Hetero Diels–Alder Reactions in Material Science

Zur Erlangung des akademischen Grades eines
DOKTOR DER NATURWISSENSCHAFTEN
(Dr. rer. nat.)

Karlsruhe Institut für Technologie (KIT),
Fakultät für Chemie und Biowissenschaften,
Institut für Technische Chemie und Polymerchemie

genehmigte
Dissertation
von

Kim K. Öhlenschläger
geboren in
Speyer, Deutschland

Dekan: Prof. Dr. Peter Roesky
Referent: Prof. Dr. Christopher Barner-Kowollik
Koreferent: Prof. Dr. Michael Meier
Tag der mündlichen Prüfung: 15.07.2014

Hiermit versichere ich, dass ich die vorliegende Arbeit selbständig und ohne Verwendung anderer Hilfsmittel und Quellen als den angegebenen verfasst habe. Die Arbeit wurde im Zeitraum vom 02.05.2011 – 04.06.2014 in einer Kollaboration zwischen dem KIT und Evonik Industries unter der Betreuung von Prof. Dr. Christopher Barner-Kowollik durchgeführt.

Ort, Datum Unterschrift

For my grandpa

Klaus König,

no better man walked ever on this earth.

IT'S GOING TO BE LEGEND… WAIT FOR IT…

Zusammenfassung

Die vorgelegte Arbeit befasst sich mit der Entwicklung und Verwendung neuartiger Verbindungen, welche in hetero Diels–Alder (HDA) Reaktionen Anwendung finden. Eine große Bandbreite an Ligationen wurde mittels neuer hocheffizienter HDA Komponenten durchgeführt um diverse funktionale makromolekulare Architekturen wie beispielsweise Netzwerke, Blockcopolymere oder Stufenwachstumspolymere zu erhalten. Die Architekturen der Netzwerke und Stufenwachstumspolymere wurde durch die HDA Reaktion von neuartigen Thiocarbonyl Dienophilen und Cyclopentadien (Cp) Funktionen aufgebaut. Die dadurch erhaltenen Thiodihydropyran-Bindungen wurden nachfolgend durch das HDA/retro-HDA Gleichgewicht zyklisiert, um so zwischen gebundenem (HDA Produkt) und ungebunden (HDA Ausgangsmaterialien) Zustand hin und her zu schalten. Während das Stufenwachstumspolymer lediglich als Modelsystem diente, um das reversible Verhalten der Thiodihydropyran-Einheiten zu untersuchen – die Analyse der Reversibilität war in einem linearen, löslichen Systemen leichter durchzuführen – wurde das schaltbare Netzwerk generiert um ein effizientes selbstheilendes Material zu erzeugen.

Elektronenarme Thiocarbonylgruppen sind naturgemäß hochreaktive Spezies und können teilweise nicht unter Umgebungsbedingungen gelagert werden, was dazu führt dass sie geschützt werden müssen. Durch die *in situ* Erzeugung der Thiocarbonylgruppen in Gegenwart eines reaktiven Diens umgeht man den Zerfall der reaktiven Gruppe und erhält direkt das gewünschte HDA Produkt. Als hochreaktive Thiocarbonylgruppen wurden in der vorgelegten Arbeit ein neuer Cyanodithioester (CDTE), bestehend aus einer angelagerten Cyanogruppe am Dithioester Kohlenstoffzentrum, und ein photogenerierter Thioaldehyde verwendet. Beide Dienophile zeigten äußerst hohe Reaktionsraten ohne die Zugabe eines Katalysators bei Raumtemperatur. Das Stufenwachstumspolymer wurde durch ein Cp_2-Polymer und einem kleinen bis-funktionalem, maskierten CDTE Linkermolekül oder mittels einer Polyethylenglycol Kette mit maskiertem Thioaldehyde an beiden Enden, erzeugt. Die temperaturabhängige Reversibilität der erzeugten Thiodihydropyran-Bindungen wurden durch on-line und off-line Experimente untersucht. Off-line Experimente basierten auf einer Dien-Metathese der

Thiodihydropyran-Einheit, bei der Cp durch eine anderes Dien ausgetauscht wurde. Der Austausch wurde via ESI-MS und GPC analysiert. Die erhaltenen Massespektren bewiesen den erfolgreichen Dien-Austausch, während GPC Daten die Depolymerisation des Stufenwachstumspolymers belegen konnten. Für on-line Nachweise der Reversibilität der Thiodihydropyran Einheiten wurden temperaturabhängige NMR und DLS Messungen durchgeführt, welche die Ergebnisse der off-line Experimente bestätigten. Darüber hinaus zeigten temperaturabhängige UV-Vis Spektroskopie-Messungen die Empfindlichkeit des DA Gleichgewichts gegenüber Temperaturänderungen, welches sich innerhalb weniger Minuten bei Temperaturänderungen wieder einstellte. Für die Erzeugung eines Netzwerkes wurde ein tetra-funktionales, maskiertes CDTE Molekül synthetisiert und die Synthese mit Hinblick auf die industrielle Anwendung optimiert. Das CDTE Netzwerk zeigte sehr gute selbstheilende Eigenschaften. Diese selbstheilenden Eigenschaften wurden qualitativ mittels wiederholter Stresstests und quantitativ durch Rheologie-Studien der Komplexenviskosität sowie des Spannungs- und Verlustmodules bewiesen.

Zusätzlich zu Studien über die reaktiven CDTE und Thioaldehyde HDA Produkte wurde ein photogeneriertes Dien in der Reaktion mit elektronenreichen Dithioestern untersucht. Das reaktive Dien basiert auf einer Dienolstruktur und wurde ebenfalls *in situ* durch die Bestrahlung von *ortho*-Methylbenzaldehyd-Vorläufern generiert. Der Erfolg der HDA Reaktion und die Isothiochroman Struktur wurde mittel ESI-MS, UV-Vis, NMR, und ESI-CID Messungen nachgewiesen. Die Eignung der neuen lichtinduzierten HDA Reaktion für die Herstellung makromolekularer Architekturen wurde durch die Blockcopolymerkonjugation von Poly(ε-caprolacton), endfunktionalisiert mit einer *ortho*-methyl Benzaldehyde-Einheit, und einem Dithiobenzoat tragendem poly(methyl methacrylat) demonstriert.

1 Abstract

The presented work focuses on the design and application of new compounds suitable for Diels–Alder (DA) and hetero Diels–Alder (HDA) reactions in material science.

A wide range of ligations leading to block copolymer formation, step-growth polymerization and network construction were carried out by employing novel, efficient and highly reactive DA/HDA units. Step-growth polymerization and network formation were performed with highly reactive thiocarbonyl-dienophiles and cyclopentadiene moieties, affording dihydro-thiopyran linked architectures. The resulting dihydro-thiopyran linkages were cycled between the bonded dihydro-thiopyran (HDA products) and debonded (retro HDA products) state by exposing the architectures to periodically changing temperatures. Whereas the step-growth polymer served as a linear test system – as it was simpler to analyze with regard to its reversible linkages – the generated network represented an efficient self-healing material.

Electron poor thiocarbonyl molecules are by nature highly reactive and can be unstable under ambient conditions, requiring their protection during storage. Their *in situ* activation in the presence of suitable dienes avoids premature decomposition and provides facile access to the desired HDA products. A new dithioester, featuring a cyano group attached to the thiocarbonyl function as well as a photochemically generated thioaldehyde served as highly activated thio-dienophiles, which showed extremely fast reaction rates at ambient temperatures without any catalyst. The step-growth polymerization was conducted with a bis-cyclopentadiene polymer and either a small molecule bearing two masked cyanodithioester units or a polyethylenglycole (PEG) chain capped with a masked thioaldehyde on both ends. The temperature switchability of the resulting dihydrothiopyran linkages formed between the thio-dienophiles and cyclopentadiene moieties were analyzed via on-line and off-line experiments. Off-line experiments were based on a diene exchange study of the HDA product assessed by ESI-MS and SEC analysis. Whereas ESI-MS confirmed the successful diene exchange reaction in a polymer end group study, SEC traces underpinned the depolymerization of the respective step-growth polymers.

Temperature dependent NMR and DLS experiments gave an on-line image of the dihydrothiopyran driven bonding/debonding process. Furthermore, fast bonding/debonding reaction kinetics were evidenced via on-line UV-Vis measurements. In order to apply the hetero Diels–Alder chemistry to networks, a tetra-functional masked CDTE molecule was synthesized and optimized with respect to its synthetic strategy in an industrial context. The healing ability and efficiency of the network was demonstrated by repetitive tensile tests and quantitatively explored by rheology studies focusing on the viscosity as well as the tension and loss module.

In addition to the development of reactive thio-dienophiles, the use of highly reactive photocaged dienes able to react with rather unreactive electron rich dienophiles, such as dithiobenzoates, was investigated. The reactive diene, based on an *ortho*-quinodimethane structure, was *in situ* generated via irradiation of a *ortho*-methyl benzaldehyde precursor with mild UV light. To assess the HDA reactions success and confirm the isothiochroman structure, ESI-MS, NMR, UV-Vis, and ESI-CID measurements were carried out. The suitability for macromolecular design was demonstrated by a block copolymer conjugation between a poly(ε-caprolacton) end capped *ortho*-methyl benzaldehyde and a 2-cyanopropyl-dithiobenzoate carrying poly(methyl methacrylate) under light irradiation.

In summary, the present thesis provides the today most efficient and rapidly switchable DA self-healing system with excellent perspectives to be employed in an industrial contest. In addition, the thesis demonstrated that polymers prepared via the RAFT process using conventional RAFT agents can readily undergo HDA ligations at their chain termini with photocaged dienes

2 Introduction and Motivation

The words ‘recycling’ and ‘pollution’ have become a hot topic in science and politics due to the growing world population. With increase in population comes a proportional increase in consumption of everyday products and consequently disposal of waste becomes an issue. This circumstance has been exacerbated by the fact that many companies have adopted high profit business models achieved by producing cheap goods with short lifetimes. As a result, waste disposal has reached an alarming rate on a global scale. An aspiring solution to the problem is the development of products with longer lifetimes and self-healing features. Self-healing materials can be repaired by certain mechanisms and thus prolong their lifespan, while also reducing pollution. Moreover, such mendable materials offer a great potential for a broad spectrum of applications. With respect to their adjustable physico mechanical properties, adaptable networks, a key class of self-healing materials, display the possibility to be employed in rapid prototyping printers, composite materials for aeronautics and car elements as adhesives and coatings, or in consumer electronics. Consequently, multiple industrial branches have shown high interest in self-healing materials and the design of special systems tailored for their purposes.

The majority of self-healing materials are networks based on reversible bond chemistry.[1] By employing a network specific trigger, it is possible to break the bonds in the network and reform them.[2] As a result, scratches and cracks are completely refurbished preventing crack progression and consequently more serious damage. Among all applied reversible bonding chemistries, the DA reaction has proven to be a powerful mechanism in the field of self-healing materials.[3] Due to its often high yields and robustness, the 4+2 cycloaddition has mostly been applied as conjugation tool enabling polymer chemists to build complex architectures or transform polymer end groups with a high end group fidelity. In addition, the high yield has sparked interest in employing the DA reaction as a polymerization technique itself[4] and to perform step-growth polymerizations not requiring a catalyst, an inert atmosphere or elevated temperatures.[5] By employing the heat triggered cycling between the bonded (i.e. the DA product) and the debonded state (i.e. the retro DA product), damages and cracks can be completely healed. The repairing process of such DA

based material relies on a metathesis exchange between DA connections on the edge of the fracture, which reforms crosslinks and mends the DA based material on a microscopic scale.

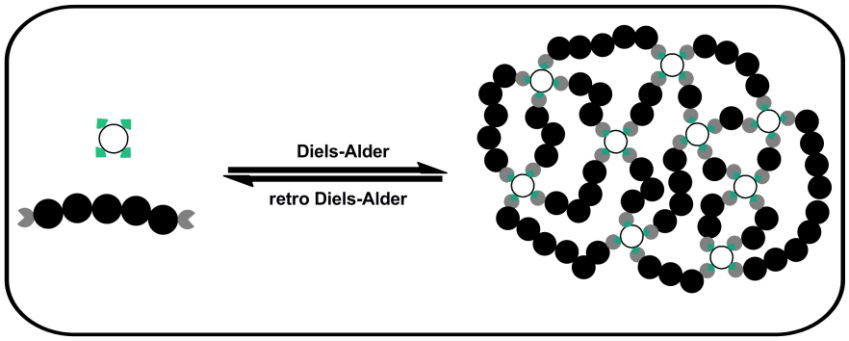

Figure 2.1 Idealized schematic reaction scheme of a DA based self-healing network.

Despite the great potential such materials offer, the number of chemical systems in the field of self-healing materials is scarce. The lack of publications reporting new DA systems for self-healing materials can simply be attributed to the deficiency of reversible DA reactions that can be achieved at reasonable temperatures, essential for the healing processes. The design of such new DA systems, reversible at relatively mild temperatures (i.e. approximately 100 °C), not requiring a catalyst and demonstrating high reaction rates are a crucial challenge in the field of self-healing materials. Furthermore, it is essential from an industrial point of view to reduce the synthetic costs for an industrial product. These problems were addressed in the present thesis by developing a new rapid DA system suitable for self-healing material applications and industrial scale production.

However, aside from the work on new self-healing materials, it is also important to broaden the scope of conjugation tools and increase the number of available end groups able to serve as ligation points. Thus, the concept of HDA chemistry based on reversible addition fragmentation chain transfer agents was extended. So far, only three examples of reversible addition fragmentation chain transfer agents exist which can on the one hand act as controlling agent in a radical polymerization process and on the other hand function as reactive end group in a HDA ligation.[6] However, the intrinsic activation of the RAFT agents for the coupling reaction reduces the stabilization of radical intermediates and limits the number of monomers which can

be polymerized in a controlled fashion. To enlarge the number of RAFT polymers which are suitable for HDA conjugation, a new photocaged diene was designed, able to react with the highly versatile RAFT agent cyanopropyldithiobenzoate (CPDB) under light irradiation.

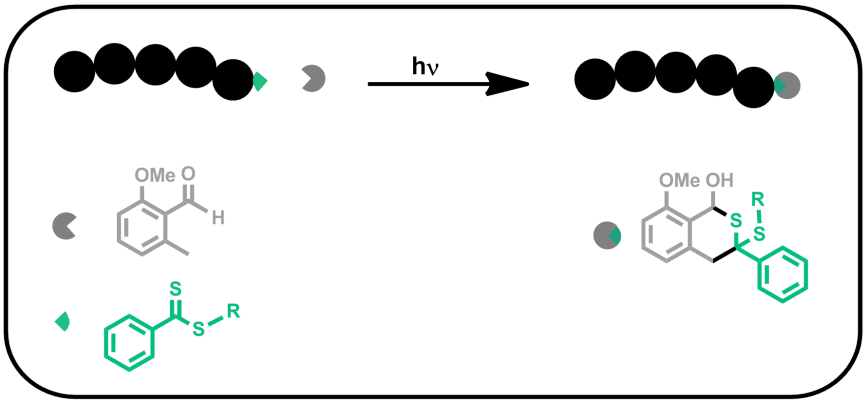

Figure 2.2 Schematic light-induced ligation reaction of a dithiobenzoate containing polymer with a photocaged diene.

3 Theoretical Background and Literature Overview

3.1 Modular ligation and *click* chemistry

Perhaps no other synthetic concept has revolutionized the abilities of chemists as much as the *click chemistry* philosophy. The entire field of chemical synthesis was advanced by following the example of nature, circumventing complex multiple step synthesis by simple modular chemical procedures. Sharpless and coworkers were the first to realize the advantage of distinctive modularity in bio-synthesis which led to the development of the *click chemistry* concept.[7] The *click* chemistry approach addressed the problem of sophisticated natural product synthesis in an unorthodox manner. In contrast to the arduous strategy of building a molecule step by step– the usual approach – Sharpless and coworkers decided to synthesize multiple fragments of the targeted molecule separately. Finally, they assembled the single fragments via special orthogonal reactions with high yields, obtaining the desired natural product or derivatives of the targeted molecule with the same biological properties.

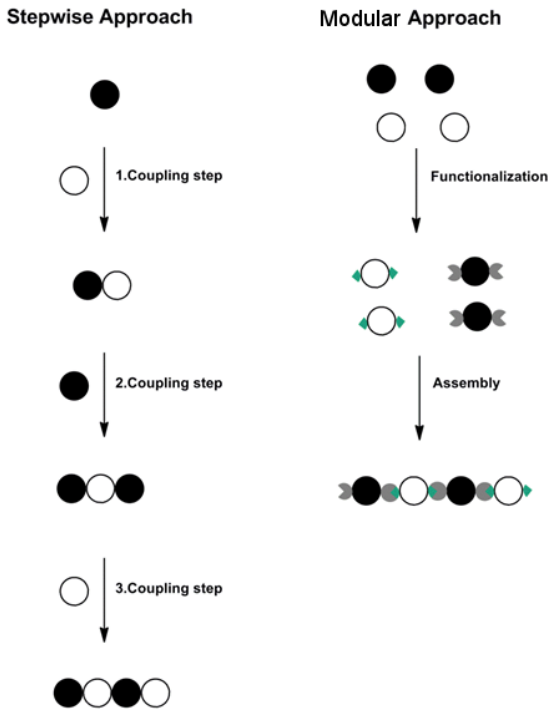

Figure 3.1 Stepwise and modular ligation approach to a target molecule. In contrast to the stepwise construction of the targeted molecule, the modular approach utilizes the specific assembly of prefunctionalized fragments.

Replicating the sound of a closing seat belt, these authors coined the new concept *click chemistry,* symbolic for the formed linkages between the fragments and the modular ligation principle. The crucial point in the concept was the question of which chemical reactions should be utilized for the covalent assembly of the fragments. To address this issue, Sharpless and coworkers defined certain criteria for their conjugation reactions, limiting the amount of possible reactions to a small number of very efficient synthetic protocols. According to their criteria, a *click* reaction has to:

i. be wide in scope.

ii. be modular.

iii. reach very high yields.

iv. be stereospecific.

v. has a high thermodynamic driving force.

Moreover, it is necessary that the process:

vi. is benign to environmental parameters, such as oxygen and moisture.

vii. has a high reaction rate.

viii. can be conducted in benign solvents, such as water.

ix. yields no offensive by-products.

x. requires no purification via column chromatography.

xi. utilizes readily available starting materials.

xii. be selective for a single product.

Considering all these characteristics, only reactions such as cycloadditions, ring opening reactions, special condensations and Michael addition reactions are allowed to be considered as highly efficient ligations worthy to be defined as *click* reactions.

Originally exhibited as a new way of natural product synthesis, soon the *click* approach became an attractive strategy for other chemical fields, which simplified

reaction pathways by using modular ligation techniques.[8] In particular, the field of polymer and material chemistry has been drastically advanced via the context of *click* chemistry.[9] By combining *click* reactions with powerful polymerization techniques, a novel modular ligation strategy has evolved, representing a tool for the design of any imaginable macromolecular architecture while sparing the tedious orthodox synthetic pathways.[9a,10] Common examples for such polymeric architectures which are achieved via modular ligations are block copolymers,[6a,11] star-[12], cyclic-[13] and brush polymers[14] as well as dendrimers.[15]

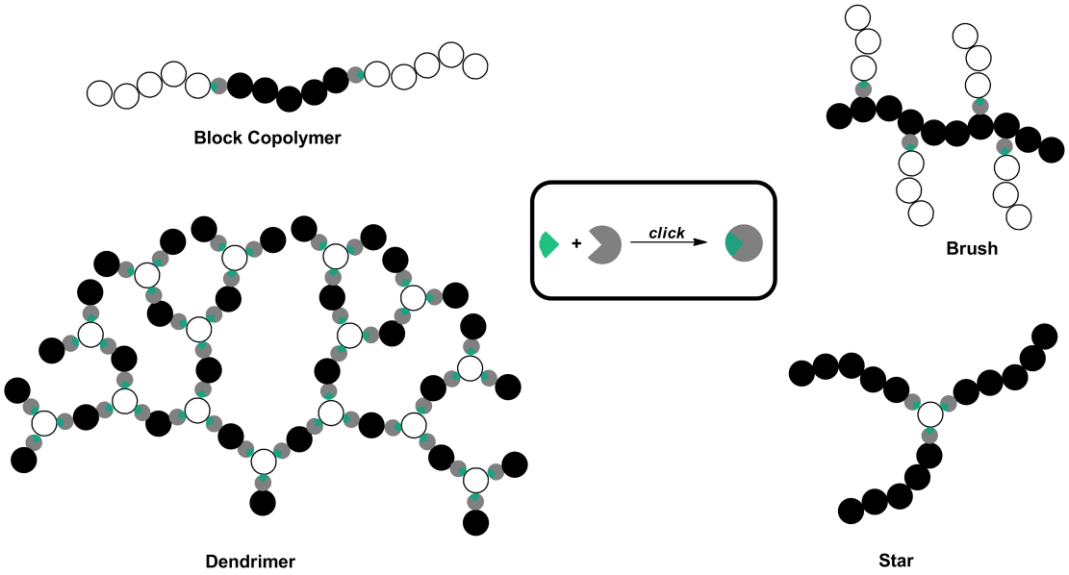

Figure 3.2 Macromolecular architectures designed by the utilization of modular ligation protocols.

However, the original *click* criteria are not applicable to every chemical field. Some require more defined criteria, whereas others can not include all of the entire original criteria. For example the copper catalyzed azide alkyne cycloaddition cannot be utilized in medicinal chemistry, because of the cytotoxic character of copper traces. On the other hand, the field of polymer chemistry does not require stereospecific conjugation reactions, which are essential for natural product synthesis. Understanding this, chemists started to modify the original *click* criteria for different chemical fields according to their requirements. One of the most famous examples of refined *click* criteria is the selection for synthetic polymer chemistry established by a group of leading polymer chemists.[16] Their refined selection addressed certain issues by adding the following criteria:

xiii. equimolarity.

xiv. large-scale purification.

xv. short timescale.

At the same time they specified some original criteria by rephrasing them to:

vii. high reaction rates in a reasonable timeframe.

viii. benign solvent as low boiling organic solvent.

and additionally discarded:

iv. stereospecificity.

Following these assessment rules, the established *click* reactions in synthetic polymer chemistry can be narrowed to:

- The Diels–Alder and hetero Diels–Alder cycloaddition
- The copper catalyzed azide alkyne cycloaddition
- The nitril oxide cycloadition
- The oxime condensation
- The thiol-ene addition of Michael systems
- The thiol or amine addition with isocyanates and isothiocyanates
- The ring opening of epoxides with amines or thioles
- The thiol-bromo nucleophilic substitution
- The copper catalyzed nitriloxide radical coupling

Various literature reviews have addressed the topic of complex polymeric architectures and *click* chemistry which highlight the achievements reached through the use of the aforementioned reactions.[17] Among the above listed *click* reactions, the Diels–Alder (DA)[18], the copper catalyzed azide alkyne click[19] and the Michael-typ thiol-ene[20] reactions have attracted the most attention and have been employed extensively.

3.2 Polymerization techniques

3.2.1 Free radical polymerization (FRP)

With approximately 50% of all synthetic polymers produced via free radical polymerization (FRP), the technique can be considered as the most important method in an industrial context.[21] Of the two polymerization mechanisms, i.e. step-growth and chain growth, FRP follows the later one, adding monomer units repetitively via radicals to a chain end, resulting in a polymer. The process can be divided into four elementary reaction steps. Firstly, *initiation* generates radicals, secondly the repetitive addition (*propagation*) of monomers, i.e. the growth of the polymer chains, and thirdly the *termination* which ceases macromolecular growth by quenching the highly reactive radical species, leading to dead polymer chains. In addition to these three steps, a forth step (*transfer*) can occur during FRP. The transfer reaction can be considered as a special termination reaction in which highly reactive growing polymer chain radical species are quenched by a transfer of the active center to a small molecule (i.e. monomer units, solvent or polymer chains), which subsequently restarts macromolecular growth. As every radical reaction requires all four steps, the absence of oxygen and other oxidizing agents which would quench the radical and therefore inhibit the FRP is essential. Scheme 3.1 presents the four elementary steps.

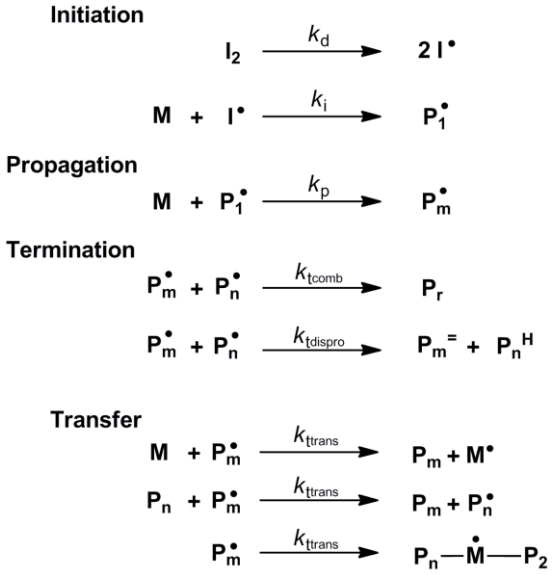

Scheme 3.1 The four elementary reactions in a free radical polymerization process.

For the initiation process, highly energetic molecules such as diazo- or peroxy compounds are utilized to generate the radicals. When heated or irradiated, the diazo- and peroxy compounds decompose under a homolytical bond cleavage to form the highly reactive primary radical species often producing an inert stable gas (i.e. nitrogen and carbon dioxide) as a byproduct. In the following steps, the radical adds to a monomer unit, producing the first monomer radical which then commences macromolecular growth. Arguably the addition of the first monomer unit to the radical can already be considered as a growth step; however, the fate of the radicals past the initiator decomposition is uncertain. When two radicals are generated in close proximity to each other, the two radicals may not only initiate chain growth, but may also recombine, leading to an inactive small molecule. As a result, the addition of the first monomer unit to a generated radical is treated separately from the other monomer unit addition steps and specified as an additional sub-reaction in the initiation process. Typical rate coefficients for the initiator decomposition and the monomer addition are 10^{-5} s^{-1} for k_d and 10^4 s^{-1} for k_i at moderately elevated temperatures. The growth of the chain, i.e. propagation, results from an attack of the radical on a monomer unit which leads to a new bond between the monomer and the former radical, generating a new radical species on the monomer unit. Mostly activated C=C double bond carrying·molecules such as styrenes, acrylates or methacrylate derivatives are utilized in FRP, but heterocyclic compounds such as oxiranes or oxazolines can be polymerized by FRP as well. The propagation rate coefficient k_p depends on the stabilization of the produced monomer radical and therefore depends on the chemical nature of the monomer, varying from 10^5 to 10 $M^{-1}s^{-1}$.[22] Termination of the growing polymer chains can occur by either the combination of two radicals, disproportionation via a hydrogen radical transfer from one chain to the other or the aforementioned transfer to another small molecule. A special case in the radical transfer process is the transfer to a polymer chain. A radical transfer reaction can be subdivided in an intermolecular transfer leading to long branches of the chain and an intramolecular transfer (backbiting), which produces short side chains of two monomer units.[23] The transfer reaction does not change the overall number of radicals in the polymerization mixture, yet it influences the molecular weight distribution. Moreover, the transfer reaction results – if reinitiation is slow – in the retardation of the polymerization, affecting the entire polymerization process. All termination reactions are a product of the movement of

the polymer chains, implying that the rate coefficient is determined by the diffusion of the macroradicals within the polymerization mixture. Therefore, the chain length and conversion are critical factors affecting the termination rate coefficient of the individual macroradicals.[24] Common values for the average termination rate coefficient k_t range between 10^8 $M^{-1}s^{-1}$ and 10^5 $M^{-1}s^{-1}$.[25] Tolerating water and further protic impurities allows the FRP of a wide range of monomers. However, in the context of modular ligation FRP has to be discarded for that purpose, as it does not provide telechelic functionalities in the polymer in addition to the limited control over the polymer distribution, which is required for the use of polymers in conjugation reactions to achieve precisely engineered macromolecular architectures.

3.2.2 Anionic polymerization

The polymerization of monomers by anionic techniques provides extraordinary control over the molecular weight distribution, functionality, composition, reaction rate and reaction time. Consequently, anionic polymerization represents a chain growth process without ideally chain termination reactions (termination and/or transfer) and thus the technique is considered to be truly living in character,[26] as the reactive anionic species are still present and active after the consumption of all monomer units. However, extreme conditions are required to ensure a living anionic polymerization. Slight traces of moisture and oxygen can interfere with the reactive anionic species and quench it. Furthermore, carbon anions, a common anionic species in the case of styrene monomers, are highly reactive compounds which are able to even react with nitrogen. Therefore, anionic polymerizations have to be carried out under argon atmosphere with highly pure starting materials. A further result of the high reactivity of such anionic species is the monomer limitation. Ester containing monomers such as acrylates and methacylates are vulnerable to attack by nucleophiles (i.e. anions) meaning that special initiator systems are required for their anionic polymerization. ,Accordingly only styrenes, butadienes, heterocycles and vinylic derivatives are possible monomers for a standard anionic polymerization process.

In an effort to combine the living character of anionic techniques with the tolerance of functionality and moisture of FRP, chemists focused on the development of controlled

radical polymerizations (CRP), providing a compromise of all the desired characteristics. However, a radical chain growth process can never be entirely living as the termination reactions cannot be completely suppressed. Nevertheless, several radical polymerization techniques have been designed to prevent transfer reactions and termination processes.

Reversible degeneration is the key component to CRP processes.[27] The most widely utilized CRP techniques are the nitroxide mediated polymerization (NMP), [28] atom transfer radical polymerization (ATRP),[29] and reversible addition-fragmentation chain transfer (RAFT)[30] polymerization. Those techniques are highlighted in the following CRP section.

3.2.3 Controlled radical polymerization (CRP)

3.2.3.1 Nitroxide mediated polymerization (NMP)

In the NMP process, the radical concentration is reduced via a temperature dependent dynamic equilibrium of alkoxyamine compounds to suppress the termination processes.[28] At elevated temperatures, alkoxyamines undergo a homolytic cleavage of the carbon-oxygen bond resulting in a stable persistent nitroxide radical and an active growing carbon radical species.[31] The persistent radical recombines only with growing radical chains and not with itself as the combination product would be a highly energetic peroxy form, which would decompose immediately to the nitroxide radical.[32] Consequently, the cross-combination is favored, enabling NMP to suppress termination reactions. (Scheme 3.2).[33]

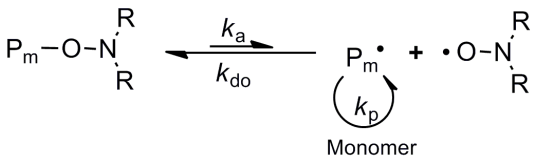

Scheme 3.2 General NMP mechanism. R stands for specific carbon moieties, which are presented in Scheme 3.4.

The phenomenon of such stable radicals which do not recombine is known as the persistent radical effect discovered by Gomberg.[34] Despite the persistent radical effect, a growing radical chain can still recombine and form inactive polymer chains leaving an excess of persistent radicals in the polymerization mixture. The NMP process can be conducted in two ways, either via a stable nitroxide radical such as 2,2,6,6-tetramethylpiperidine-1-oxyl (TEMPO)[31] and a radical initiator or by heating an alkoxyamine unit. Both approaches lead to a dynamic equilibrium which minimizes termination. The fact that alkoxyamines can be reactivated and remain, after the NMP, as a polymer end group makes the technique very attractive for block copolymer synthesis, similar to anionic polymerizations.

Scheme 3.3 Block copolymer synthesis by employing consecutive NMP of two monomers.[35]

However, post-polymerization modifications, apart from block copolymer formation, remain challenging because of the limited chemistry which can be carried out with the alkoxyamine group. For further macromolecular architectures functionalized initiators are required with suitable functional groups, tolerating the polymerization conditions and representing a reactive center for conjugation reactions.[36] Moreover, high temperatures are required to reach the dynamic equilibrium as TEMPO derivatives form relatively stable alkoxyamines ($K_{NMP} = k_a / k_{do} = 2.1\ 10^{-11}$ M for TEMPO/styrene at 125 °C). With those TEMPO derivatives only styrenes are suitable monomers as acryltes and methacrylates induce uncontrolled self-polymerizations at 125 °C. Therefore, other nitroxides have been synthesized with the ability to control the polymerization process of a broad variety of monomers in lower temperatures ranges (Scheme 3.4).[37]

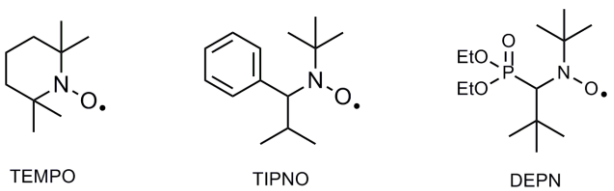

Scheme 3.4 Typical nitroxides utilized in NMP processes

3.2.3.2 Atom transfer radical polymerization (ATRP)

The ATRP process is based upon a simple redox equilibrium, which yields the active radical species by the reduction of a halogen alkane and terminates the radical by oxidizing it back to the halogen form. Equilibrium constants $K_{ATRP} = k_a / k_{do}$, of the redox process lie generally in the range of 10^{-11} to 10^{-3}, [38] favoring the oxidized halogen alkane (dormant) form and yielding the growing radical species in a very low concentration. As a result of the low amount of radicals, disproportionation and combination are mostly suppressed. The transfer process is not affected by the low radical concentration, but can be prevented in the ATRP process by the short life time of the radical species, terminating a growing chain by reversible reduction rather than by a transfer mechanism, due to the dynamic nature of the redox equilibrium. The atom transfer radical species is commonly a transition metal complex formed between a transition metal salt and an amine containing ligand. The reversible redox process between the active reduced radical species and the dormant oxidized halogen specie is presented in Scheme 3.5.

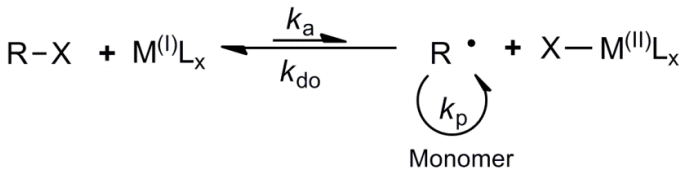

Scheme 3.5 Accepted general ATRP mechanism. X represents a halid and L a ligand.

Matyjaszewski[39] and Sawamoto[40] were the first to realize the potential of the reversible redox mechanism, utilizing copper and ruthenium, respectively, for polymer chemistry, which was formerly employed in organic synthesis for carbon-carbon bond formation.[41] Copper is among the most utilized transition metals and certainly the most efficient. The low potential between the Cu(I) and Cu(II) states makes it the perfect reducing/oxidizing agent for the reversible process. However, the transition metal complex's stability and reactivity in the equilibrium depends strongly on the employed ligand which is added to the copper salt.[29] The metal/ligand reactivity together with the stability of the monomer radical dictates the polymerization process which suppresses termination. These two factors have to be considered for every

ATRP process, implying that the ligand has to be chosen with respect to the polymerized monomer. Common ATRP ligands are shown in Scheme 3.6.

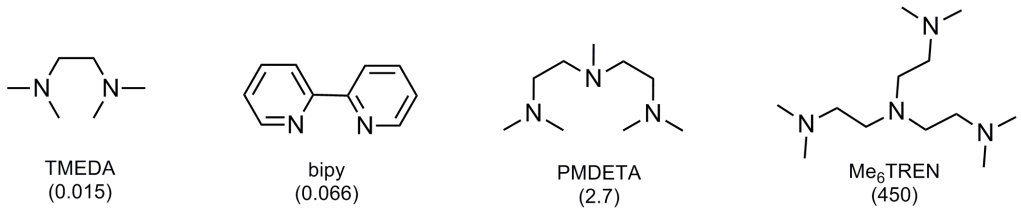

Scheme 3.6 Typical ligands for copper catalysed ATRP. The numbers represent activation rate coefficients (k_a / $M^{-1}s^{-1}$) with 2-bromoisobutyrate in the presence of CuBr in MeCN at 35 °C.[29]

In addition to the living polymerization characteristics, ATRP offers additional advantages compared to other CRP techniques. As the reversible redox process produces the active radical species, no radical initiator, such as the aforementioned peroxy- or azo- compounds, are required. The lack of small radical initiator molecules which could quench the growing chain reduces the amount of inactive polymer chains and leads – at least at low conversions –[42] to significant end group fidelities. The retention of a halide end group is an additional advantage, giving synthetic polymer chemists a handle for post-polymerization modifications and further modular ligations which makes ATRP an efficient and powerful tool for the construction of macromolecular architectures.[43] In addition, ATRP offers a wide variety of readily available organo halids which can be employed as ATRP initiators. Essentially all compounds with a halogen functionality next to an α-carbonyl, phenyl, vinyl, or cyano group are efficient initiators (Scheme 3.7).

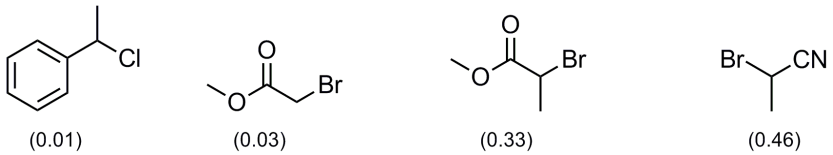

Scheme 3.7 Examples of ATRP initiators. The numbers represent activation rate coefficients (k_a /$M^{-1}s^{-1}$) with CuX/PMDETA (X = Br or Cl) in MeCN at 35 °C.[29]

Despite of the advantages of ATRP there is no suitable polymer process for all desired materials and applications. The cyctotoxic effect of even small traces of transition metals such as copper prohibits the use of ATRP polymerized products in biomedical applications. Nevertheless, new ATRP procedures such as activator regenerated by electron transfer (ARGET) ATRP proceed with very small concentrations of Cu complexes.[44] However, the removal of the copper as well as the improvement of the termination suppression remains as the critically limiting factors for ATRP.

3.2.3.3 Reversible addition-fragmentation chain transfer (RAFT) polymerization

The RAFT polymerization process differs from the aforementioned CRP techniques fundamentally. In contrast to NMP and ATRP, which suppress termination processes by keeping the radical concentration low via a dormant equilibrium process, the RAFT process follows a regressive approach. In the course of the polymerization a special chain transfer agent (CTA) is added to the mixture which reacts with the growing chain ends. Consequently, the growing chain is terminated and another active radical is released by the CTA. The generated radical can propagate and re-react with the CTA setting the former growing chain free again. This exchange process is occurring permanently during the polymerization, affording polymers with a high end group fidelity.[45] Typically employed CTAs are thiocarbonylthio compounds such as dithioesters, xanthates and trithiocarbonates known for their high radical affinity.[46] The accepted RAFT mechanism and its multiple equilibria are shown in Scheme 3.8.[45]

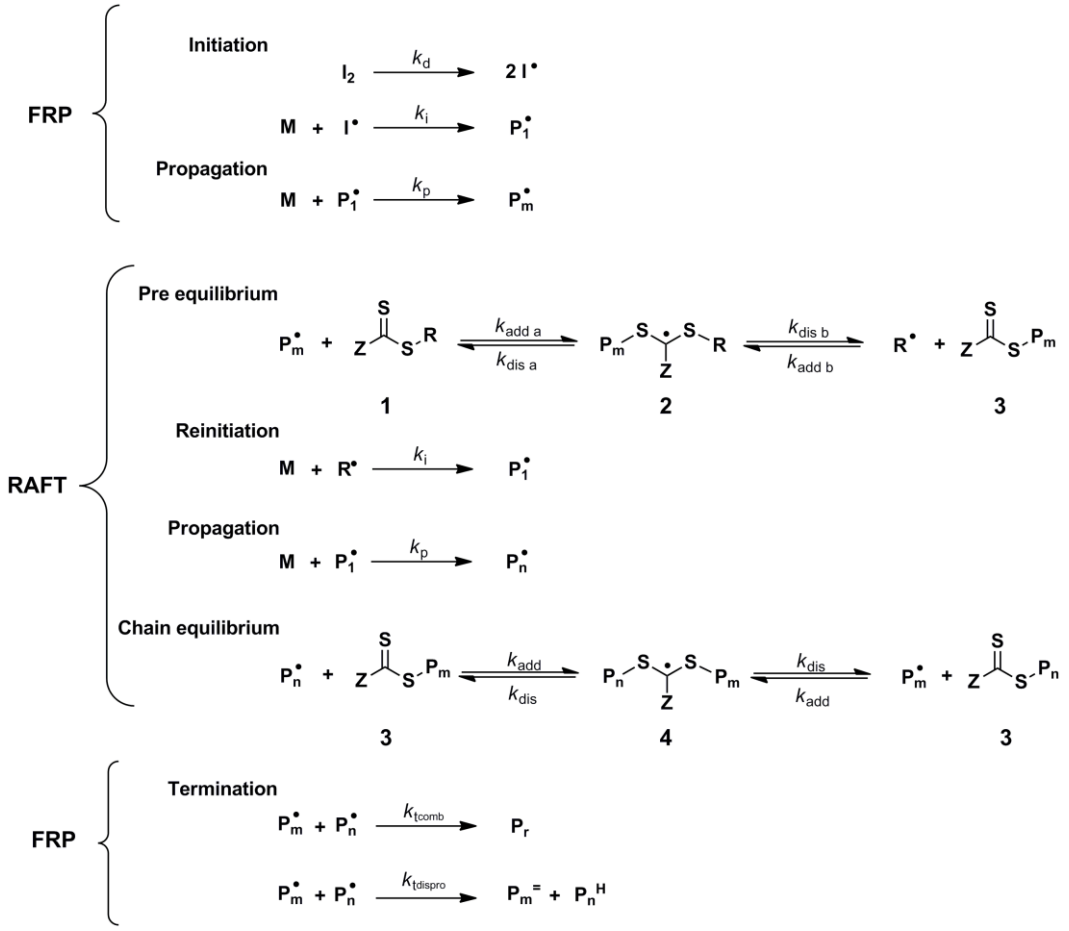

Scheme 3.8 Accepted mechanism for the RAFT process. After a FRP initiation and propagation, the pre- and main equilibrium lead to thiocarbonylthio terminal polymers. Upon cooling, the polymerization is stopped by the termination processes of FRP, quenching still growing radicals.

The beginning of the RAFT polymerization process does not differ from a conventional FRP. An initiator molecule is heated to its decomposition temperature, yielding the initiating radicals, which attack monomer units and start growing chains. However, after a short time of propagation – ideally already at chain length one – the growing radicals add to the thiocarbonylthio molecule **1** and form the intermediate radical **2**. The intermediate radical **2** fragments into a new thiocarbonylthio compound **3** and the respective radical. Addition of the generated radical to a monomer unit affords a new growing polymer chain, which adds after a short growing period again to the thiocarbonylthio compound **3**. Once the entire thiocarbonylthio species **1** is consumed only polymeric radicals are present in the mixture. A rapid equilibrium between growing polymer chains and the dormant radicals **4** is reached when the

addition fragmentation process repeats. The exchange reaction of the polymer chains with the dormant species **4** ensures an average equal protection for all propagating chains and enables molecular weight control over the process, resulting in a narrow molecular weight distribution with excellent end group fidelity (i.e. thiocarbonylthio groups). Nevertheless, some inactive polymer chains are formed when employing RAFT, although the majority of polymer chains is end capped with the utilized CTA. The known termination processes from the FRP applies to the growing polymer chains which are not end capped with a CTA unit.[47] Consequently, the amount of inactive polymer chains can be controlled to a certain point by choosing the CTA to initiator ratio wisely.[48]

As can be seen in the mechanism, the number of radicals is constant during the entire polymerization. Accordingly, the reaction rates of the RAFT process are higher than in NMP or ATRP due to no inherent retardation by persistent radicals. This advantage makes RAFT very attractive for industrial processes as shorter reaction times are required. Moreover, the thiocarbonyl thio end group gives synthetic chemists a handle for modular ligation by either simple end group transformations or direct modular ligation on the end group. The choice of a suitable CTA depends on the nature of every specific monomer. Important points for the assessment of the suitability of a CTA are:[49]

- The thiocarbonyl thio compounds should be active towards the attack of a radical (high k_{add}).
- The dormant radical species **2** should fragment towards the macromolecular thiocarbonyl thio molecule ($k_{diss\ b} > k_{diss\ a}$).
- The addition of radicals to the thiocarbonyl thio function should be favored over termination ($k_{add} >> k_t$).
- The radical generated from the attack of a growing radical to the thiocarbonyl thio compound **2** should initiate a new chain without inhibiting the entire polymerization process ($k_i > k_p$).

With respect to these points, synthetic polymer chemists have established a table of different Z-groups and R-groups of CTAs and assessed their suitability with different monomers.[50]

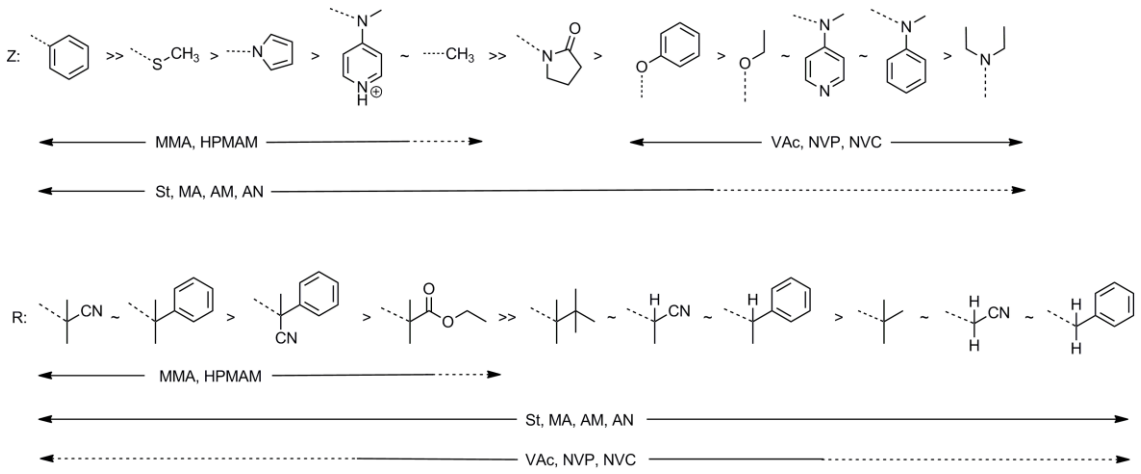

Scheme 3.9 Guidelines for the selection of a suitable RAFT agent in a controlled polymerization, adapted from reference 51. (Dashed lines represent limited control over the reaction and poor polydispersities) AM = acrylamide, AN = acrylonitrile, HPMAM = N-(2-hydroxypropyl) methacrylamide, MA = methacrylate, MMA = methyl methacrylate, NVC = N-vinyl carbazole, NVP = N-vinyl pyrrolidone, St = styrene, VAc = vinylacetate.[51]

In the context of modular ligation, the RAFT process displays a living character, providing the ability to form well defined linear polymers and suitability for complex macromolecular architectures. Due to very high end group fidelity it is possible to perform consecutive RAFT polymerizations of different monomers leading to well defined block copolymers.[52] Moreover, functionalized RAFT agents can be employed for modular ligations post polymerization, enabling synthetic chemists to built structures such as dendrimers and mikto arm star shaped polymers.[12,30,53] However, star shaped polymers can also be achieved via the RAFT process without the need of modular ligations. Molecules bearing multiple RAFT groups, connected via either Z- or R-group, can be utilized as core structure, growing polymer chains from the core to obtain star structures.[54]

3.2.3.4 Ring opening polymerization (ROP)

The ROP process represents a special polymerization technique in the field of synthetic polymer chemistry. In contrast to the aforementioned polymerizations it is possible to initiate a ROP process via different methods. Cyclic monomers can be opened either via the addition of a radical[55] or an ion (i.e. cation or anion) giving

synthetic chemists variable opportunities to conduct the polymerization process with many functionalities in the monomer (see Scheme 3.10).

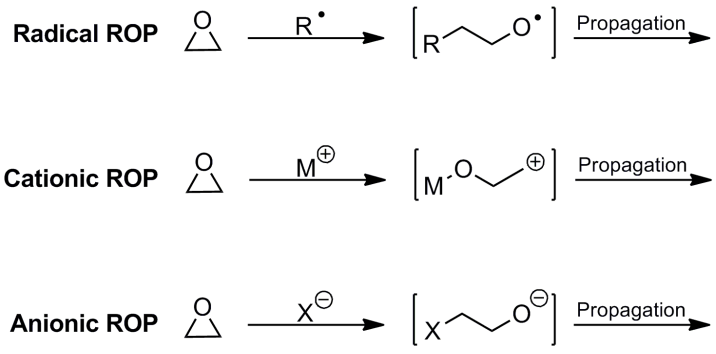

Scheme 3.10 Different ROP initiation processes.

However, cationic and radical induced ROP processes can undergo side reactions such as disproportionation and elimination reactions, leading to undesired chain termination.[56] Consequently, only the anionic ROP process which lacks such termination reactions when carried out under dry conditions can be considered as a living polymerization technique. The nucleophilic anion can only be terminated by moisture or protic impurities. Working under inert gas atmosphere reduces such terminations, leaving reactive end groups at the terminus of the polymer chains past polymerization. As a result, anionic ROP is the most widely employed ROP techniques and often misleadingly equaled with the term ROP. It is noteworthy that it is possible to perform cationic and radical ROP in a living fashion, however, intentional addition of reversible termination agents is required[56-57] changing the original mechanism of the ROP process. A large variety of cyclic monomers, including lactames, lactones, cyclic ethers or siloxanes can be polymerized via the ROP process. Such cyclic functionalities are mostly found in biocompatible molecules, making ROP the polymerization of choice when targeting a polymer for biomedical applications. Despite that, the most prominent examples for industrial ROP products are Nylon 6 and poly(ethylene glycol) obtained by the polymerization of ε-caprolactam and ethylene oxide, respectively.

The ability of cyclic monomers to form macromolecules by sequential ring-opening depends strongly on the size and the possible conformations of the ring as well as the possible conformations of the linear polymer chain. Ring strain is key to the

polymerization of cyclic monomers. As a result of the ring strain, the single monomer units represent highly energetic small molecules. Once attacked by an initiator molecule or activated chain end, the ring opens and releases the rings strain leading to a more stable conformation. Therefore, thermodynamics favor the ring opening of the monomer and drive the polymerization forward. However, the ROP polymerization can be reversed from the linear polymer back to cyclic analogs by intramolecular backbiting of the growing specie. This polymerization-depolymerization equilibrium features much slower propagation rates than in CRP or anionic polymerizations, increasing the reaction times of ROP. Furthermore, high monomer conversions lead to very broad molecular weight distributions as a result of intramolecular transfer reactions of growing polymer chains.

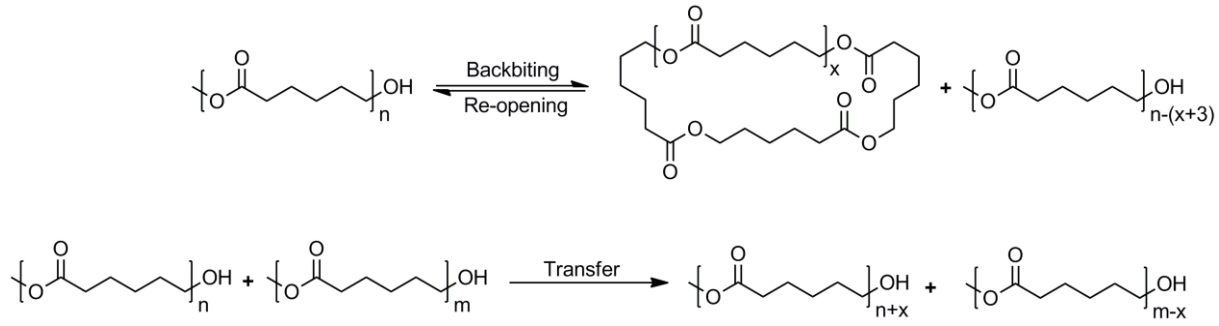

Scheme 3.11 Main side reactions occurring in the ROP process, exemplified on the ROP of ε-caprolacton.

To drive the equilibrium of the polymerization process towards linear polymer chains, variable catalytic systems have been developed and employed for ROP systems. The three main catalytic systems rely on metal complexes, small organic molecules and enzyms. Metal complexes and small organic molecules coordinate onto the growing polymer chain and a cyclic monomer unit bringing both reactive centers in close contact to each other to ensure no backbiting. Enzymes on the other hand react with the cyclic monomer to an open chain conformation, yielding more reactive monomers which rapidly react with the growing polymer chain. These synthetic approaches cannot prevent transfer reactions but indeed improve the reaction times of ROP processes and lead to a better control of the molecular weight distribution (i.e. smaller PDI) by suppressing reversible backbiting.

3.2.3.5 Ring opening metathesis polymerization (ROMP)

A special type of ring opening polymerization is the ROMP process. It enables the polymerization of unsatured alkene molecules with ring strain such as cyclohexene, cyclopentene or dicyclopentadiene by a ring opening process. Completely orthogonal to radical or ionic polymerization, the basis of the ROMP process is the transition metal complex catalyzed metathesis reaction between two unsaturated compounds. The metathesis process was developed by Scott and coworkers already in the late sixties,[58] yet did not gain much attention as the harsh reaction condition prevented the use of functional starting materials. Due to the Nobel Prize winning work of Chauvin, Schrock and Grubbs in the seventies, new oxygen resistant catalysts were available, catalyzing the alkene exchange under very mild conditions. Their ground breaking work helped to establish the alkene metathesis in synthetic laboratories. Inspired by the work of so-called metal coordinating living polymerization by Ziegler and Natta, Grubbs decided to combine the alkene metatheses reaction with the concept of coordinating polymerizations, conducting the first living ROMP processes (see Scheme 3.12).

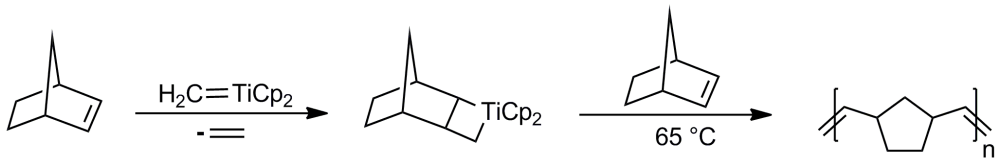

Scheme 3.12 First reported living ROMP process by Grubbs and coworkers.[59]

In the ROMP process, a cyclic alkene is attacked by the transition metal catalyst, which opens the cycle, following Chauvin's mechanism, and yields a linear α,ω-functionalized structure. Bearing an alkene on one side and the transition metal catalyst on the other, the linear monomer structure can grow further by sequentially adding cyclic monomer units to the chain via the repetitive attack on monomers of the transition metal catalyst function.[60] Similar to the aforementioned anionic ROP process, the ROMP process is a living polymerization technique showing limited termination reactions. Moreover, the process – in contrast to every other discussed living polymerization technique – is inert against moisture, protic impurities and

oxygen as a result of the new transition metal catalysts designed by the groups of Grubbs and Hoveyda. However, side reactions such as transfer reactions and depolymerization, noted in the ROP section, apply to ROMP as well, leading to longer reaction times and broader molecular weight distributions. Regardless of those disadvantages, ROMP represents a very powerful tool in synthetic polymer chemistry. Especially when combined with the DA reaction, ROMP can be a more favorable choice over other polymerization techniques. The 4+2 cycloaddition produces a cyclohexene structure which can act as monomer in the ROMP process. This combination has led to multiple architectures and applications such as brush copolymers or self-healing materials (see Scheme 3.13).[61] However, the ring strain of the DA product has to be significant. Accordingly, bridged DA products obtained from Cp or furan are preferred.

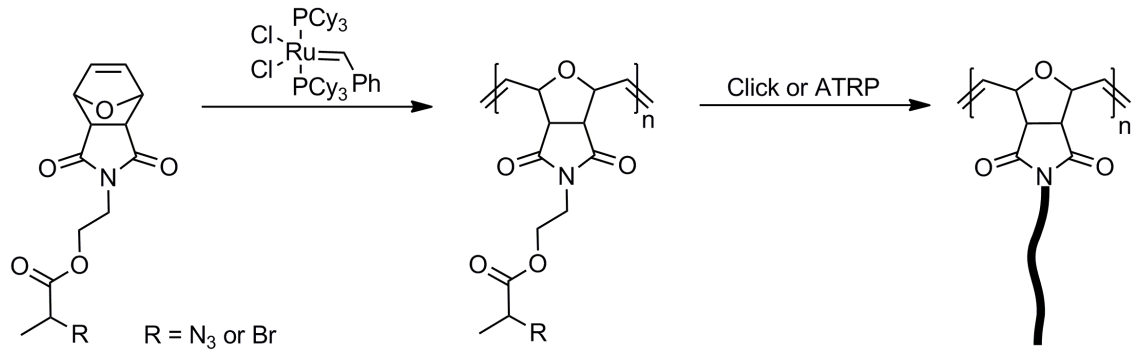

Scheme 3.13 Brush polymer obtained via the combination of the furan/maleimide DA pair and ROMP followed by ATRP polymerization or copper catalyzed azide alkyne click reaction.[61]

3.3 The Diels–Alder reaction

3.3.1 The history of the Diels–Alder and hetero Diels–Alder reaction

In January 1928, Otto Diels and Kurt Alder described their structural analysis of the reaction product of a mixture of chinone and Cp.[62] In contrast to Albrecht and Staudinger, who suggested a reductive addition of the methylen group,[63] the duo assumed a cycloaddition of the diene structure of Cp on the double bond units of chinone. Their assumption based on a previous study of Diels, adressing the reaction of Cp with an azodiester (see Scheme 3.14) [64] as well as on an old report of Euler[65] regarding the reaction of chinone with isoprene. Both publications evidenced an unsaturated cyclic reaction product, suggesting a 4+2 cycloadditions between the diene and en reactants. Proven to be right with their assumption, the work of Diels and Alder focused the attention of scientists on the 4+2 cycloaddition and made the reaction between a diene and an en state of the art for the synthesis of 6-membered rings

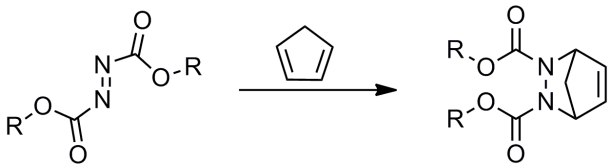

Scheme 3.14 Diels study addressing the reaction of an azidoester and cyclopentadiene to yield N,N-dicarbonyl-tetrahydro-pyridazine.[64]

In the following years Diels and Alder published a comprehensive manuscript with the name “Synthesis in the Hydroaromatic Series”, divided in multiple parts[62,66] about their results of different dienes and dienophiles in 4+2 cycloaddition reactions. The original idea of their work was to demonstrate the high potential of the cycloaddition for synthetic strategies of natural products. Therefore, the first sections of their publications focused on the synthesis of different terpenoides such as cantharidin[66b] or camphor.[66d] When they studied the synthesis of cantharidin, they realized an uncommon decomposition of the cantharidin product back to the starting materials upon heating to the melting point.[66b] This observation represented the first notation

of a concerted cyclorevison. Later on they decided to reduce their efforts in natural product synthesis and rather focus on the reactivity of different “dienes” and “dienophiles” as they termed the reactants. In the following they explored many dienes and dienophiles which are today still frequently used in chemistry. Among their analyzed compounds were maleic anhydride,[66c] antracene,[66f] furan,[66h] Cp[66a] as well as pyrrole.[66j] Hence, due to the great contribution to the field of 4+2 cycloadditions the reaction was eventually named after the two pioneers. Moreover, their work was honored with multiple prices, among them the Noble Price in 1950.

Inspired by the great potential of the new cycloaddition, chemists in different fields explored multiple diene/dienophile combinations, either in all-carbon conformations or with hetero atoms in the reactive center. The later version of the DA reaction was eventually named hetero Diels–Alder (HDA) reaction. However, besides the very first example of Diels, not many hetero dienophiles or hetero dienes were described after their pioneering work. Most synthetic chemists saw the HDA reaction only as a curiosity and focused rather on the substitution patterns of the starting materials.[67] However, the first reaction of an imine in a DA reaction, conducted by Alder,[68] showed the versatility and ready availability of starting materials for HDA reactions, leading to a higher publication output in the following years.[69] Consequently, further groups such as carbonyls, serving as dienophiles, or α,β-unsaturated carbonyl functions serving as dienes, were employed in HDA reactions, enabling chemists to built carbonhydrate derivatives in one step reactions.[69a,70] In contrast to carbonyl groups their sulfur analogues found less interest in HDA reactions.[69c] Although most thiocarbonyl functions were found to react rapidly with a wide range of dienes at exceptionally low temperatures,[71] their tendency to undergo a thermal decomposition back to the starting materials complicated the further use of the HDA products. Moreover, many thiocarbonyl functions are not stable under atmospheric conditions, making a HDA reaction difficult to conduct. Despite these obstacles different thiocarbonyl functional groups such as thioaldehydes,[72] thioketones[73] and dithioesters[74] were successfully employed as hetero dienophiles in HDA reactions.

Developed by Diels and Alder, the 4+2 cycloaddition has become one of the most studied and employed reactions in chemical history. This popularity can simply be attributed to the special features associated with the Diels–Alder reaction, comprising:

1. **No byproducts.**

   As the Diels–Alder reaction is a cycloaddition no byproducts are generated.

2. **Simple work up.**

   Due to the lack of byproducts no complex column purification is necessary.

3. **Cheap starting materials.**

   The starting materials are often readily available and do not require complex synthesis and can often be found in the pool of natural products.

4. **High yields.**

   In many cases high conversions can be achieved.

5. **Orthogonality.**

   The cycloaddition provides high functional group tolerance as the starting materials react exclusively with each other.

6. **Robustness.**

   The reaction can be performed in many solvents and in most cases under air.

7. **Reversibility.**

   Like all thermally allowed cycloadditions, the Diels–Alder reaction is reversible and undergoes a retro Diels–Alder cyclorevision at elevated temperatures back to the starting materials.

3.3.2 The frontier molecular orbital (FMO) theory

To better understand the nature of the DA reaction and predict the behavior of different diene/dienophile pairs, multiple studies were carried out. In this context, the pericyclic character of the cycloaddition was also explored and evidenced.[75] Only in special cases indications for a diradical or diionic mechanism were found.[76] Due to the concerted mechanism, DA reactions are highly stereospecific, i.e. the conformation of the starting materials is transferred into the product. However, diastereospecificy of the reaction product is not given. If two diastereomers are

possible, the product will mostly be obtained as a mixture, whereby the *endo*-product represents the kinetic product and the *exo*-product the thermodynamically one (see Scheme 3.15).

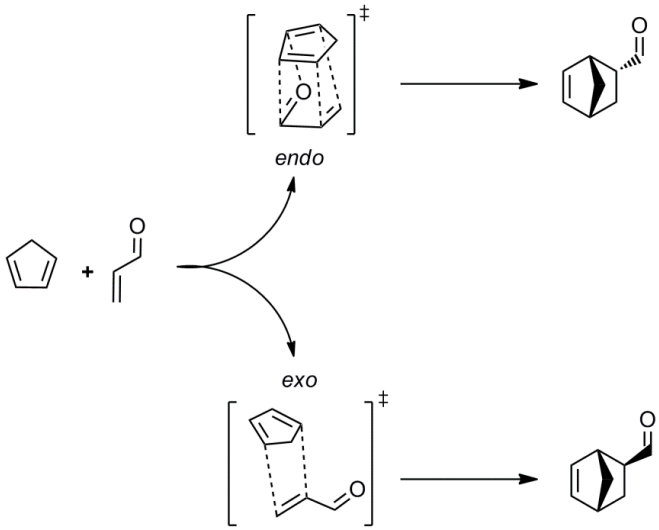

Scheme 3.15 Both possible diastereomers obtained from a Diels–Alder reaction with the respective transition state.

Based on various studies regarding different diene/dienophile pairs, a trend in the substitution pattern of the starting materials was observed. By comparing the reaction rates of similar DA pairs it became obvious that electron withdrawing groups on the dienophile and electron donating groups on the diene favored the cycloaddition and led to shorter reaction times. This observation can be explained by the empiric FMO theory. In this theory, all molecular orbitals are neglected except on the FMO, i.e. the highest occupied molecular orbital (HOMO) and the lowest unoccupied molecular orbital (LUMO). The reaction proceeds via a six membered transition state which is based on the positive overlap of the HOMO and the LUMO of the two reactants. Positive overlap implies that the wave functions of the two overlapping·molecular orbitals (MO), which form the new σ-bond, are in phase. Such a positive overlap can either occur on the same plane of the molecule (suprafacial) or on different planes (antarafacial). Suprafacial overlaps are the common conformation in cycloadditions whereas antarafacial overlaps are rare and proceed only in the case of long flexible π-systems which can twist around their axis. Passing the transition state, the two new bonds are eventually formed via the cycloaddition. Crucial for the FMO approach

is only the smallest HOMO-LUMO gap and the matching of the MOs as the reaction proceeds faster the easier the transition state (i.e. the HOMO-LUMO overlap) is reached (refer to Figure 3.3).

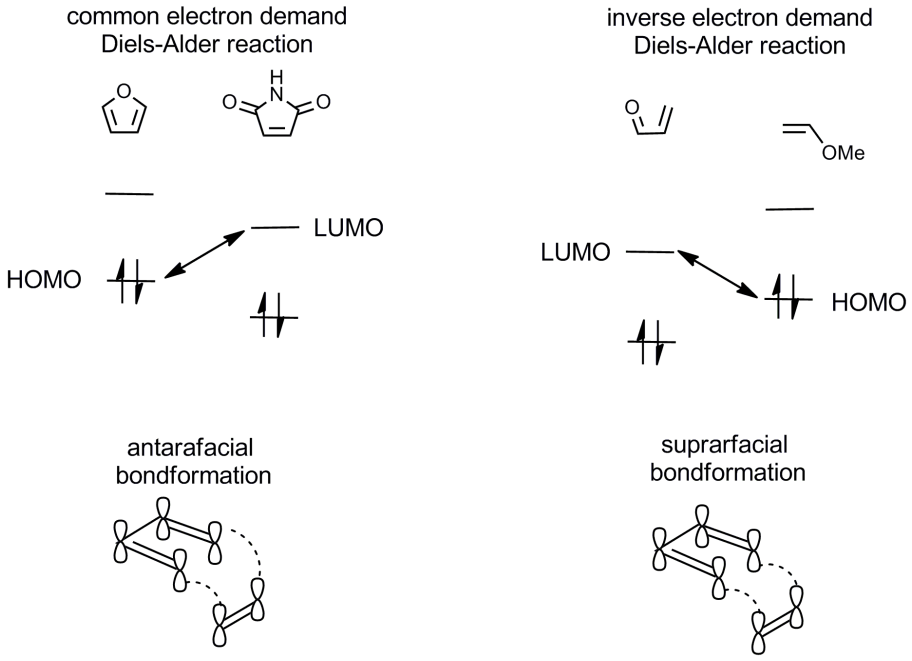

Figure 3.3 HOMO-LUMO gap of a common and inverse electron demand Diels–Alder reaction as well as the suprafacial and antarafacial bond formation.

Due to the relative electronic energy levels of a diene and a dienophile, the transition state is usually reached via the overlap of the $HOMO_{diene}$ and $LUMO_{dienophile}$ (normal electron demand DA reaction). By functionalizing the diene with electron donating and the dienophile with electron withdrawing moieties, the HOMO-LUMO gap can be reduced leading to a lower energy barrier and therefore to faster reaction rates. However, the DA reaction can also proceed via the interaction between the $HOMO_{dienophile}$ and the $LUMO_{diene}$ (inverse electron demand DA reaction). Such an uncommon interaction can only be observed if electron poor dienes and electron rich dienophiles are utilized, reducing the respective HOMO-LUMO gap significantly. In addition to predicting relative reaction rates, the FMO theory also helps to understand the regiochemistry of DA reactions. With respect to the FMO coefficients of the reactive atom center, it can be explained why the DA reaction shows such a high regioselectivity towards *ortho* and *para* substituted products compared to *meta* products.

By employing the simple FMO theory it becomes clear why some diene/dienophile pairs react in a fast fashion whereas others do not proceed at all. In addition, questions regarding regioselectivity and substitution effects can be answered with the FMO theory. Nevertheless, the theory cannot explain why the cycloaddition proceeds at all and what the differences are between the heat triggered cycloadditions and the light-induced ones. For understanding what the differences between 2+2 and 4+2 cycloadditions are, it is necessary to follow the more refined Woodward-Hoffmann rules which are highlighted in the next section.

3.3.3 The Woodward–Hoffmann rules

Despite the great success and numerous studies on the Diels–Alder reaction, the formulation of a rule predicting pericyclic reactions in general was unknown for a long time. Although the FMO theory developed and served as tool to predict tendencies in kinetic rates, it could not be explained why the 4+2 reaction proceeded at ambient or elevated temperatures whereas the 2+2 reaction did not.

Not until 1965, when Woodward and Hoffman published their results about the stereo chemistry of electrocyclic reactions, progress was made in the field.[77] In their work they followed the simple thought of keeping the symmetry of all MO during any kind of structural change constant. Consequently, not only the character of an MO (σ or π, positive or negative wave function) should be considered to assess the reaction, but most importantly their symmetry should be taken into account. Transformed into a scheme, Woodward and Hoffmann were able to predict and explain the stereo chemistry of electro cyclic reactions triggered by either heat or light (see Figure 3.4).

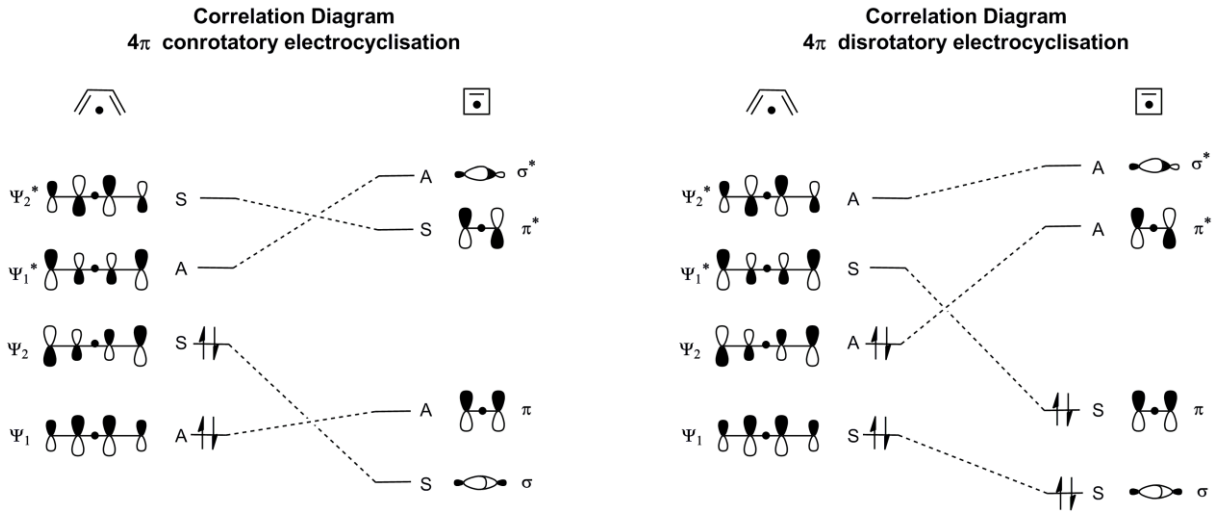

Figure 3.4 Correlation diagram for the disrotatory and conrotatory electrocyclisation of butadiene. The conrotatory cyclisation is thermally allowed and proceeds via the ground state of the π-system. In contrast, photochemical excitation is essential for the disrotatory cyclisation. The spot in the upper chemical structure represents the symmetry element of the cyclisation.

To simplify the MO correlations scheme, Woodward and Hoffmann neglected the high and low energetic σ and σ* orbitals and focused only on the reactive π, n, and π* MO, which eventually generate the new bond. The correlation diagram depicted in a simple way the dependency of the obtained product's stereochemistry on the electro cyclic trigger and the relationship to the length of the conjugated π-system. In case of heat as a trigger in a four π-electron system for example, the cyclisation proceeds from the HOMO and yields via a conrotatory movement of both end π-MOs the anti-product. Light, on the other hand, leads to a disrotatory movement of the two π-MOs and to the syn-product as the cyclisation proceeds via a single occupied molecular orbital (SOMO) in the π*-orbital. With a stepwise increase of the π-system, the rotatory movement of the end π-MOs alternates with the trigger as a result of the changed phase of the end π-MOs.

The correlation diagram was initially created as a tool for the prediction of the stereochemistry of electrocyclic reactions, but was shown to be the key for understanding pericyclic reactions in general.[78] Transferred to cycloadditions, the correlation diagram dictates that the symmetry of the MOs should not change throughout the reaction. However, the energetic level of each MO can shift and change the character of the reaction. Due to this energy shift an antibonding MO of

the starting materials can become a bonding MO in the product and vice versa, if the symmetry of the orbitals match. Considering these possibilities, the correlation diagram explained why 2+2 reactions are not allowed to be triggered by heat and why a Diels–Alder reaction is per se not possible to be conducted via light irradiation. Figure 3.5 presents the two correlation diagrams of the thermally allowed DA reaction and a light-induced 2+2 cycloaddition as published by Woodward and Hoffmann.[78-79]

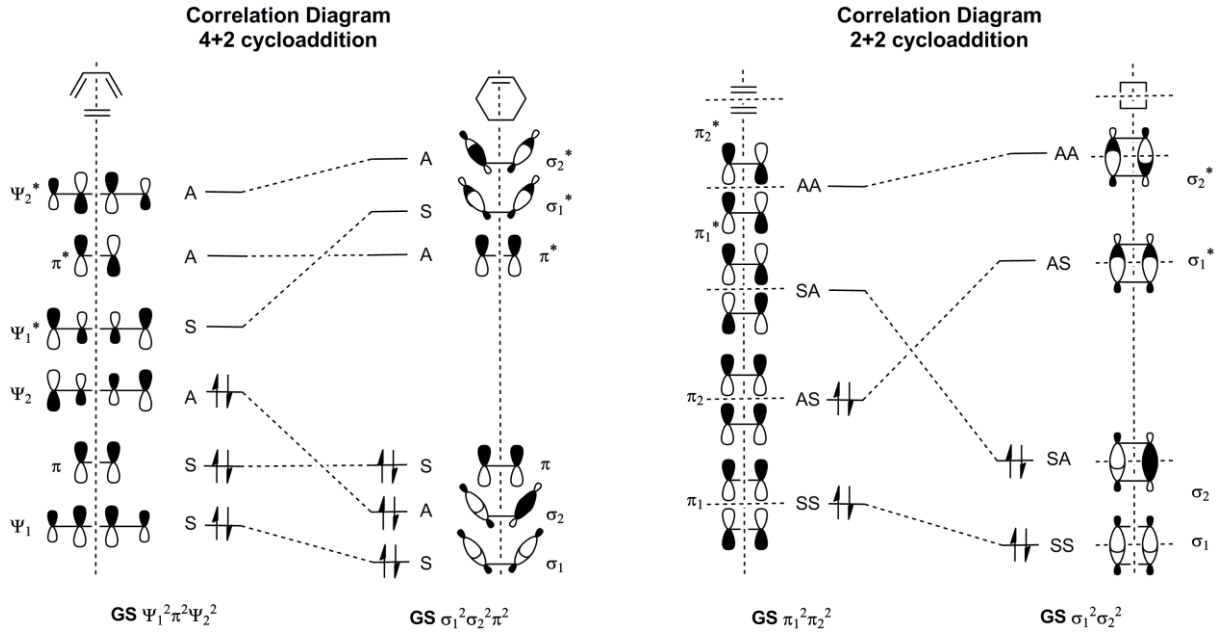

Figure 3.5 Correlation diagrams of the 4+2 and 2+2 cycloaddition reaction. The 4+2 cycloaddition proceeds via the ground state (thermally allowed), whereas the 2+2 cycloaddition requires excitation (photochemically allowed) to the first excited state to proceed.

As can be seen in the diagrams in Figure 3.5, the occupied bonding MOs (i.e. ψ_1 (S), π (S), and ψ_2 (A)) of diene/dienophile lead to the new bonding MOs (i.e. σ_1 (S), σ_2 (A), and π (S)) of the product. The process yields an energetically lower ground state which is reached without passing an energetic barrier. Thus, no excitation is required for the DA reaction allowing the cycloaddition to proceed without any light irradiation. Conversely, the new bonding MOs of the 2+2 cycloaddition product (i.e. σ_1 (SS) and σ_2 (AS)) are formed from both the π-MO (i.e. π_1 (SS)) and the π*-MO (i.e. π^*_3 (AS)). Consequently, an excitation of an π-electron from π_2 to π^*_3 is required for the 2+2 cycloaddition. The required excitation represents the energetic barrier which has to be overcome when eventually generating the new bonding MOs in the 2+2

cycloaddition. Due to this fact only light or enhanced temperatures can introduce the 2+2 cycloaddition. In an effort to simplify the correlation diagram approach, Woodward and Hoffman distilled the essence of their idea into two statements governing all pericyclic reactions that are today known as the Woodward-Hoffmann rules. Thanks to the ground breaking work Hoffmann was awarded with the Nobel Prize in 1981. The formulation of their rules was:[78]

- A ground state pericyclic reaction is symmetry-allowed when the total number of $(4q+2)_s$ and $(4r)_a$ components is odd.
- A pericyclic change in the first electronically excited state is symmetry-allowed when the total number of (4q+2)s and (4r)a components is even.

The rules imply that a thermally allowed cycloaddition has to have an odd overall number of suprafacial (4q+2) π-electron species and antarafacial (4r) π-electron species whereas the overall number has to be even in the case of photochemically allowed cycloadditions. Figure 3.6 represents examples for both cases.

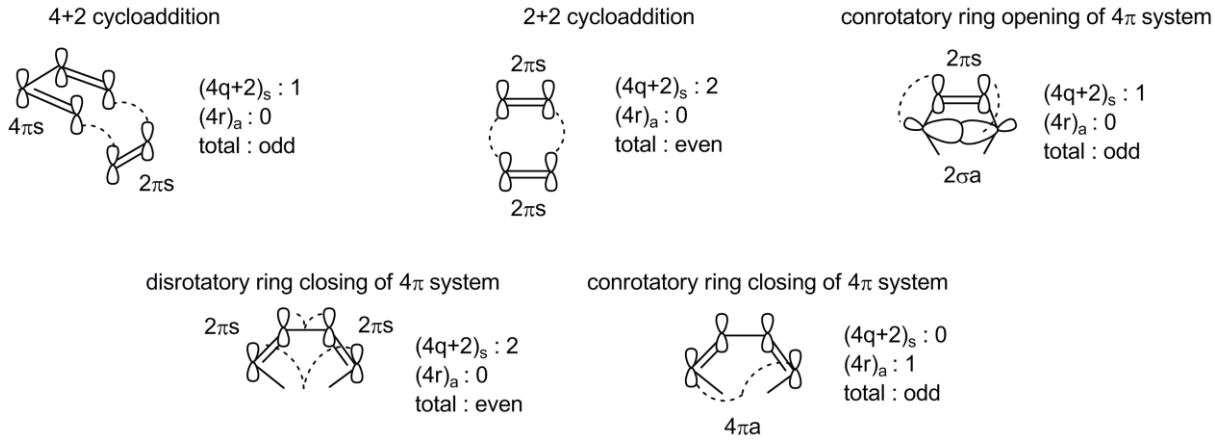

Figure 3.6 Examples of the Woodward-Hoffmann rules for photochemically and thermally allowed pericyclic reactions.

3.3.4 The retro Diels–Alder reaction – an equilibrium

As the majority of chemical reactions, the Diels–Alder cycloaddition follows the rule of micro reversibility.[80] Through the course of the DA reaction an equilibrium is established between the starting materials and the cycloaddition product. The

equilibrium has a dynamic nature implying that the starting materials and the product react or debond permanently. Thus, the kinetic rate coefficients of decomposition and product formation determine the state of the equilibrium. By comparing the two rate coefficients, the equilibrium constant $K_{eq} = k_{DA} / k_{rDA}$ is defined, describing the product/starting material ratio. As dynamic equilibria follow the rules of Le Chatelier, the state of the DA equilibrium can be manipulated by changing concentration, pressure or temperature leading to a different product/starting material ratio (see Scheme 3.16).

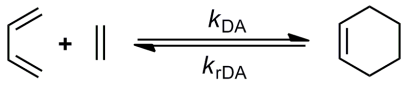

Scheme 3.16 The Diels–Alder equilibrium with the respective rate coefficient k_{DA} and k_{rDA}.

The process of retrodiene decomposition, or so-called retro Diels–Alder (rDA) reaction, was already noted in one of the first publications from Diels and Alder.[66b] During their study regarding the terpen cantharidin synthesis, they realized the dissociation of the cantharidin species back to the starting materials when heated to the melting point of 125 °C. However, their publication was not the first report regarding a rDA reaction. In his study addressing the famous Cp chinone reaction, Albrecht described already in 1906 that the reaction between chinone and Cp could be reversed by heating the obtained product to its melting point.[63] As aforementioned, Albrecht assumed jointly with Staudinger a reductive addition mechanism of the methylene group of Cp, which was later on proven to be wrong by Diels and Alder. Nevertheless, the publication of Albrecht represents one of the first observations of the rDA reaction in the chemical literature.

The ability to form and break covalent bonds by shifting the equilibrium via the temperature makes the DA/rDA reaction sequence a powerful tool in materials design. Examples for the use of the DA/rDA reaction in bonding/debonding on demand materials are adaptable networks,[81] protecting groups[82] or macromolecular architectures.[13] Despite all these applications, the number of suitable DA pairings which can be cycled in a reasonable temperature range (i.e. below the materials' degradation temperature) are scarce. To date, only a few DA systems are used,

offering cyclability at mild temperatures in a reasonable time frame (those DA pairing examples are presented in the subsequent sections). The main problem in designing a reversible DA equilibrium is that most DA equilibria show rather degradation than dissociation due to thermodynamics. The thermodynamics of the DA reaction shows a high negative enthalpy based on the transformation of two π-bonds into to new σ-bonds. The entropy is negative as well, but more than compensated by the enthalpy. As a result, the Gibbs-Helmholtz equation leads to a negative free Gibbs energy favoring the DA reaction. In the course of the reaction, the entropy rises with conversion until the product of temperature and entropy matches the enthalpy value. At this point the free Gibbs energy is zero representing the equilibrium state.

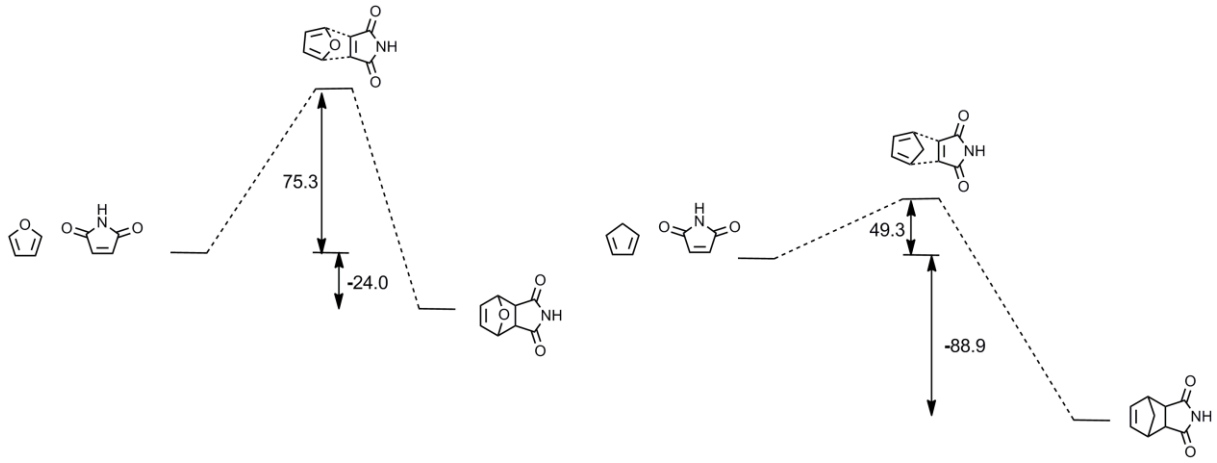

Figure 3.7 Gibbs energy diagram with transition state for the furan/maleimide and the Cp/maleimide DA pair. The energy values are given in kJ·mol^{-1}.[83]

To reverse the DA process, it is necessary to increase the temperature and add energy to the system favoring the entropy factor. Accordingly, the equilibrium shifts towards the starting materials. However, to produce a significant amount of starting materials from the DA product, the added energy in the form of temperature has to match at least the DA reaction enthalpy and the kinetic energy barrier. As noted above, most DA products degrade at such temperatures. Therefore, a low DA reaction enthalpy is key to a reversible system.[83] The three pairs, which will be discussed at a later stage, ensure the above by either utilizing stable aromatic starting materials, i.e. furan, or by producing less stable DA product, i.e. 3,6-dihydro-2H-thiopyrane or dicyclopentadiene. Despite a low reaction enthalpy, the starting materials still have to be activated for the cycloaddition transitions state, i.e. electron

rich and electron poor with a favoring conformation, to reduce the kinetic barrier.[83] It is important to understand the compromise between a low reaction enthalpy and activated starting materials when studying and designing a reversible DA equilibrium.

Moreover, the molecular weight and size of dienophile and diene play an important role in the retro DA process. The larger the utilized starting materials, the more possible conformations can be taken. Consequently, more entropy is gained via the decomposition of the DA product to the starting materials. Accordingly, a higher percentage of debonding is obtained for heavier and larger starting materials at a given temperature. This highly significant finding was concluded and published recently by Guimard *et al*. who studied the rHDA behavior of block copolymers of various lengths, generated by the modular HDA reaction of telechelic RAFT polymers.[84]

3.3.4.1 The furan/N-maleimide couple

The DA/rDA equilibrium between maleimides and furans is probably the most studied system among DA pairs. Its strong temperature dependence together with the fact that side reactions and possible thermal degradation are negligible makes the furan/maleimide pair highly suitable for materials applications. Especially the field of self-healing materials has greatly benefited from the maleimide/furan DA equilibrium due to its relatively low cycling temperatures. [18b,85] An approximate indication of the temperature effect on the equilibrium implies that close to 60 °C, the DA reaction to the adduct dominates, whereas above 110 °C the rDA reaction becomes preponderant.[18b] A study of Goiti *et al.* revealed that the DA product starts slowly to decompose to the starting materials at 77 °C.[86] However, in their study Goiti *et al.* extracted the maleimide species from the reaction mixture, raising concerns about the concentration effect on the DA equilibrium. Nevertheless, a slow shift towards the furan and maleimide starting material and the begin of the rDA reaction at 77 °C is evidenced. These finding is supported by other studies describing a very slow shift of the DA equilibrium towards the more thermodynamically stable *exo* diastereomer at 65 °C.[83] Such a shift of the equilibrium can only be observed if the dynamic exchange is accelerated, symbolizing the beginning of the rDA onset temperature.

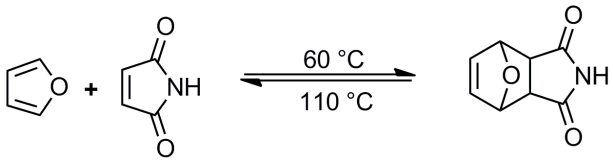

Scheme 3.17 The Diels–Alder equilibrium of furan and maleimide. At 60 °C the Diels–Alder product dominates, whereas at 110 °C the retro reaction becomes dominant.

On the other hand, the maleimide/furan DA reaction shows almost no progress when mixed at ambient temperatures. Due to the relatively high kinetic barrier of the DA pair, reaction times of days are required when performing the cycloaddition at ambient temperatures.[83] Accordingly, elevated temperatures in the range of 60 °C are usually employed for the DA cycloaddition, reducing the reaction time to hours. In extreme examples temperatures of 80 °C are applied to the maleimide/furan pair.[87] At 80 °C the equilibrium starts already to shift towards the DA starting materials. However, the amount of present starting materials is in a very low range and reacts to the DA product during slowly cooling. Therefore, reaction times of a few hours are observed from 80 °C.

3.3.4.2 The thiocarbonyl/cyclopentadiene couple

The product of a thiocarbonyl function and a diene is a so-called 3,6-dihydro-2H-thiopyrane (DHTP). Such DHTPs are well known to be unstable molecules, dissociating into the respective DA starting materials upon heating to relatively low temperatures.[88] This statement is confirmed for any kind of thiocarbonyl function, i.e. thioketones, thioaldehydes and dithioester. In organic synthesis thioketones and thioaldehydes are rather exotic compounds due to their strong incompatibility with oxygen and moisture. Moreover, thioaldehydes are such reactive compounds that they likely undergo self condensation. Nevertheless, once reacted in a HDA reaction the DHTPs of thioaldehydes are stable against both and display similar temperature dependencies as the DHTPs of dithioesters or thioketones. Dithioester represent a more convenient thiocarbonyl species for HDA reactions as they are less vulnerable towards oxidation and hydrolysis. Studies addressing the retro hetero Diels–Alder

(rHDA) reaction of DHTPs, by exploring a cyanodithioester (CDTE)/Cp HDA adduct, imply that the onset rHDA temperatures for DHTPs formed from Cp, lie in general in temperature ranges close to 70 °C.[89] At 70 °C a slight increase in HDA starting materials can be observed via ^{1}H NMR spectroscopy. With increasing temperature the equilibrium shifts further towards the stating materials, reaching a conversion of 19% starting materials at 130 °C.[89] These values can be seen as approximate indication for the rHDA temperature of DHTP, disregarding the concentration effect on the equilibria. An advanced study addressing the rHDA dependency of reaction time, temperature and concentration was performed by Zhou *et al.*, exploring the behavior of DHTPs from pyridinyl- and phosphoryl dithioester with sorbic alcohol.[4] However, the study addressing the DHTP of CDTE was conducted with Cp which is known to have lower rDA temperatures than open chain dienes such as sorbic compounds.[90] For those DHTP derivatives derived from butadiene species, a slight increase in rHDA temperatures can be assumed.[4]

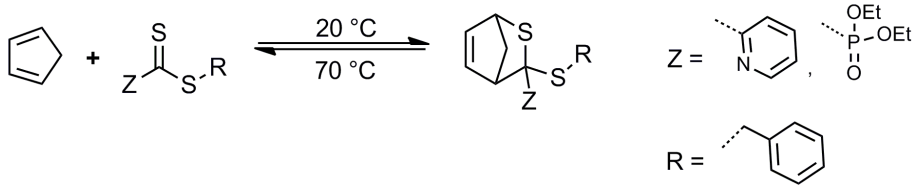

Scheme 3.18 The Diels–Alder equilibrium of cyclopentadiene and a model activated dithioester. At 20 °C the Diels–Alder proceeds forward whereas at 70 °C the retro reaction occurs. Z = electron withdrawing group, R = leaving group of the RAFT process.

The HDA forward reaction proceeds with highly reactive thioaldehydes and thioketones already at ambient temperature in a very fast fashion.[72,88b,91] Dithioesters on the other hand show the potential to react as fast as thioaldehydes and thioketones; however, the attached functional group on the dithioester is crucial for its activation towards the HDA cycloaddition. Strong electron withdrawing groups such as carbonyl,[92] cyano,[93] or sulfonyl groups[6d] decrease the electron rich character of the C=S bond and activate the dithioester. Due to the activation comparable reaction rates to thioaldehydes and thioketones are reached. However, as a result of the electron poor character, the thiocarbonyl function becomes more vulnerable towards hydrolysis and oxidation. On the other hand, strong electron

donating groups such as thiols and alcohols (i.e. trithiocarbonates and xanthates) or conjugated groups, i.e. aromatic systems, lead to an electron rich character of the C=S deactivating the dithioester for normal electron demand HDA reactions. As a compromise between activation for HDA reactions and tendency to undergo degradation, dithioesters with pyridinyl and phosphoryl groups are employed. Those groups activated the dithioester function less towards the HDA reaction but offer the opportunity to increase the electron poor character of the thiocarbonyl group by adding a catalyst.[6b,6c,94] Trifluoroacetic acid (TFA) or $ZnCl_2$ are frequently used catalysts for the pyridinyl and phosphoryl groups bearing dithioester. While TFA protonates the pyridinyl moiety, $ZnCl_2$ coordinates onto the phosphoryl group, transforming both functions into strong electron withdrawing groups. However, without the addition of a catalyst both, pyridinyl- and phosphoryl-groups do not decrease the electron rich nature of the C=S double bond too much, reducing the activation towards oxidation and hydrolysis. As a result of the stabilized thiocarbonyl group, pyridinyl- and phosphoryl dithioester represent suitable CTAs in RAFT polymerizations of certain monomers (i.e. styrenes and acrylates). Consequently, by employing pyridinyl- and phosphoryl dithioester in RAFT processes, telechelic polymers with end groups suitable for HDA reactions are obtained. This powerful combination led already to multiple publications, describing different macromolecular architectures and bonding/debonding on demand systems.[6a-c,12,81,95] Moreover, the RAFT process of pyridinyl- and phosphoryl dithioester enables the defined synthesis of HDA starting materials with tailored chain length and molecular weight.[6a] This fact becomes important in the context of recent studies published by Guimard *et al.* describing the effects of chain length and molecular weight on the HDA reactions of telechelic pyridinyl- and phosphoryl dithioester polymers. According to their work, longer chain length and higher molecular weights shift the HDA equilibrium towards the starting materials at elevated temperatures.[84]

3.3.4.3 The cyclopentadiene dimerization

Cp moieties can dimerize at ambient temperatures in a DA reaction, acting as both diene and dienophile. In the course of the dimerization not only two new σ-bonds are formed, making the reaction exothermic, but in addition the ring strain of both

reacting Cp units is drastically reduced, being the driving force of the cycloaddition. Although the process is naturally favored – as Cp can only be obtained in its dimerized form – the kinetic barrier for the dimerization is relatively high. Thus, it is possible to prepare and store mono-Cp species, once obtained by cracking the dicyclopentadiene.[96] Nevertheless, only low temperatures close to -70 °C can prevent the naturally favored self-reaction which proceeds in hours at ambient temperature. Stored at temperatures around -20 °C the Cp dimerization is considerably slowed, requiring weeks for the DA reaction which enables chemists to work with the mono Cp species.

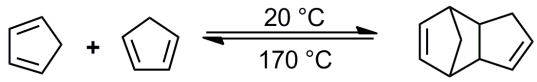

Scheme 3.19 Cyclopentadiene dimerization via a Diels–Alder reaction. The self reaction proceeds within hours at 20 °C and can be reversed at 170 °C by cracking the dicyclopentadiene species.

The rDA reaction of pure dicyclopentadiene is usually carried out at temperatures close to 170 °C, if no catalyst as iron chips are added. At such high temperatures, the DA equilibrium is slowly shifted towards the mono Cp units, which can be distilled from the reaction mixture in parallel. Incorporated in networks, temperatures of 120 °C to 150 °C are utilized to induce the rDA process of dicyclopentadiene linkages and consequently open the network. Closing is on the other hand achieved by slow cooling to ambient temperature.[97]

3.4 Thiocarbonyl compounds

3.4.1 Categories and synthesis

The reactivity of thiocarbonyl groups in reactions such as condensations or cycloadditions is strongly dependent on the attached substituents, i.e. the nature of the functional groups. Known thiocarbonyl groups which were explored and employed in organic synthesis are: thioketones, thioaldehydes, dithioesters, thioamides, sulfoxides, trithiocarbonates, or xanthates (see Scheme 3.20).

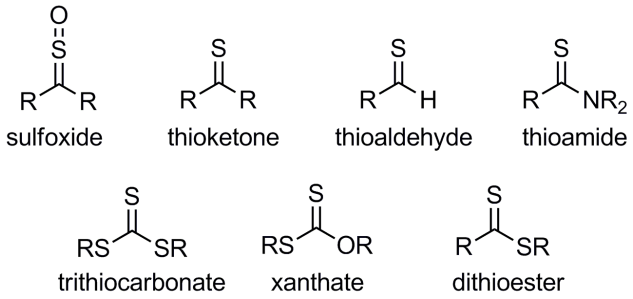

Scheme 3.20 Different thiocarbonyl groups. R represents a carbon moiety.

Each of these sulfur species displays special characteristics which found applications in chemical science. Strongly electron withdrawing thiocarbonyl groups for example can be generated by oxidizing the sulfur to sulfoxides, finding use as activating groups in cycloadditions. Dithioester, on the other hand, have a stabilizing effect on radicals yielding a dynamic equilibrium between reactive and dormant radical species which is utilized in the RAFT polymerization. A similar behavior is displayed by trithiocarbonates,[51] xanthates[51] and stable thioketones[98] compounds. Consequently, these compounds are also used in CRP processes. Besides stabilizing radicals, trithiocarbonates and xanthates provide moderate leaving group properties. As a result, trithiocarbonates and xanthates can be applied in the Tschugajew elimination and other pyrolysis reactions.[99] Thioaldehydes and thioamides are rather exotic species in organic reactions, mostly evolving as reactive intermediates or starting materials in natural product synthesis.

The generation of these thiocarbonyl functions is a complex synthetic problem, which was addressed by chemists in multiple ways. A general method for the preparation of thiocarbonyl functions is the transformation from their oxygen carbonyl analogues via the addition of phosphorous pentasulfide or the Laweson reagent. Both reagents exchange every oxygen atom present in the molecule (i.e. in ketones, aldehydes, ester, or amides) to a sulfur atom and therefore into the respective thiocarbonyl groups.[100] A more specific synthetic reaction to thioaldehydes or ketones, is based on an elimination mechanism of thiol derivatives. Via basic treatment of secondary or primary tosylates or xanthates, the attached carbon center can be oxidized through HX elimination to the corresponding thioketone or thioaldehyde.[88b] An additional elegant way towards the synthesis of thioaldehydes was described by Vejeds *et al.* employing the light triggered fragmentation of phenacylsulfides to acetophenone and a thioaldehyde to introduce thioaldehydes in a molecule.[72]

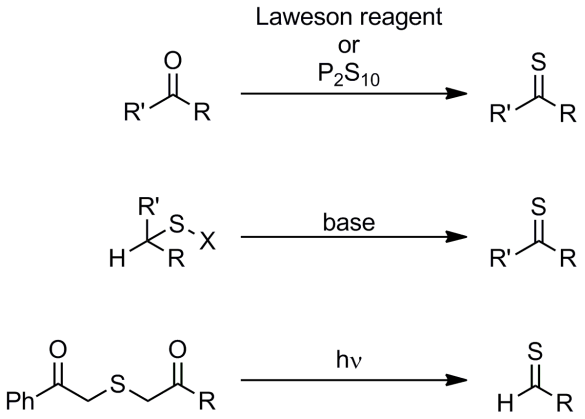

Scheme 3.21 Synthesis of thioketones and thioaldehydes. In case of a thioketone R' = CR_3, for a thioaldehyde R' = H. R symbolizes always a carbon moiety. X = xanthate or tosylate. The light-induced fragmentation of phenacylsulfides yields only thioaldehydes.

The synthesis of dithioesters, trithiocarbonates and xanthates caught more attention in chemical labs than other thiocarbonyl functions, related to the high demand of functionalized RAFT agents in the context of modular ligation protocols. By closer inspection of the majority of RAFT agent syntheses, it becomes obvious that three synthetic strategies are mainly employed.[51] One of them is the aforementioned Laweson reagent or phosphorous pentasulfide transformation of thioester groups to dithioesters.[101] Alternatively, thiophosgene is converted in a two step reaction

sequence via the reactive chlorodithioformiate intermediate. Eventually carbon disulfide is reacted with a nucleophile to yield the carbodithioate salt, which is subsequently transferred into a thiocarbonylthio compound by an alkylating agent. In addition to carbon disulfide and nucleophiles, carbodithioate salts can be obtained by the oxidation of primary halogen species via adding elemental sulfur and a base. Besides these three techniques, mostly transfer reactions of already existing thiocarbonyl functions are followed for the synthesis of dithioester, trithiocarbonates, or xanthates. Among the listed strategies, the carbon disulfide conversion is certainly the most common approach, especially in the synthesis of trithiocarbonates and xanthates, as the soft thiolates and alcoholate ions readily attack the soft carbon center of carbon disulfide.

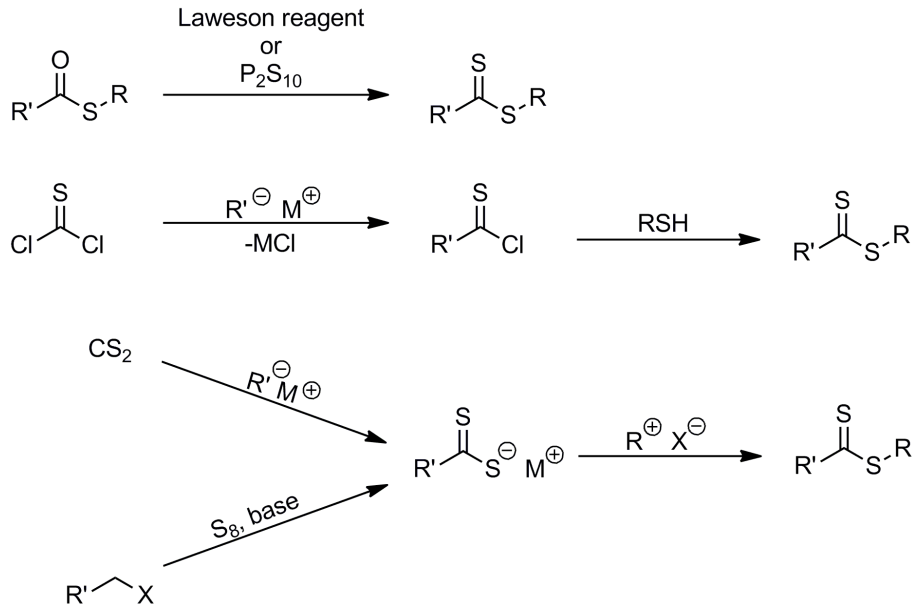

Scheme 3.22 Synthetic approaches to dithioesters, trithiocarbonates and xanthates. In case of dithioesters R' = CR_3, for xanthates R' = OR and for trithiocarbonates R' = SR. R represents always a carbon moiety and X = halogen.

3.4.2 Thiocarbonyl groups in hetero Diels–Alder reactions

Virtually all types of thiocarbonyl groups have been found to undergo rapid HDA cycloadditions with suitable dienes. Unlike their oxygen analogues (i.e. ketones and aldehydes), which require extremely activated dienes with alkoxy groups,[102] the addition of a catalyst[103] or extraordinary activation temperatures,[103-104] the HDA

reactions of thiocarbonyl groups proceed mostly at ambient temperatures with less activated dienes such as butadiene derivatives, displaying high reaction rate. This difference in reactivity between carbonyl and thiocarbonyl groups can be attributed to the relative HOMO and LUMO energy levels. Molecular orbital calculations for the model systems formaldehyde and thioformaldehyde revealed that the π^*_{CS} LUMO orbital of thioformaldehyde is about 2.8 eV lower than the respective π^*_{CO} LUMO orbital of formaldehyde (see Figure 3.8).[105] Consequently, the HOMO-LUMO gap between a thiocarbonyl group and a diene is smaller than the HOMO-LUMO gap of the respective carbonyl group, resulting in a higher reactivity of the thiocarbonyl group towards the HDA product. Moreover, the sulfur lone-pair orbital in thioformaldehyde, representing the HOMO, is calculated to be 2.1 eV higher in energy than the oxygen lone pair of formaldehyde, being the respective HOMO of the carbonyl compound. As a result, thiocarbonyl compounds are also more activated towards electron inverse demand HDA reaction. The energy lowering of the π^*_{CS} LUMO and the energy elevating of n_S HOMO in thiocarbonyl can easily be seen in the color of the compound, being a side effect of the smaller HOMO-LUMO gap of thiocarbonyl species.

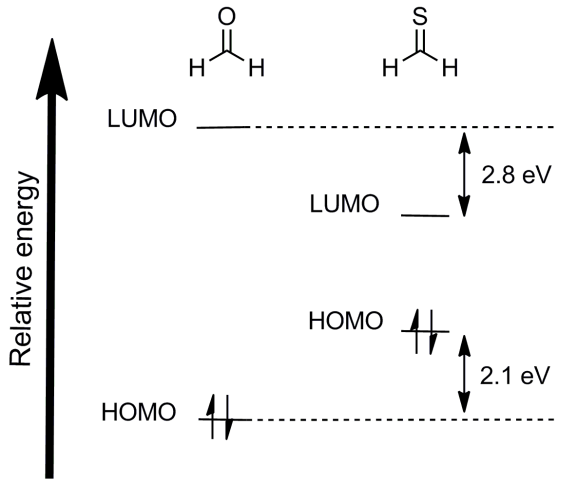

Figure 3.8 Molecular orbital levels of formaldehyde and thioformaldehyde. The energy difference of the HOMO and LUMO was obtained by quantum calculations of Vejeds et al.[105]

While the reaction rates are higher in thiocarbonyl HDA reactions, the regioselectivity is reduced compared to the HDA reactions of carbonyl groups. As sulfur displays a

very similar electronegativity as carbon, the C=S double bond is poorly polarized. Thus, the orbital coefficient values of both double bond centers are close to each other, resulting in a small bonding difference between the regioisomer transition states and therefore in a less regioselectivity product mixture. However, the regioselectivity can be increased and switched by the thiocarbonyl substituents, which have an enormous effect on the thiocarbonyl group polarization.[105] While electron withdrawing groups polarize the double bond towards the carbon center, electron donating and conjugation groups polarize C=S toward the sulfur. Accordingly, the orbital coefficients values of sulfur and carbon are exchanged, leading to an inverse selectivity of the respective substituent.

3.5 Self-healing materials[i]

3.5.1 Origin of self-healing materials

Self-healing materials is a field of chemistry which developed from some observations in the early 1970s, when it was noted that viscoelastic polymers, such as hard elastic polypropylene, consisted of a stacked lamellar morphology perpendicular to the axis of polymer extrusions. The lamellar morphology enabled the plastics to heal interlamellar microvoids formed by stretching in the perpendicular direction. This deformation recovery process was simply attributed to an energy balance in the material. Upon polymer stretching, surface energies are converted to strain energy. The strain is subsequent converted into mechanical work, which reorganizes the lamellar morphology and eventually closes cracks.[106] Despite this mending process and other repairing techniques such as resin injection and welding, the properties of the material are not completely restored. In all cases the site of repair generally remains the weakest point in the material. Moreover, resin injection and welding can only be applied to damaged material if the site is accessible. From these limitations stems the need for a new material able to undergo self-healing at the molecular level, preventing crack propagation and restoring the physical and mechanical properties completely. Consequently, many research groups designed different intelligent materials to realize such an ideal self-healing behavior. However, the different approaches can in general be classified as either intrinsically or extrinsically processes. Intrinsic healing is bases on reversible bond formation, opening and closing linkages in the material. Extrinsic healing on the other hand employs a pre-added encapsulated healing agent which is released to the network. Alternatively, materials with low glass transition temperatures (T_g) can be considered as healable as heating above their T_g permits the material to flow and fill microcracks (refer to Scheme 3.23). Such materials are already commercially available, but display healing only via a physical rearrangement on the macroscopic level and not by chemical changes in the molecular structure.

[i] Parts of the current chapter were reproduced from N. K. Guimard, K. K. Oehlenschlaeger, J. Zhou, S. Hilf, F. G. Schmidt, C. Barner-Kowollik, *Macromol. Chem. Phys.* **2012**, *213*, 131, with permission from John Wiley & Sons, Inc. all rights reserved.

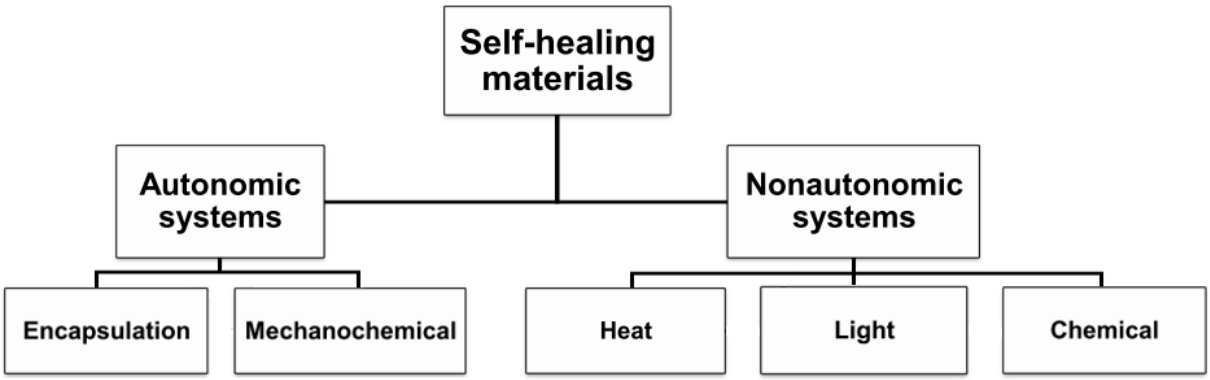

Scheme 3.23 Organization scheme of self-healing materials based on their healing trigger and their ability of autonomous or non-autonomous healing. The organization comprises only the broad applications of self-healing materials, neglecting special cases such as light triggered self-healing under sunlight irradiation which is consequently autonomic.

In all cases of the aforementioned healing strategies a stimulus or trigger, initiating the healing of the system, is essential. Most materials that heal autonomously – whether through extrinsic or intrinsic means – require mechanical force (i.e., damage) as a trigger. Only a couple of strategies lack a trigger healing damage by permanently reorganizing their molecular structure.[107] However, the majority of intrinsically and extrinsically healing systems were designed to heal in response to a predetermined external trigger, other than damage, such as optical,[108] thermal,[87,109] electrical,[110] ballistic,[111] or chemical.[112] In all cases, microscopic cracks in the material are mended, preventing crack propagation and as a result potentially catastrophic failure. The first self-healing materials, designed by Dry, provided extrinsically self-healing and consisted of fiber reinforced concrete. The fibers were filled with a self-repair fluid which healed the composite materials autonomously when set free by damage.[113]

Inspired by the work of Dry, many material scientists faced the challenge of developing other self-healing systems for a variety of applications over the past decades.[114] In this context, autonomously and non-autonomously healing approaches were combined with the aforementioned trigger providing engineers with multiple possibilities when designing a self-healing material. Consequently, not every existing self-healing material is suitable for every use. It is important to consider the targeted application when choosing the trigger and healing mechanism. Additional

points to consider are the repeatability of healing at the same fracture point, the extent to which the original mechanical properties are restored at the damage site, the complexity of the fabrication, stability of the network and cost of the system.

3.5.2 Mechanically triggered healing

As already noted, the earliest mechanical trigger design for self-healing materials consisted of concrete reinforced with cyanoacrylate-filled fibers.[113a] The fibers broke through mechanical force and released a healing fluid which repaired the caused damage. In a further development of mechanical triggered self-healing materials, scientist switched their strategy from one healing fluid to a two component mixture preventing ageing or self reaction of the healing fluid. The two compounds are in general a resin (e.g., epoxy) and a hardener (e.g., diamine), which are supplied to the material by fiber-reinforced polymer (FRP) systems, either via separately loaded adjacent fibers or via embedding one compound in the matrix by encapsuling the other in the fibers.[115] Conversely to the FRP approach, White *et al.* developed a new self-healing material design based on microcapsules. In their work, a mixture of a healing agent and an encapsulated catalyst was embedded in the network. Upon mechanical force the capsule broke, releasing the catalyst to the healing agent which subsequently initiated the repair. Besides their new encapsulated design, these authors also utilized a new chemistry for the healing process, employing typically dicyclopentadiene as healing agent and a Grubbs' catalyst as encapsulated compound.[61c] The parameters for these type of self-healing materials (i.e., FRP and microcapsule-polymer composite system) such as fiber or capsule wall thickness,[116] capsule size and concentration,[117] healing agent,[118] fiber diameter,[116a] and catalyst incorporation method,[118b,119] were studied in-depth to optimize every step of the healing process (i.e.,release of the healing agent, mixing of the healing agent with the catalyst, rate of polymerization/curing). Although FRP and microcapsule-based polymeric systems (MBPS) are similar in many ways, the latter system permits a finer tuning of the material properties. A common problem with matrix embedded self-healing systems is the preparation of the material and the breakage of fibers and capsules through manufacturing. However, by a judicious selection of microcapsule material, size and concentration, the preparation of materials with an increased

toughness of the original polymer composite can be realized.[117a,120] Accordingly, enhanced healing efficiency and, therefore, increased resistance to bulk material crack formation is gained from such a fine tuned MBPS.[61c] Compared to other self-healing material designs, FRP and MBPS display substantial potential for special applications. An adaptable matrix and autonomous healing is provided by systems that employ a microencapsulated repairing agent. Moreover, such self-healing systems show a potential for quantitative healing, which makes FRP and MBPS very attractive for isolations and composite materials. Nevertheless, systems with embedded healing agents also have limitations. A major issue is the inability to repeatedly heal the polymer at the same location due to limited healing agent distributed throughout the polymer matrix. In this context, a new biomimetical self-healing polymer systems containing a microvascular network was developed by White *et al*.[121] The vascular network was connected to a refillable pump, supplying the matrix permanently with healing agent and encapsulated catalyst in order to circumvent the repetitive healing problem (refer to Figure 3.9).

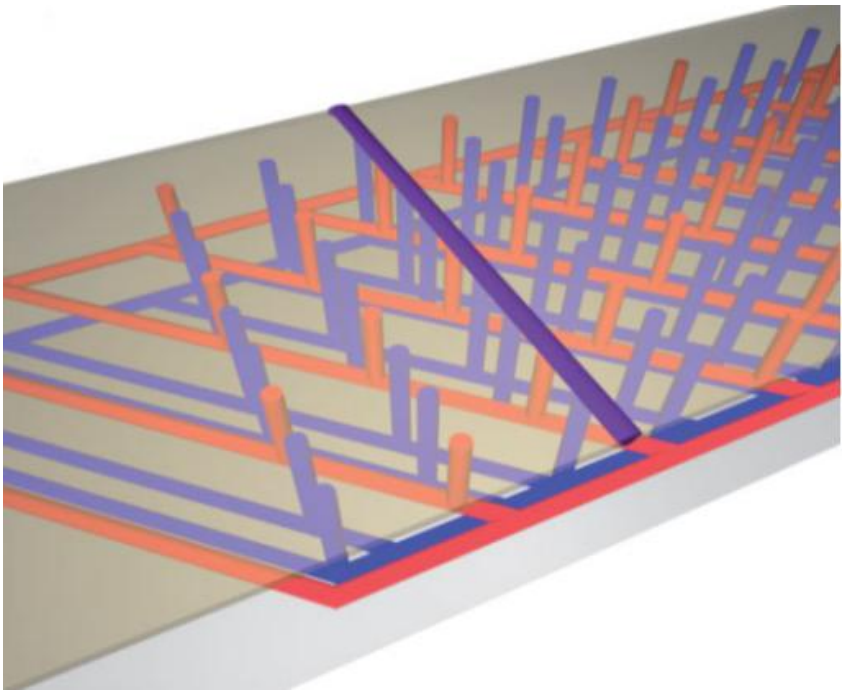

Figure 3.9 Schematic view of an interpenetrating microvascular network that supplies two fluids (red and blue) to a crack plane, where mixing occurs (purple). Reproduced with permission from Ref 122.[122]

Despite the required human intervention of the microvascular network system (to refill the microvascular network with healing agent), this type of self-healing system features a major advantage over FRPs and MBPSs, as it can heal multiple times at the same fracture site.[121] More refined microvascular network systems containing incorporated perpendicular channels which were connected with a new supply system in the polymer matrix, eliminated the need for human intervention.[122-123]

Regardless of the attractive advantages of autonomous healing, FRPs and MBPSs do not represent suitable systems for a broad range of applications. Rather autonomously, intrinsically healing materials composed of dynamically bonding components are appealing for multiple applications as these materials are theoretically capable of repeatedly healing at the same damage site. These dynamic bonds may either be covalent or non-covalent, yet require heat, light, or a chemical to trigger healing.

3.5.3 Light triggered healing

The first optically triggered self-healing systems employed reversible cycloadditions as cross-link reactions in polymer networks, enabling the network linkages to open and close under suitable irradiation. Typical examples for such light-induced, reversible cycloadditions are the [2 + 2] reaction of coumarin[108a] and cinnamoyl groups,[108c] as well as the [4 + 4] reaction of anthracene.[108b] Cycloadditions of coumarin and cinnamoyl groups afford reversible dimerization only under irradiation with very short wavelength (i.e. highly energetic irradiation). Anthracene cycloaddition on the contrary occurs under milder irradiation at 340 nm. In this wavelength region most functional groups stay intact, giving the anthracene dimerization an advantage over coumarin and cinnamoyl. Moreover, 340 nm is present in the irradiation spectrum of the sun, affording a possible autonomously, intrinsically self-healing material for environmentally exposed surfaces.[124] However, two wavelength are required for the aforementioned systems to open and close the network linkages in a controlled fashion. This does not interfere with the healing process, because the linkages formed by the cycloaddition of cumarins, cinnamic acids, or anthracenes are the first to cleave under mechanical stress;[108c] however, it renders the applications of such light-induced reversible network challenging, as multiple applications require

a controlled opening of the network in order to (re)form/build their shape and composition. Thus, most recently developed optically triggered self-healing systems require irradiation by only one wavelength to undergo healing. In such self-healing materials, healing proceeds via a metathesis mechanism of highly reactive radical species which are generated by irradiation. The challenge in the approach is to identify suitable functional groups which yield such radical species under longer wavelength irradiation. Examples of bonds that can undergo light triggered metathesis are disulphide bonds, as demonstrated by Otsuka *et al.*,[108e] and allyl sulfide bonds,[108f] although allyl sulfide groups require the addition of a photoinitiator which generates radicals and initiates the metathesis process.

Trithiocarbonates represent an additional possibility for metathesis based optically healable materials, requiring irradiation at 330 nm at ambient temperature without the need of a photoinitiator, as shown by Matyjaszewski and coworkers (refer to Scheme 3.24).[108g] Moreover, trithiocarbonates can be employed as RAFT agents in CRP, offering an advantage in the design of a polymer matrix. In particular, polymer branches of a preselected molecular weight can be synthesized from the trithiocarbonate center using living radical polymerization.

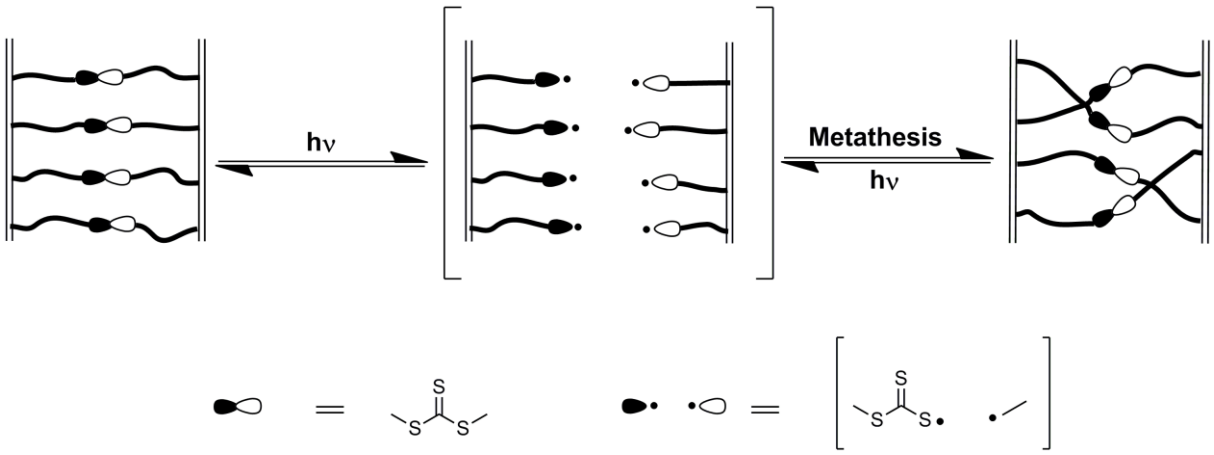

Scheme 3.24 Metathesis of trithiocarbonate bonds in a polymer following photoirradiation (330 nm). Adapted from reference 125.[125]

A combination of light-induced bond cleavage and inorganic chemistry was presented by Burnworth *et al.* contributing to the field of metathesis-based healing materials.[126] In their work, the authors utilized the dynamic bond exchange of a

metal complex M-L to achieve healing under long wavelength irradiation. At already 340 to 390 nm, the metal complex absorbs light which is transferred into heat, causing M-L bond cleavage. Rebonding of the respective M and L species results in a newly distributed M-L matrix and consequently in a healed material.[108g] A different interesting approach to generate optically self-healing materials consisted of a modified natural polysaccharide, chitosan, with urea crosslinks and oxetan.[108h] Mechanical stress resulted in bond cleavage of the urea linkages and chitosan ether bonds. However, under the irradiation of visible light the oxetan rings open and form radical species. Those radical species re-crosslink the damaged network by adding to the chitosan units. Accordingly, the chitosan network, functionalized with oxetan moieties, displays the properties to heal caused damaged under sunlight irradiation which is a considerable advantage. Nevertheless, the system relies on the concentration of oxetan functions in the network which is reduced with the number of healing cycles.

3.5.4 Chemically triggered healing

Many intrinsically self-healing materials utilize the addition of a chemical trigger to induce reversible bond formation (refer to Scheme 3.25). Mostly, acids and bases or redox agents are added to the material in order to change either the pH value[127] or oxidation state.[128] Common pH-sensitive systems based on boronic-acid-salicylhydroxy complexation,[129] hydrazone formation of acylhydrazines,[127b] and crown ether-benzylammonium salt ionic interactions.[130] Typical redox sensitive self-healing systems contain disulfide linkages in the network system, switching from disulfide to thiolate after adding the redox agent.[108b,128] Therefore, it is no surprise that polymers containing disulfide linkages have become increasingly attractive for self-healing material applications given the fact that healing can be stimulated and controlled by redox agents in addition to heat[131] and irradiation.[108e]

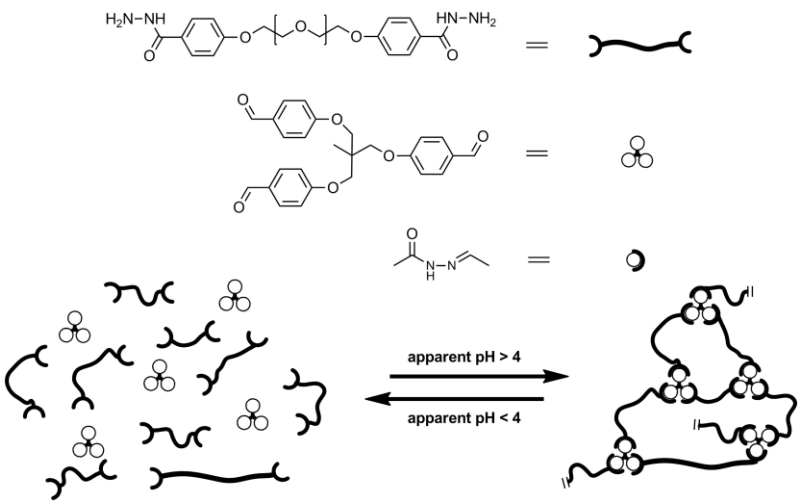

Scheme 3.25 Schematic representation of the pH-sensitive reversible polymerization of a bisacylhydrazine functionalized poly(ethylene glycol) with an acylhydrazone tri-linker. Adapted from reference 132.[132]

In comparison with other self-healing materials, chemically triggered intelligent materials offer the advantage of total control over the extent of bonding and, therefore, over the healing process, yet also the disadvantage of non-autonomous healing.

3.5.5 Heat triggered healing

Heating of a material symbolizes the input of energy and therefore the manipulation of dynamic equilibria. Accordingly to Le Chatelier, the dynamic equilibrium is shifted, resulting in chemical bonds cleavage within the material. The reformation of such broken bonds proceeds in a form of metathesis which leads to a reshaped and restored polymer matrix. Such dynamic equilibria can either be based on cycloadditions,[97,109a,109c,133] disulfides,[131] alkoxyamines,[109b,134] or secondary interactions,[130,135] whereas every system displays its own temperature dependency. The majority of secondary interactions, for example crownether complexation, π–π stacking, or hydrogen bonding, show a strong dynamic exchange behavior already at ambient temperatures providing consequently autonomous healing. Similar results can be achieved by the use of specific DA systems which exchange also at ambient temperatures.[136] Alkoxyamine and different DA systems on the other hand require

elevated temperatures to shift the equilibrium towards the cleaved bond form of the network linkages. Although such elevated temperature requiring self-healing systems would no longer be capable of autonomous healing, these materials would benefit from improved mechanical properties, which may be necessary for certain applications. Moreover, it is very appealing to specific applications, requiring heat for the depolymerization process of the polymer matrix.[137]

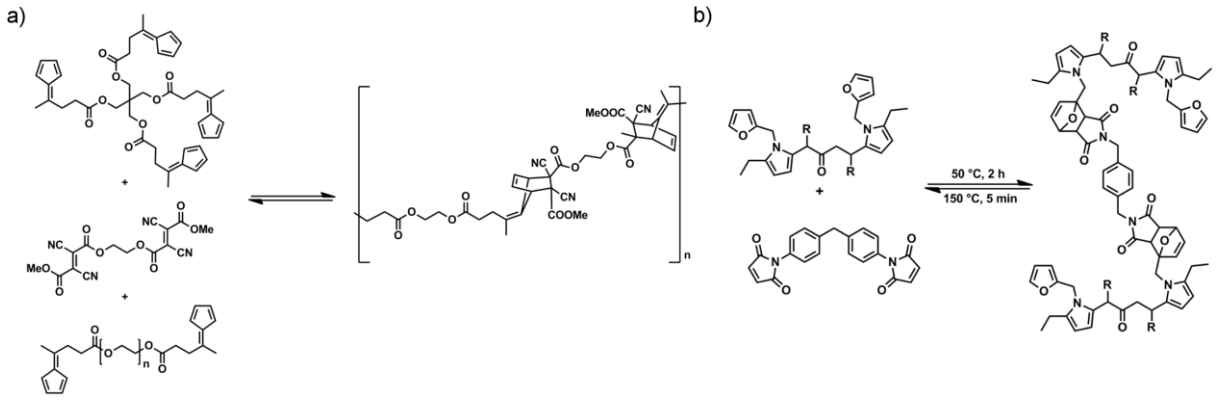

Scheme 3.26 Reversible DA systems for self-healing applications. a) The reversible cross-linking of a furan functionalized polyketone (PK-furan) with a bismaleimide using Diels–Alder chemistry (adapted from reference 133a). b) Diels–Alder chemistry used to reversibly cross-link fulvene functionalized glycol-based polymers with a cyanfumarate di-linker at room temperature (adapted from reference 109a).

Among the temperature dependent dynamic equilibria, DA chemistry represents the most promising technique for generating polymeric systems with thermally triggered self-healing.[114d,114e,138] The first study regarding thermally reversible polymeric networks containing DA functionalities was reported by Craven in 1969.[139] Since then, two main strategies have evolved in the field of thermally reversible DA networks for the construction of networks. One approach consist of multifunctional linker molecules, whereas the other follows the polymerization of di- or multifunctional monomers (e.g., a bis- or multifuran functionalized monomer with a bis- or multimaleimide functionalized monomer) which are converted with a difunctional molecule.[140] The first to utilize the technique of multifunctional linker molecules were Wudle and coworkers, who published their pioneering work in 2002 about a cross-linked material obtained from a furan tetra-linker (diene) and a maleimide tri-linker (dienophile), which showed healing above 120 °C.[87] The work of Wudle motivated many scientists to focus on DA based self-healing materials, yielding multiple

publications addressing the topic of reversible DA networks.[3] A wide variety of self-healing polymer networks employed the same diene–dienophile pairing as Wudle in an effort to alter the equilibrium constant and decrease the required temperature.[141] However, also combinations of different material compositions have been constructed by employing reversible DA chemistry. Ghezzo *et al*., for example, coated carbon FRP laminates with the reversible bismaleimide/tetra-furan DA pair.[142] The carbon fiber reinforcement improved the mechanical properties of the material, gaining a self-healing material with a high mechanical load capacity, potentially being used for applications demanding stronger materials. Other notable contributions comprised glass fibers reinforced furan functionalized epoxy-amine thermosets that heals in the presence of a bismaleimide healing agent[143] and the heat dependent reversible polymerization of furfuryl carrying ABA triblock copolymer with a bismaleimide.[141a,144] The strategy of polymeric multifunctional linker units was explored by Zhang *et al.* who developed a recyclable network from a thermosetting polyketone bearing furan moieties which cross-linked with bismaleimide.[109a] The DA reaction, i.e. the network formation, required temperatures of close to 50 °C for 2–24 h. In contrast to long reaction times the rDA reaction, i.e. the dissociation of the polymer network, preceded within 20 min at 120 °C (or at 150 °C for 5–10 min). Aside from different composite and architecture combinations of the furan/maleimide DA pair, other dienes and dienophiles have been explored for their DA reactivity and potential for self-healing applications.[97,133b,136,145] Consequently, a pool of variable dienophile and diene pairs is available for engineers planning to utilize a self-healing material in an application. However, the careful selection of the DA pair can drastically improve the self-healing properties of the targeted application.

Although DA chemistry is the most widely employed mechanism for heat triggered self-healing materials, it is not the only thermally reversible dynamic bond formation method as aforementioned. Alkoxyamines are, for example, a very interesting reversible covalent technique, which also finds use in CRP in the form of NMP. Opening and closing of polymer networks by homolytical cleavage of the carbon oxygen bonds has shown to be a suitable approach for heat triggered self-healing materials. Nevertheless, very high temperatures are required for alkoxyamine bond cleavage, disabling the use of functional matrixes.[146] Recent results of Zhang *et al.* showed that healing with alkoxyamines can be conducted under ambient temperature (i.e. autonomously). By attaching a stabilizing carbon moiety on the

alkoxy group the required healing temperature were reduced, yielding a healed specimen when storing the damaged material at ambient temperature for two days.[147] Disulfide bridges display homolytical bond cleavage, too, when heated to temperatures close to 60 °C. Klumperman and co-workers followed this approach and demonstrates that an epoxy resin cross-linked with disulfide bonds is capable of healing at 60 °C after 1 h due to the dynamic nature of the disulfide bonds and the low T_g of polyesters.[131] Secondary bonding interactions represent an additional heat triggered reversible bonding approach. Mostly ionic interactions between cations and anions in the form of ammonium salts and crownether are utilized as network linkages, but π–π stacking of certain benzene derivatives was explored, too. Although such materials are composed of non-covalent dynamic bonds, it has been demonstrated that a robust free standing film that heals at 80 °C within seconds can be formed from a mixture of a diimide-containing polymer and a pyrene end capped polymer.[135a,148] As becomes apparent, there has been an enormous amount of effort spent attempting to discover and characterize other thermally reversible linkages. However, so far most alkoxyamines require very high temperatures for healing, most disulfides are vulnerable towards degradation, and most secondary interactions lack a high mechanical capacity, leaving the robust, covalently bonded, and low temperature requiring DA reaction as the mechanism of choice for heat triggered self-healing material application.

3.6 Light–induced chemistry

3.6.1 History and fundamentals of photochemistry

The first photochemical reaction was discovered by Trommsdorf in 1834.[149] Following the color change of an *α*-santonin crystal and its bursting by exposure to sunlight, Trommsdorf hypothized that light could interact with matter and invoke a chemical reaction. Despite a report about his observation and further research into the topic, he was unable to exactly explain the occurring phenomenon. Einstein was the first who understood the interaction of matter and light, published in his work from 1905 about the photo effect, which later was honored with the Nobel prize.[150] He imagined light as an alternative form of energy and stated that the energy of light is dependent on its wavelength in a proportional fashion. Furthermore, he noted that light would be delivered in small packs of specific values. Combined with Max Planck's quantum hypothesis[151] the idea of Einstein defined a new physical theory, the light quantum theory. Evidence for his hypothesis can be found in the well known experiment measuring the electronic tension and current between a photo and a ring cathode while irradiating the photocathode with different intensity and wavelength of light. Johannes Stark related, in 1908, the light quantum theory with the kinetic energy of radiated molecules. He claimed that molecules, which absorb light, increase their kinetic energy, leading to a higher rate of collision and finally to a chemical reaction. Aside from the kinetic energy of irradiated molecules, Stark also assumed that the absorption of light could involve a change in valence electrons of the irradiated compound. Inspired by the idea of changing valence electrons, Einstein developed the theory of light equivalence. In the light equivalence theory, the number of molecules which are activated per unit of time is proportional to the intensity of light radiation. More simply, every exited molecule consumes one pack per unit of light.[152] In these publications Einstein defined for the first time the words photon and quantum yield, which are to date known by all chemists. Experiments which confirmed the assumption of Einstein and measured the quantum yield of chemical processes were provided by Warburg[153] in a number of studies. These fundamental works of Einstein, Stark and other physicists and chemists, pioneered the field of photochemistry and enabled following generations of scientists to utilize photochemical reactions in synthetic chemistry. The typical photochemical processes

which take place in an irradiated molecule can be schematically followed by a Jablonski diagram. Such a scheme was first established by A. Jablonski in 1935,[154] in an effort to explain the photochemical phenomenon of phosphorescence. Through the years many scientists have often cited and referred to the famous graphical representation from Jablonski, so that the Jablonski diagram became universally accepted. A Jablonski diagram simply depicts the relative energy of all existing states in a molecules (ground and exited) considering the spin orientation of every state (singulet and triplet) and connects the existing states with the respective photochemical transitions which take place in a molecule (Figure 3.10). The advantage of such a Jablonski diagram is the simplicity and traceability of photochemical processes. In general, the reconstruction of photochemical processes is extremely complex considering the multiple transitions which may take place between different degrees of freedom. However, with the Jablonski diagram only focusing on electronic and vibrational transitions, the view of a photochemical reaction simplifies allowing the understanding of the occurring transitions.

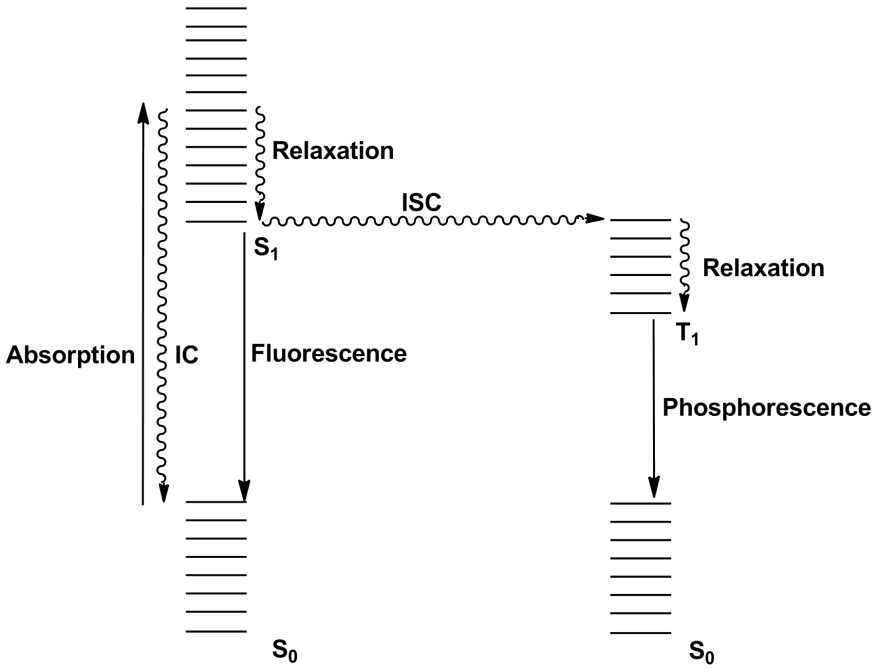

Figure 3.10 Typical Jablonski diagram containing possible photochemical processes.

Upon absorbing a photon, the irradiated molecule gains energy and is promoted from the singlet ground state (S_0) to the first exited singlet state (S_1). Excitation from the ground state to higher singulet states is possible as well, but highly unlikely so that

the concentration of molecules in higher excited singulet states is small. Aside from the transition of the electronic state, vibrational transitions also take place following the Franck-Condon principle. Due to the dissipation of thermal energy from the molecule via the loss of vibrational energy, the molecule reaches the vibrational ground state of the first exited singlet state (S_1). From here, several further photochemical processes can take place:

- Fluorescence: The molecule loses the energy of the first excited state via emission of a photon and relaxes back to the ground state (S_0).
- Internal conversion (IC): The molecule loses its energy due to vibrational transition from the exited singlet state to the singlet ground state. The procedure is similar to the relaxation from the exited vibrational level of the first exited singlet state to its ground vibrational level.
- Chemical reaction: In the presence of a reactant, the exited molecule either transfers its energy, through collision, to the reactant or undergoes the reaction with the reactant directly.
- Intersystem crossing (ISC): Compounds which contain a carbonyl- or an amine-group or very heavy atoms (e.g. iodine) in their structure can undergo a spin inversion to a triplet state of the molecule, which has a lower potential energy.

Fluorescence, chemical reaction or IC yield a singulet ground state molecule. In contrast thereto, ISC leads to a spin inversion and therefore to the first excited triplet state (T_1). From this first excited triplet state only two fates are possible for the excited molecule:

- Chemical reaction: The exited molecule undergoes a chemical reaction and rearranges to a single ground state (S_0) in the process of the reaction.
- Phosphorescence: By emitting a photon, the exited molecule loses its energy and relaxes back to the singlet ground state (The likelihood of the spin change from singulet to triplet is drastically reduced leading to a longer emission time compared to fluorescence).

To decide which of the aforementioned photochemical processes are favored in a given system, the quantity of the quantum yield is defined. It describes the

percentage of molecules which will follow a specific process after absorption of photons, implying that the quantum yield can only be less or equal to 1 for each process.

3.6.2 Photoenol chemistry

The reactivity of carbonyl groups in photochemical reactions, when exposed to sunlight or an artificial source of light, has been known for a long time.[155] Martin *et al.* and Hammond *et al.* were the first who described the utilization of light as a tool to reduce benzophenone in protic solvents to diphenylmethanol.[156] Martin used several alcohols to obtain the reduced diphenylmethanol, whereas Hammond extended these results by adding an equimolar ratio of the obtained secondary alcohol to produce a benzopinacol product in quantitative yields (refere to Scheme 3.27).

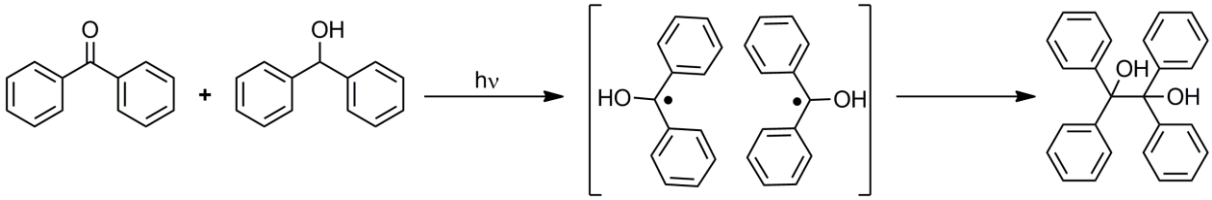

Scheme 3.27 The photo-induced benzopinacol reaction of Hammond which inspired Yang and led to the discovery of photoenol chemistry.[156b]

Inspired by the work of Hammond *et al.*, Yang *et al.* increased the library of benzopinacol derivates obtained from the photo reduction and subsequent benzopinacol reaction of different benzophenones. In the course of their study, they noticed that *ortho*-alkyl substituents on the benzophenone rings inhibited the pinacol reaction, yielding the benzopinacol and diphenylmethanol intermediate with low conversions.[157] A study with deuterated methanol as solvent for the photo reaction revealed that an exchange of approximately one deuterium per molecule indeed took place under irradiation. However, the carbonyl group was not reduced to the secondary alcohol as the exchange took place on the benzylic position. Consequently they assumed an internal hydrogen abstraction at the benzylic position of the exited carbonyl group. The resulting diradical species would then *in situ*

rearrange with the aromatic system to a dienol ground state species following a 1,5-hydrogen rearrangement back to the *ortho*-alkyl benzophenone. In order to confirm the stated hypothesis, they tried to trap the formed diene species *in situ* by adding dimethyl-but-2-ynedioate as reactive dienophile to the mixture (see Scheme 3.28).

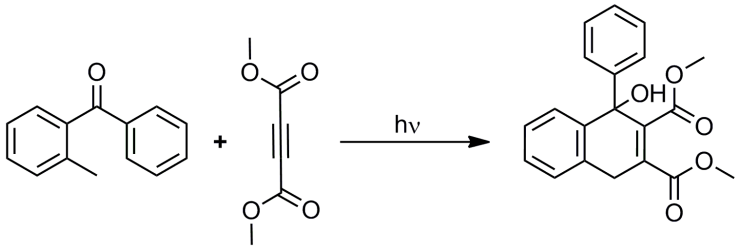

Scheme 3.28 The light-induced DA trapping reaction carried out by Yang *et al.* to prove the existence and long lifetime of the dienol species.[157]

The experiment did not only prove the existence of the reactive dienol ground state species, it also showed that the lifetime of the diene was sufficient long to trap it with an adequate dienophile, making the reaction attractive for organic synthesis. The strategy of adding a reactive diene or dienophile species to a mixture in order to prove reactive DA intermediates was later on coined DA trapping technique.[157-158] Aside from confirming the dienol species, Young was also able to detect an excited triplet state species by flash spectroscopy,[159] underpinning the assumption of an internal hydrogen abstraction. However, he was neither able to prove the remaining mechanistic steps nor to establish which formed intermediate was responsible for the reactivity in the DA reaction. Therefore, many groups tried to decode and prove the complete photoenol mechanism but failed, till finally Tchir and Porter detected every occurring species by employing extensive flash photolysis experiments. Their work confirmed the assumption of Young and revealed the number of photochemical transients and the exact lifetime of the occurring species.[160] The detailed photoenol mechanism can be seen in Scheme 3.29

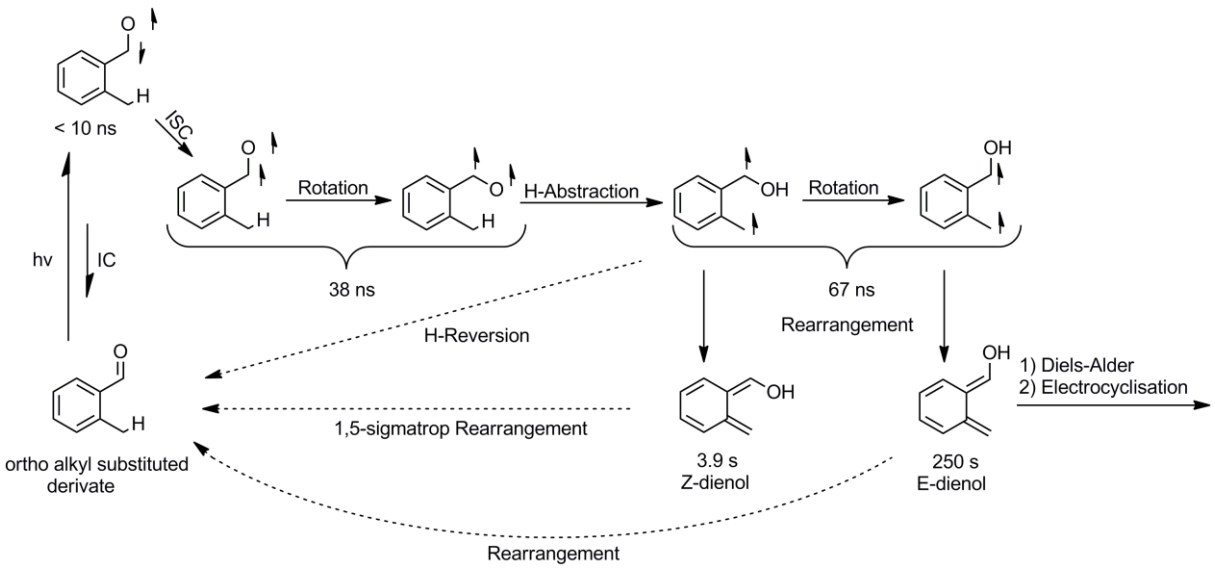

Scheme 3.29 Established mechanism of the photoenol-formation by Tchir and Porter.[160a]

The times below each molecule are the lifetimes, measured in degassed cyclohexane, of the various species occurring in the photoenol mechanism. After absorption of a photon from the exited singlet state, the molecule undergoes intersystem crossing to the triplet state which was detected by Young. The triplet state species then rotates around the aromatic-radical bearing carbon bond in order to move the exited carbonyl function into the proximity to the benzylic hydrogen. Following the abstraction of this proton, the formed biradical species has three possible opportunities to decay. It may rearrange and form the Z-dienol ground state directly, it could again rotate around the same bond and subsequently rearrange to the E-dienol ground state or it may follow the third possibility which is the return to the normal singlet ground state.[161] The fates of the two possible stereo isomers are very different. Both of them have a much longer lifetime than the radical states, but while the more stable E-dienol offers different possibilities to react, the Z-dienol undergoes a rapid 1,5-hydrogen rearrangement back to the *ortho*-alkyle benzophenone. Thus, there is no proof that the Z-dienol can only undergo the 1,5-hydrogen rearrangement, but results of Sammes *et al.* showed that other reactions such as the DA trapping are unlikely.[162] The E-dienol, in contrast, has a much longer lifetime due to the fact that it cannot undergo an H-shift to the starting materials. Consequently, the lifetime of the E-dienol is increased, enabling the E-isomer to react in a DA reaction as diene and –

provide the temperature is sufficiently – to undergo a 4π-electrocyclisation to benzocyclobutenol.[163] The selective synthesis of both products is a question of the employed precursor. Several facts which lead either to the DA product or the photocyclisation product were demonstrated by Samanta and Morthy.[158a] It was shown that every variable which stabilizes the dienol species or destabilizes the abstracted hydrogen carbon bond assists with the DA trapping, while steric congestion leads instead to the electrocyclization product. A further side product which can occur from both isomers is the photo-Elbs product.[158b] The Elbs reaction can be avoided, however, through the use of a filter which protects the sample for longer wavelength light.[160b] The decryption of the mechanism has helped in understanding of the entire process of the dienol formation which aids improving the reaction conditions.[158a,164] Moreover, the carbonyl group bearing starting material library was increased to include acetophenone and benzaldehyde derivatives. In addition, *ortho*-alkyl functionalized hetero cyclic compounds such as pyrones were explored for their suitability in the photoenolisation by Ullman *et al.*[165] Today, the photoenol DA trapping reaction represents a very efficient protocol, suitable for organic synthesis as demonstrated by Nicolaou *et al.*[166] The need of light as a reaction trigger makes the photoenol reaction completely orthogonal to common temperature dependent cycloadditions like the thermally DA reaction or the CuAAC,[11] giving synthetic polymer chemist a new light-induced *click* reaction for macromolecular architecture design.[167] Furthermore, it symbolizes the combination of highly efficient DA conjugation and light triggered reaction as a very attractive tool for soft lithography as well as,[168] direct laser writing and any kind of light triggered application.

3.6.3 Other light-induced Diels–Alder reactions

Aside from the photoenol rearrangement other light triggered DA trapping reactions have emerged, yielding *in situ* diene or dienophile species while irradiated. A prominent alternative to the photoenol chemistry is the DA trapping of *ortho*-napthoquinone-methide species. Exposed to wavelength around 300 nm, 3-hydroxy-2-naphtalenemethanol derivatives undergo a dehydration of the non-aromatic alcohol function and the hydrogen atom of the naphtol group. The respective 2,3-

napthoquinone-3-methide is subsequently obtained from an ionic rearrangement and represents a highly reactive hetero diene species which can be trapped with adequate dienophiles, similar to the photoenol chemistry (refer to Scheme 3.30). However, the *ortho*-napthoquinone-methide is an electron poor diene which is deactivated for normal electron demand HDA reactions. Consequently, only exotic electron rich dienophiles such as vinyl ether or thiovinyl ether groups undergo an electron inverse demand HDA reaction with *ortho*-napthoquinone-methide moieties.

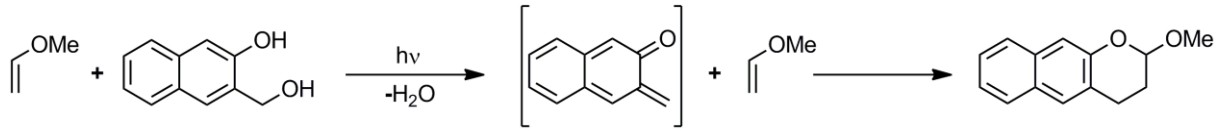

Scheme 3.30 The light triggered *ortho*-napthoquinone-methide chemistry.

Nevertheless, Popik and coworkers utilized the *ortho*-napthoquinone-methide chemistry extensively for several surface grafting approaches with different adjustments (vinylether in solution or as anchor on the surface).[169] They were thus able to spatially immobilize fluorescent dyes on glass slides.[169b] Moreover, they explored different leaving groups for the dehydration processes such as ether and ammonium salts as substituent for the alcohol group, expanding the scope of light sensitive 3-hydroxy-2-naphtalenemethane derivatives. Furthermore, they presented an interesting Michael addition strategy on the *ortho*-napthoquinone-methide structure, demonstrating that highly nucleophilic groups such as thiols were able to add to the methide group.[170] Although the Michael addition reaction displays a useful feature of the *ortho*-napthoquinone-methide chemistry, this study revealed as well the low orthogonality of the HDA reaction, discarding the *ortho*-napthoquinone-methide HDA trapping as *click* chemistry in contrast to the photoenol approach.

An additional photo triggered HDA system was already designed in the early 80s by Vedejs *et al.* employing the aforementioned photo fragmentation of phenacylsulfides to thioaldehydes.[72,171] The fragmentation required wavelengths between 300 and 370 nm. As already mentioned in previous sections, thioaldehydes represent highly reactive dienophile compounds for HDA reactions. In an effort to separate and purify thioaldehyde species, Vedejs added diene species such as 2,3-dimethylbutandiene and Cp to the reaction mixture in order to trap the generated thioaldehyde *in situ*.

Inspired by the work of Vedejs, the photo fragmentation of phenacylsulfides was recently employed in different surface grafting approaches (refer to Scheme 3.31).[172] Moreover, the photo generated thioaldehyde displays the same reactivity towards nucleophilic addition as *ortho*-napthoquinone-methide,[173] proving additional synthetic feature by reducing the orthogonality of the HDA reaction and discarding it as *click* reaction.

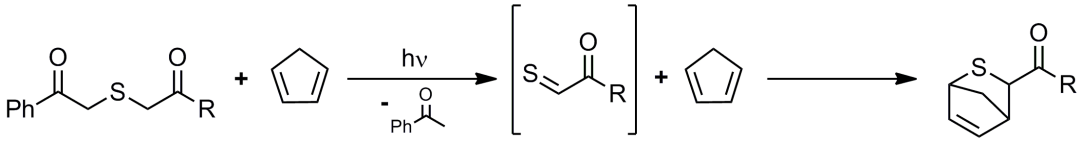

Scheme 3.31 The light-induced phenacylsulfide fragmentation and subsequent thioaldehyde hetero Diels–Alder trapping chemistry.

4 The Cyanodithioester-Cyclopentadiene Pair[ii]

As stated in the previous chapters, adaptable networks based on DA chemistry feature a high potential for multiple applications, resulting in special industrial products such as rapid proto typing printers, composite materials for aeronautic and car elements, or adhesives and coatings.[174] The first and most commonly employed DA system for reversible bonding/debonding applications is the N-maleimide/furan pair which is already applied in commercially available products.[175] Providing reversibility above 120 °C, the N-maleimide/furan pair is suitable for a large variety of moderately low cycling temperature applications.[85a,109a,176] However, the reaction rates for the shift of the N-maleimide/furan DA equilibrium either require extended times or the addition of a Lewis acid as catalyst which is either way not acceptable for certain industrial products based on self-healing materials. Considering the fabrication of car elements for example, which are produced on assembly lines within seconds, reaction times of minutes cannot be tolerated for the utilization in such applications. On the other hand, the addition of a Lewis acid as a catalyst indeed reduce the reaction time, yet would cause corrosion in the material and higher production costs as an additional compound had to be added to the polymer matrix. Consequently – from an industrial point of view – both approaches (with and without a catalyst) cannot be realized. Therefore, new DA pairs displaying extremely high reaction rates without the addition of a catalyst have to be designed to satisfy the industrial demands. A step towards the solution of this occurring problem was the development and employment of reactive dithioester species which showed ideal reaction kinetics for the HDA reaction with several dienes. However, the so far utilized dithioesters showed either no reversibility, due to fragmentation post HDA reaction,[177] or required – as the N-maleimide/furan pair – a catalyst to proceed within seconds.[6a,178] Nevertheless, the strategy of employing dithioesters offers two major advantage over the N-maleimide/furan DA. Firstly, activated dithioester react with multiple dienes reversible in HDA reactions (not only with one),[4,94] and secondly, the attached group on the dithioester function gives synthetic chemists a

[ii] Parts of the current chapter were reproduced from K. K. Oehlenschlaeger, N. K. Guimard, J. Brandt, J. O. Mueller, C. Y. Lin, S. Hilf, A. Lederer, M. L. Coote, F. G. Schmidt, C. Barner-Kowollik, *Polymer Chemistry* **2013**, *4*, 4348, with permission from the Royal Society of Chemistry 2014 all rights reserved. The temperature dependent DLS study was carried out in Dresden at the Leibniz-Institut for polymer research by Josef Brandt.

possibility to tune the reactivity of the dienophile species in HDA reactions. The last argument becomes clear by comparing reaction times of a sulfonyl[177] and carbonyl[92a] dithioester species. In other words, by attaching strong electron withdrawing groups onto the dithioester function the reaction times can be drastically improved, as illustrated by Vyas *et al*.[93] who employed highly reactive methyl cyanodithioformate towards several dienes in HDA reactions to obtain sulfur-containing carbohydrates. The reported reaction times from Vyas *et al.* matched the reaction times of catalyzed HDA reactions of dithioesters by showing no decomposition after the cycloaddition. However, the complex synthesis associated with generating·molecules substituted with cyanodithioate units prevented research groups to further explore this chemistry.

In the following a novel synthetic strategy for the synthesis of two hitherto unknown CDTE compounds (**1a**, **1b**) as well as a detailed rHDA study of the DHTP generated by the reaction between Cp and an CDTE end capped poly(ε-caprolactone) (PCL) **2** is described. The fast, catalyst free cyclability between 40 °C and 100 °C of the HDA reaction is initially studied on the polymer end group model by on-line (*in situ*) UV-Vis spectroscopy. Furthermore, off-line experiments based on a diene exchange study, analyzed by electrospray ionization-mass spectrometry (ESI-MS) are carried out to support the UV-VIS measurements and to determine the reaction kinetics of the diene exchange. In order to apply this reversible chemistry to a polymeric material, a CDTE based di-linker molecule **3** is generated and analyzed for its reversible rHDA properties. Therefore, on-line (*in situ*) UV-VIS cycling between 40 °C and 100 °C and on-line (*in situ*) ^{1}H NMR spectroscopy measurements are conducted with di-linker **3**. To demonstrate the reversibility of the CDTE HDA chemistry a step-growth polymer is generated by reacting the di-linker **3** with a bis-Cp polymer (provided by Stefan Hilf, Evonik industries) to form a linear polymer. Size exclusion chromatography (SEC), and on-line (*in situ*) ^{1}H NMR spectroscopy measurements demonstrate the repeatedly reversible nature of the HDA-based linear polymer and evidence its chemical structure, whereas on-line (*in situ*) UV-Vis spectroscopy reveal short reaction times when going from ambient temperature to 100 °C. Moreover, on-line (*in situ*) high temperature dynamic light scattering (HT-DLS) from the IPF in Dresden (J. Brandt) underpin the reversible nature of the HDA step-growth polymer by qualitatively showing the temperature responsible growth and shrinkage of the hydrodynamic radius (R_h) of the HDA step-growth polymer.

4.1 Synthesis of cyanodithioester molecules

In contrast to many other dithioesters, it is not possible to simply introduce a CDTE unit into a molecule by performing one of the three major approaches presented in previous chapter (nucleophilic substitution with the dithioate salt, stepwise substitution on thiophosgen, thioester transformation with Lawson reagent). As a result of the attached cyano group, the electron deficient character of the thiocarbonyl group is increased so strong, that the thiocarbonyl thio group is vulnerable to attack by any possible nucleophile at the electrophilic sulfur of the thiocarbonyl function.[179] Such a nucleophile can even be the leaving group of a nucleophilic substitution reaction, in case of a synthetic approach via the dithioate salt. The nucleophilic attack initializes a dimerization process of two CDTE units which was described by Bähr *et al*.[180] A suggested mechanism for the dimerization was later on published by Simmons *et al.* and is presented in Scheme 4.1.[181] After the nucleophilic attack on the thiocarbonyl sulfur, the negative charge is stabilized on the thiocarbonyl carbon center, which subsequently accumulates to a second CDTE molecule. Following elimination of elemental sulfur and desorption of the leaving group a bis-(mercapto)-furmaronitrile derivative remains.[181] The dimerization process can also take place in the sodium cyanodithioate salt precursor itself, although the dimerization proceeds slowly over several weeks. Nevertheless, a cation transfer to the ammonium cyanodithioate salt by heating the sodium salt with an ammonium bromine salt in ethanol, has to be performed when storing the cyanodithioate salt for longer times.

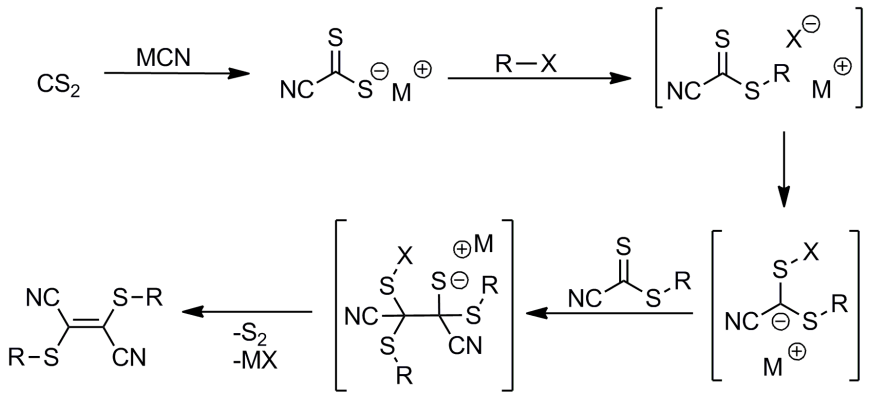

Scheme 4.1 Suggested mechanism of the cyanodithioester dimerization by Simmons *et al*.[181]

Hence, for the complex CDTE molecule synthesis, only two CDTE compounds, the methyl- and ethyl- cyanodithioate, were literature known.[93b,182] To circumvent the dimerization problem, a new procedure for the synthesis of CDTE compounds was developed. Three equivalents of Cp were added during the cyano-dithioate nucleophilic substitution reaction in order to trap the *in situ* formed CDTE in the HDA product and, therefore, protect it against dimerization, allowing the purification by flash column chromatography. In addition to dimerization, the *in situ* generated HDA product also prevented oxidation of the thiocarbonyl group. Accordingly, the protected CDTE is stable under air, at ambient temperature and in the presence of light, which is not usually the case for dithioesters.[183] As secondary benzylic halogens are known to be activated for nucleophilic substitutions of second order (SN2), functionalized benzyl bromine derivatives with a handle for further chemistry were employed for the synthesis of functionalized CDTE molecules employing the described synthesis strategy. Consequently, CDTE-benzylic alcohol (**1a**) and CDTE-benzoic acid (**1b**) were obtained from the *in situ* HDA trapping approach in moderate yields. Following purification, **1a** was utilized in a ROP of ε-caprolactone to yield a protected CDTE end capped PCL (**2**) with number average molar mass (M_n) of 2000 g·mol^{-1} and a molar mass dispersity ($Đ_M$) of 1.20.

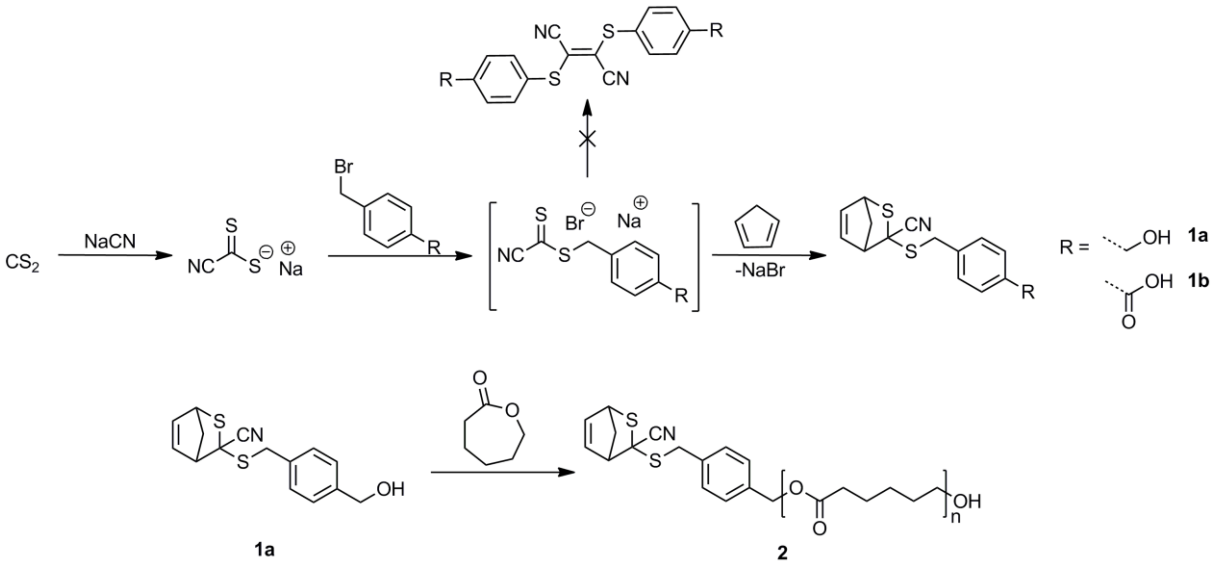

Scheme 4.2 Synthesis of the functionalized CDTE molecules **1a** and **1b** by *in situ* HDA trapping, preventing the dimerization process (upper reaction sequence). ROP process of ε-caprolactone to polymer **2** (lower reaction).

In an effort to apply the CDTE-based HDA reversible chemistry to material science, a di-linker, end capped with two protected CDTE groups, was synthesized. In a one-step synthesis, isophorone diisocyanate (IPDI) was reacted with two equivalents of **1a** at 55 °C as depicted in Scheme 4.3. The pure product, isophorone diisocyanate-cyanodithioester (IPDI-CDTE) **3**, was obtained following column chromatography as confirmed by ESI-MS and ^{1}H NMR.

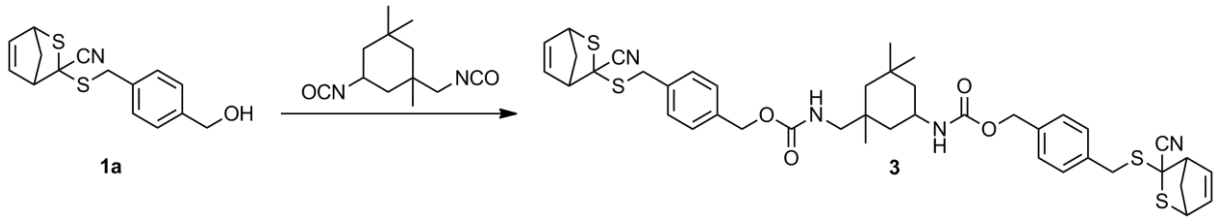

Scheme 4.3 Synthesis of dilinker IPDI-CDTE **3** from the starting materials **1a** and isophorone diisocyanate (IPDI).

4.2 Analysis of the reversibility

The rHDA deprotection reaction was first evaluated by temperature-dependent on-line UV-Vis spectroscopy of polymer **2**. This analytical technique was selected because in contrast to the protected CDTE **2** the deprotected species, **4**, undergoes a strong π-π* transition characteristic of dithioester functions and thus, it absorbs UV light. Therefore, polymer **2** was dissolved in toluene in a sealed cuvette and heated to different temperatures between 50 °C and 100 °C. At each temperature a full absorption spectrum was recorded in order to detect the increasing absorption of **4** at elevated temperatures. As can be seen in the spectra depicted in Figure 4.1, the absorption of the polymer mixture increases at elevated temperatures between 300 nm and 380 nm, implying that the HDA reaction equilibrium is shifted towards **4** and Cp (i.e., the rHDA products). Interestingly, the strong π-π* transition absorption decreased when cooling to ambient temperatures immediately, pointing to extremely high reaction rates and to a switchable reaction equilibrium, showing no degradation.

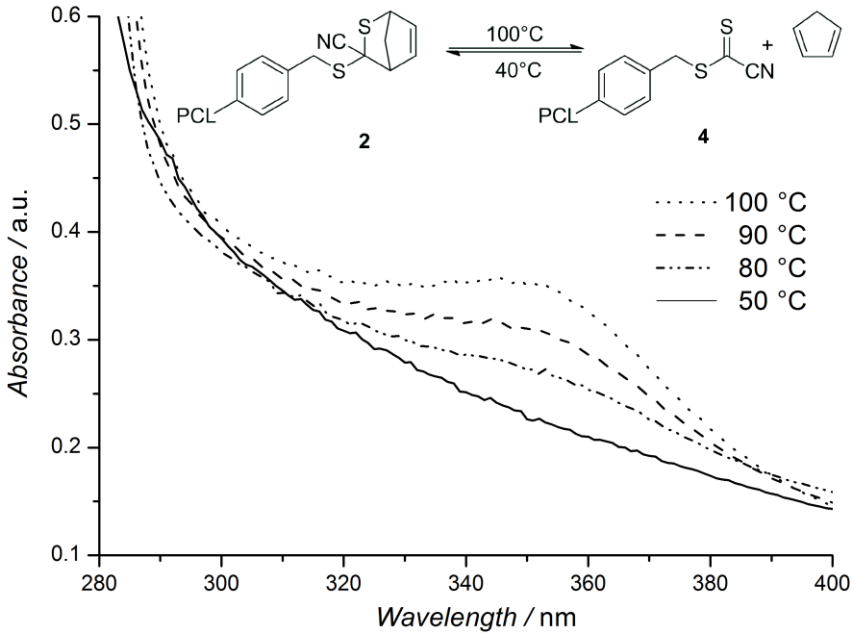

Figure 4.1 Absorption spectra of CDTE end capped PCL **2** at different temperatures. With increasing temperature, the HDA equilibrium is shifted towards the diene/dienophile side which results in more free CDTE **4** featuring the typical dithioester π-π* transition.

In order to explore the reversibility of the HDA equilibrium further and to determine whether hysteresis was present or not, a repetitive temperature cycling experiment was performed. Again, temperature-dependent on-line UV-Vis spectroscopy was chosen for the cycling test. Consequently, the same sealed cuvette with polymer **2** dissolved in toluene was cycled between 40 °C and 100 °C for eight times (refer to Figure 4.2), while recording the absorption of the solution at 347 nm (the absorption maximum of **4** according to Figure 4.1). Higher temperatures could unfortunately not reached because of the limitations of the UV-Vis spectrometer.

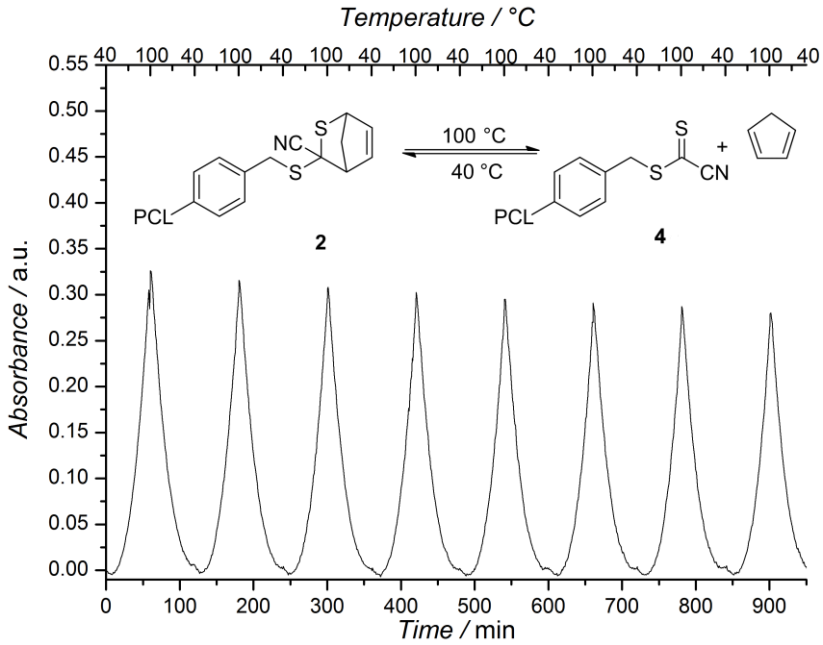

Figure 4.2 Temperature dependent UV-Vis spectroscopy data (heating/cooling rate was 1 °C/min) of trapped CDTE **2** during the cycling between 40 °C and 100 °C. The absorption was recorded at 347 nm. A baseline correction was applied according to a literature procedure.[184]

As expected, the absorption at 347 nm increased at elevated temperatures and decreased back to the starting point during cooling, thus clearly demonstrating the feasibility of repeatedly cycling between **2** and **4**. Moreover, a heating rate of 1 °C per minute was applied for the cycling experiment, which was four to eight times faster than earlier temperature-dependent on-line UV-Vis spectroscopy experiments of other dithioester HDA pairs.[184] Accordingly, it can be concluded that the CDTE/Cp system is so far the fastest explored dithioester HDA pair. Although a slight decrease in the maximum absorption signal is observed over time, chemical hysteresis was discarded as the source for the slight signal decrease since UV-Vis spectra of the CDTE species (i.e., **2** and **3**) showed no decrease in absorption intensity after the cycling experiments relative to the initial spectra collected prior to the start of the experiment (i.e., time = 0).

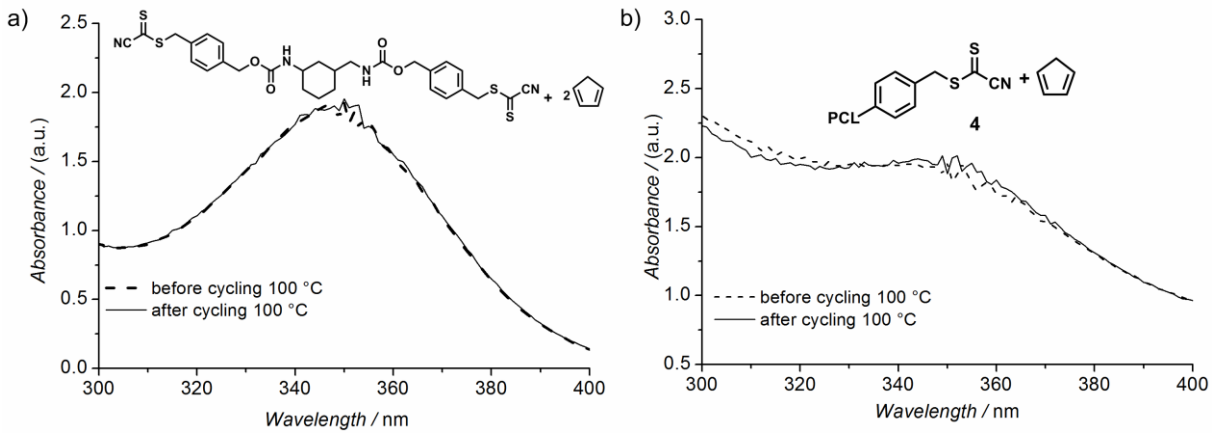

Figure 4.3. a) and b) depict the samples absorption spectra prior (striped) and after (solid) the heat cycling experiment of **2** and **3**. The absorption was recorded at 347 nm. Evaporated toluene was refilled after the cycling, to ensure an identical concentration as before the cycling experiment.

Therefore, it was concluded that the decrease in the absorption maximum over time resulted from a baseline shift, attributed to detector drift over time and temperature. The UV-Vis study thus demonstrates the on demand cyclability of the CDTE HDA/rHDA reaction. To quantitatively assess the rHDA reaction of **2**, the kinetics of a diene exchange reaction were analyzed by ESI-MS. The protected CDTE **2** was heated in toluene with two equivalents of 1,3-dimethylbutadiene (DMBD) (i.e., the diene to be exchanged with Cp). DMBD was chosen as the replacing diene because the corresponding HDA products are known to have generally higher rHDA temperatures than the HDA products obtained from Cp.[90b] Consequently, the rHDA reaction of the DMBD trapped CDTE functionalized PCL, **5**, to form **2**, could be avoided. In this experiment, the extent of diene exchange at 120 °C was assessed over time. Figure 4.4 depicts the mass spectrum after 0, 10, and 30 min of the diene exchange reaction of Cp with DMBD at 120 °C.

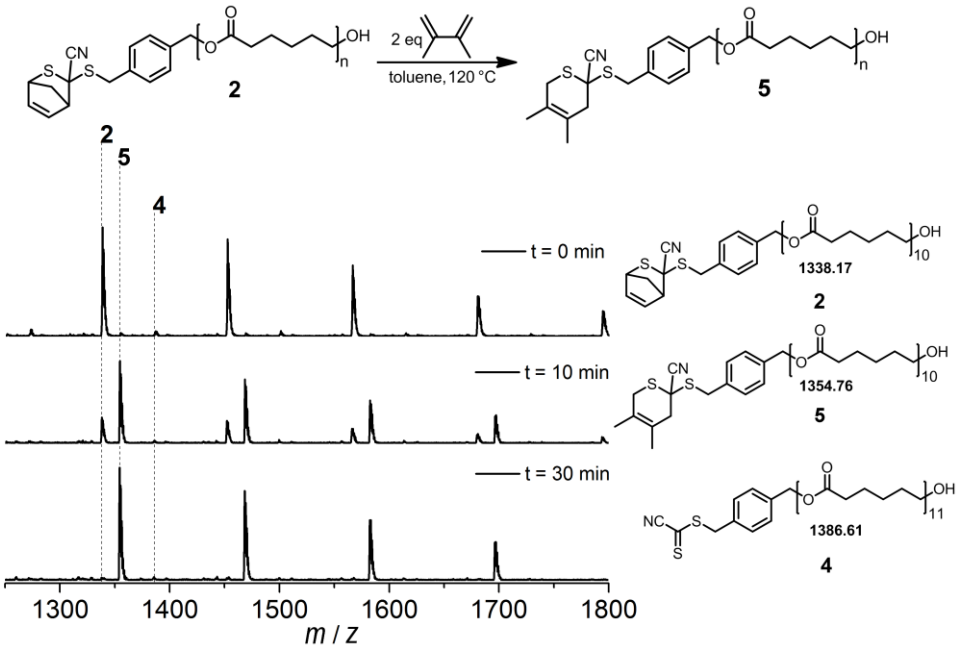

Figure 4.4 ESI-MS spectra of the kinetic study for the diene exchange reaction between Cp and DMBD. In addition to the starting material **2** and the product **4**, the deprotected CDTE **3** is also present in the t = 0 min sample. The masses below the chemical structures refer to the sodium adducts of the polymers.

The 0 min (i.e., ambient temperature) starting material spectrum suggests that a small amount of unprotected CDTE **4** exists in addition to **2**. The presence of **4** in this MS spectrum can be explained by the fact that the rHDA reaction occurs during the ESI-MS measurement which was already observed in former ESI-MS studies.[6a] After 10 min the MS data evidence that the rHDA reaction has proceeded to approximately 66% completion, calculated from the signal intensities of **2** and **5**, which supports the notion that the CDTE deprotection occurs rapidly in the presence of DMBD. After 30 min of reaction time no starting material **2** was detectable. The kinetics of the diene exchange reaction were studied at 80 °C and 100 °C, in addition to 120 °C, the results of which are presented in the Figure 4.5. In all cases, a fast conversion of **2** to **5** proceeds at the beginning; however, while a conversion of 100% is reached at 120 °C and 100 °C within less than 2 h, at 80 °C full conversion is not obtained even after more than 6 h. This observation points to a small amount of free CDTE **3** at 80 °C, suggesting the onset rHDA temperature is close to 80 °C. Nevertheless the exchange from **2** to **4** was successful, evidencing a rHDA reaction of the CDTE/Cp HDA pair at mild temperatures.

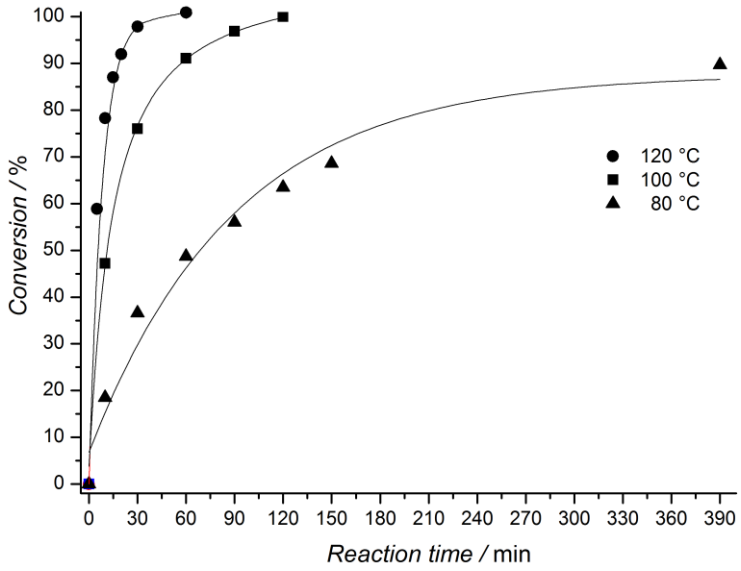

Figure 4.5 Kinetic plot of the diene exchange reaction between **2** and DMBD to form **4** at 80 °C, 100 °C, and 120 °C in toluene.

Before utilizing the novel di-linker **3** in a polymerization reaction, its ability to switch between the protected and deprotected state, without undergoing degradation, was explored. Therefore, the same temperature dependent on-line UV-Vis spectroscopy cycling experiment as in case of compound **2** was performed, recording the raising and decreasing absorption of the π-π* transition from free CDTE at 347 nm.

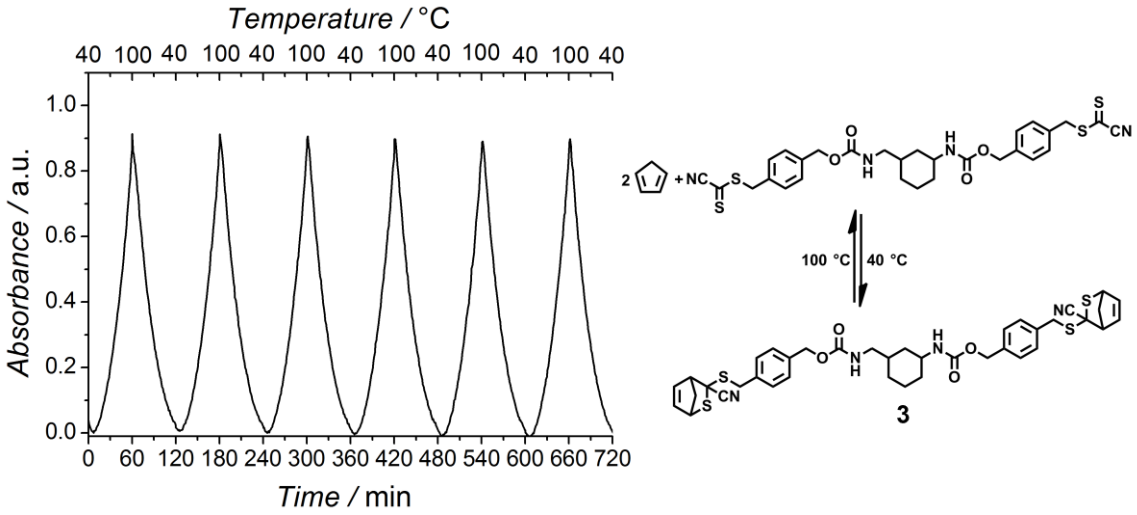

Figure 4.6 Temperature dependent UV-Vis spectroscopy data of di-linker molecule **3** in toluene during the cycling between 40 °C and 100 °C (heating/cooling rate was 1 °C/minute). The absorption was recorded at 347 nm. A baseline correction was applied according to a literature procedure.[184]

Identical to the temperature dependent on-line UV-Vis spectroscopy cycling experiment of polymer **2**, di-linker **3** displayed ideal cyclability properties by following the fast temperature changes without showing any hysteresis (refer to Figure 4.6). In addition, temperature dependent ^{1}H NMR spectroscopy was utilized to support the findings of the UV-Vis cycling experiment. The advantage of on-line high temperature ^{1}H NMR spectroscopy is that it combines the qualitative proof of the on-line UV-Vis experiment with the quantitative findings of the diene exchange studies analyzed by ESI-MS, giving an additional on-line view of the HDA reaction. The cycling was performed in a NMR pressure tube in toluene-d_8 as the NMR solvent at a substrate concentration of 0.02 mol·L^{-1}. Figure 4.7 shows a zoom into the region between 5 and 7 ppm of **3** at the different temperatures.

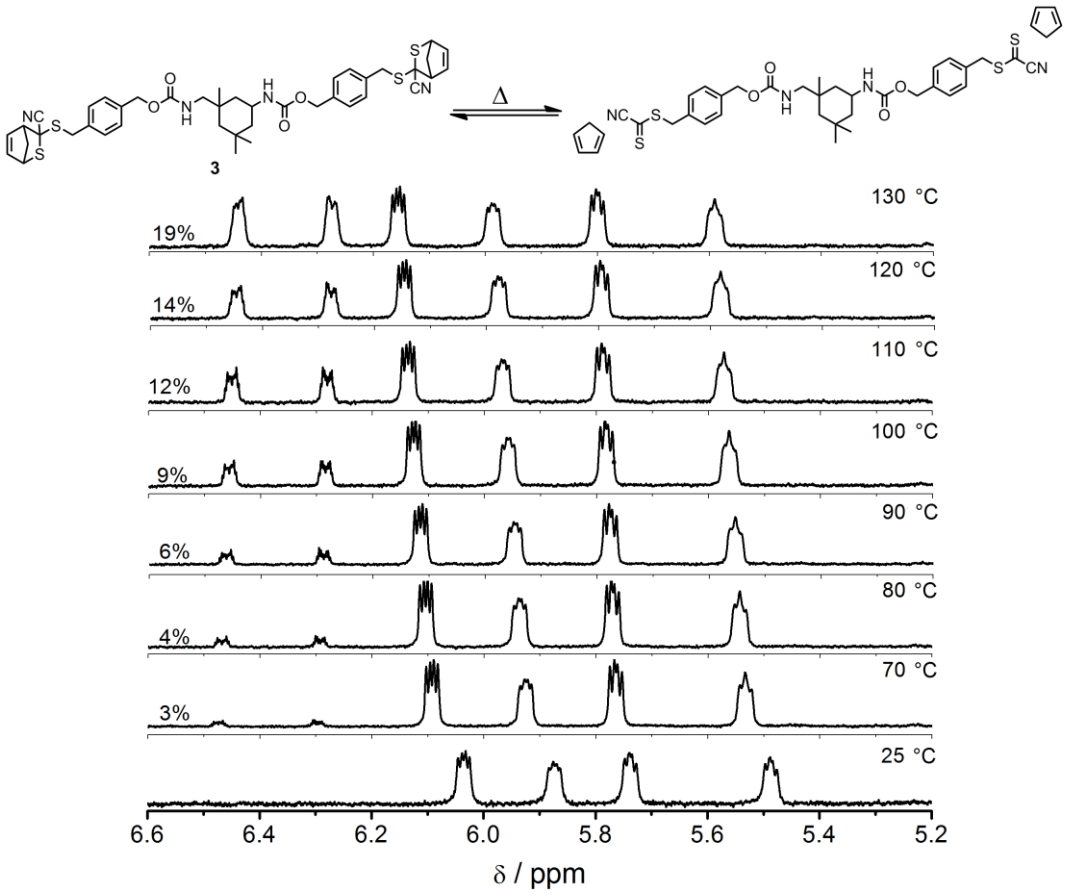

Figure 4.7 NMR spectra of **3** in deuterated toluene-d_8 at different temperatures. Next to the HDA product signals of **3**, a set of signals that corresponds to free Cp can be seen, increasing with the temperature. Left hand side of the increasing peaks, the calculated mol% of deprotected **3** is noted. The resonance set disappears again when cooled below 70 °C. In addition, a general shift of all signals towards lower field can be observed, associated with the increasing temperature.

In agreement with the UV-Vis study, the NMR spectra at elevated temperature revealed additional signals in the double bond region associated with free Cp, formed by the rHDA reaction. The additional signals started to increase already at 70 °C and increased with climbing temperature. Unfortunately, it was not possible to increase the temperature above 130 °C due to device limitations. Subsequent to heating to 130 °C, the sample was cooled to 25 °C, no longer showing free Cp signals in the NMR spectrum. Additionally, the same peak intensity of free Cp was reached, compared to the spectra recorded prior to heating to 130 °C and cooling to 25 °C, when heated again to any temperature above 70 °C. Such cycling experiments were carried out several times with arbitrary temperatures between 70-130 °C and every time the same Cp intensity at the given temperature was detected. These findings imply 100% cyclability of **3** by repetitive heating to 130 °C and cooling, and its stability at the elevated temperatures that are necessary for the polymerization reaction and for the cycling process.

4.3 Hetero Diels–Alder based step-growth polymerization

Next, the HDA based AA-BB step-growth polymerization of the CDTE di-linker **3** was targeted. Attempts to remove the Cp protecting groups of di-linker molecule **3** in order to gain the unprotected CDTE species which would react rapidly with any di-functional diene, failed. Pure heating of the protected compound resulted in either no change of the ^{1}H NMR spectrum of **3** or in various side reactions. Considering the clean reaction of the diene exchange study from **2** to **5**, it appeared reasonable to polymerize the protected di-linker **3** *in situ* with an adequate diene di-linker via a diene exchange reaction. Following the diene exchange study, a di-functional diene with general higher rHDA temperatures than Cp – to avoid the depolymerization of the generated polymer by free Cp – was employed. Therefore, a di-functional sorbic alcohol diene (IPDI-SA) was utilized in the polymerization of di-linker **3**. In order to prove the concept of the HDA polymerization of **3**, the first polymerization was performed in solution. Dissolved in toluene, an equimolar mixture of **3** and IPDI-SA was heated in a sealed pressure tube to 120 °C, triggering the polymerization.

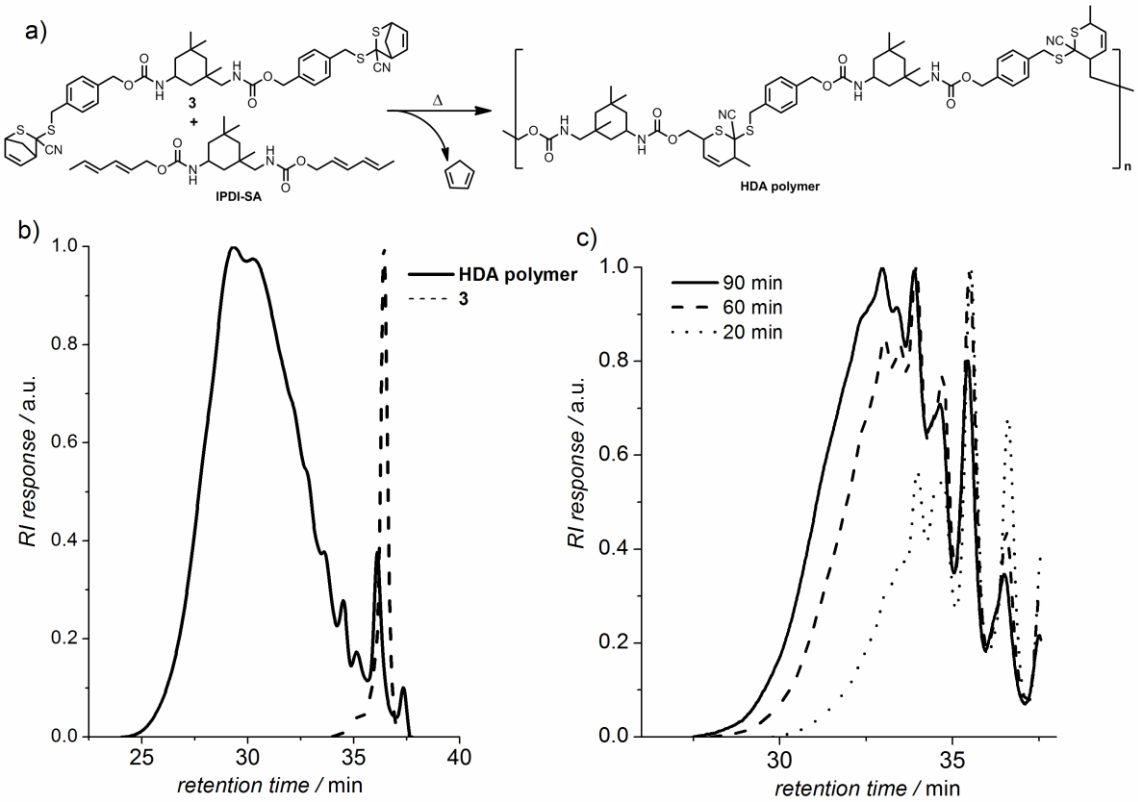

Figure 4.8 a) Reaction scheme of the diene exchange HDA polymerization. b) Normalized SEC traces of **3** (dotted line, M_n = 900 g·mol^{-1}, $Đ_M$ = 1.0), and the heated mixture of **3** and IPDI-SA in solution, resulting in HDA polymer (solid line, M_n = 6500 g·mol^{-1}, $Đ_M$ = 3.7). c) Normalized SEC traces of the bulk polymerization between **3** and IPDI-SA after 20 min (dotted line, M_n = 1600 g·mol^{-1}, $Đ_M$ =1.7), 60 min (dashed line, M_n = 2400 g·mol^{-1}, $Đ_M$ = 1.9), and 90 min (solid line, M_n = 3000 g·mol^{-1}, $Đ_M$ = 2.0).

Elevated temperatures were required for the polymerization reaction with **3** to remove via rHDA chemistry, the Cp protecting group (refer to Figure 4.8 a). The polymerization temperature was selected based on the fast reaction rates observed at 120 °C in the diene exchange study. Figure 4.8 b) depicts the obtained HDA step-growth polymer after 1 h reaction time. A significant shift towards higher molecular weights (i.e., low retention time) results from the diene exchange reaction of the di-functional linker molecules, evidencing the suitability of the HDA *in situ* trapping technique as polymerization method. To mimic the conditions in a self-healing material, the second polymerization of **3** and IPDI-SA was conducted in bulk. Therefore, a homogeneous bulk mixture of the building blocks had to be generated by dissolving the building blocks in dichloromethane, stirring the solution for 1 min, and removing the solvent. The bulk material was heated to 120 °C in an open flask

and kinetic samples were taken to monitor the process of the polymerization (refer to Figure 4.8 c). As can be seen in the SEC spectra, the bulk step-growth polymerization proceeds to lower conversion than the polymerization in solution. Such a behavior is not suppressing given that the viscosity is drastically increased in the melt compared to solution. Moreover, after a certain conversion the HDA-polymer appears to be too viscous for further growing steps, remaining at the molecular weight obtained after 1 h. In order to explore the structure of the obtained polymer and to confirm its HDA character, ^{1}H NMR spectra were recorded in DMSO-d_6 of the building blocks **3** and IPDI-SA as well as of the product HDA-polymer.

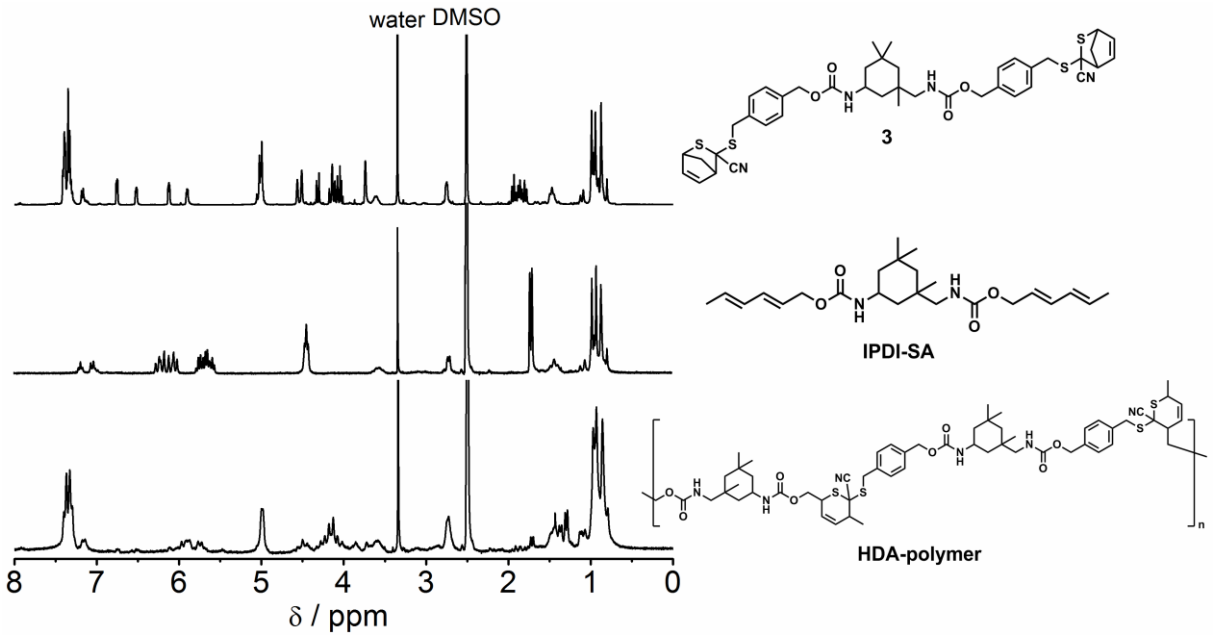

Figure 4.9 ^{1}H NMR analysis of the obtained polymer from **3** and the sorbic alcohol derivative of IPDI recorded in DMSO-d_6. The resonances of the bridge-head protons of the Cp HDA product (top) vanish in the HDA-polymer spectrum (bottom), as well as the signals of the terminal methyl groups (middle) of IPDI-SA. Moreover, a significant change in the double bond region evidences the generation of the HDA product.

Inspection of the^{1}H NMR spectra presented in Figure 4.9 reveals that indeed a diene exchange of the Cp protecting group against the sorbic alcohol moieties is responsible for the step-growth polymerization. Comparing the region between 1 and 2 ppm for every spectrum shows that the signals of the bridge head protons of the Cp HDA adduct as well as the methyl groups of the sorbic alcohol groups vanish in the course of the reaction. Moreover, the double bond region between 5 and 7 ppm changes completely from sharp doublets (Figure 9 top spectrum of **3**) and good

resolved multipletts (Figure 9 middel spectrum of IPDI-SA) to one broad double bond resonance (Figure 9 bottom spectrum of HDA-polymer), typically observed for polymer groups. Consequently, it can be summerized that the HDA adduct changed, the Cp group vanished, the sorbic alcohol groups were consumed and the polymer consists of double bond units, leading to the conclusion that the HDA step-growth polymerization in bulk was successful. Despite the success of the HDA trapping polymerization, the obtained HDA polymer based on the CDTE/sorbic alcohol HDA pair, should have slower reaction kinetics and higher rHDA temperatures than the CDTE/Cp system.[94] In order to transfer the observed reaction kinetics and temperature dependency of di-linker molecule **3** to material science, a HDA step-growth polymer with the same HDA linkages (i.e. based on the CDTE/Cp HDA pair) had to be constructed. In other words, a bis-functional Cp polymer had to be used for the step-growth polymerization. Consequently, a readily available bis-Cp polymer (Cp_2-P(*i*BoA-*n*BA); M_n = 12000 g·mol^{-1}, $Đ_M$ = 1.4) was employed for the HDA step-growth polymerization, following the same diene exchange reaction polymerization strategy.

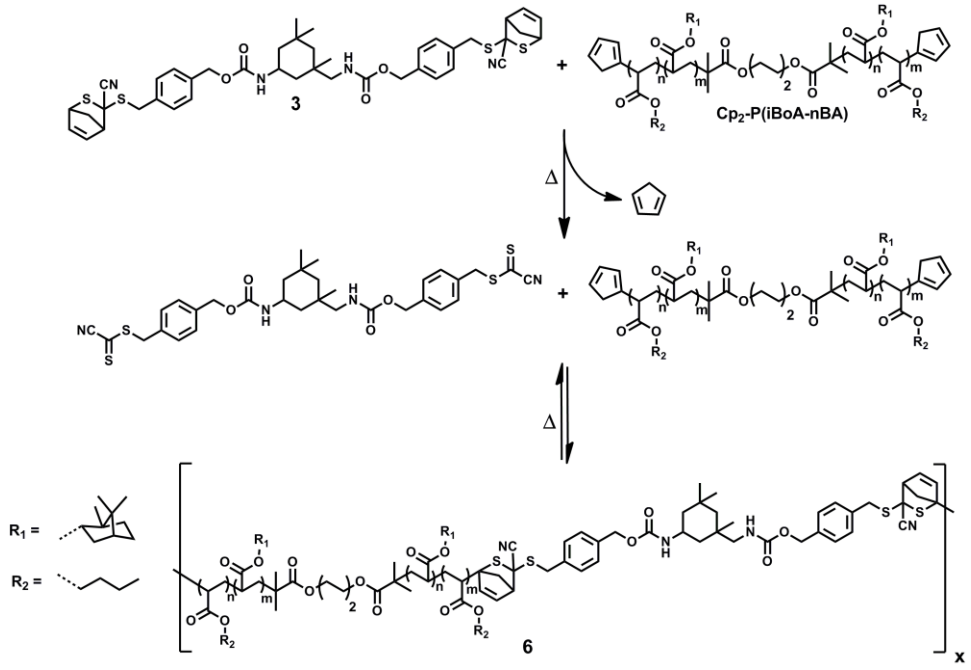

Scheme 4.4 Polymerization process of **3** with Cp_2-P(*i*BoA-*n*BA) to polymer **6**.

As the polymerization of **3** with IPDI-SA, the diene exchange polymerization with Cp_2-P(*i*BoA-*n*BA) was performed in bulk to mimic a self-healing process, which would be

expected of such an applied material. The polymerization mixture of **3** and Cp_2-P(*i*BoA-*n*BA) was prepared in the same fashion as the previous bulk polymerization sample and subsequently heated to 120 °C for 1 h after which it was slowly allowed to reach ambient temperature, yielding the HDA based polymer **6**. To further confirm that heating is required for the deprotection of the CDTE di-linker in order to permit polymerization, a 1 to 1 molar mixture of **3** and Cp_2-P(*i*BoA-*n*BA), prior to heating, was analyzing by SEC (see Figure 4.10).

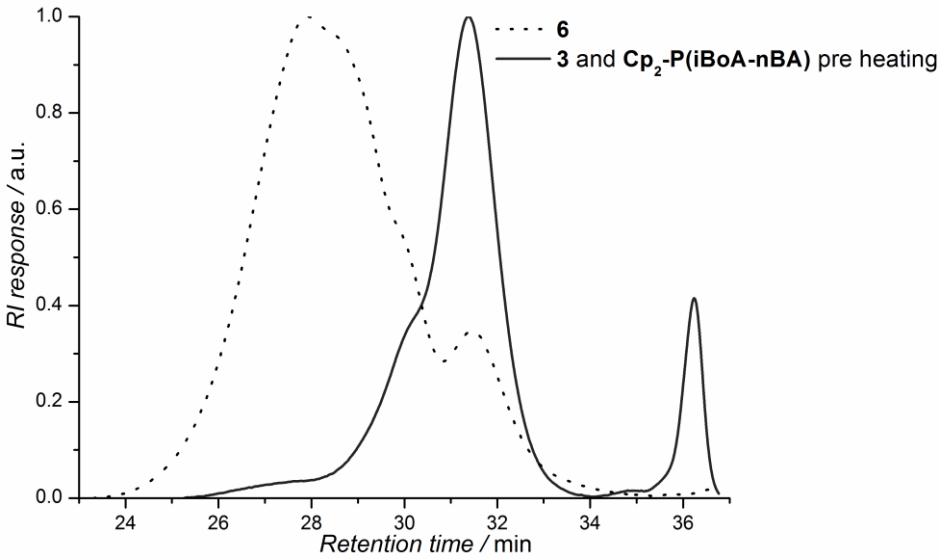

Figure 4.10 Normalized SEC traces of the mixture of **3** and Cp_2 -P(*i*BoA-*n*BA) before heating (solid line, M_n = 7100 g·mol^{-1}), and the obtained polymer **6** (dotted line, M_n = 34200 g·mol^{-1}).

As expected, the obtained chromatogram demonstrates that the building blocks do not undergo any reaction at low temperatures since their corresponding·molecular weight distributions remain unchanged. The smaller peak appearing at higher retention times correlates well with **3** and the high molecular weight polymer distribution (i.e., lower retention times) associated with the larger peak is attributed to Cp_2-P(*i*BoA-*n*BA). Note that the high molecular weight shoulders associated with the Cp_2-P(*i*BoA-*n*BA) peak can be explained by the slow Cp-Cp dimerization that occurs over time despite storing the Cp_2-P(*i*BoA-*n*BA) at -20 °C. Due to the Cp dimerization reaction, the polymer distribution changes slowly over an extended period of time making it challenging to accurately prepare a 1 to 1 ratio of the building blocks, with respect to their available functional groups. Once **3** was deprotected, *in situ*, the deprotected **3** was subsequently available to react further with other dienes present

in the mixture, i.e., Cp_2-P(*i*BoA-*n*BA). The polymerization reaction was allowed to proceed for an hour instead of thirty minutes because it is reasonable to assume that the polymerization process requires more time to achieve complete conversion given the exchange of Cp against another Cp species and the nature of HDA equilibrium. In addition to initializing the rHDA deprotection process, the high temperature also permits the vaporization of Cp, which theoretically should drive the polymerization forward. The near tripling of the M_n of polymer **6** compared to the M_n of Cp_2-P(*i*BoA-*n*BA) and the increase of the $Đ_M$ from 1.6 to 2.5 indicates the success of the HDA polymerization. Of course, the concern that the high molecular weight product results from the HDA self-reaction of Cp_2-P(*i*BoA-*n*BA) is real; however, a control reaction in which Cp_2-P(*i*BoA-*n*BA) was heated to 140 °C for 12 h revealed no change in the M_n of Cp_2-P(*i*BoA-*n*BA). Moreover, the disappearance of IPDI-CDTE (i.e., **3**) in the elugram of **6** clearly indicates that **3** is consumed during the polymerization process and incorporated into polymer **6**. Despite the complete disappearance of **3**, a shoulder at higher retention times that clearly corresponds to Cp_2-P(*i*BoA-*n*BA), remains. The shoulder could not be eliminated by performing an optimization study of the molar endgroup equivalents of the building blocks used in the HDA polymerization suggesting that the remaining Cp_2-P(*i*BoA-*n*BA) actually lacks both Cp end groups, rendering it unreactive. Given that both atom-transfer radical polymerization and polymer Cp functionalization, which were utilized to synthesize Cp_2-P(*i*BoA-*n*BA), commonly yield dead chains (i.e., non Cp-functionalized polymer chains) the remaining Cp_2-P(*i*BoA-*n*BA)-derived shoulder is less surprising. Taking the aforementioned results into account, the HDA-based polymerization was considered to be successful.

4.4 Reversibility of the synthesized step-growth polymer

The reversibility of the HDA based polymerization reaction of **3** and Cp_2-P(*i*BoA-*n*BA) was assessed utilizing essentially the same procedure as that employed for the diene exchange study. A sample of polymer **6** was heated in toluene to 120 °C for 1 h with 10 equivalents of DMBD to trap all **3** that is released from the depolymerization reaction. SEC analysis of the product suggests that complete depolymerization, followed by the cycloaddition of DMBD with the CPDE end groups of the di-linker, was achieved because the elugram is nearly identical to that of the mixture of **3** and Cp_2-P(*i*BoA-*n*BA) prior to heating (refer to Figure 4.11). The only difference is a slight shift of the peak corresponding to **3** to higher molecular weight values, which would be expected if DMBD were to add to both sides of **3**. In essence, the SEC elugram demonstrates that the IPDI-CDTE di-linker **3** can be regenerated at high temperatures and upon cooling will re-undergo a HDA reaction if a diene is present (i.e., in this case DMBD). Naturally, it would be more satisfying to observe both the depolymerized **6** product in the absence of DMBD and the repolymerized **6** by SEC; however, repolymerization (the HDA reaction) proceeds too rapidly to allow for the isolation and analysis of the untrapped depolymerized product. Therefore, the results of the trapping study are considered to be the next best option to demonstrate the reversibility of the system via SEC.

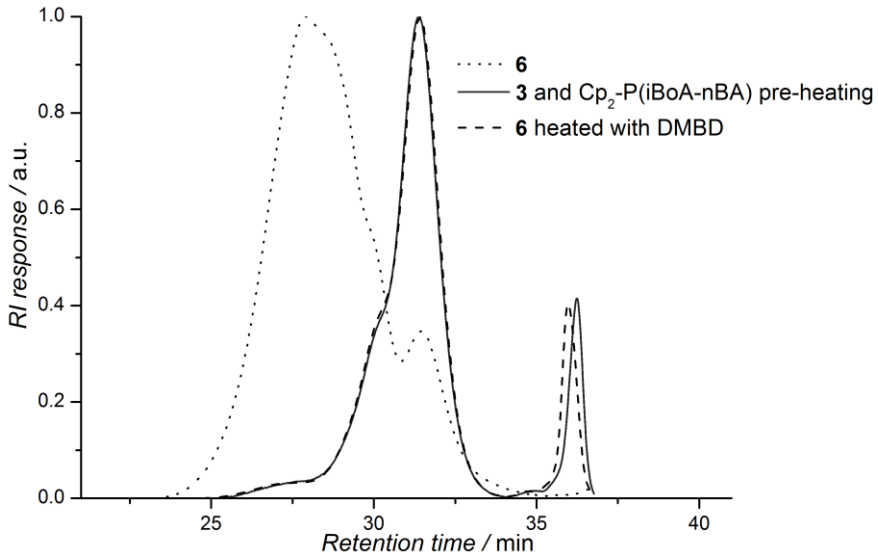

Figure 4.11 Normalized SEC traces of the mixture of **3** and Cp_2-P(*i*BoA-*n*BA) before heating (solid line, M_n = 7100 g·mol^{-1}), polymer **6** (dotted line, M_n= 34200 g·mol^{-1}), and **6** heated in the presence of the trapping agent, 1,3-dimethylbutadiene (dashed line, M_n = 7400 g·mol^{-1}).

However, an on-line analysis technique would finally demonstrate the cyclable properties of the HDA polymer **6**. Consequently, a HT-DLS experiment was performed to detect the shrinking (depolymerization) by heating and expansion (repolymerization) by cooling of the HDA polymer (refer to Figure 4.12). Therefore, a solution of **6** in trichlorobenzene (TCB), with a concentration of 17 $mg \cdot mL^{-1}$, was cycled five times between 30 °C and 120 °C while recording the R_h of the solution over time. Starting with an R_h of 2.43 nm, polymer **6** indeed shrank when heated to 120 °C to 2.19 nm and expanded again when cooled to 30 °C. This constant switching behavior can be observed over the entire cycling process, which is depicted in Figure 4.12 (solid line), giving final evidence of the reversible properties of **6**. Only slight fluctuations of about 0.05 nm can be observed at the end of the first and fourth cycle, yet such small values are within experimental error of DLS measurements. To assess the fluctuation, and especially to monitor the temperature dependence of the DLS results, a sample of Cp_2-P(*i*BoA-*n*BA) was cycled under identical conditions (dashed line) to compare the obtained values as reference to the results from polymer **6**. With an R_h of 1.83 nm at 30 °C and 2.00 nm at 120 °C, the R_h of the reference also shows a dependence on the temperature. This finding is expected, as the temperature has a significant influence on the coil dimension of polymers in solution. At higher temperatures the polymer usually expands and occupies a larger volume, resulting in a higher R_h value while in a cooled state it collapses, which reduces the R_h. Whereas the R_h of the reference expands during heating and shrinks during cooling, the R_h of the sample behaves inversely, as it is expected for rHDA caused de- and HDA caused repolymerization.

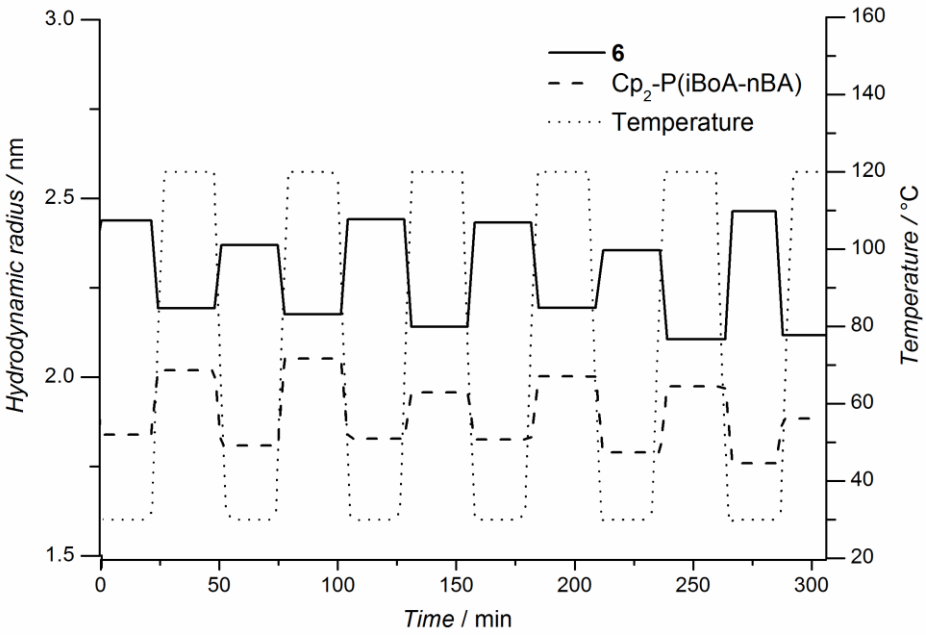

Figure 4.12 Temperature dependent DLS experiments of HDA polymer **6** (M_n = 34200 g·mol^{-1}) and Cp_2-P(*i*BoA-*n*BA) (M_n = 13000 g·mol^{-1}). The traces in the diagram present the average of the R_h of **6** (solid line) and Cp_2-P(*i*BoA-*n*BA) (dashed line) during the temperature (dotted line) cycling between 30-120 °C. TCB was employed as solvent and both samples had a concentration of 17 mg·mL^{-1}.

To further explore the depolymerization and to analyze the depolymerized structure, on-line HT-NMR analysis of polymer **6** was carried out. Similar to the on-line HT-NMR experiments of **3**, the spectra of **6** and Cp_2-P(*i*BoA-*n*BA) were recorded in toluene-d_8 with a relaxation time of 1 s and 100 scans. With this set up, polymer **6** was cycled between 40 °C and 120 °C, similar to the HT-DLS experiment. As compound **3** and **6** contain the same HDA linkage, the proton resonances of the double bond appear at 40 °C at the same shifts(5.7 and 5.9 ppm; refer to Figure 4.13, top three spectra). The Cp end group resonances of Cp_2-P(*i*BoA-*n*BA) are found at 6.1 to 6.6 ppm. A spectrum of Cp_2-P(*i*BoA-*n*BA) recorded at 120 °C uncovered that the shift of the Cp end group resonances is not influenced by temperature. At 120 °C, polymer **6** showed the expected Cp signal between 6.1 and 6.6 ppm. When cooled to 40 °C, the Cp resonances vanished again, implying a full repolymerization of the end groups. To confirm the reversibility also via the on-line HT-NMR technique, the cycling between 40 °C and 120 °C was repeated two times, yielding spectra which perfectly match each other when taken at the same temperature (Figure 4.13, bottom five spectra). To determine the percentage of

debonding of **6** at 120 °C, the integral values of the HDA product resonances and the Cp resonances were compared. With approximately 37 mol% of starting material at 120 °C, the system is well suitable for bonding/debonding applications. The debonding is even stronger than for the N-maleimide/furan system of Chen *et al.* (12% debonding at 130 °C for 25 min), although it has to be noted that their values are obtained by solid state analysis of a network. Overall, the HT-NMR and HT-DLS results evidence the system's reversibility, stability, lack of hysteresis and structure of the debonded state. Moreover, the on-line HT-NMR results point to an extremely fast equilibrium that is reached already after 15 min.

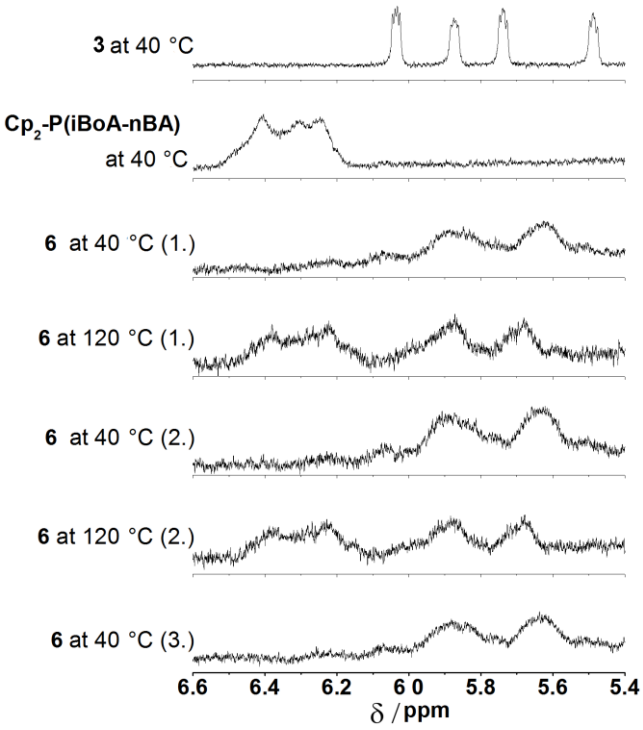

Figure 4.13 Temperature dependent ^{1}H NMR spectra of HDA polymer **6**. The stacked spectra depict a zoom into the double bond region of the starting materials for the HDA polymerization **3** and Cp_2-P(*i*BoA-*n*BA) (two upper spectra) as well as the spectra of **6** recorded during the cycling between 40-120 °C (five lower spectra). The two cycles were recorded in toluene-d_8 with a concentration of 20 mg·mL^{-1}.

4.5 Bonding/debonding reaction kinetics of the step-growth polymer

In an effort to observe the depolymerized state of the HDA polymer **6** and to understand the kinetics of the polymerization and depolymerization processes in detail, the reactions were additionally performed in a temperature dependent UV-Vis instrument, which permits the on-line observation of the evolution of the CDTE di-linker during the reactions. Each step of the reversible process, deprotection of **3,** polymerization of deprotected **3** with Cp_2-P(*i*BoA-*n*BA), and depolymerization of **6**, was analyzed separately. To assess the kinetics of the deprotection step, an ambient temperature solution of **3** in toluene was injected into a 100 °C preheated cuvette containing a small amount of toluene and was immediately analyzed for absorption at 347 nm over 5 min (value taken every 0.16 s). The small amount of toluene that was heated with the cuvette served to drastically reduce the time required for the solution of **3** to attain 100 °C. The change in the absorption at 347 nm over time revealed that the deprotection of **3** is essentially already complete after 2.5 min. Next, the kinetics of (re)polymerization (to form **6**) were characterized by first heating **6** to obtain the depolymerized state of the system and subsequently observing the repolymerization process by UV-Vis spectroscopy. More specifically, a solution of **6** in toluene was heated to 110 °C for 5 min, added immediately into the cuvette held at 20 °C in the UV-Vis spectrophotometer, and then analyzed for absorption at 347 nm, which was recorded every 0.16 s for 5 min. The results of the analysis, plotted in Figure 4.14, indicate that the repolymerization of deprotected **3** with Cp_2-P(*i*BoA-*n*BA) is even faster than the deprotection step with reaction completion occurring after just 1 min of cooling to 20 °C. Finally, characterization of the depolymerization step, which was performed utilizing the same procedure as that employed to assess the deprotection reaction, suggests that depolymerization of **6** takes 4 min to reach equilibrium. The fact that this step takes longer than either of the other two steps is not surprising considering the greater heat capacity of the HDA polymer compared to the building blocks, Cp_2-P(*i*BoA-*n*BA) and **3**.

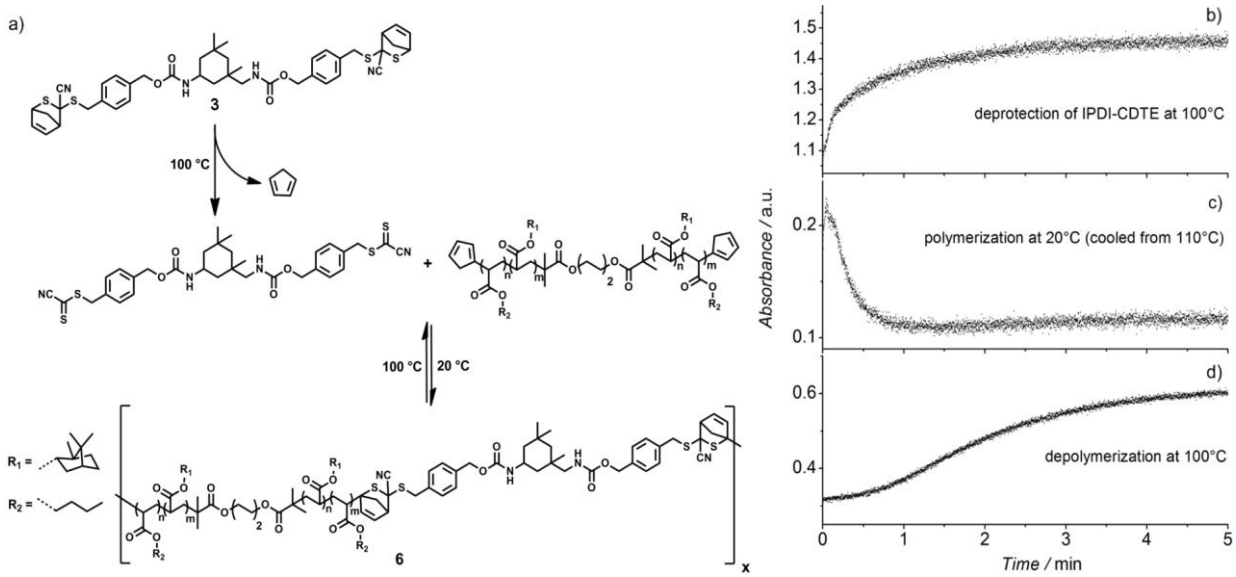

Figure 4.14 Absorption traces, recorded at 347 nm, of all three processes presented on the left side, vs. time. The left side scheme. a) depicts the three processes. Spectrum b) shows the deprotection of **3** by heating to 100 °C, c) depicts the forward polymerization of deprotected **3** with Cp_2-P(*i*BoA-*n*BA) when heated to 110 °C and cooled to 20 °C, d) shows the depolymerization of **6** when heated to 100 °C. On the left side, the polymerization process is schematically depicted.

All three traces demonstrate that none of the processes takes more than 5 min to reach the equilibrium state, which is indicated by the plateauing of the absorption signal. It should be noted that the y-axis scale differs for each graph because the molar concentration of released CDTE-di-linker for each solution differed. Additionally – although evidenced by on-line HT-NMR that **6** is not 100% depolymerized at 100 °C – instrument limitations prevented the characterization of the depolymerization process at higher temperatures. Regardless, the entire process of de- and re-polymerization at 100 °C takes a total of only 5 min. It is reasonable to assume that the equilibrium for each reaction step is reached within a similar time frame at higher temperatures.

4.6 Conclusions

In the current chapter a new reversible, fast, and catalyst free HDA reaction based on CDTE was developed. A novel synthetic approach for isolating functionalized CDTEs, suitable for further chemistry, employing an *in situ* trapping with Cp, was pioneered. The rHDA behavior of the Cp protected CDTE was explored by temperature dependent on-line UV-Vis and NMR spectroscopy as well as by ESI-MS measurements. All experimental techniques demonstrated the reversibility of the HDA reaction and the relatively low rHDA temperature. The practical relevance of the new bonding/debonding on demand chemistry was explored in a polymer system by generating a CDTE-based di-linker, which was polymerized with a bis-Cp polymer (i.e., di-functional diene) in a HDA-based step-growth polymerization reaction. The AA-BB polymer obtained was demonstrated to undergo reversible polymerization by SEC analysis, pre and post *in situ* trapping of the polymer with DMBD, and high temperature on-line dynamic light scattering as well as ^{1}H NMR spectroscopy. Time resolved on-line UV-Vis measurements revealed a rapid CDTE deprotection, polymerization and depolymerization. None of the three steps required more than 5 min reaction time. Thus, the HDA reaction presented is a key innovation in heat triggered, reversible covalent bond-based systems.

5 Alternative Cyanodithioester Synthesis Approaches – A Cost Reduction Strategy

The presented CDTE/Cp HDA pair displays great reversible properties for the use in self-healing materials application. However, the synthesis of di-linker molecule **3** contains expensive starting materials as well as a complex purification work up, i.e. column chromatography. Considering the need of simple and cheap synthetic strategies for industrial products, an alternative linker molecule had to be designed, satisfying the industrial demands. Important points to consider for the new linker molecule synthesis comprised:

- Cheap, non toxic and readily available starting materials.
- simple purification (i.e. no column chromatography).
- minimal number of reaction steps.
- no sophisticated reaction conditions.
- lack of byproducts.
- if byproducts occurred they should be non-toxic.
- multiple HDA functionalities to act as a multi-linker.

The first six points represent general factors industrial processes have to address during the developing phase of the process. However, the last point becomes important for further applications of the novel CDTE/Cp chemistry. Designed for self-healing material applications, the new HDA pair has to be incorporated in polymer matrixes, generating adaptable networks. Cp moieties tend to dimerize rapidly preventing the use of a multi-functional Cp linker molecule for the network formation. Consequently, a new linker molecule bearing at least three CDTE functions had to be synthesized, in order to form network structures. Among the three dithioester synthesis strategies, two can already be discarded for an industrial process. Thiophosgene represents a highly toxic compound with expensive substitute chemicals, requiring column chromatography purification after the substitution reaction. P_2S_{10} and the Lawesson's reagent on the other hand produce the dithioester species in insufficient yields while generating plenty of byproducts. Thus,

the reaction with a cyanodithioate salts was the best possibility for a suitable linker synthesis. Nevertheless, the reaction to the cyanodithioate salt contains carbon disulfide, sodium cyanide and dimethylformamide, i.e. highly toxic substances. Regardless, the synthesis via a dithioate salt is still suitable for an industrial process as it is also possible to generate the salt via the sulfur oxidation of chloro-cyanomethane with sulfur and a base, circumventing the toxic compounds.

Lab scale synthesis

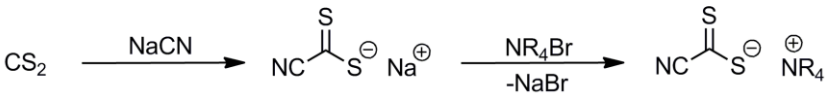

Industrial suitbale synthesis

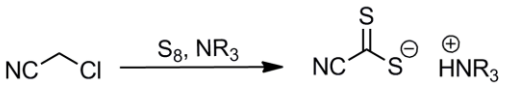

Scheme 5.1 Two synthetic routs to the cyanodithioate salt.[180,185] The lab scale strategy contains a second step, the transformation of the sodium to an ammonium salt. This second step was necessary to produce a stable (i.e. storable) cyanodithioate salt in order to use in every reaction sequence the same batch of the salt.

However, for the exploration of a new synthesis at the lab scale, carbon disulfide and sodium cyanide were employed for the cyanodithioate generation, starting from already available starting materials. Therefore, the following reaction sequences will always start form the cyanodithioate salt, produced from carbon disulfide and sodium cyanide, assuming that for an industrial process the alternative reaction via chloro-cyanomethane, sulfur and a base is employed. The following chapter describes the search and development of an industrial friendly synthesis to a multifunctional linker molecule able to generate adaptable networks with a suitable diene linker molecule.

5.1 Identifying an industrial viable route to cyanodithioester

When designing the synthesis of a multi-linker it is always important to be aware of how to construct the basic structure of the functional molecule. The design can either occur by direct attachment of the functional group to a core structure, or require the transformation of the desired functional group into another functionality, more suitable for linking to the core unit.

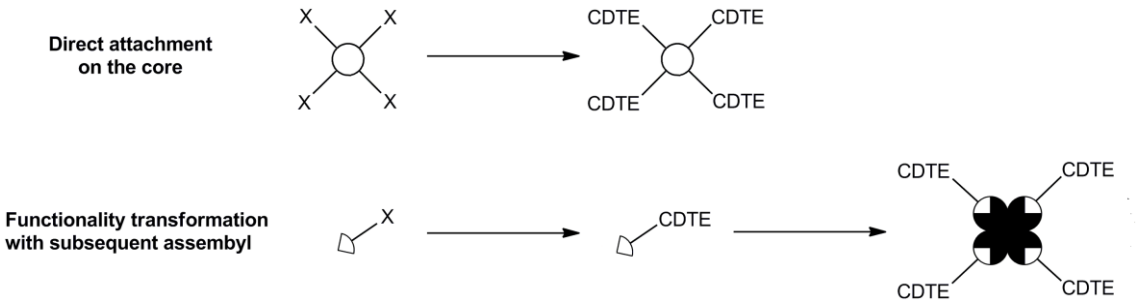

Scheme 5.2 Different synthetic approaches to a linker molecule. Either via the direct functionalization of a core molecule or by the two step synthesis of a functionalized precursor which is subsequently linked to the core.

In the case of the cyanodithioate salt, it appeared to be reasonable to transform the salt initially into a trapped CDTE compound with a suitable handle rather than converting it directly on a core molecular structure into trapped CDTE units, due to the lower yields obtained in the synthesis of molecules **1a** and **1b**. Following the above strategy, a clean and simple conjugation reaction, such as an esterification, amidation or an isocyanate addition, would be ideally suitable to link a functionalized trapped CDTE compound to a multifunctional core molecule. However, a suitable reaction yielding the functionalized trapped CDTE had to be found first. Therefore, the nature of the cyanodithioate salt had to be considered. In general, dithioate salts represent soft nucleophiles with variable reactivities, depending on the attached functional group of the dithioate salt. The cyano group, as a strong electron withdrawing group, stabilizes the negative charge in the anion and leads to a less reactive nucleophilic species. Nevertheless, the synthesis of linker molecule **3** showed that the cyanodithioate salt can react as nuclophile in substitution reactions. Consequently, different reactions strategies for nucleophiles were applied to the cyanodithioester salt in order to generate a functionalized trapped CDTE molecule.

The ring opening of epoxides is considered as a *click* reaction when performed with stronger nucleophiles such as amines and thiols, representing an extreme atom-economic reaction.[7,186] Thus, the first synthetic strategy focused on the ring opening reaction of epoxides by the cyanodithioate salt in the presence of Cp, targeting a trapped CDTE species with an alcohol group. Styrene oxide represents a cheap and readily available epoxide compound which is additionally activated for the ring opening reaction, giving hope to obtain the opened epoxides trapped CDTE species in quantitative yields. Accordingly, the salt was converted with styrene oxide, at various temperatures (i.e. ambient, 50 °C) in a range of solvents (acetonitrile, acetone, ethanol) for different times (2 h, 4 h, 24 h) and analyzed via ^{1}H NMR spectroscopy.

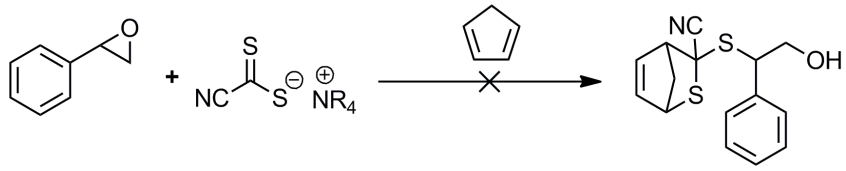

Scheme 5.3 Attempted ring opening reaction of styrene oxide with the cyanodithioate salt.

The obtained ^{1}H NMR spectra (refer to Figure 5.1) revealed the conversion of the characteristic epoxides resonances, yet lacked the typical HDA C=C double bond signals between 5 and 7 ppm (refer to Figure 4.7). Moreover, the recorded spectra displayed multiple resonances between 1 and 5 ppm, pointing to several side reactions occurring during the epoxide opening. In an effort to optimize the reaction and catalyze the ring opening of styrene oxide by the cyanodithioate salt, Lewis acids which are known to support the ring opening of epoxides,[187] were added to the reaction. Unfortunately, the catalyst addition had no effect on the conversion to the epoxides opened trapped CDTE molecule. Therefore, the ring opening reaction of epoxides by the salt was discarded for the synthesis of a functionalized trapped CDTE compound.

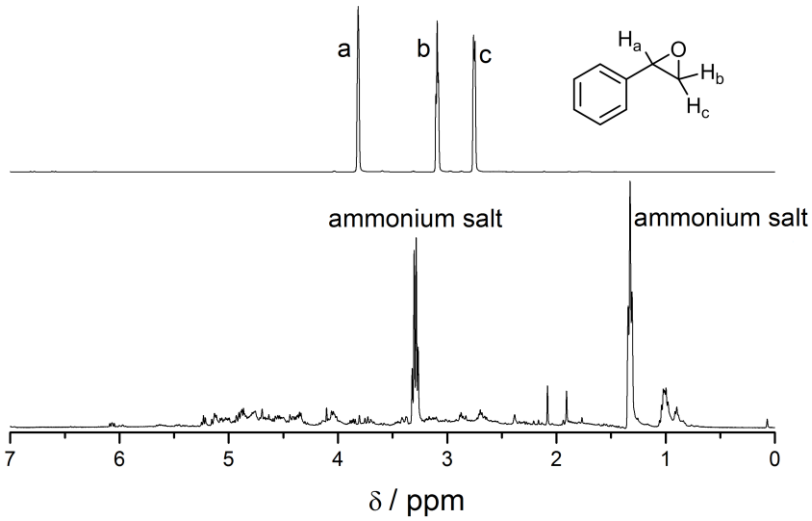

Figure 5.1 ^{1}H NMR spectra of styreneoxide (upper spectrum) and of the reaction mixture from the reaction between styreneoxide and cyanodithioate salt, recorded in deuterated chloroform-d.

As an alternative suitable synthetic strategy to a functionalized trapped CDTE molecule, a Michael addition reaction was explored. Acrylates contain an electron withdrawing carbonyl group with a negative mesomeric effect, activating the carbon double bond for the Michael addition with nucleophiles. The soft electrophilic position 4 on the acrylate Michael system is suitable for the attack of soft nuclephiles such as the cyanodithioate salt. Furthermore, the Michael addition on activated carbon double bonds of amines and thiols is considered as an atom economic *click* reaction similar to the ring opening reaction of epoxides,[7,188] fulfilling the characteristics required for the synthesis of a multi-linker. 2-Hydroxyethyl acrylate (HEA) is such an activated Michael system, having an alcohol function as possible handle and being a cheap starting material for industrial processes. Consequently, the Michael addition on HEA of the cyanodithioate salt was targeted. However, the *in situ* HDA trapping strategy with Cp could not be employed in the case of HEA, as the electron poor double bond of the Michael addition represents a DA activated dienophile which would rather rapidly react with Cp before adding the salt onto the double bond. It was believed that the Cp could be added after the successful conjugation to the reaction as the dimerization of formed CDTE should proceed slowly, given the fact that no leaving group or nucleophile is present.

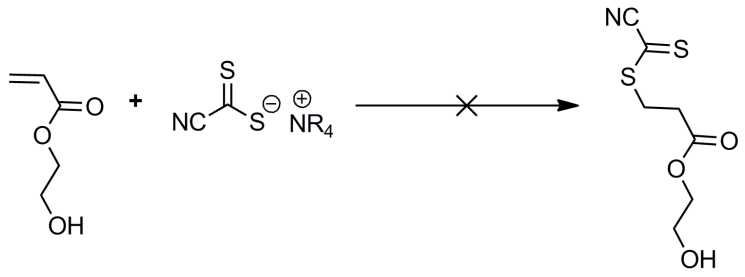

Scheme 5.4 Attempted Michael addition reaction of the cyanodithioate salt on HEA.

Therefore, the Michael addition was initially performed without Cp. Despite varying temperature (ambient, 50 °C) and solvent (acetonitrile, acetone, ethanol), no reaction of the acrylate unit was observed. ^{1}H NMR spectra recorded prior and after stirring for 24 h matched perfectly, implying that no reaction of the Michael system had occurred at all. Thus, it was concluded that the cyanodithioate salt is too unreactive for the attack on the here applied Michael system.

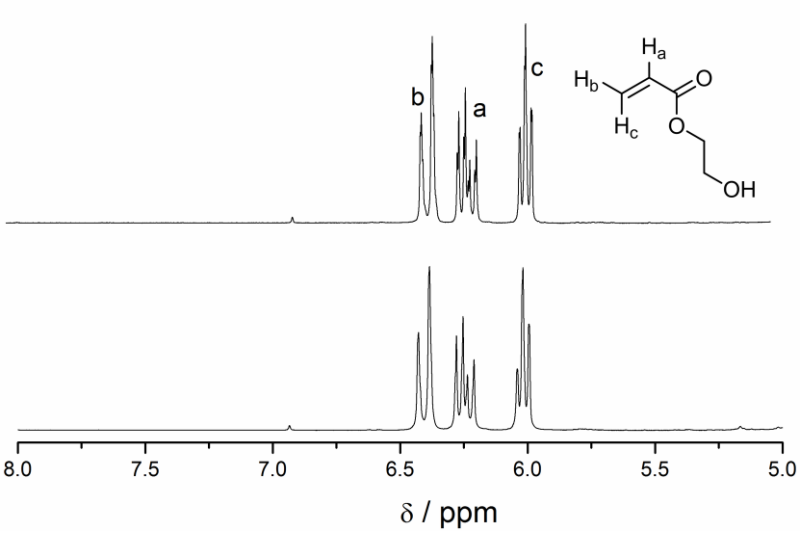

Figure 5.2 ^{1}H NMR spectra of HEA (upper spectrum) and the reaction mixture from the reaction between HEA and cyanodithioate salt, recorded in deuterated DMSO-d_6.

The third targeted reaction for the functionalized trapped CDTE molecule synthesis is based on a nucleophilc substitution reaction of the cyanodithioate salt. In contrast to the epoxides ring opening and Michael addition reaction, the simple nucleophilic substitution is not considered as a *click* reaction and displays no atom economy;

however, the cyanodithioate salt showed at least some reactivity towards the nucleophilic substitution in the synthesis of molecule **1a** and **1b**, in contrast to the aforementioned reactions. The synthesis of **1a** and **1b** proceeded with benzyl bromine derivatives which are known to be activated for SN2 reactions. Accordingly, a compound suitable for a SN2 reaction with a primary carbon atom, bearing a good leaving group for the nucleophilic substitution and being readily available, such as tosylethanol, was employed. Tosylethanol was synthesized by a simple reaction between tosylcholride and an excess of ethylenglycol, yielding the desired tosylethanol pure after washing with water and subsequent recrystalization from ethanol.

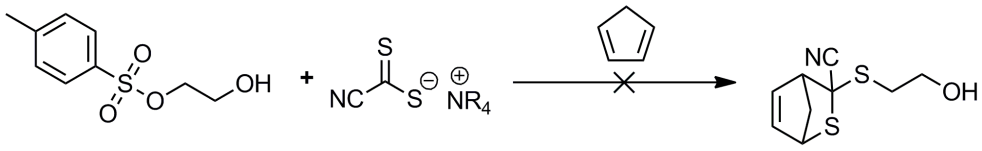

Scheme 5.5 Attempted nucleophilic substitution of tosylethanol with the cyanodithioate salt.

The nucleophilic substitution with the cyanodithioate salt would certainly not proceed to full conversion, but it was thought that the remaining unreacted starting material could be separated by washing and recrystalization. In the following, cyanodithioate, tosylethanol and Cp were dissolved in acetone and stirred for 24 h at ambient and elevated temperature (50 °C). The resulting ^{1}H NMR spectra revealed a shift of the aromatic tosyl resonances, but exhibited no signals in the double bond region where the HDA product of the *in situ* trapped CDTE was expected.

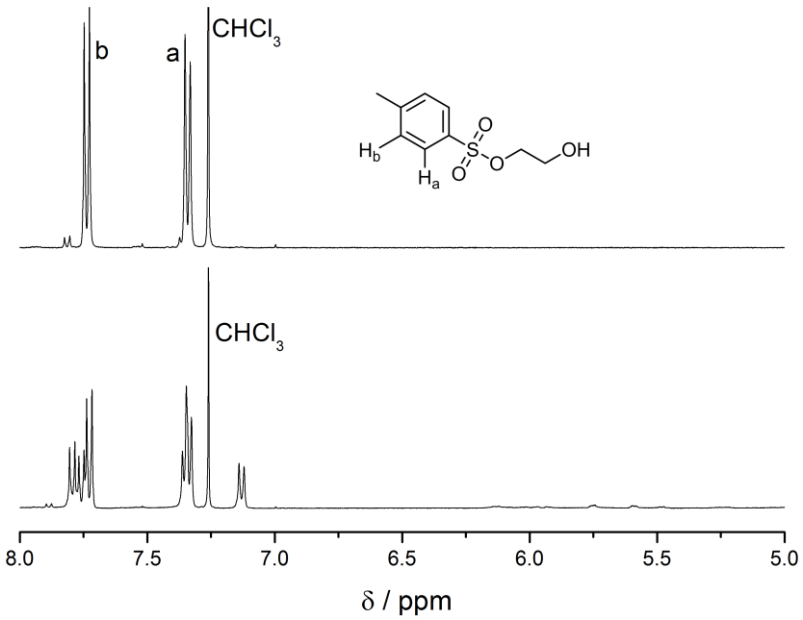

Figure 5.3 ^{1}H NMR spectra of tosylethanol (upper spectrum) and the reaction mixture from the reaction between tosylethanol and cyanodithioate salt, recorded in deuterated chloroform-d.

Consequently, it was concluded that the cyanodithioate salt would either be sufficiently reactive to exchange the tosyl group or that the generated CDTE molecule would not be sufficiently reactive in a HDA reaction. Considering the reactivity of the salt in the ring opening and the Michael addition reaction, the low reactivity seemed to be more reasonable. However, the reduced reactivity in the nucleophilic substitution on the tosylethanol showed – interestingly – that reduced sterical hindrance was not the main issue for the reactivity of the cyanodithioate salt in the SN2 reaction with benzyl bromine. Rather stereoelectronic effects can be attributed for the reactivity of the cyanodithioate salt. At the benzylic positions the carbon center is partly sp^2 hybridized, favoring the plane SN2 transition state and stabilizing the attack of a nucleophile. Moreover, the antibonding π* MO of the aromatic ring can interact with the antibonding $\sigma^*_{C\text{-}X}$ of the leaving group, lowering the energetic level of the $\sigma^*_{C\text{-}X}$ MO which supports the nucleophilic attack.

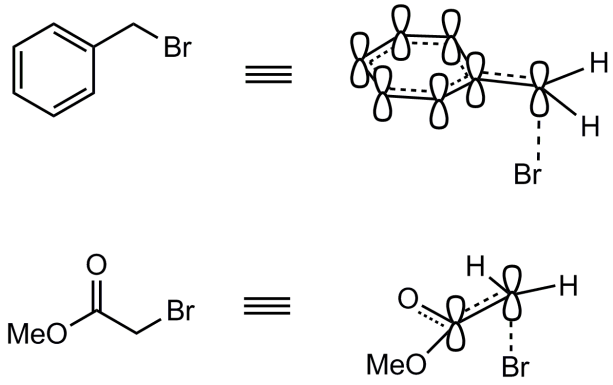

Scheme 5.6 Mesomeric structures of benzylic and α-halogen carbonyl functions, which are activated towards SN2 reactions due to the sp^2 hybridized carbon center, favoring the plane SN2 transition state.

Taking the stereoelectronic effect of benzylic positions into account, another starting material, containing a primary halogen compound in conjugation to a π-electron system (preferably with an electron withdrawing group), had to be employed. A cheap and simple molecule which fulfilled the demands was 2-bromo methylacetate.

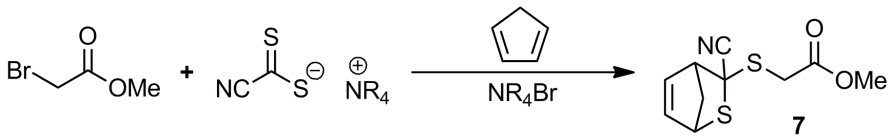

Scheme 5.7 Successful synthesis of an *in situ* trapped CDTE molecule from the reaction between cyanodithioate salt and 2-bromo methylacetate.

A first reactivity test of 2-bromo methylacetate towards the SN2 reaction with the cyanodithioate salt in acetone, pointed to extremely high reaction rates, as a solid – likely the bromine ammonium salt and elemental sulfur – precipitated immediately from the reaction mixture before adding Cp. This observation is associated with the successful formation and subsequent dimerization of the CDTE species within seconds. Indeed, the obtained ^{1}H NMR spectrum of the resulting mixture displayed a set of resonances in the double bond region between 5 and 7 ppm, matching perfectly with the HDA double bond signals of molecule **3** (refer to Figure 4.7). With respect to the observation of the 2-bromo methylacetate and cyanodithioate mixing, the order of compounds added to the solution was changed when repeating the

experiment. After dissolving the cyanodithioate salt in acetone, three molecular equivalents of Cp were added before adding the 2-bromo methylacetate. Consequently, only a minor amount of solid precipitated, implying that the dimerization process was suppressed and only the bromine ammonium salt precipitated. Surprisingly, the ^{1}H NMR study revealed that the nucleophilic exchange between the bromine and the cyanodithioate salt with subsequent HDA *in situ* trapping processes with quantitative conversion to compound **7**.

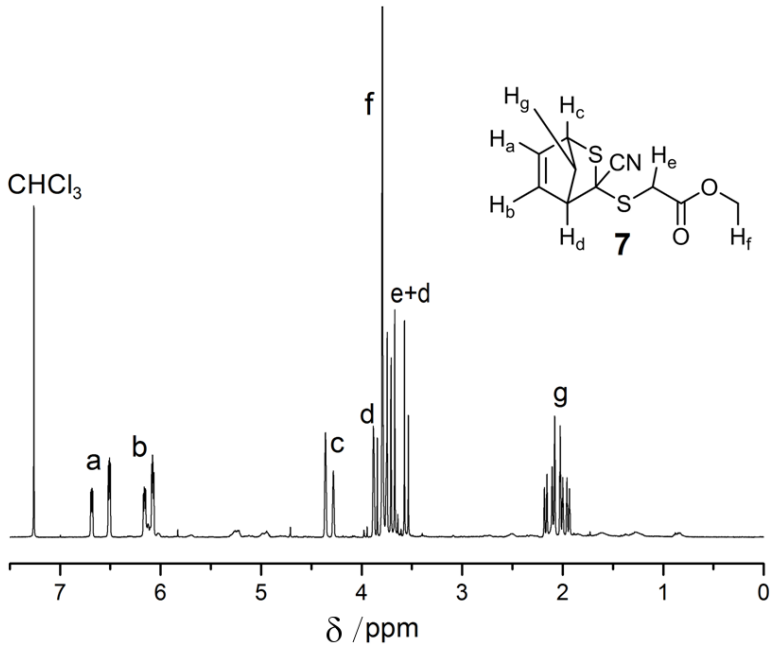

Figure 5.4 ^{1}H NMR spectrum of the crude reaction product **7** from the nucleophilic substitution between 2-bromo-methylacetate and cyanodithioate recorded in chloroform-d. A quantitative conversion is achieved within 1 h.

Quantitative conversion can be expected from a stereoelectronical point of view, as the conjugation to the electron withdrawing carbonyl function lowers the antibonding $\sigma^*_{C\text{-}X}$ more than the benzene ring which supports the nucleophilic substitution reaction and increases the reaction rate. However, the reaction was performed on a milligram scale. When scaling up the synthesis to gram scale, an excess of the cyanodithioate salt was required to obtain a high conversion which had to be removed by silica gel filtration. Moreover, even with an excess of the cyanodithioate salt, a quantitative conversion was not achieved. Best yields are close to 90%.

5.2 Reversibility of the new trapped cyanodithioester molecule

Although the new synthesis yielded CDTE bearing·molecules in high yield, the effect of the proximity to the carbonyl function on the reversible CDTE/Cp HDA pair was uncertain. In order to explore whether the reaction of the new CDTE molecule **7** was as reversible as the benzyl structure based molecules, such as **3**, temperature dependent spectroscopy experiments were conducted. First, on-line UV-Vis spectroscopy experiments were carried out to assess the tendency of **7** to undergo the rHDA reaction. The same set up as for the temperature dependent UV-Vis spectroscopy cycling of **2** was employed (refer to Figure 10.1). However the experiment was slightly changed in order to improve the data base. In contrast to the monochromatic UV-Vis temperature cycling experiment of **2**, a full spectrum of **7** was recorded at each temperature step. Therefore, hysteresis was immediately discarded for the cycling process, as a result of the perfect match of the absorption spectra at each temperature. For the measurements, **7** was dissolved in toluene and consecutively heated to 100 °C and cooled to 20 °C in a sealed cuvette. The recorded spectra are depicted in Figure 5.5.

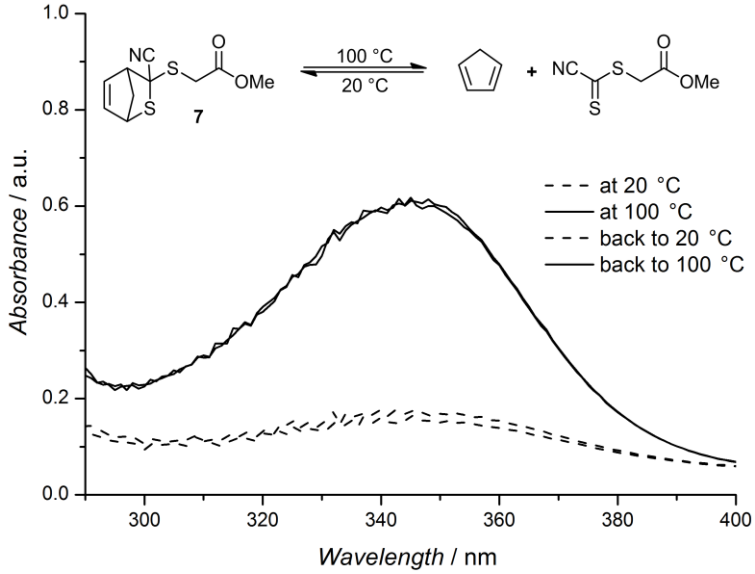

Figure 5.5 UV-Vis spectra of compound **7** recorded during the temperature cycling between 20 °C and 100 °C.

Equally to the recorded UV-Vis spectra of **2** (Figure 4.1) the obtained data of molecule **7** display an increasing absorption between 300 and 400 nm at elevated temperature, which can be attributed to the π-π* transition of free CDTE. During the

cooling phase to 20 °C, the absorption decreases to the starting point, associated with the complete reoccurring of the HDA reaction. In addition to UV-Vis spectroscopy, temperature dependent ^{1}H NMR spectroscopy was performed to quantify the percentage of debonding. Identical to the temperature dependent ^{1}H NMR spectroscopy cycling of di-linker **3**, molecule **7** was dissolved in toluene-d_8 in a NMR pressure tube with a concentration of 0.02 mol·L^{-1}.

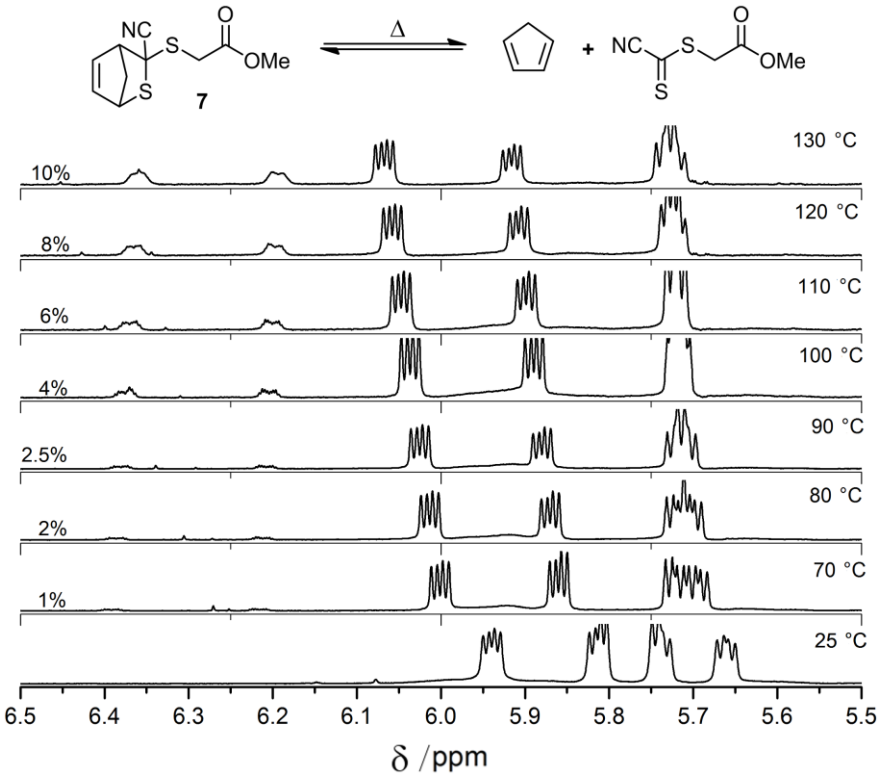

Figure 5.6 Zoom into the region between 5.5 and 6.5 ppm of stacked temperature dependent ^{1}H NMR spectra of **7** recorded in toluene-d_8 during the temperature cycling. Next to the HDA product resonances of **7**, a set of signals that corresponds to free Cp can be identified, increasing with the temperature. On the left hand side to the increasing peaks, the calculated mol% of deprotected **7** is depicted. The resonance set disappears again when cooled below 70 °C. In addition, a general shift of all signals towards lower field can be observed, associated with the increasing temperature.

The obtained spectra, recorded at elevated temperatures and depicted in Figure 5.6, are in excellent agreement with the UV-Vis cycling experiment of **7** and display the same bonding/debonding behavior as **3**. The rising Cp resonances at lower field decrease during cooling and increase by heating in the same fashion as in the temperature dependent ^{1}H NMR experiment of **3**. In addition, the rHDA on set temperature for the HDA equilibrium of **7** lies with 70 °C at the same value the HDA

equilibrium of **3**. Nonetheless, the percentage of debonding differs from the debonding values obtained for di-linker **3** at the given temperature. This finding can be explained by the calculation of the debonding and the nature of the molecules **3** and **7**. The noted values represent the percentage of debonding in mol%. Considering that linker **3** is bi-functional whereas molecule **7** is mono functional, the concentration of functional groups is doubled in the solution of **3** compared to the solution of **7**, resulting in a higher percentage of Cp at elevated temperatures. With respect to the UV-Vis and the NMR results of **7**, it can be concluded that the proximity of the trapped CDTE unit to the carbonyl group has no effect on the reversibility of the HDA equilibrium. To further substantiate the hypothesis, the reaction time for the rHDA reaction was determined via UV-Vis spectroscopy. As in the experiment for di-linker **3**, molecule **7** was dissolved in toluene in a sealed cuvette and placed in the heated UV-Vis spectrometer, recording the absorption of the mixture at 347 nm (refer to Figure 5.7).

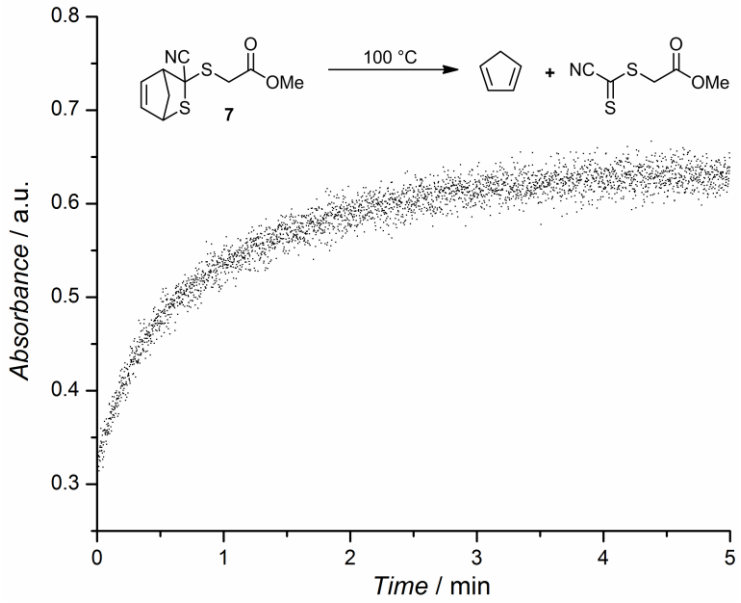

Figure 5.7 Absorption spectra, recorded at 347 nm for the deprotection process of **7**.

The absorption increases and reaches a plateau after approximately 3 min, symbolizing the equilibrium of the HDA reaction at 100 °C. The reaction time of 3 min lies in the same time range as the deprotection of di-linker **3**, giving final evidence for the same temperature dependent kinetic rates of molecule **7** compared to **3**.

5.3 Synthesis of a tetra-functional linker molecule

Proven to provide a molecule with the same reversible properties as the benzylic species **3**, the synthesis of **7** had to be implemented in a multi-linker synthesis. Given the quantitative yields obtained from the nucleophilic substitution reaction, it was believed that the linker could be generated by direct attachment of the trapped CDTE onto a core molecule. Consequently, a core structure with the appropriate α-halogen carbonyl function had to be designed. A simple and cheap synthetic strategy to introduce such α-halogen carbonyl functions into a molecule, is the esterification reaction with the respective acid. Therefore, a multi functional alcohol species, pentaerythritol, was reacted with the acidic bromine (2-bromoacetyl bromide) to obtain the tetra-functional precursor molecule **8**.

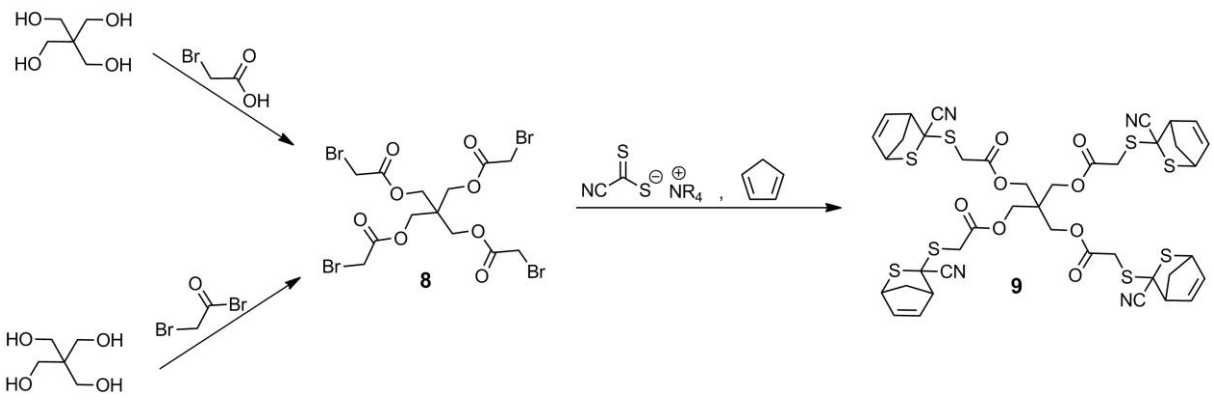

Scheme 5.8 Novel synthetic strategy to multi-functional trapped CDTE molecules.

The use of water soluble starting materials (i.e., pentaerytritol, and 2-bromo acetic acid, resulting from the quenching of 2-bromoacetyl bromide) simplified the purification as both starting materials as well as partly esterified pentaerytritol, could be removed by multiple washing with water. Despite the simple, industrially friendly work up, the synthesis had to be modified because of the corrosive byproduct hydrogen bromide. Accordingly, the acidic bromine was substituted in the reaction by the carboxylic acid which reacted under modified conditions as readily as the acidic bromine, producing only water as an industrial friendly byproduct. Finally, the precursor molecule **8** was utilized in the nucleophilic substitution reaction with the cyanodithioate salt and *in situ* trapped with Cp. Consequently, the pure tetra-functional linker molecule **9** was obtained after multiple washing procedures to

remove precipitated ammonium salt. The recorded ^{1}H NMR spectrum of **9** revealed no remaining starting materials as well as a reasonable purity of approximately 95%.

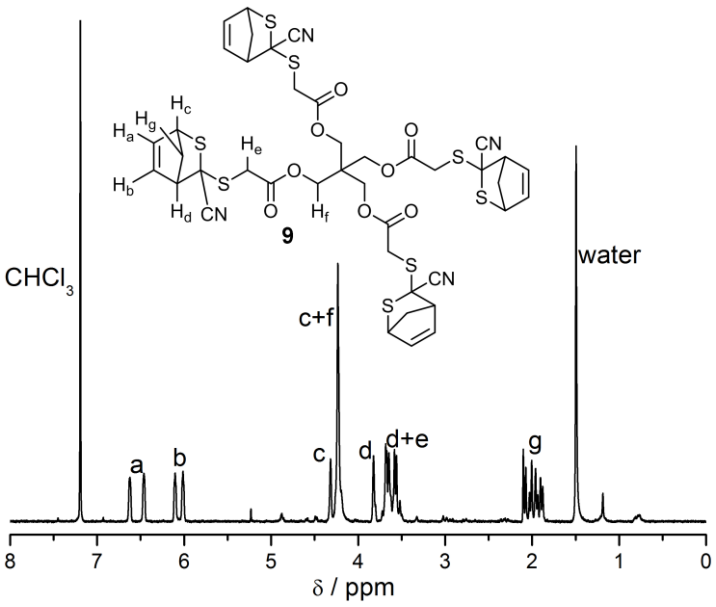

Figure 5.8 ^{1}H NMR spectrum of the crude tetra-linker **9**, recorded in chloroform-d.

5.4 Conclusions

The presented study has demonstrated the complexities associated with the introduction of CDTE units in a molecule. Several attempts via a ring opening reaction of epoxides, a Michael addition on acrylates or a nucleophilic substitution on primary tosylates failed in producing a functional CDTE molecule. However, by closer inspection of the failed reactions, the importance of stereoelctronic factors for the nucleophilic substitution reaction of cyanodithioates was realized. As a result, the highly efficient substitution on α-halogen carbonyl functionalities with the cyanodithioate salt was conducted and explored for the very first time. Temperature dependent ^{1}H NMR and UV-Vis spectroscopy experiments of the novel trapped CDTE molecule ensured that the new chemical structure and surrounding of the HDA product had no effect on the reversibility and reaction kinetics. Thus, the substitution on α-halogen carbonyl functions was combined with a simple esterification reaction to design an industrial friendly synthesis strategy for the tetra-linker molecule **9** via the synthesis of precursor **8**. The new synthesis is based on extremely cheap starting materials, yielded only salts and water as byproducts and required no complex purification by column chromatography to obtain a multifunctional molecule in moderate purities.

6 Reversible Networks Based on Cyanodithioester Chemistry – A New Designed Self-Healing Material[iii]

Following the development and study of the novel fast, catalyst free, reversible CDTE/Cp HDA chemistry as well as the cheap and simple synthesis of a multi-functionalized linker molecule, the transfer to material science was targeted. Therefore, an adaptable network based on the new tetra-linker **9** and Cp_2-P(*i*BoA-*n*BA) was generated and analyzed for its self-healing properties. In the following chapter the generation as well as the performed self-healing tests of the CDTE/Cp based adaptable network is presented. The cross-linked character of the material is qualitatively analyzed by a swelling test, whereas the adaptable character of the obtained network is demonstrated by temperature dependent complex viscosity cycling between 40 °C and 120 °C. The characteristic transitions of the storage (G`) and the loss (G``) moduli unambiguously demonstrate that a cross-linked network is formed, revealing a glassy state, the glass transition state, the rubber plateau, and after release of the cross-linking points, a liquid state. Furthermore, repetitive tensile tests of original and healed samples are conducted to assess the healing efficiency after each cycle, while temperature dependent solid-state NMR is utilized to explore the chemical structure of the material in its heated state.

[iii] Parts of the current chapter were reproduced from K. K. Oehlenschlaeger, J. O. Mueller, J. Brandt, S. Hilf, A. Lederer, M. Wilhelm, R. Graf, M. L. Coote, F. G. Schmidt, C. Barner-Kowollik, *Adv. Mater.* **2014**, DOI: 10.1002/adma.201306258, with permission from John Wiley & Sons, Inc. all rights reserved. The temperature dependent MAS ^{1}H NMR spectra were recorded at the Max-Planck-Institut for polymer science in Mainz by Dr. Robert Graf.

6.1 Network formation

With the novel CDTE tetra-linker **9** in hand, the formation of a HDA based network with the available Cp_2-polymer (P(*i*BoA-*n*BA), M_n = 12,000 g·mol^{-1}, $Đ_M$ = 1.4) was targeted. Accordingly, a homogeneous solution of **9** and Cp_2-P(*i*BoA-*n*BA) was prepared in anisole with a molar ratio of 1:2 and a molar concentration of 0.01 mol L^{-1} of **9**. The viscous solution was subsequently introduced into a 120 °C heated teflon template and held for 2 h. After cooling to ambient temperature, the desired network **10** was obtained.

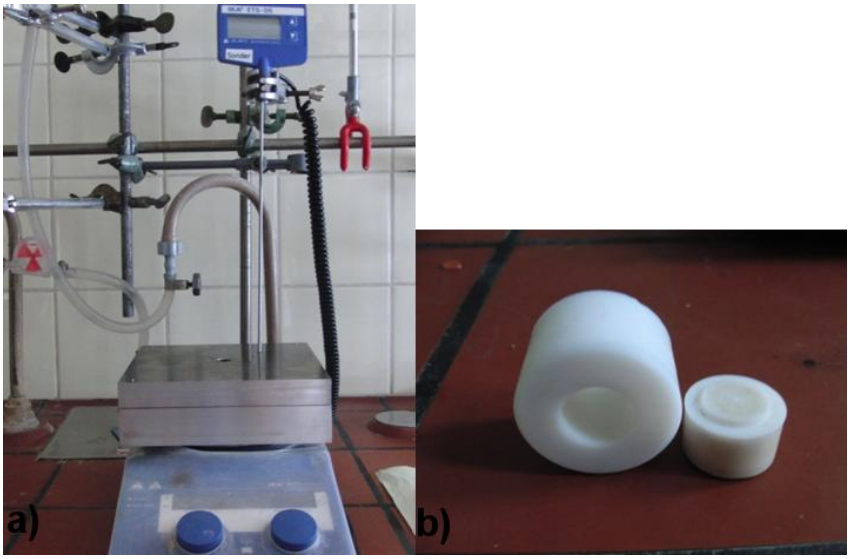

Figure 6.1 a) Picture of the network template: alluminium block (heated to 125 °C). The hole in the middle of the block is the reaction chamber and contains two teflon inlets b), which can be removed from the block.

Elevated temperature is essential for the synthesis of the cross-linked material as it triggers the rHDA reaction of linker **9**, necessary to remove the Cp protecting group. The unprotected linker species (i.e. the cyano dithioester) reacts upon cooling with the Cp end groups of Cp_2-P(*i*BoA-*n*BA) to form network **10** (refer to Scheme 6.1). The use of anisole as high boiling solvent, which evaporates slowly at 120 °C, supports the immediate vaporization of the released Cp. Thus, the HDA equilibrium cascade is driven towards the unprotected linker species, resulting in high conversions (84 wt% gel) compared with cross-linking reactions performed neat (34 wt% gel).

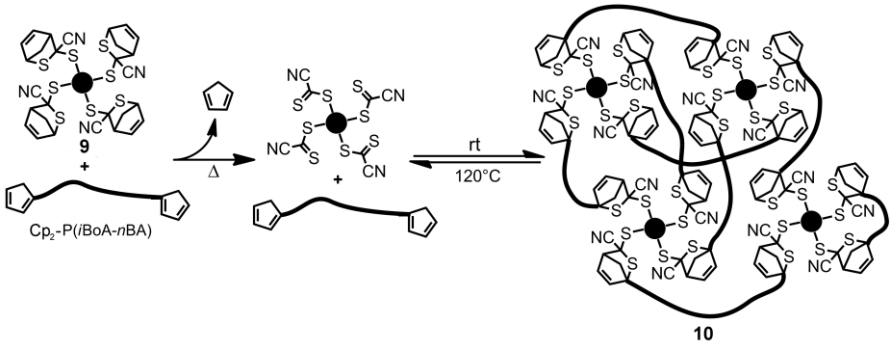

Scheme 6.1 Network formation of **10** via HDA/rHDA chemistry during the deprotection of tetra-linker **9** in the presence of Cp_2-P(*i*BoA-*n*BA) as well as the idealized schematic cycling process.

However, at elevated temperature a weak entangled network of polymer chains is already formed. During the cooling process, the network density increases with the proceeding HDA reaction between free CDTE and Cp end groups in the network. To qualitatively assess the extent of cross-linking, a swelling test was performed with the obtained material **10**. The employed Cp_2-P(*i*BoA-*n*BA) served as reference and was treated in the same fashion as the 1:2 mixtures of **9** and Cp_2-P(*i*BoA-*n*BA). The control sample dissolved in toluene within 10 min of shaking, whereas upon similar treatment of network **10** swelling was observed, proving the cross-linking reaction to be successful.

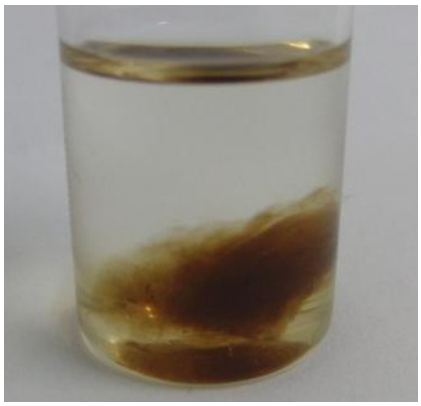

Figure 6.2 Swelling test results of network **10** in toluene after 24 h.

By comparing the measured weight of network **10** prior (w0) and after (w1) the swelling process, the degree of swelling (Ds) was calculated according to the common formula:

$$Ds = \frac{(\mathrm{w1} - \mathrm{w0}) \cdot 100}{\mathrm{w0}}$$

The Ds can be seen as an approximate indication for the network density of a cross-linked material, following the rule of thumb: the higher the network density, the lower the swelling of the network. For network **10**, a Ds of 338 wt% was found. This value appears to be high for a cross-linked material; however, it has to be taken into account that a polymer with the molecular weight of M_n = 12,000 g·mol^{-1} (Cp_2-P(*i*BoA-*n*BA)) was employed in the network formation. In an idealized network with a quantitative conversion of the diene exchange between Cp and Cp_2-P(*i*BoA-*n*BA), the end-to-end distance of the polymer end groups is the shortest network mesh length. To calculate the end-to-end distance of the polymer end groups a simplified approach can be applied.

$$h^2 = 2 \cdot N \cdot l^2$$

h^2 = square of the end-to-end distance

N = number of repeating units

l^2 = square of the length of one repeating unit (l^2 = 0.0948 nm^2 = (2·0.154nm)^2)

2 = factor obtained for perfect tetraeder angle of 109.5 °

Assuming a perfect tetraeder angle for the polymer conformation, a C-C single bond distances of 0.154 nm, a precise M_n = 12,000 g·mol^{-1} for Cp_2-P(*i*BoA-*n*BA) and a perfect molecular weight distribution of 80% weight (iBoA) and 20% weight (nBA) in every polymer chain (synthesized by Evonik with this monomer mixture) which results in an average of 65 acrylate repeating units (46.1 iBoA and 18.7 nBA) per chain, leads to an end to end distance of 3.51 nm. With respect to the molecular weight of the polymer and the resulting minimum mesh length of 3-4 nm, the swelling behavior of network **10** appears to be reasonable. For a more detailed analysis of the network properties, temperature dependent rheology experiments were performed with an 8 mm plate-plate geometry on an ARES G2 rheometer in the oscillating shear mode.

Therefore, a pellet of **10** was produced in a heatable press at 120 °C and 1 kN for 5 min, matching perfectly with the 8 mm plate geometry (refer to Figure 6.3).

Figure 6.3 Heatable press with vacuum connection.

The rheology experiments were conducted with a fixed strain of 1%, a frequency of 1 Hz, and a heating rate of 2.5 °C min^{-1}. With such a rheology set up, measurements below 30 °C could not be performed due to the high module of the sample causing an overload of the torque detection, which can be attributed to the hardness of the sample and insufficient adhesion at low temperatures. Inspection of Figure 6.4, which depicts G` and G`` as a function of temperature, suggests a simple explanation for such a behavior.

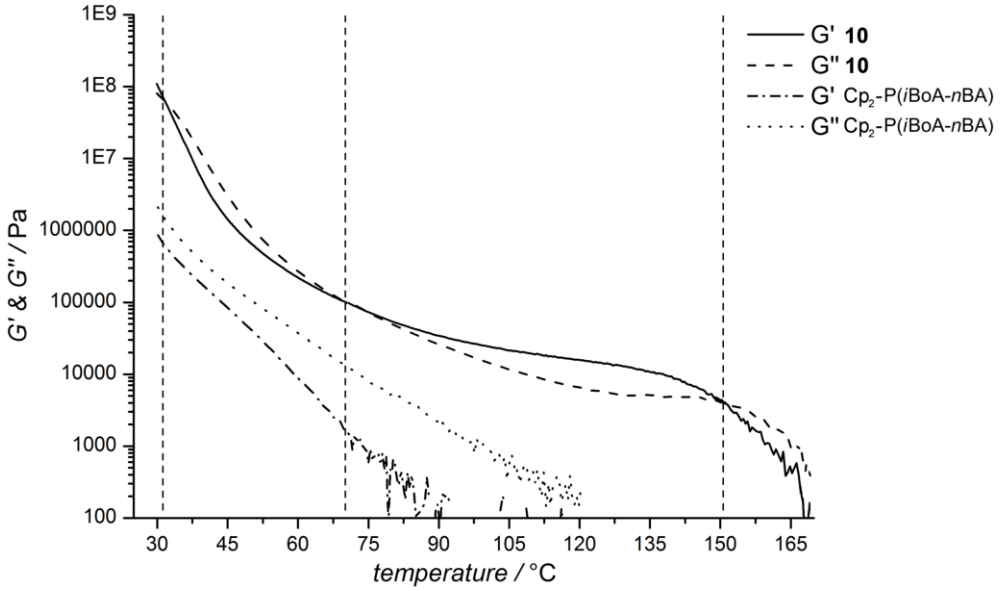

Figure 6.4 Evolution of the modulus G` and G`` from network 10 as a function of the temperature (γ0 = 1%, 8 mm geometry, ω/2π = 1 Hz). The applied heating rate was 2.5 °C min^{-1}.

Below 31 °C, the G` modulus becomes higher than the value of G``, indicating the transition to the hard and brittle glassy state, thus causing the measurement problem with the plate-plate geometry. Above 31 °C, the material reaches the so-called glass transition or leather state, where the network can be plastically reshaped although it remains fragile. At 72 °C, G` becomes again the dominant modulus leading to a state where the material has strong elastomeric properties, representing the rubber state. The elastic rubber state turns into the liquid state with a strong moduli and viscosity decrease at temperatures higher than 150 °C. All of these states of cross-linked materials are well known and described in the literature for variable network systems.[189] However, the given network examples in the literature describe either permanently cross-linked networks or adaptable networks with a high network density and consequently a small mesh length. Compared with the reversible network **10**, weak cross-linked permanent networks show a glassy state, glass transition, and a rubber state, yet degradation (rather than a liquid state) is observed at higher temperatures due to their permanent linkages. In the case of adaptable networks with a small mesh length, only two significant states – a hard glassy and a more viscous liquid state – are detected, due to suppression of the network transition states (glass transition and rubber state) by the high network density. In other words, the HDA

network **10** is not only able to heal damage by heat treatment, but is also able to specifically adjust the mechanical properties of the network by setting the temperature, making network **10** unique and distinguishes it from the dynamic covalent systems that have been reported to date.

6.2 Healing

Next, a repetitive tensile test was performed to study the healing efficiency after repetitive cycles of breaking and repairing the material. A rod shaped sample was stretched till breakage and consecutively healed in the heat press for 10 min at 120 °C and 1 kN. Although the healing should already proceed in a reasonable timeframe above 70 °C, at the beginning of the rubber state a healing temperature of 120 °C was selected based on the G` and G`` moduli traces depicted in Figure 6.4. At 120 °C the network is opened further, resulting in a lower value of the G` modulus, thus providing more rapid healing while still being sufficiently mild to tolerate most functional groups. Figure 6.5 depicts the obtained load vs. displacement curves for the original and the healed specimens.

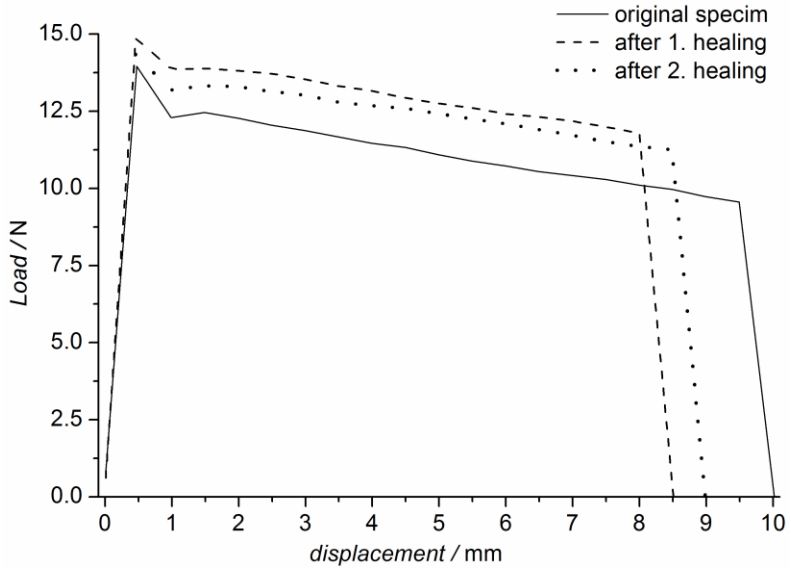

Figure 6.5 Repetitive tensile tests of a rod sample of **10**.

All samples display a small decrease in force while displacing the sample over time, so called creep. Creep is a well-known deformation phenomenon in material science appearing for example in metals and glassy polymer materials.[190] As the tensile test was performed at ambient temperature, such a behavior confirms the finding of the temperature dependent G moduli measurement and reveals a transition to the glassy state below 31 °C. Regarding the healing, a higher force was required to displace the healed specimens compared to the original. Keeping in mind the reversible nature and the synthesis of network **10**, it is not surprising that a healed (cycled) sample shows – after the first cycle – slightly higher toughness properties than the original one. Through the healing process the chemical structure of the network is refurbished leading to a different microscopic order and a slightly higher cross-linking density. Such a process is underpinned by the smaller displacement, which is needed to break the healed specimens. As a higher cross-linking density is obtained, the more restricted movement of the chains results in a smaller deformation of the material before breakage. According to the equations used by White and coworkers, a healing efficiency of 106% for the first healing cycle and 96% for the second one are obtained, being in excellent agreement with the published data of White.[190a] However, these healing efficiency values should not be considered as absolute numbers as the tensile test can easily deviate with fluctuations of inner stress or fabrication errors of the sample and the temperature. Nonetheless, a very high healing efficiency is certain for the system.

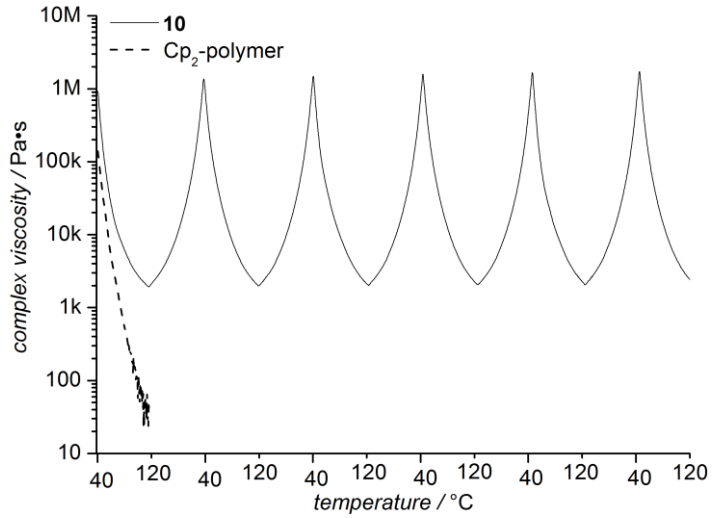

Figure 6.6 Complex viscosity of network **10** (solide curve) and Cp_2-P(*i*BoA-*n*BA) (doted curve) during the temperature cycling between 40 °C and 120 °C (γ_0 = 1%, 8 mm geometry, $\omega/2\pi$ = 1 Hz).

In order to further demonstrate the regulating properties of the material, additional on-line analyses were carried out. Since the flow of a network is directly dependent on its cross-linking density, on-line complex viscosity measurements were considered to be a suitable tool for the inspection of the cyclability of the reversible HDA linkages. Consequently, a pressed pellet was cycled in the rheometer between 40 °C and 120 °C with the same set-up as used for the G modulus measurements, while recording the complex viscosity of the system. As can be seen in Figure 6.6, the viscosity of network **10** is close to a factor of ten higher than the reference sample, containing the Cp_2-polymer only, at the starting temperature of 40 °C. However, with increasing temperature this factor increases strongly. At 110 °C, for instance, the viscosity of the reference sample decreases below 50 Pa s to a region where the 8 mm plate-plate rheology setup does not provide accurate measurements. In contrast to the behavior of the reference sample, **10** shows still a reproducible viscosity above 2000 Pa s at 120 °C, which is not surprising considering the G modulus traces shown in Figure 6.4. At a temperature of 120 °C, the material displays elastomeric behavior, implying that a few cross-linking points are still present in the material. Nonetheless, the significant viscosity decrease (by a factor of 500) during heating for network **10** points to a strong loss of cross-linking density and a high percentage of debonding. In an effort to identify the temperature at which complete debonding of network **10** occurs, a temperature ramp to 180 °C was applied.

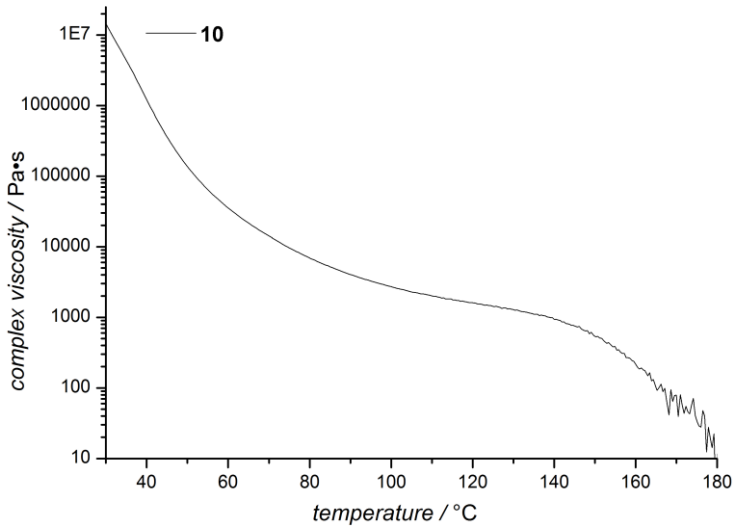

Figure 6.7 Complex viscosity of network **10** during a temperature ramp from 30-180° C measured with a heating rate of 2.5 °C min^{-1}.

The temperature ramp revealed that the viscosity reached the value measured for the Cp_2-P(*i*BoA-*n*BA) (at 110 °C) – just above 170 °C – indicating complete debonding in this temperature range. This value appears to be lower than expected considering the debonding values obtained from the temperature dependent ^{1}H NMR spectroscopy experiment of di-linker **3** (refer to Figure 4.7). In case of **3,** 19% debonding is obtained at 130 °C, calling into doubts about an increase of 81% debonding when raising the temperature only about 40 °C. However, the drastic gain in debonding can be explained by the significantly greater entropic gain on debonding the networked system **10**, compared with the small molecule **3**.[84] Nonetheless, the 5 repetitive viscosity cycles of **10** exhibit a perfect reproducibility of the measurements with a viscosity of approximately 2000 Pa s at 120 °C and a viscosity that is ten times higher than the reference sample at 40 °C without any hysteresis. The reproducibility of the low temperature values after each cycle suggests that complete re-bonding occurs during the cooling periods. Considering the relatively fast heating rate of 2.5 °C min^{-1}, very fast reaction kinetics can be assumed, comparable to those found for the linear step polymer system **6**. Thus, the on-line viscosity measurements are indicative of very fast reversible chemistry showing no hysteresis during the cycling of the bulk material.

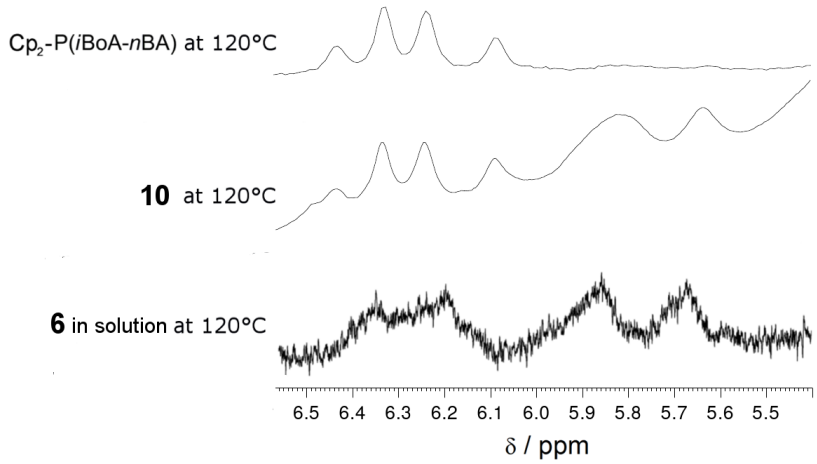

Figure 6.8 ^{1}H MAS-NMR spectra of Cp_2-P(*i*BoA-*n*BA) and network **10** at 120 °C (vMAS = 25 kHz, v1H Larmor = 700 MHz, upper and middle spectra) and ^{1}H-solution NMR spectrum (400 MHz) of the step-growth polymer **6** recorded in d_8-toluene at 120 °C (lower spectrum).

For a detailed structural analysis of the debonded network material, high temperature solid-state NMR spectra were recorded. Inspection of the ^{1}H MAS-NMR spectrum of network **10**, taken at 120° C with 25 kHz MAS spinning and 700 MHz 1H Larmor frequency (see Figure 6.8, middle spectrum), revealed a set of resonances between 6.5 and 6.1 ppm. A comparison with the MAS-NMR spectrum of Cp_2-P(*i*BoA-*n*BA) (Figure 6.8, top spectrum) recorded under the same conditions, suggests that the new set of resonances can be attributed to Cp-polymer end groups generated by the retro-HDA reaction of the network linkages as the shift and the signal splitting of both MAS-NMR spectra between 6.5 and 6.1 ppm matches perfectly. To further corroborate the hypotheses of the responses between 6.5 and 6.1 ppm in the MAS-NMR spectrum of **10** being Cp-polymer end group resonances, the spectrum of the step-growth polymer **6** (Figure 6.8, bottom spectrum, recorded in d_8-toluene at 120° C), was considered. The liquid state NMR spectrum of **6** displays the same shift of the Cp-polymer end group responses to the region between 6.5 and 6.1 ppm, underpinning the assignment of the MAS-NMR spectrum of **10**. In the liquid state NMR spectrum of step-growth polymer **6,** the resonances between 6.0 and 5.4 ppm were assigned to the HDA product isomers. Interestingly, the same resonances between 6.0 and 5.4 are also present in the MAS-NMR spectrum of **10**, which supports on the one hand, the correct assignment of the responses between 6.5 and 6.1 to the Cp-polymer end groups and on the other hand the presence of the HDA product isomers in the network.

6.3 Conclusions

The current chapter demonstrated the transfer of the novel HDA chemistry of a CDTE with Cp to a self-healing material. The success of the cross-linking process was assessed by a swelling test as well as plate-plate rheology measurements, while the chemical structures of the network debonding were confirmed via high temperature ^{1}H MAS-NMR analysis. Temperature dependent on-line viscosity data demonstrated the successful cross-linking of the material and confirmed the extremely fast reaction kinetics for the de- and re-bonding of the network system. The recorded temperature dependent traces of G` and G`` display the typical properties of a network with long mesh lengths, pointing to a material with excellent self-regulating qualities. Thus, in contrast to previously reported dynamic covalent systems, the current material is not only able to heal damage by heat treatment, but is also able to specifically adjust the mechanical properties of the network by setting the temperature, making it highly appealing for multiple reversible bonding applications. Not only can the properties of the network be set specifically by controlling the operating temperature in a very mild range, but also the property changes arise within a very short time as a result of the fast reaction kinetics. Such properties make the designed network very applying for application such as rapid prototyping, adhesives, composite materials, coatings and paints as well as sealants.

7 The Thioaldehyde-Cyclopentadiene Pair

As described in the previous chapter, the CDTE system shows excellent properties for self-healing materials applications, providing ideal reversibility and extremely fast reaction kinetics which lead to efficient healing within 10 min. Such a fast reaction behavior can only be displayed by highly reactive molecules such as the deprotected CDTE molecule. Unfortunately, the handling and storage of such highly reactive molecules is complex. As a result of the high reactivity, degradation can easily occur. Consequently, the highly reactive species has to be protected or masked in order to prevent degradation. In case of the CDTE molecule, the *in situ* HDA trapping with Cp served as protecting group, avoiding the loss of CDTE groups while still providing the reactive free CDTE species at elevate temperatures. However, deprotection via rHDA chemistry is not the only possibility to activate a masked highly reactive molecule *in situ*. The approach of Vedejs *et al*. generating highly reactive thioaldehyde compounds via the light-induced fragmentation of phenacyl sulfides appears to be suitable for the utilization in fast HDA step-growth polymerization as well. Moreover, the resulting HDA step-growth polymer would be based on DHTP linkages in the polymer backbone, similar to the step-growth polymer **6** from the CDTE/Cp chemistry, allowing to possibly generate a reversible step-growth polymer. Accordingly, the use of light-induced phenacyl sulfide fragmentation to generate highly reactive thioaldehydes in reversible HDA step-growth polymerizations was explored. In the following chapter the synthesis of a phenacyl sulfide di-linker **12** as well as its utilization in the reversible HDA step-growth polymerizations with a readily available bis-Cp P$_t$Bu is presented. To assess the reversible character of the DHTP product obtained from thioaldehydes and Cp, an SEC-ESI-MS exchange study of Cp against DMBD was conducted. Furthermore, the successful polymerization and reversing of the HDA step-growth polymer **15** was analyzed by off-line SEC and on-line temperature dependent ^{1}H NMR spectroscopy measurements.

7.1 Phenacyl sulfide fragmentation and synthesis

The phenacyl sulfide fragmentation mechanism follows a similar route as the photoenol rearrangement. Under relative mild irradiation (310-400 nm), the phenacyl sulfide function absorbs light and reaches the excited singulet state. Following an ISC to the excited triplet state, a classical Norrish type two reaction occurs, entailing a γ-hydrogen abstraction and subsequent fragmentation to the thioaldehyde species.[191]

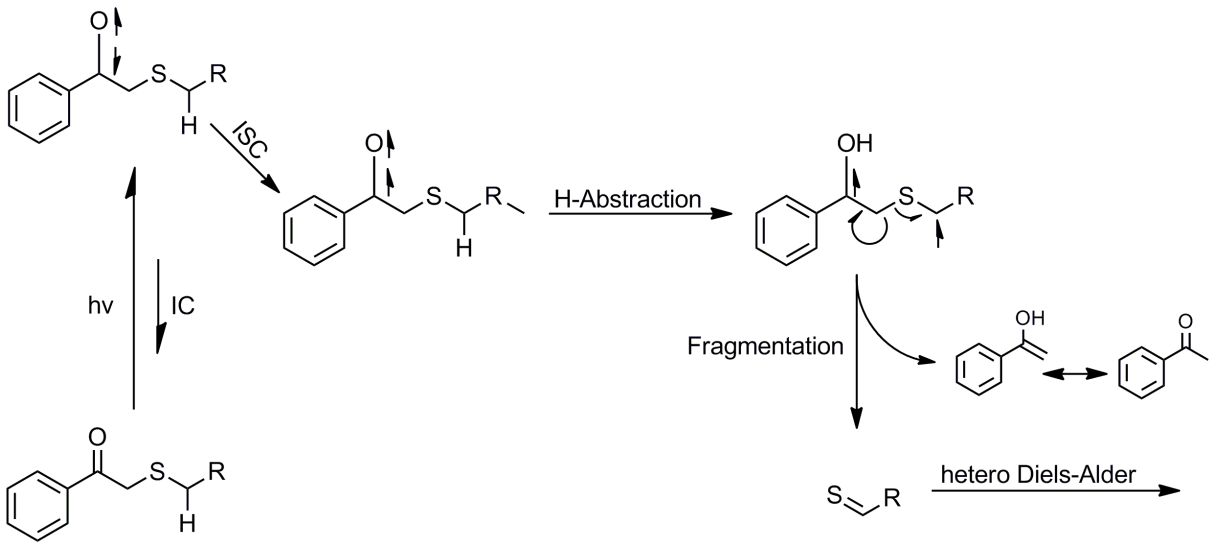

Scheme 7.1 Light-induced fragmentation mechanism of the phenacylsulfides fragmentation. R = variable group.[191]

Vedeys *et al*. were the first to explore the effect of the functional group in proximity to the new generated thioaldehyde (R), revealing that electron withdrawing groups lead to a higher conversion of *in situ* trapped HDA products. This finding is not surprising, as electron withdrawing groups activate dienophiles for normal electron demand DA reactions and increase the reaction rate. Consequently, the thioaldehyde reacts faster in the HDA reaction than undergoing side reactions such as condensation and self polymerization. Moreover, via the electron withdrawing character of R, the C=S double bond is polarized which leads to an excellent regioselectivity. Despite the increased reactivity towards HDA reactions, degradation reaction cannot completely be avoided. However, in the same publication which addressed the effect of R on the reactivity of thioaldehydes, the simple synthesis of functionalized phenacyl sulfide compounds via the nucleophilic substitution of chloro-acetophenone with

functionalized thiols was described. Consequently, mercapto acetic acid was utilized in the reaction with chloro-acetophenone yielding (phenacylthio) acetic acid in excellent yields. The attached acid group on the small molecule precursor served, on the one hand, as electron withdrawing group increasing the HDA conversion of the *in situ* generated thioaldehyde functional and, on the other, as functional handle for the synthesis of linker molecules. In order to gain access to a di functional and a polymeric phenacylsulfides molecule, a Steglich esterification with di- and mono-functional poly(ethylene glycol) (PEG) was carried out yielding PEG functionalized phenacylsulfides **11** as well as di-linker **12**.

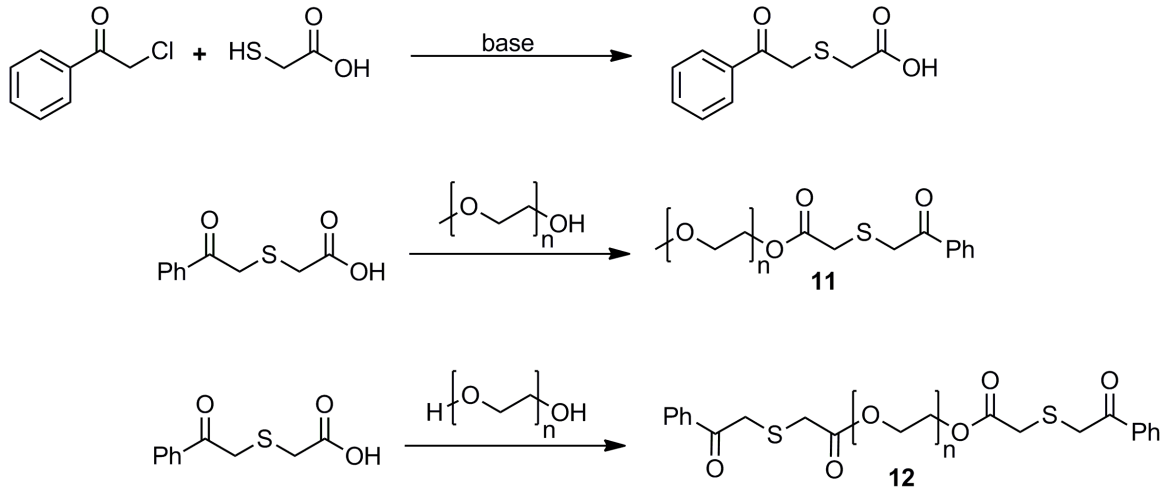

Scheme 7.2 Synthesis of the (phenacylthio) acetic acid via the nucleophilic substation of chloro-acetophenone and mercapto acetic acid (top reaction) as well as the reaction to the mono functionalized PEG **11** and di-linker **12** obtained via a Steglich esterification with (phenacylthio) acetic acid.

7.2 Reversibility of the thioaldehyde hetero Diels–Alder adduct

To investigate the efficiency and feasibility of the retro HDA reaction of the *in situ* trapped thioaldehyde, the model system **11** was utilized for a diene exchange study of polymer end groups. Consequently, the phenacyl sulfide bearing PEG was irradiated in the presence of Cp, with a Philips CLEO compact PL-L lamp (λ_{max} = 355 nm), to give the respective HDA cycloadduct **13**. The Philips CLEO compact lamp was chosen for the reaction as its emission spectrum showed a significant overlap with the absorption spectrum of model system **11** (see Figure 7.1).

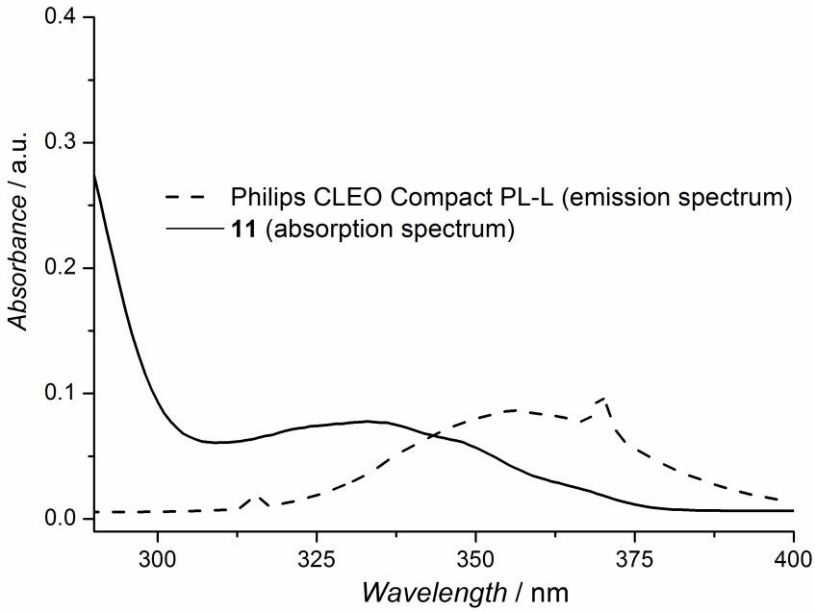

Figure 7.1 Emission spectrum of the Philips CLEO compact PL-L plotted together with the measured absorption spectrum of **11**.

Following isolation by precipitation, the HDA product from the *in situ* generated thioaldehyde and Cp was subsequently heated to 110 °C in a toluene solution containing 5 equivalents of DMBD, in order to exchange the Cp and yield the cycloadduct of thioaldehyde and DMBD **14.**

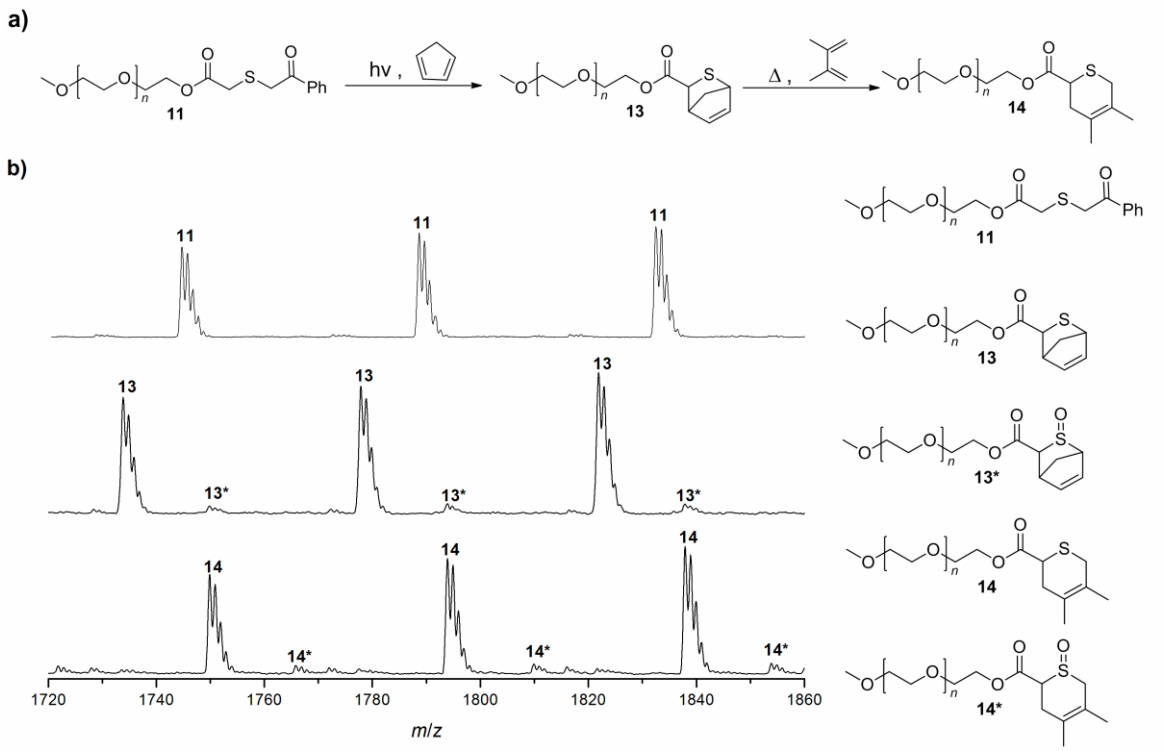

Figure 7.2 Diene exchange study of Cp against DMBD in the DHTP unit. a) depicts the reaction sequence to the presented mass spectra b).

Inspecting the respective ESI-MS spectra, the diene exchange study revealed that photolysis of **11** in the presence of cyclopentadiene yields the expected cycloadduct **13** in high yield. A small amount of a side product (~ 10% peak intensity) occurs at 16 amu higher mass to charge ration (*m / z)* ratios which can be explained by oxidation of the thioether **13** to the corresponding sulfoxide. After 5 h at 110 °C in the presence of an excess of DMBD, **13** is completely absent in the ESI-MS spectrum and the main product is the cycloadduct **14**. The side product present in the starting material shows the same shift as **13** which is consistent with the assumption of oxidation to the sulfoxide because those can undergo rHDA cleavage and *in-situ* trapping as well.[90a]

7.3 Photo-polymerization and heat de-polymerization

Based on the knowledge of the diene exchange study, the transfer to materials science of the light-induced HAD chemistry was addressed. Therefore, polymer **12**

and a readily available Cp_2-P$_t$Bu were mixed in acetonitrile, and irradiated for 3 h (subsequent to bubbling with nitrogen) to yield step-growth polymer **15**. In order to prove the reversibility of the HDA linkages in the polymer, an SEC off-line experiment was conducted to evidence the depolymerization **15**. For the off-line experiment, polymer **15** was heated with DMBD in toluene to 120 °C to trap the de-polymerized thioaldehyde species in the corresponding HDA product.

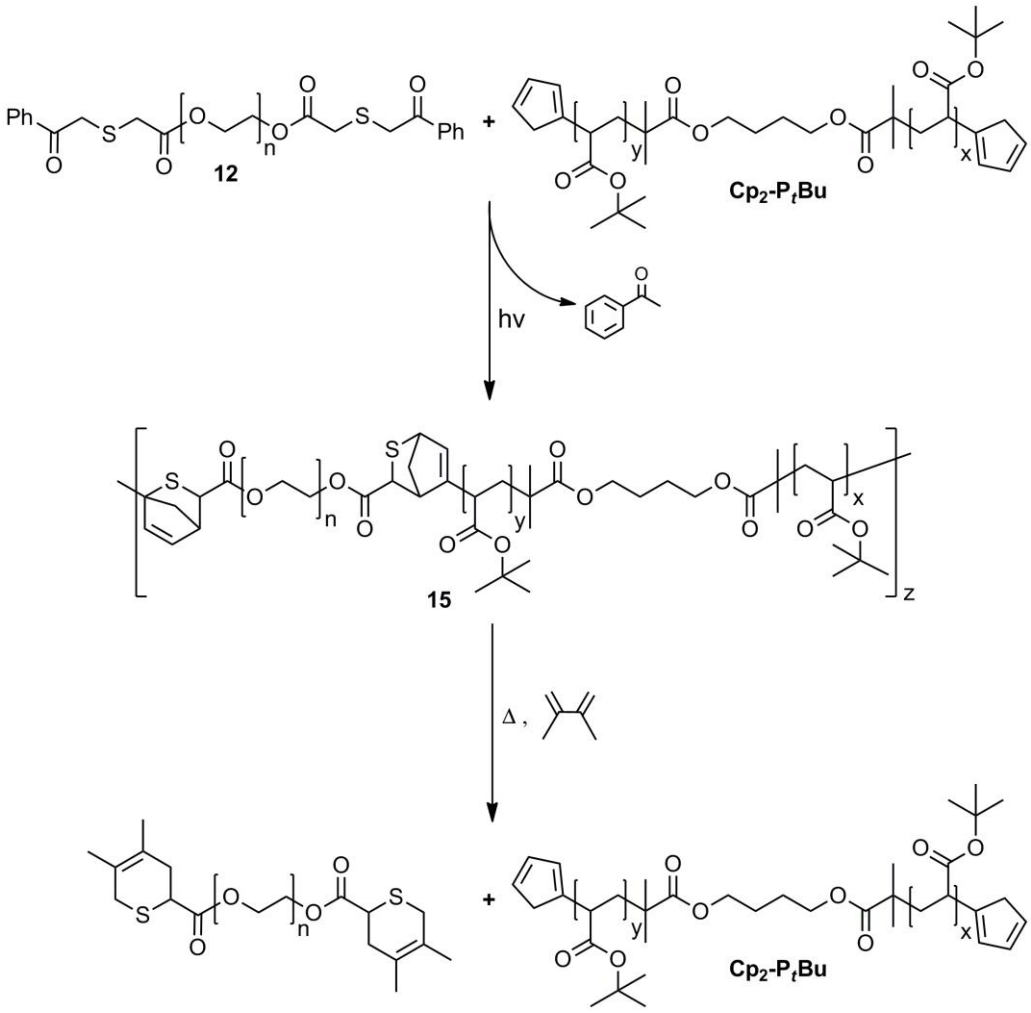

Scheme 7.3 Schematic presentation of light-induced HDA polymerization and heat triggered depolymerization by *in situ* trapping with DMBD.

DMBD was chosen as trapping agent, as its DA products are known to have higher rDA temperatures compared to those obtained with Cp.[192] Consequently, the obtained de-polymerized DMBD trapped thioaldehyde linker was not able to re-polymerize with the present Cp_2-P$_t$Bu. Figure 7.2 presents the SEC traces of the

mixture of polymer **12** and Cp_2-P$_t$Bu prior to irradiation, the obtained polymer **15** and the heated sample of **15** with DMBD.

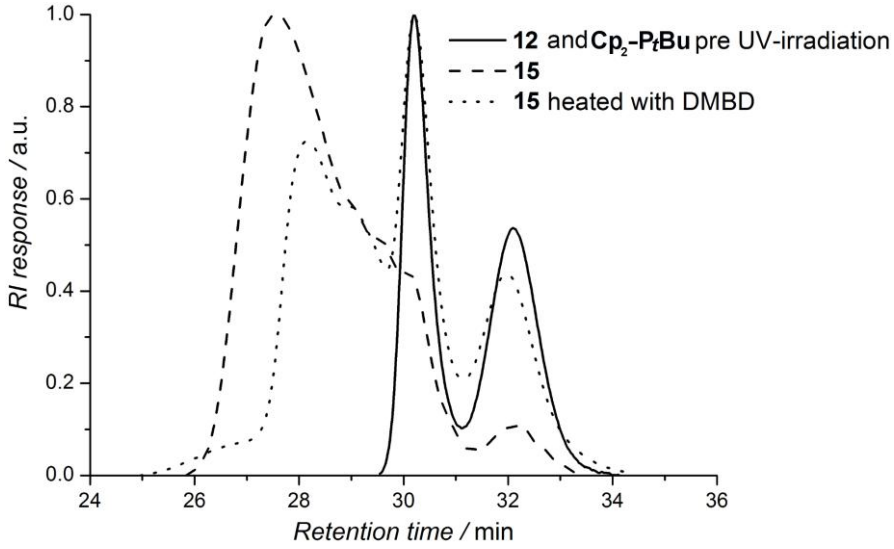

Figure 7.3 Normalized SEC traces of the mixture between **12** and Cp_2-P$_t$Bu prior to UV irradiation (M_n = 8400 g·mol^{-1}), the obtained step-growth polymer **15** (M_n = 26100 g·mol^{-1}) and the heated mixture of **15** with DMBD (M_n = 13200 g·mol^{-1}).

As expected, the chromatograms in Figure 7.2 evidence that light is crucial for the polymerization as the non-irradiated mixture of **12** and Cp_2-P$_t$Bu – in contrast to the irradiated mixture – show no shift to lower retention times (i.e., higher molecular weight). However, the observed shift to higher molecular weight, in the chromatogram of polymer **15**, can be reversed by heating the polymer with DMBD as the trace of the sample displays. The reappearance of Cp_2-P$_t$Bu and **12** in the chromatogram of the heated sample points to the successful depolymerization polymer **15**. Nevertheless, a significant amount of polymer with higher molecular weight, in the same trace, cannot be neglected. It is assumed that the remaining shoulder could be a result of occurring coupling reactions of the highly reactive thioaldehyde itself. To give further evidence for the reversible nature of the HDA polymer and gain more information about the depolymerisation process, temperature dependent on-line ^{1}H NMR spectroscopy experiments of polymer **3** in toluene-d_8 with a relaxation time of 1 s and 32 scans were performed.

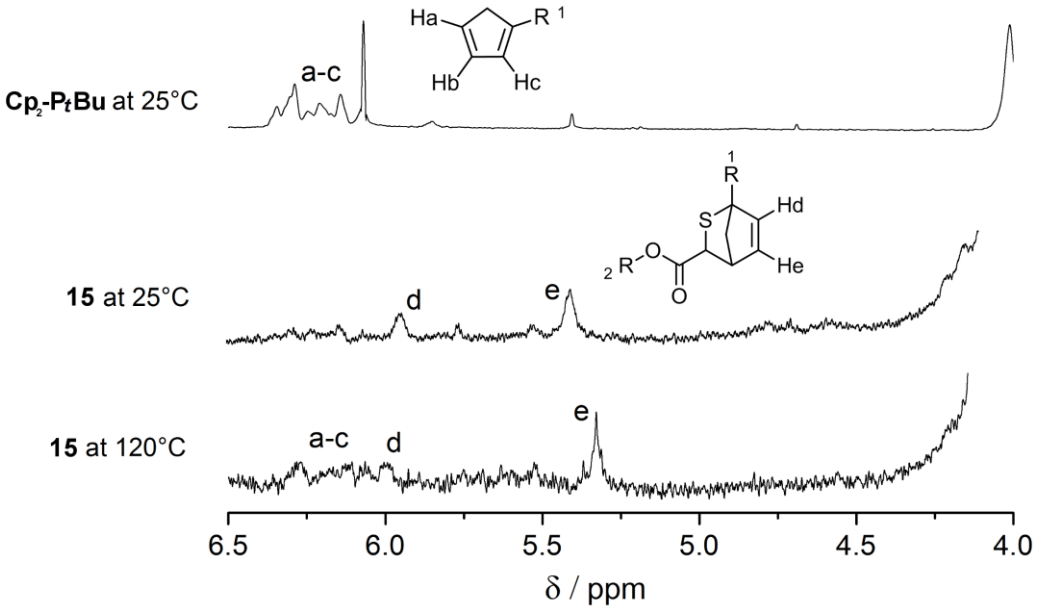

Figure 7.4 Temperature dependent ^{1}H NMR study of the obtained step-growth polymer **15** in toluene-d_8. Spectrum of polymer Cp_2-P$_t$Bu at 25 °C (top spectraum), spectrum of **15** at 25 °C (middle spectrum) and the spectrum of **15** at 120 °C (bottom spectrum) depict the reversing of the dihydrothiopyrane units back to the starting materials.

Figure 7.3 presents spectra of polymer Cp_2-P$_t$Bu and **15** recorded at ambient temperature as well as a spectrum of **15** taken at 120 °C. As can be seen in the top spectrum the Cp end groups yield a broad multiplet response between 6.4 and 6.1 ppm, whereas the middle spectrum exhibits two singulet resonances at 6.0 and 5.3 ppm representing the HDA linkages of polymer **15**. Heated to 120 °C, the spectrum of polymer **15** changes, as can be seen in the bottom spectrum revealing an additional set of responses in the region between 6.4 and 6.1, clearly matching with the Cp end groups of polymer Cp_2-P$_t$Bu. This finding underpins the assumption of a retro HDA reaction of the thioaldyhed-Cp linkages and stands in excellent agreement with results of the SEC off-line study presented in Figure 7.2.

7.4 Conclusions

In the present chapter, a new reversible, light triggered step-growth polymerization technique based on the HDA reaction between thioaldehyde and Cp moieties was introduced. The high conversion and rate of the light-induced HDA reaction as well as the reversible nature of the formed dihydrothiopyrane unit was examined by an ESI-MS trapping and diene exchange study with a mono functionalized PEG. Transferred to materials science, an AA-BB step-growth polymer was synthesized from bis-functional polymers. Depolymerization of the step-growth polymer was analyzed with an offline SEC experiment, trapping the de-polymerized starting materials, and a temperature dependent ^{1}H NMR study which evidenced the opening of the DHTP linkages in the polymer. The presented HDA chemistry concept appears to be very special due to its unique trigger by light that reverses with heat. Given that different triggers are required for the polymerization and de-polymerization, the presented chemistry appeals to a wide range of applications such as soft lithography or direct laser writing.

8 Light-Induced RAFT Hetero Diels–Alder Chemistry[iv]

The previous chapter employed light as activating source for the generation of highly reactive thioaldehyde functionalized molecules. As shown and noted, such thioaldehydes are highly activated towards HDA reactions, yielding DHTPs also with deactivated dienes.[172] The high reactivity is for certain applications strongly desired as it enables chemists to utilize simple, cheap and less reactive starting materials for HDA reactions such as sorbic acid and the respective esters for example. However, thioaldehydes can only act as dienophiles in HDA reactions. For the reaction with less or deactivated dienophiles in DA reactions, a highly reactive diene species would be required. Keeping this in mind, stable dienes are not sufficiently reactive to undergo HDA reactions with such electron rich dienophiles as dithiobenzoates RAFT agents for example. Consequently, a highly reactive diene has to be generated *in situ* from a protected or masked form in order to provide such high reactivities. In the context of highly reactive dienes, the photoenol has proven to be a versatile tool, undergoing DA reactions with several dienophiles within a short time frame.[193] Similar to the thioaldehyde, the photoenol requires light as trigger to rearrange *in situ* to the highly reactive dienol species. In order to apply this photoenol chemistry to the HDA reaction of electron rich RAFT agents, a detailed study regarding the HDA reaction between a photoenol precursor and the universal RAFT agent 2-cyanopropyl dithiobenzoate (CPDB), was carried out. In an exploratory study, the HDA reaction between a CPDB-functionalized poly(methyl methacrylate) (PMMA) **16** and the photoenol precursor (2-methoxy-6-methylbenzaldehyde) **17** was confirmed. The nature and success of this reaction was determined by size-exclusion chromatography/electrospray ionisation-mass spectrometry (SEC/ESI-MS), electrospray ionisation-collision-induced dissociation-mass spectrometry (ESI-CID-MS), ^{1}H NMR spectroscopy, and UV-Vis spectroscopy. After confirming that the HDA reaction proceeded, a block-copolymer was formed from **16** and a photoenol end-functionalized poly(ε-caprolactone) (PCL) and analyzed by SEC.

[iv] Parts of the current chapter were reproduced from K. K. Oehlenschlaeger, J. O. Mueller, N. B. Heine, M. Glassner, N. K. Guimard, G. Delaittre, F. G. Schmidt, C. Barner-Kowollik, *Angew. Chem. Int. Ed.* **2013**, *52*, 762, with permission from John Wiley & Sons, Inc. all rights reserved. The project was carried out in collaboration with Jan Mueller from our working group. He evidenced the broad applicability of the RAFT-PE conjugation by performing further block copolymer conjugations with variable polymers, such as polyacrylates, styrenes and polyacrylamides bearing CPDB end groups. Moreover, he explored the reaction kinetics of the conjugation as well as the effect of the deoxygenation method on the ligation.

8.1 Qualitative assessment of RAFT-photoenol hetero Diels–Alder

The first step of the study comprised the synthesis of CPDB (according to literature)[194] and its subsequent utilization as a chain transfer agent in the RAFT polymerization of methyl methacrylate to yield a dithiobenzoate end capped poly(methyl methacrylate) (PMMA) (M_n = 3300 g·mol^{-1}, $Đ_M$ = 1.27) **16**. With the obtained polymer **16** a model study on polymer end groups was performed, in order to explore the light-induced HDA reaction as well as a block copolymer formation to demonstrate its efficiency and suitability for material science. The end group functionalization of **16** with the photoenol precursor, 2-methoxy-6-methylbenzaldehyde **17,** was achieved by irradiating a deoxygenated solution of **16** with a concentration of 10 mg·mL^{-1} and 1.1 equivalents **17** in acetonitrile for 3 h at ambient temperature.

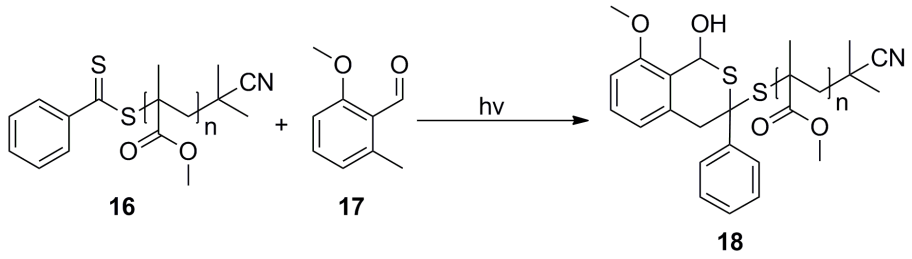

Scheme 8.1 Photo-conjugation of dithiobenzoate end capped poly(methyl methacrylate) (**16**) with 2-methoxy-6-methylbenzaldehyde (**17**), yielding the isothiochroman (**18**).

The photoenol precursor **17** was selected for this reaction, as it is the most reactive photoenol tested so far. Its high reactivity is believed to originate from the significant overlap of its absorption spectrum (λ_{max} = 315 nm) with the emission spectrum of the employed UV lamp (Comedico Arimed B6; λ_{max} = 320 nm). Both, the emission spectrum of the Comedico Arimed B6 and the absorption spectrum of **17** are depicted in Figure 8.1.

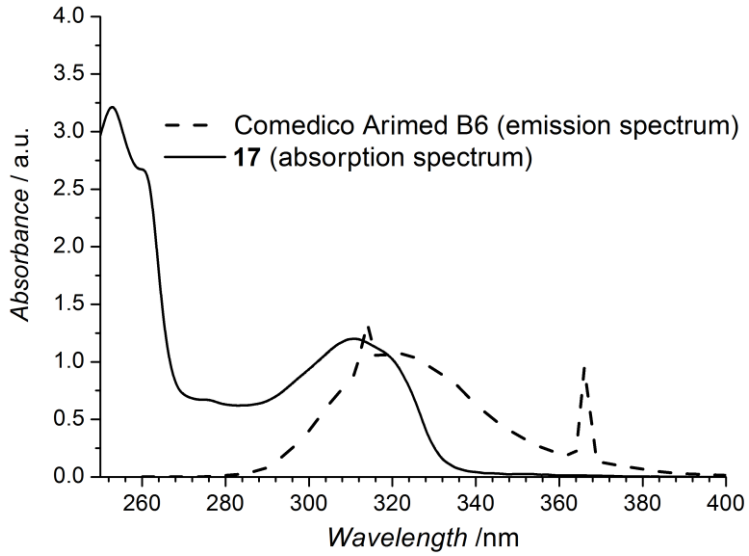

Figure 8.1 Emission spectrum of the Comedico Arimed B6, plotted together with the measured absorption spectrum of **17**.

Following irradiation, the product was isolated by precipitation in cold *n*-hexane. The success of the reaction can be qualitatively assessed by comparing the color of the reaction mixture prior to and after irradiation. The initially pink solution became colorless during irradiation indicating the consumption of the chromophoric dithioester end group. In addition, a control experiment consisting of a pure solution of **16** that was exposed to UV light for an extended period of time revealed the persistence of the pink coloration and suggested that the dithioester is stable under these conditions. Thus, it is reasonable to assume that **16** undergoes a reaction with **17** in the presence of UV light. In order to qualitatively assess the success of the HDA reaction, UV-Vis spectroscopy measurements of polymer **16** and **18** were carried out. UV-Vis spectroscopy was chosen as first analysis technique because of the typical strong π-π* and weak n-π* transitions of the thiocarbonyl moiety in polymer **16**, which should be absent in the absorption spectrum of the irradiated mixture if **16** partakes in the desired HDA cycloaddition, making UV-Vis spectroscopy a rapid assessment for the success of the reaction. Indeed, the absorption maximum at 300 nm corresponding to the π-π* transition is drastically reduced after the reaction in comparison to the transition of the starting material. The presence of aromatic substituents in the product can explain the existence of a remaining low absorbance

in this region. In addition, the absence of a n-π* transition further indicates that there is no longer any detectable thiocarbonyl functional group present in the product.

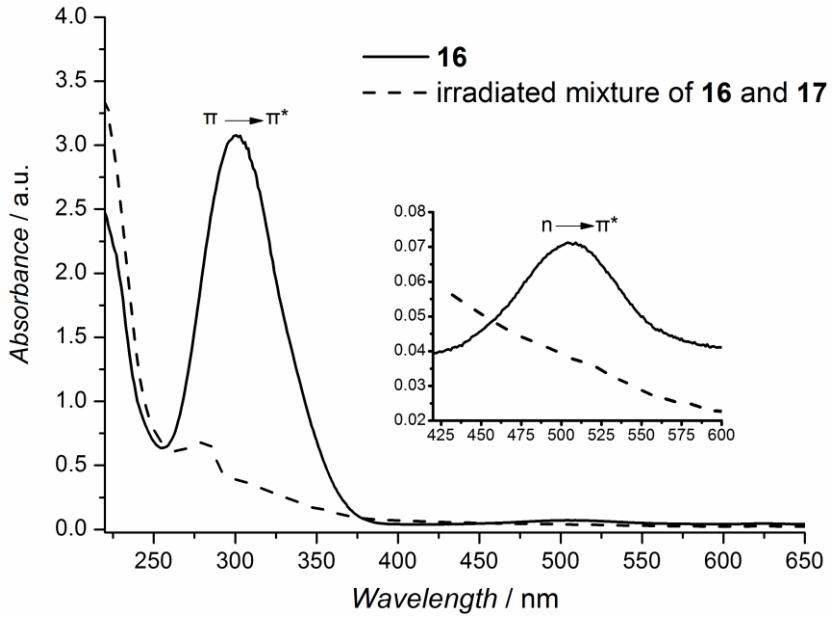

Figure 8.2 UV-Vis spectra of the RAFT polymer **16** (solid line) and the irradiated mixture of **16** and **17** (dashed line) after precipitation from the reaction mixture.

To support the positive finding of the UV-Vis study, ESI-MS experiments of the obtained polymer **18** were conducted. SEC/ESI-MS analysis confirmed that the conjugation reaction occurred, since a comparison of the MS spectra of the starting material and the product clearly reveals that the *m / z* signal associated with the RAFT polymer **16** is shifted by 149.9 amu, which corresponds very well to the exact mass of **17** (M = 150.07 g·mol^{-1}) (refer to Figure 8.3). The SEC/ESI-MS spectrum of the product also reveals the presence of a minor impurity, as well as a trace amount of starting material. Although the presence of starting material would seem to contradict the UV-Vis results, it should be noted that the detection limit of ESI-MS is lower than that of UV-Vis spectroscopy and it is possible that the presence of a small amount of starting material could easily be masked by the absorption spectrum of the product.

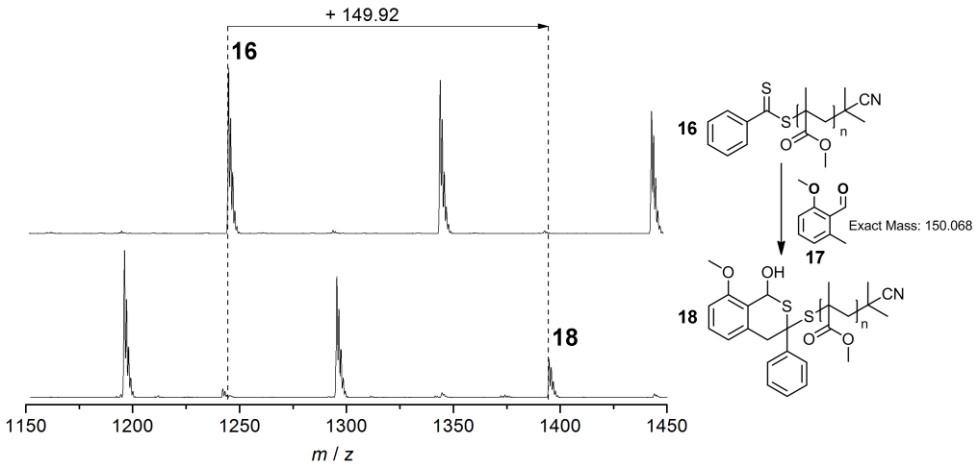

Figure 8.3 SEC/ESI-MS spectra of the PMMA **16** before (top) and after (bottom) the conjugation reaction with **17**. The spectra correspond to the polymer eluted at later retention times with single sodium ion (lower molar masses).

8.2 Structure analysis of the isothiochroman product

Although the results from SEC/ESI-MS and UV-Vis spectroscopy both confirm the successful coupling of PMMA **16** with **17**, these results do not reveal any information about the nature of the chemical bond formed. Therefore, ESI-CID-MS was carried out to determine the chemical structure of the obtained polymer product **18**. Polymer **16** served as reference sample for the ESI-CID-MS experiment, demonstrating the typical fragmentation patter of a dithiobenzoate end capped PMMA (refer to Figure 8.4). Following the collision with a helium atom, benzodithioic acid is eliminated from the RAFT end capped polymer, yielding a daughter ion with a terminal double bond and a decreased molecular weight of 154 amu compared to the mother ion. Such a fragmentation is known to proceed for most methacrylates polymers generated via the RAFT polymerization with dithiobenzoate derivatives.[195]

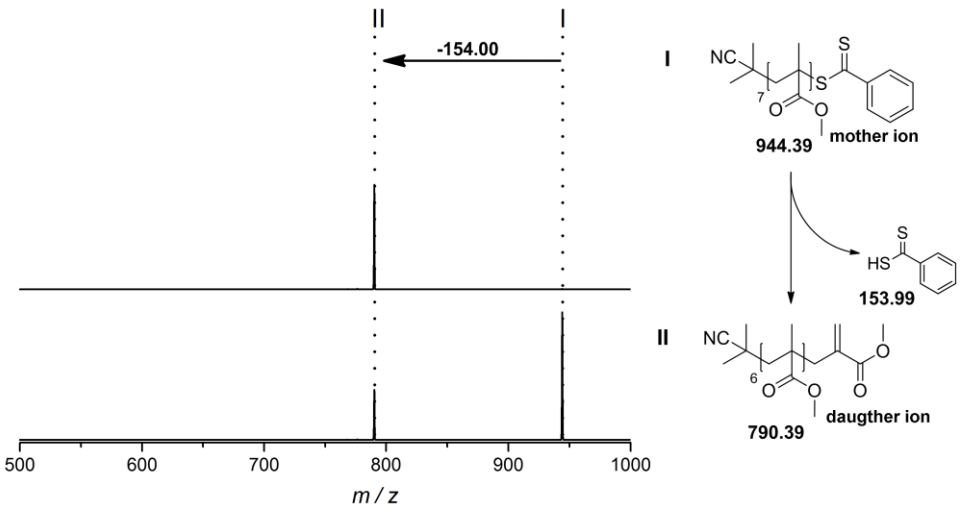

Figure 8.4 ESI-CID-MS spectra of polymer **16**. The labeled numbers under the polymer structures represent the exact mass of the single charged sodium adducts from the depicted polymers. The bottom spectrum (measured with lower collision energy) depicts the fragmentation pattern with remaining mother ion **16**. The top spectrum (measured with higher collision energy) shows neither remaining mother ion **16** nor addition fragments of the daughter ion, indicating a very clean fragmentation. Such a fragmentation pattern is typically observed for dithiobenzoate end capped polymers.

In contrast to the fragmentation pattern of the dithioester-based polymer, the RAFT-HDA product was found to generate no unsaturated fragment. Instead, the primary daughter ion obtained from the fragmentation of the HDA product is a thiol end capped polymer (*m / z* = 824.38 amu) that results from the cleavage of the S-C bond which was previously part of the dithioester group. Such a process is only conceivable if the thiocarbonyl group is converted into a thioketal, permitting the generation of two stable fragments (i.e., the polymeric thiol and a cyclic thioether). Additional ESI-CID-MS experiments performed on the daughter ion resulted in a fragmentation pattern that would be expected for methyl methacrylate polymers, although an isobaric thiolactone series would also give rise to the same fragmentation pattern. These results support the hypothesis that a polymeric thiol fragment was obtained as the daughter ion of the product.

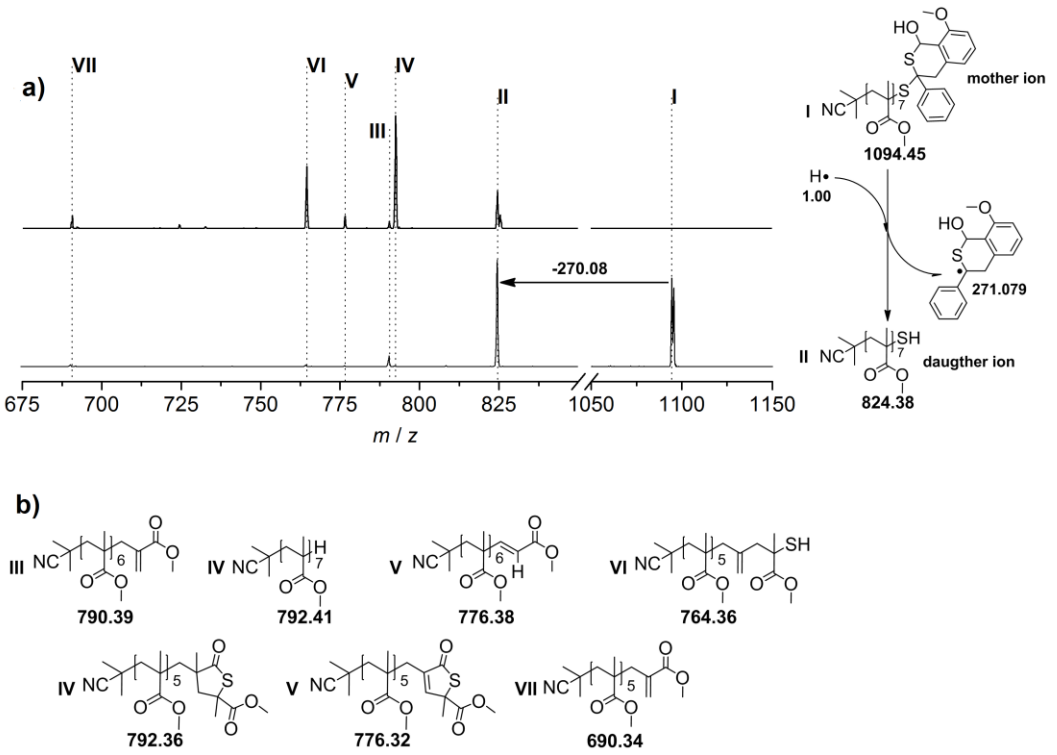

Figure 8.5 a) ESI-CID-MS spectra of the RAFT-HDA product (bottom) and the resulting daughter ion (top). The labeled numbers under the polymer structures represent the exact mass of the single charged sodium adducts from the depicted polymers. The right-hand-side scheme depicts the proposed fragmentation process of the mother ion. b) Structures predicted to result from the fragmentation of the daughter ion.

Finally, the most conclusive evidence for the successful HDA cycloaddition between the non-activated dithioester-terminated polymer **16** and the highly reactive diene precursor **17** was obtained by NMR analysis (see Figure 8.6). The ^{1}H NMR spectrum of the irradiated solution of **16** and **17** revealed a significant change in the signals between 6.5 and 8 ppm that are associated with the aromatic protons. Specifically, the NMR signals associated with the phenyl protons a-c shift upfield and new resonances in the 6.5 to 8 ppm region emerge, which correlate well with the aromatic protons k', l', and m' of the cycloadduct **18**. In addition, the total integration value for the aromatic region corresponds to eight protons, which is in perfect agreement with the number of aromatic protons expected for the product. Moreover, the presence of two new resonances at 5 ppm and 5.5 ppm further suggests the formation of the desired product since these signals can be attributed to the new protons i' and p' of the isothiochroman.

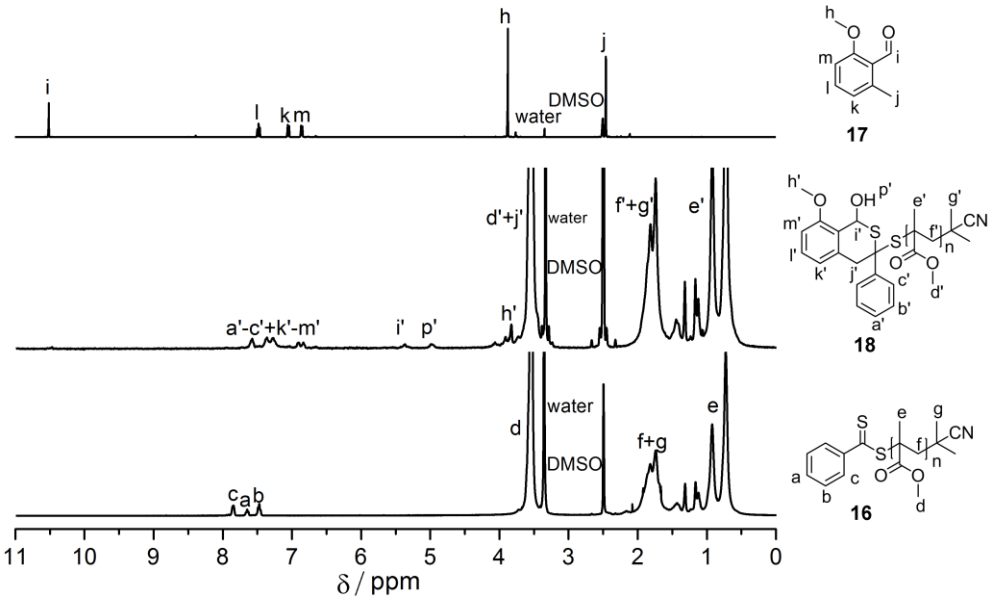

Figure 8.6 ^{1}H NMR spectra of the reactants 2-methoxy-6-methylbenzaldehyde (**17**) and dithiobenzoate end capped PMMA (**16**), as well as the isothiochroman (**18**) formed after irradiation for 3 h at ambient temperature.

8.3 Block copolymer formation

To assess the scope of the photo-induced HDA reaction, modular formation of block copolymers consisting of a RAFT polymer, (i.e., PMMA **16**) and a photoenol-functionalized PCL **19** were investigated. Therefore, a ROP initiator carrying the photoenol moiety was synthesized following the synthetic route depicted in the Scheme 8.2 below.

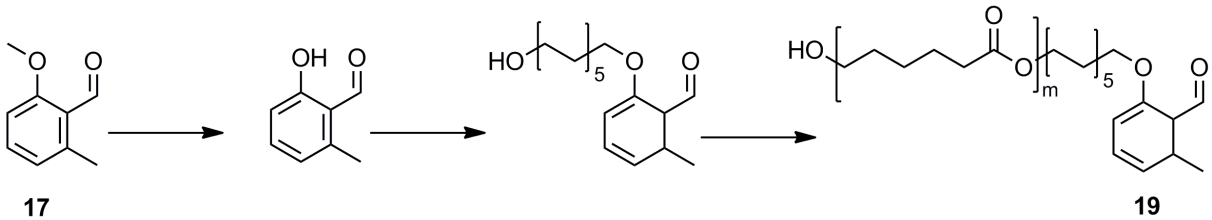

Scheme 8.2 Synthesis of the photoenol-functionalized PCL **19** starting from the photoenol precursor **17**.

The ROP of ε-caprolactone was performed in the presence of the photoenol-based initiator and triazabicyclodecene in toluene under inert gas at ambient temperature

for 5 h. Subsequent precipitation of the product from cold *n*-hexane resulted in a PCL with a M_n of 2000 g·mol^{-1} and a $Đ_M$ of 1.25. Comparing the ^{1}H NMR signals corresponding to the aromatic end group protons (7.35 ppm and 6.8 ppm in $CDCl_3$) to the characteristic terminal hydroxymethylene proton signals (3.64 ppm in $CDCl_3$) revealed quantitative end group functionalization.

Next, polymer conjugation was performed using an equimolar ratio of each block component, based on the M_n calculated from the ^{1}H NMR spectra of the polymer blocks. The procedure that was employed for the previously described HDA reaction (deoxygenation and subsequent irradiation in acetonitrile for 3 h) was also utilized for the block copolymer formation. SEC chromatograms for the individual building blocks and the copolymer product are illustrated in Figure 8.7.

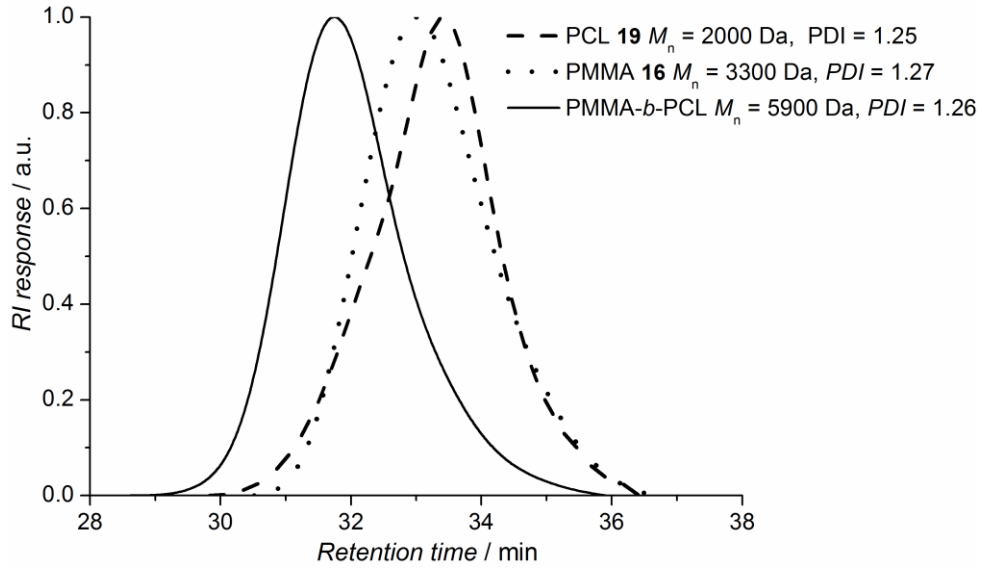

Figure 8.7 Normalized SEC traces of PMMA **16** (M_n = 3300 g·mol^{-1}), PCL **19** (M_n = 2000 g·mol^{-1}) and the block copolymer (M_n = 5900 g·mol^{-1}).

In comparison to the SEC chromatogram of each starting material, the chromatogram of the block copolymer is significantly shifted towards higher molecular weight values and indicates that the copolymer has a polydispersity ranging between the values found for **16** and **19**. These results clearly indicate the successful coupling of the single blocks. The SEC chromatogram of the block copolymer suggests that quantitative conversion is achieved since the measured M_n ($M_{n(measured)}$ = 5900 g·mol^{-1}) was found to be effectively equal to the theoretical M_n ($M_{n(theoretical)}$ = 5300 g·mol^{-1})

predicted for the copolymer. However, there is some error associated with the SEC results obtained for block copolymers because of the differing properties of each block. Nevertheless, the SEC analysis of a non-UV irradiated, equimolar mixture of **16** and **19** results in neither a shift in the molecular weight distribution, nor a change in the shape of the chromatogram, evidencing the necessity of UV light exposure for achieving the HDA conjugation.

In an effort to prove the HDA conjugation and to confirm the block copolymer formation, ESI-MS measurements were carried out. Figure 8.8 presents a zoom into the recorded ESI-MS spectrum of the block copolymer from **16** and **19**. With a molecular weight above 4000 Da, the block copolymer exceeds the ESI-MS limitations for single charged peaks. Nevertheless, a series of quadruple charged peaks can be identified and assigned to the possible block copolymer compositions of PCL and PMMA, evidencing the clean and successful HDA conjugation.

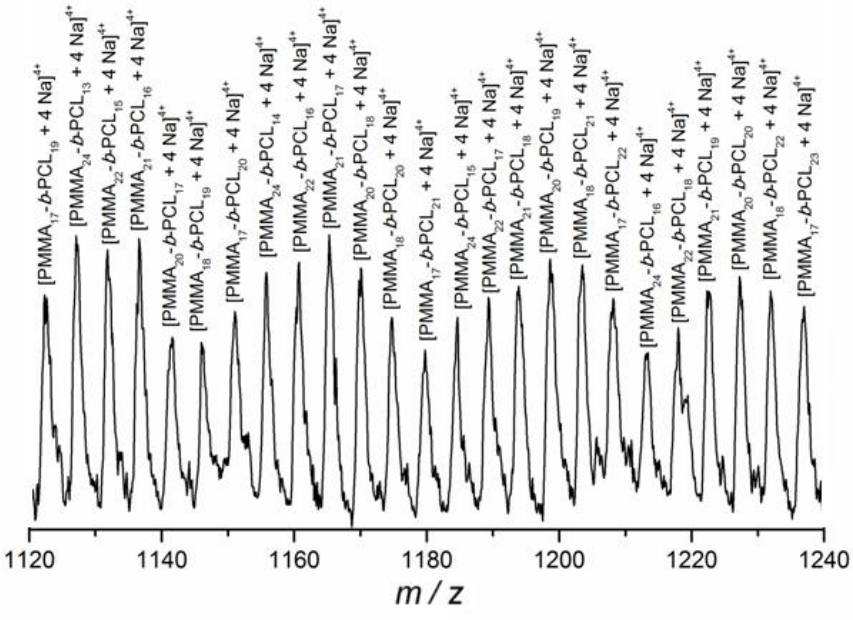

Figure 8.8 Expanded region of the SEC/ESI-MS spectrum of PMMA-b-PCL in the charge state z = 4.

8.4 Conclusions

In the current chapter, a novel polymer conjugation reaction for a non-activated dithioester was presented, which is based on a light-triggered HDA reaction with a highly reactive photoenol diene. Close to quantitative coupling is achieved within short reaction times at ambient temperature and the absence of a catalyst. Coupling of a RAFT polymer with a small photoenol molecule was first verified by ESI-MS. ^{1}H NMR and ESI-CID-MS techniques were utilized to confirm the isothiochroman linkage formation in the HDA-RAFT product. Furthermore, the applicability of the conjugation technique to the formation of block copolymers was demonstrated. The novel polymer conjugation reaction presented herein increases the number of well-defined photo-*clickable* polymers that can be generated as it can be applied for a *conventional* RAFT agent, which is suitable for the controlled radical polymerization of a wide range of monomers. Therefore, the novel reaction provides a key advantage for synthetic chemists in a variety of applications, such as surface patterning, macromolecular architecture design, three-dimensional network formation, bio-conjugation and step-growth polymer synthesis. The ability to perform modular ligation on conventional RAFT polymers greatly expands the synthetic toolbox available to macromolecular chemists.

9 Concluding Remarks

The current thesis addresses the utilization of highly reactive functional groups in HDA reactions for material science. In chapter 4 a new reversible HDA chemistry is presented which is based on the CDTE/Cp HDA pair. To establish the new HDA pair, a novel synthetic strategy to functionalize CDTE molecules is developed comprising *in situ* trapping of the generated CDTE unit by Cp. A small molecule model study demonstrates the extremely fast reaction rates and equilibrium shifts at elevated temperatures of the CDTE/Cp pair without the need of a catalyst. Moreover, the *in situ* trapping strategy is transferred to material science by employing bisfunctional CDTE and diene linker molecules to afford HDA based step-growth polymers. By utilizing a Cp_2-polymer as building block, the fast, catalyst free, reversible HDA chemistry is implemented into a HDA step-growth polymer, demonstrating the suitability of the novel chemistry for reversible material science applications such as self-healing materials. Chapter 5 addresses the need for an economically viable CDTE multi-linker molecule, able to be produced on an industrial scale. Therefore, multiple synthetic strategies are followed to yield a multi-functional linker molecule from cheap starting materials without the need of complex purification techniques such as column chromatography. Subsequently, the novel CDTE multi-linker molecule is employed in order to generate a self-healing material based on the novel CDTE/Cp HDA pair, described in chapter 6. The obtained self-healing material is analyzed with several state-of-the-art analysis techniques for the exploration of adaptable networks.

The completely new reversible HDA chemistry is an extremely powerful tool for any application regarding adaptable network or dynamic covalent bond chemistry. To date, the presented work in Chapter 4,5 and 6 represents to the best of the candidate's knowledge, the currently most advanced, fast, catalyst free reversible covalent bond chemistry proceeding at ambient temperatures for self-healing materials.

In further studies addressing highly reactive functional groups, a light-induced reversible step-growth polymerization is presented in chapter 7. The step-growth polymerization is based on the light triggered generation of thioaldehydes which react *in situ* with Cp_2-polymers to HDA linkages. Those HDA linkages show a reversible

behavior towards the starting materials at elevated temperatures, as evidenced in off-line and on-line experiments. Such a new reversible polymer displays attractive properties for dynamic covalent bond applications and represents one of the first examples of a light triggered, heat reversible polymerization.

In the last chapter of the thesis (chapter 8) a new approach towards the HDA reaction of electron rich dithiobenzoate groups is presented. Normally inhibited by their electron rich character, the HDA reaction of dithiobenzoate groups is realized by employing highly reactive photoenol moieties as dienes in the cycloaddition with conventional RAFT agents. The successful conjugation reaction is analyzed by multiple analysis techniques and eventually used in a block copolymer synthesis to exhibit its high efficiency of the ligation and suitability for macromolecular architecture design.

The candidate submits that all three presented projects (CDTE/CP chemistry, thioaldehyde/Cp chemistry, RAFT/PE chemistry) contribute strongly to the field of HDA reactions in material science and form a platform future studies can be based on. The reversible CDTE/Cp chemistry certainly entails a high potential for the field of dynamic covalent bonding chemistry. For self-healing materials, the influence of the nature of the Cp_2-polymer should be explored in the context of lowering the rHDA temperature to achieve self-healing at lower temperatures than already demonstrated. Moreover, polymeric CDTE linker molecules could be employed for the network generation to gain a higher cross-linking density in the polymer matrix, further enhancing the bonding/debonding properties of the HDA product. Soft lithography is another field which benefits from fast reversible covalent chemistry, especially the micro contact printing technique. The same field could benefit from the light triggered conjugation and heat triggered reverse of the thioaldehyde/Cp HDA adduct. Finally, the entire field of macromolecular architectures and surface grafting will benefit from the conjugation of well-defined non-modified RAFT polymers, via the use of the RAFT–HDA–PE concept.

10 Materials and Analytic Instrumentation section

10.1 Materials

ε-Caprolactone (ε-CL, Sigma Aldrich) was distilled from CaH_2 and stored over molecular sieves. Dichloromethane (DCM, VWR) and *N,N*-dimethyl formamide (DMF, 99+%, Alfa Aesar) were dried and stored over $CaCl_2$ prior to use. Cyclopentadiene was obtained by cracking and distilling dicyclopentadiene (97% Sigma Aldrich) at 170 °C. Acetonitrile (MeCN, LC-MS chromasolve, Fluka), magnesium sulfate (99%, ROTH), methyl-4-(bromomethyl)benzoate (97%, Alfa Aesar), 4-(bromomethyl)benzoate (97%, ABCR), diisobutylaluminium hydride (25% solution in hexane, Alfa Aesar), carbondisulfide (Merck), sodium cyanide (98% ABCR), 1,3-dimethylbutadiene (Merck), tetraethylammoniumbromide (Sigma Aldrich), isophorone diisocyanate (97% Sigma Aldrich), dibutyltin dilaurate (Sigma Aldrich), triethylamine (Sigma Aldrich), tetrahydrofuran (THF, GPC-grade, VWR), trichlorobenzene (TCB, GPC-grade, VWR), toluene (Acros), ethanol (Acros), 1,5,7-triazabicyclo[4.4.0]dec-5-ene (TBD, Sigma Aldrich) were used as received, Cp_2-P(iBoA-BA) (M_n = 13,000 g·mol^{-1}, $Đ_M$ = 1.6) and isophorone diisocyanate-sorbic alcohol (IPDI-SA) was supplied by Evonik industries. Methyl methacrylate (MMA, 99+%, Acros), styrene (99%, extra pure, Acros) and methyl acrylate (MA, 99+%, Acros) were passed through a column of basic alumina (VWR) to remove inhibitor and subsequently stored at -19 °C. 2,2'-Azobis(2-methylpropionitrile) (AIBN, Sigma-Aldrich) was recrystallized twice from methanol (MeOH, VWR) and stored at -19 °C. ε-Caprolactone (ε-CL, Sigma-aldrich) was distilled from CaH_2 and stored over molecular sieves. Dichloromethane (DCM, VWR) and *N,N*-dimethyl formamide (DMF, 99+%, Alfa Aesar) were dried and stored over $CaCl_2$ prior to use. Aluminium chloride (anhydrous, >99%, ROTH), benzoic acid (99.5%, Sigma-Aldrich), 11-bromo-1-undecanol (purum, Fluka), copper sulfate pentahydrate (99+%, Acros), 2-cyano propyldithiobenzoate (CPDB, >97%, Sigma-Aldrich), 2,3-dimethyl anisole (97%, Alfa-Aesar), acetonitrile (MeCN, LC-MS chromasolve, Fluka), magnesium sulfate (99%, ROTH), potassium peroxodisulfate (97%, Sigma-aldrich), tetrahydrofuran (THF, GPC-grade, VWR), toluene (extra dry, water < 30 ppm, Acros), 1,5,7-triazabicyclo[4.4.0]dec-5-ene (TBD, Sigma-Aldrich) were used as received.

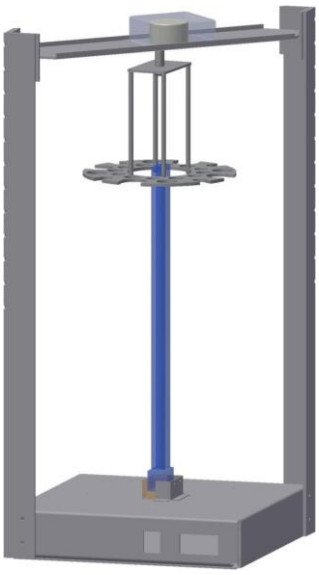

Drawing of the custom-built photoreactor employed in the light triggered studies of chapter 7 and 8.

10.2 Analytic Instrumentation

Electrospray ionization-mass spectrometry (ESI-MS)

ESI-MS spectra were recorded on an LXQ mass spectrometer (ThermoFisher Scientific, San Jose, CA, USA) equipped with an atmospheric pressure ionization source operating in the nebulizer assisted electrospray mode. The instrument was calibrated in the *m / z* range 195-1822 using a standard containing caffeine, Met-Arg-Phe-Ala acetate (MRFA) and a mixture of fluorinated phosphazenes (Ultramark 1621) (all from Sigma-Aldrich). A constant spray voltage of 4.5 kV was used and nitrogen was applied with a dimensionless sweep gas flow-rate of 2 (approx. 3 $L \cdot min^{-1}$) and a dimensionless sheath gas flow-rate of 12 (approx. 1 $L \cdot min^{-1}$). The capillary voltage, the tube lens offset voltage and the capillary temperature was set to 60 V, 110 V and 300 °C, respectively. A typical polymer concentration of approximately 3 $mg \cdot mL^{-1}$ (in a 3:2 THF/MeOH mixture) was utilized. Data treatment was performed using the procedure outlined in a recent publication.[v]

[v] Junkers, T.; Koo, S. P. S.; Davis, T. P.; Stenzel, M. H.; Barner-Kowollik, C. *Macromolecules* **2007**, *40, 8906-8912*.

Molar mass analysis via size exclusion chromatography (SEC)

For the determination of molar mass distributions (MWD) a SEC system (Polymer Laboratories PL-GPC 50 Plus), comprised of an auto injector, a guard column (PLgel Mixed C, 50 × 7.5 mm) followed by three linear columns (PLgel Mixed C, 300 × 7.5 mm, 5 µm bead-size) and a differential refractive index detector, was employed. THF at 40 °C at a flow rate of 1 $mL \cdot min^{-1}$ was used as the eluent. The SEC system was calibrated using narrow poly(methyl methacrylate) standards ranging from 600 to 5105 $g \cdot mol^{-1}$ (Polymer Standards Service (PSS), Mainz, Germany). The resulting·molar mass distributions were determined by universal calibration using Mark-Houwink parameters for PiBoA (K = 5 10^{-5} dL g^{-1}, α = 0.745), PS (K = 14 10^{-5} dL g^{-1}, α = 0.7) and PCL (K = 13.95 10^{-5} dL g^{-1}, α = 0.786),[vi] respectively.

UV-Vis spectroscopy

UV-visible spectroscopy was performed using a Cary 300 Bio spectrophotometer (Varian) featuring a thermostated sample cell holder. Absorption spectra for samples dissolved in toluene at a ratio of 10 $mg \cdot mL^{-1}$ were measured from 200 to 800 nm with a resolution of 1 nm and slit width of 2 nm in a 1 cm UV cuvette. In case of the kinetic measurement, the concentration of the samples was different. 0.2 mL of toluene were placed in the cuvette and 10 mg of the sample were dissolved in 0.5 mL toluene for the measurements. The sample that was taken for repolymerisation analysis had a different concentration, due to the evaporation of toluene which took place during heating.

High temperature dynamic light scattering (HT-DLS)

The HT-DLS experiments have been carried out using a DynaPro NanoStar photospectrometer (WYATT Technology Corporation, USA). A solution of **6** (17

[vi] Schindler, A.; Hibionada, Y. M.; Pitt, C. G. *Journal of Polymer Science, Polymer Chemistry Edition* **1982**, *20*, 319.

mg·mL^{-1} in 1,2,4-triclorobenzene (TCB)) was prepared and filtered through a 0.2 µm PTFE syring filter after 20 minutes of dissolution. In multiple cycles, the temperature has been changed from 30 to 120 °C (heating/cooling rate = 15 °C min^{-1}) and the hydrodynamic radius has been determined continuously (each data point represents an average of 15 single acquisitions (see Figure S4, p. S26)) by light scattering at 658 nm. The control sample (Cp_2-P(*i*BoA-*n*BA), 17 mg·mL^{-1} in TCB, filtration was not necessary) was measured under identical conditions. In both cases, the solution was kept in the quartz-glass cuvette during the whole experiment to avoid introducing dust or other impurities, thus shaking or stirring for increasing the reaction rate was not possible.

Nuclear Magnetic Resonance Spectroscopy (NMR and on-line HT-NMR)

^{1}H NMR spectroscopy was carried out on a Bruker AM 400 MHz spectrometer. The samples were dissolved in DMSO-d_6 and measured with 16 scans for **5,** 100 for **6**, and a relaxation time of 1 s for both. The δ-scale is referenced to tetramethylsilane (δ = 0.00 ppm) as internal standard. For the on-line high temperature measurements the samples were dissolved in toluene-d_8. The temperatures were kept constant by continuous heating with a thermo element (20% heating power), while cooling was performed with a compressed air stream (400 L·h^{-1})

11 Experimental Section

11.1 The cyanodithioester–cyclopentadiene pair

Synthesis of the carbonocyanidodithioate

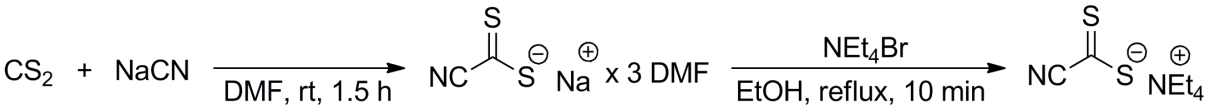

A suspension of 5.46 g (0.111 mol, 1.1 eq) sodiumcyanide in 20.0 mL DMF was cooled with an ice-bath to 0 °C. Under strong stirring 6.20 mL (7.75 g, 0.102 mol, 1 eq) of carbondisulfide (CS_2), diluted with 13 mL DMF, were added over a period of 10 min. After completion of the CS_2 addition, the ice-bath was removed and the solution was stirred until complete solidification, due to the precipitation of brown needles (ca. 60 min). Isopropanol (150 mL) was added and heated to 90 °C, to dissolve the precipitated needles. The warm suspension was filtered to remove the excess of sodiumcyanide. The filtrate was cooled with liquid nitrogen and the reprecipitated solid was filtered and washed with diethylether. The mustard colored powder was recrystallized from an isopropanol/diethylether mixture (1:1). Yield: 90% (30.0 g, 0.090 mol)

The entire obtained mustard colored solid was subsequently heated to reflux in 110 mL ethanol, while – in parallel – 18.9 g (0.090 mol, 1 eq) tetraethyl-ammoniumbromide were heated to reflux in 50 mL ethanol. The two boiling solutions were combined and heated to reflux for an additional 10 min. During the slow cooling to ambient temperature a brown solid crystallized, which was filtered off and recrystallized from ethanol. The final product was a brown lustrous powder which was used without further characterization. Yield: 48% (10.0 g, 0.043 mol)

Synthesis of the 4-(bromomethyl)benzylic alcohol

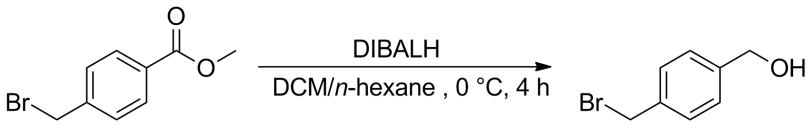

50 mL of a 25% diisobutylaluminium hydride solution (25% in hexane, 8.17 g, 57.4 mmol, 2 eq) were added to a two neck round bottom flask under an inert atmosphere (N_2). The flask was cooled to 0 °C with an ice bath before 6.57 g (28.7 mmol, 1 eq) methyl-4-(bromomethyl)benzoate, dissolved in 30.0 mL DCM (dry), were added within 30 min. After 4 h reaction time the remaining diisobutylaluminium hydride was quenched with water. To dissolve the white solid, which precipitated during the quenching process, 30 mL HCl (37%) and 30 mL DCM were added. The phases were separated and the aqueous layer was extracted 4 times with 50 mL DCM. The combined organic layers were dried over Na_2SO_4 and concentrated under reduced pressure to yield a white solid which was employed without further purification. Yield: 77% (4.40 g, 22.0 mmol).

^{1}H NMR (DMSO-d^6, 250 MHz) δ (ppm): 7.41-7.38 (d, *J* = 8.1 Hz, 2H, Ar*H*), 7.31-7.28 (d, *J* = 8.1 Hz, 2H, Ar*H*), 4.70 (s, 2H, C*H*$_2$Br), 4.49 (s, 2H, C*H*$_2$OH).

Cp-protected cyanodithioester (1a and 1b)

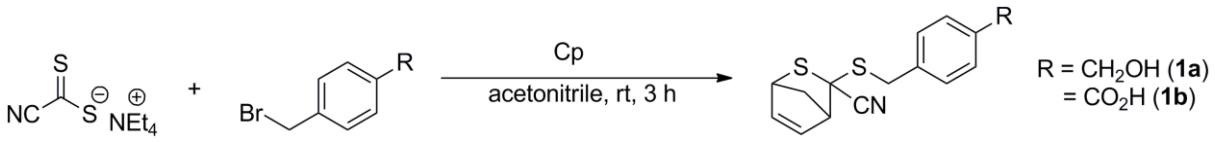

1a)

5.22 g (22.5 mmol, 1.02 eq) tetraethylammonium carbonocyanidodithioate were dissolved in 120 mL acetonitrile and stirred at ambient temperature. 4.40 g (22.0 mmol, 1 eq) 4-(bromomethyl)benzylic alcohol, dissolved in 80 mL acetonitrile, were added to the solution. After 1 min reaction time 5.22 mL (4.02 g, 60.9 mmol, 2.7 eq) cyclopentadiene were added and the mixture was stirred for 3 h. The solvent was removed under reduced pressure and the obtained yellow oil purified via flash chromatography over silica gel (hexane/ethylacetate (1:1)-(1:2)). Yield: 32% (2.03 g, 7.04 mmol), MS (ESI) calculated for sum formula $[M+Na]^+$: (found) 311.93 *m / z*, (expected) 312.03 *m / z*.

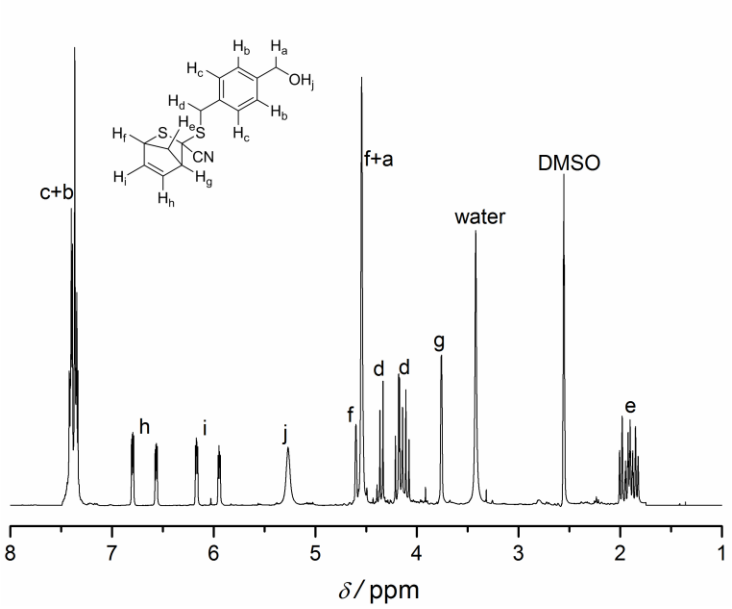

^{1}H NMR (DMSO-d^6, 250 MHz) δ (ppm): 7.37-7.28 (m, 4H, Ar*H*), 6.76-6.73 (dd, *J* = 5.4, 2.9 Hz, 0.4H, C=C*H*$_{exo}$), 6.53-6.50 (dd, *J* = 5.4, 2.9 Hz, 0.45H, C=C*H*$_{endo}$), 6.12-6.10 (dd, *J* = 5.4, 3.2 Hz, 0.4H, C=C*H*$_{exo}$), 5.88-6.86 (dd, *J* = 5.4, 3.2 Hz, 0.45H, C=C*H*$_{endo}$), 5.20 (br, 1H, CH_2OH), 4.55 (s, 0.5H, C*H*SC), 4.49 (s, 2.5H, C*H*SC + C*H*$_2$OH), 4.31-4.28 (d, *J* = 12 Hz, 0.5H, SC*H*$_2$Ar), 4.23-4.13 (m, 1.5H, SC*H*$_2$Ar), 3.70 (s, 1H, C*H*CCN), 1.95-1.77 (d+ddt+d, *J* = 10.2, 18.1, 10.2, 2.1, 10.4 Hz, 1.75H, bridge C*H*$_2$).

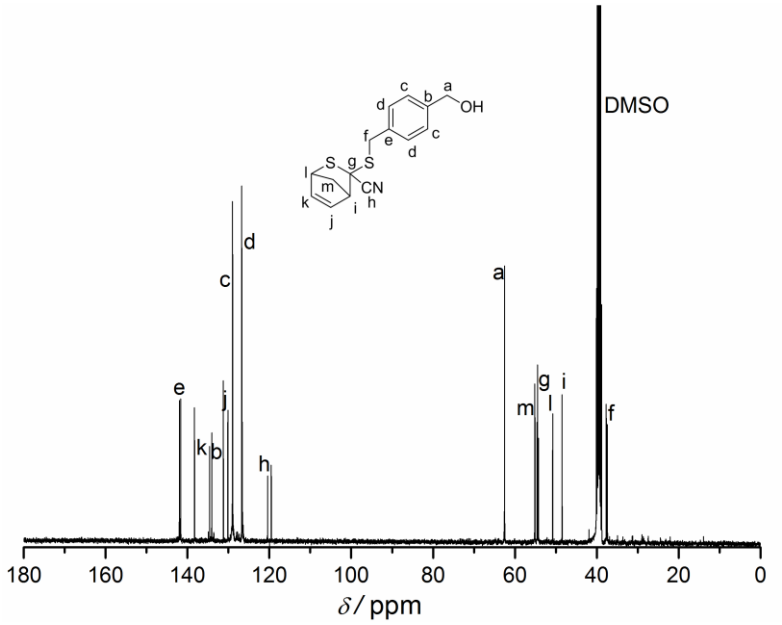

^{13}C-NMR (DMSO-d^6, 100 MHz) δ (ppm): 142.0 (e), 141.69 (e), 138.31 (k), 134.61 (k), 134.10 (b), 131.27 (j), 130.17 (j), 129.02 (c), 128.97 (c), 126.78 (d), 126.70 (d), 120.74 (h), 119.56 (h), 62.58 (a), 55.21 (m), 55.19 (m), 54.64 (l), 54.55 (g), 54.51 (g), 54.31 (l), 50.84 (i), 48.54 (i), 37.75 (f), 37.48 (f).

UV-Vis spectrum of **1a**

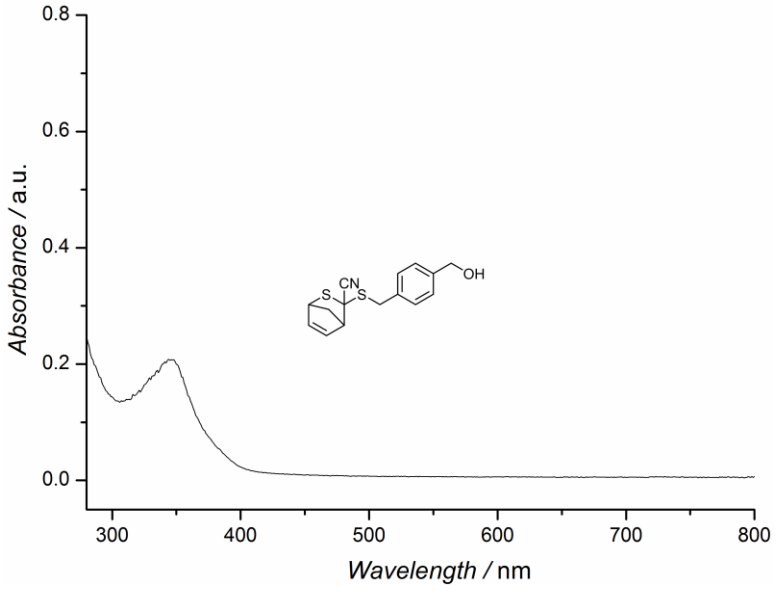

1b)

3.88 g (16.7 mmol, 1.1 eq) tetraethylammonium carbonocyanidodithioate, dissolved in 80.0 mL acetonitrile, were placed in a 100 mL round bottom flask and stirred at ambient temperature. 3.24 g (15.2 mmol, 1 eq) 4-(bromomethyl)benzoic acid, suspended in 70.0 mL acetonitrile, were added to the solution. After 1 min reaction

time, 3.80 mL (3.01 g, 45.4 mmol, 3 eq) cyclopentadiene were added and the mixture was stirred for 24 h. The solvent was removed under reduced pressure and final purification, of the yellow oil, was performed via flash chromatography (silica gel/ dichloromethane:methanol (19:1)). Yield: 32% (2.03 g, 7.04 mmol), MS (ESI) calculated for sum formula $[M+Na]^+$: (found) 326.00 *m / z*, (expected) 326.03 *m / z*.

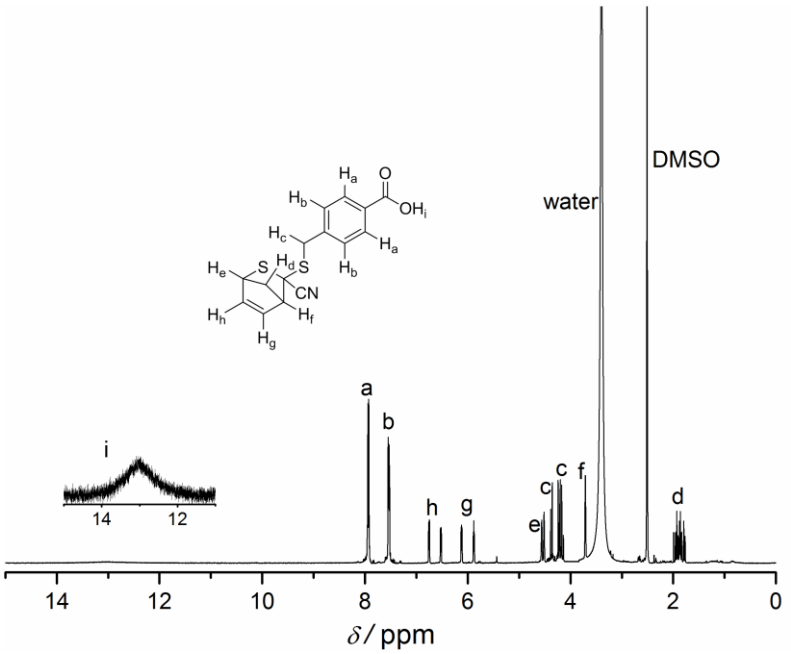

^{1}H NMR (DMSO-d^6, 250 MHz) δ (ppm): 13.01 (br, 1H, CO_2H), 7.94-7.91 (dd, *J* = 8.3, 1.7 Hz, 2H, Ar*H*), 7.54-7.51 (dd, *J* = 8.3, 3.9 Hz, 2H, Ar*H*), 6.76-6.73 (dd, *J* = 5.4, 2.9 Hz, 0.4H, C=C*H*), 6.53-6.50 (dd, *J* = 5.4, 2.9 Hz, 0.45H, C=C*H*), 6.13-6.09 (dd, *J* = 5.4, 3.2 Hz, 0.4H, C=C*H*), 5.91-6.87 (dd, *J* = 5.4, 3.2 Hz, 0.45H, C=C*H*), 4.55 (s, 0.5H, C*H*SC), 4.50 (s, 0.5H, C*H*SC), 4.38-4.35 (d, *J* = 12.6 Hz, 0.5H, SCH_2Ar), 4.16-4.02 (m, 1.5H, SCH_2Ar), 3.70 (s, 1H, C*H*CCN), 1.95-1.77 (d+ddt+d, *J* = 10.2, 18.1, 10.2, 2.1, 10.4 Hz, 1.75H, bridge CH_2).

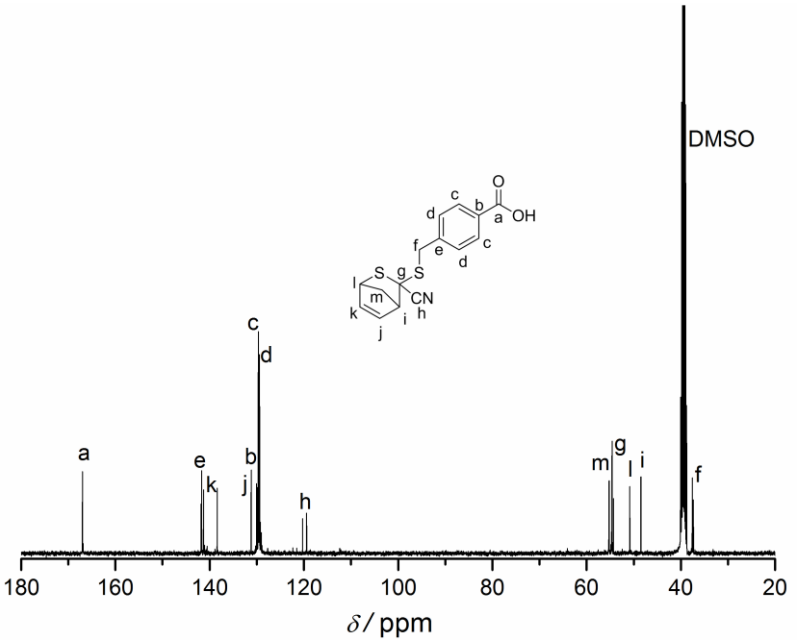

^{13}C-NMR (DMSO-d^{6}, 100 MHz) δ (ppm): 167.10 (a), 141.92 (e), 141.81 (e), 141.41 (k), 138.50 (k), 131.29 (b), 130.13 (j), 130.00 (j), 129.78 (c), 129.75 (c), 129.54 (d), 129.50 (d), 120.39 (h), 119.53 (h), 55.39 (m), 55.33 (m), 54.77 (l), 54.70 (g), 54.69 (g), 54.41 (l), 50.95 (i), 48.59 (i), 37.68 (f), 37.46 (f).

UV-Vis spectrum of **1b**

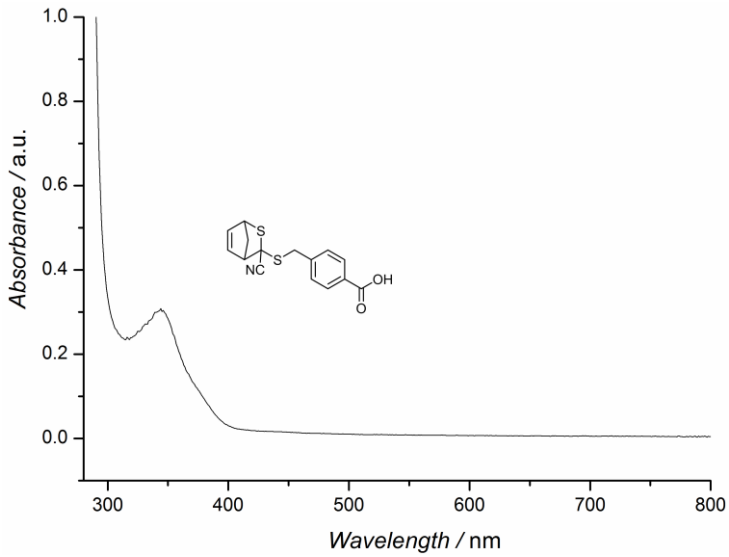

Trapped cyanodithioester end capped poly(ε-caprolactone) (2)

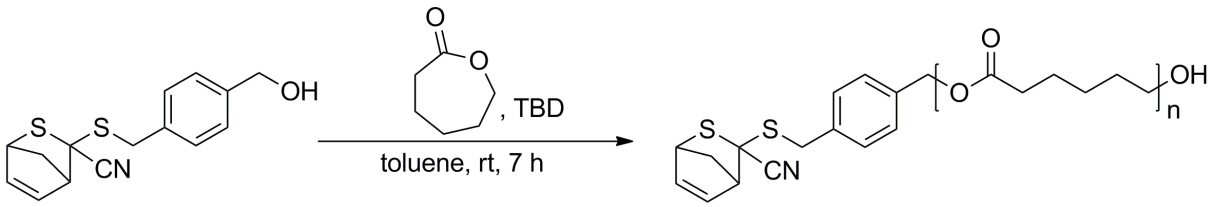

1a **2**

Alcohol **1a** (200 mg, 0.690 mmol, 1 eq) and TBD (9.60 mg, 0.069 mmol, 0.1 eq) were dissolved in toluene (4.00 mL) under inert atmosphere (Ar). ε-CL (2.22 g, 19.0 mmol, 20 eq) was added and the solution was stirred at ambient temperature for 7 h. The reaction was quenched with benzoic acid (50.0 mg, 0.400 mmol, 0.6 eq) and the polymer was precipitated in cold hexane/Et_2O (1:1 v/v, 200 mL) to yield 1.4 g of **2** (M_n = 2000 g·mol^{-1} and $Đ$ = 1.20).

ESI-MS spectrum of **2**

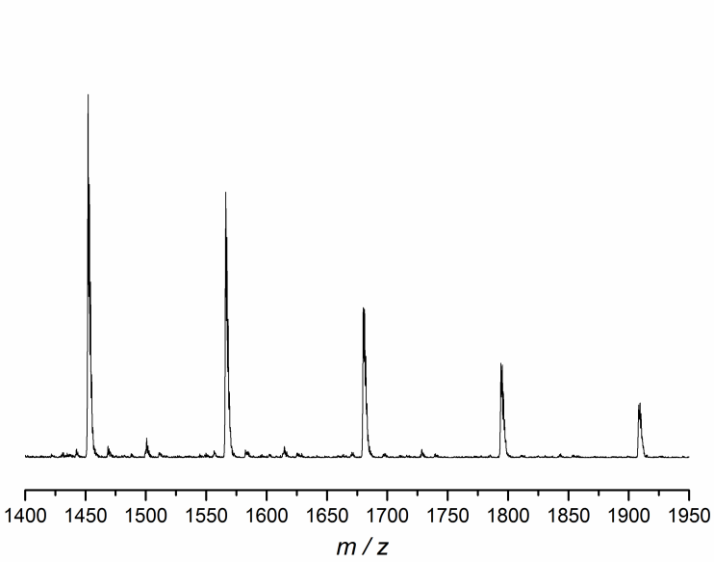

	PCL-Cp DA product (2)
Measured mass values	**1452.09**
Theoretical mass values	**1452.16**

Trapped cyanodithioester di-linker (3)

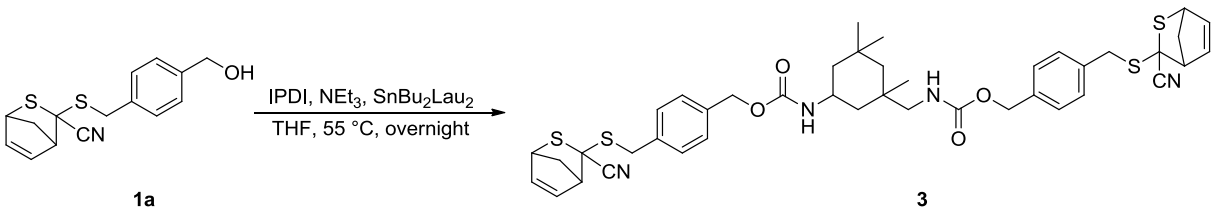

1a **3**

Alcohol **1a** (1.00 g, 3.40 mmol, 2.3 eq), isophorone diisocyanate (0.33 mg, 1.50 mmol, 1 eq) and dibutyltin dilaurate (1.00 mg, 0.015 mmol, 0.01 eq) were placed in a two neck flask under inert atmosphere (N_2). 4 mL dry THF were added and the mixture was heated to 55 °C. 0.5 mL (0.362 mg, 3.50 mmol, 2.3 eq) triethylamine were added and the reaction mixture was stirred overnight at 55 °C. To cease the reaction, the mixture was exposed to air and cooled to ambient temperature. THF was removed under reduced pressure and the residue was dissolved in 40 mL DCM. The organic layer was washed with 1 M NaOH (2·30 mL), 1 M HCl (2·30 mL), and brine. The organic layer was dried over magnesium sulfate and concentrated under reduced pressure to gain 1.40 g of a dark solid. The crude product was purified by flash chromatography (silica gel/ ethylacetate:hexane (2:1)). Yield: 53% (0.700 g, 0.800 mmol), MS (ESI) calculated for sum formula $[M+Na]^+$: (found) 823.00 *m / z*, (expected) 823.23 *m / z*.

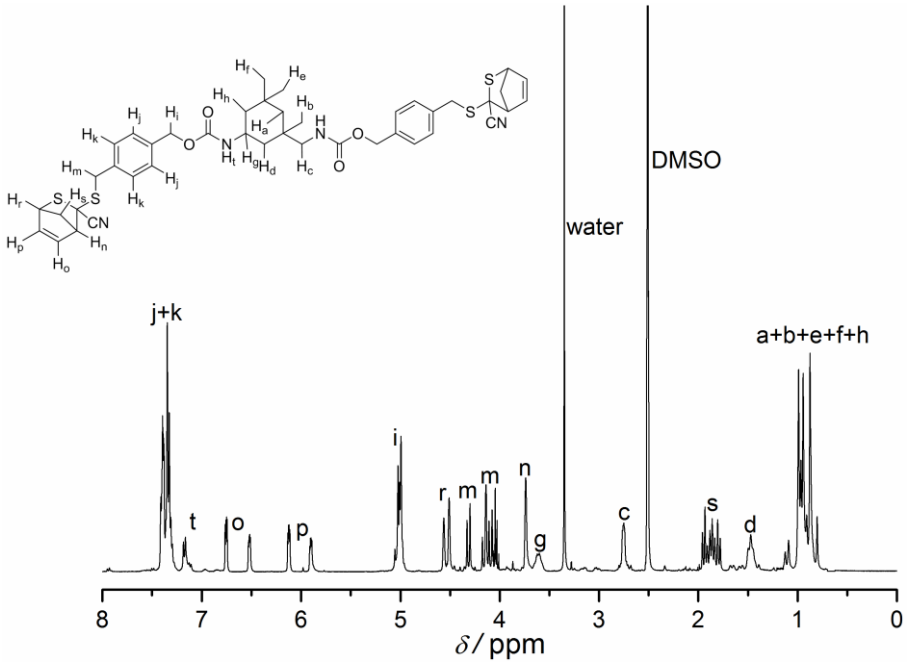

^{1}H NMR (DMSO-d^6, 250 MHz) δ (ppm): 7.40-7.29 (m, 8H, Ar*H*), 7.18-7.10 (m, 1H, N*H*), 6.76-6.74 (dd, *J* = 5.4, 2.9 Hz, 1H, C=C*H*), 6.52-6.50 (dd, *J* = 5.1, 2.9 Hz, 1H,

C=C*H*), 6.13-6.10 (dd, *J* = 5.3, 3.2 Hz, 1H, C=C*H*), 5.90-5.88 (dd, *J* = 5.0, 3.4 Hz, 1H, C=C*H*), 5.05-4-95 (m, 4H, NCOOCH_2), 4.55 (s, 1H, C*H*SC), 4.50 (s, 1H, C*H*SC), 4.32-4.29 (d, *J* = 12.1 Hz, 1H, SCH_2Ar), 4.17-4.02 (m, 3H, SCH_2Ar), 3.73 (s, 2H, C*H*CCN), 3.60 (br, 1H, OOCNC*H*), 2.74 (br, 2H, OOCNCH_2) 1.95-1.77 (m, 4H, bridge CH_2), 1.46 (br, 2H, CH2) 1.12-0.79 (m, 13H, three CH_3 groups and two CH_2 groups from the cyclohexane fragment).

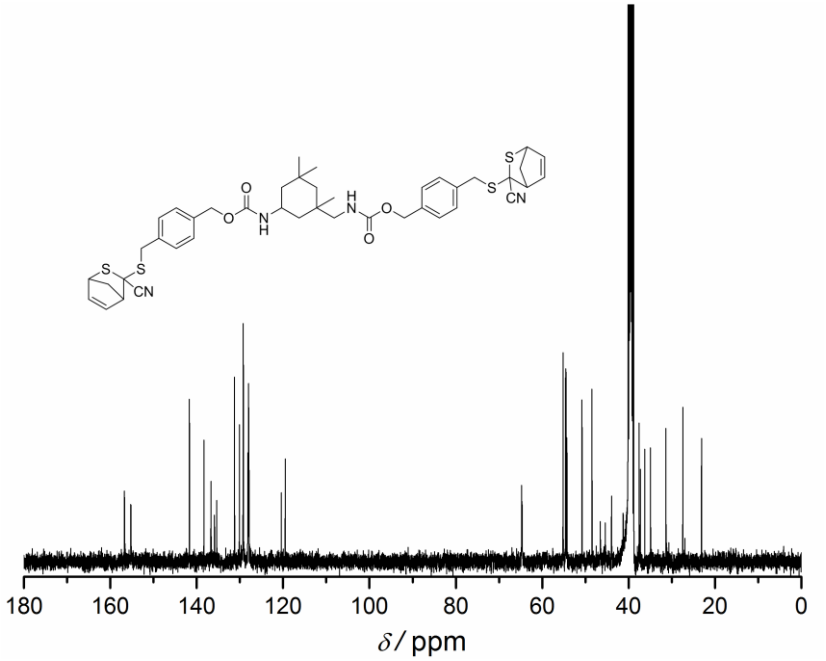

^{13}C-NMR (DMSO-d^6, 100 MHz) δ (ppm): 156.74, 155.26, 141.71, 138.35, 135.90, 135.39, 131.27, 130.14, 129.27, 129.22, 128.18, 128.11, 128.00, 127.93, 120.44, 119.54, 64.81, 64.71, 59.76, 55. 22, 54.61, 54.59, 54.53, 54.33, 50.84, 48.53, 46.60, 45.44, 44.00, 37.62, 37.34, 36.30, 34.98, 31.42, 27.50, 23.18.

ESI-MS spectrum of **3**

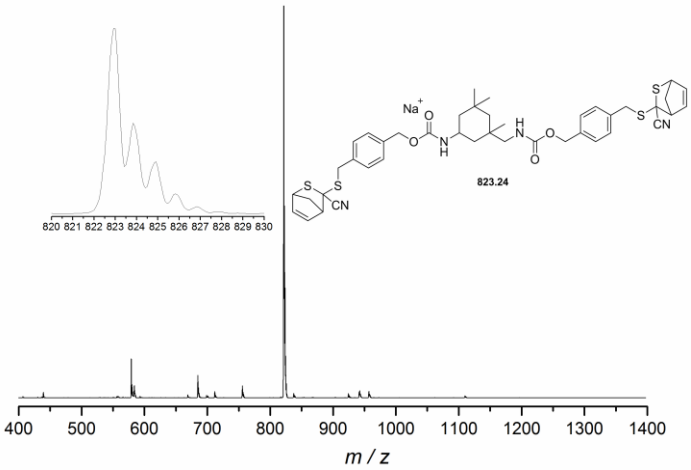

Diene exchange of cyanodithioester end capped poly(ε-caprolactone) (5)

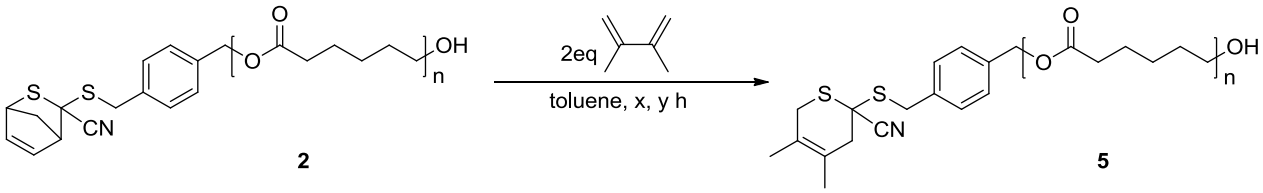

CDTE end capped PCL **2** (27.0 mg, 0.013 mmol, 1 eq) was placed in a two neck flask and dissolved in 2 mL toluene. 3.00 µL (2.21 µg, 0.026 mmol, 2 eq) DMBD were added and the mixture was heated to the desired temperature (80 °C, 100 °C or 120 °C) with a rubber septum on one neck and a reflux condenser on the other. For the kinetic studies, samples were taken after pre-defined time, and cooled to ambient temperature. The solvent was removed and the residue was dissolved in THF for ESI-MS analysis. The reaction conversion was calculated by comparing the product's and starting material's peak intensities of the first signal of the isotopic pattern. To prevent the error of chain length depended ionization, the 3 most intensive repeating units were averaged.

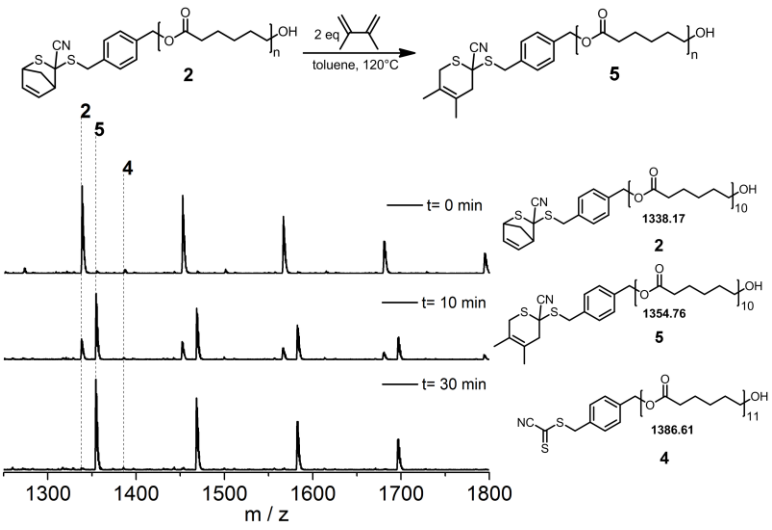

	PCL-Cp DA product (2)	PCL-unprotected CDTE (4)	PCL-DMBD DA product (5)
Measured mass values	**1338.09**	**1386.66**	**1354.67**
Theoretical mass values	**1338.17**	**1386.61**	**1354.76**

HDA step-growth polymerization reactions (6 and HDA-polymer)

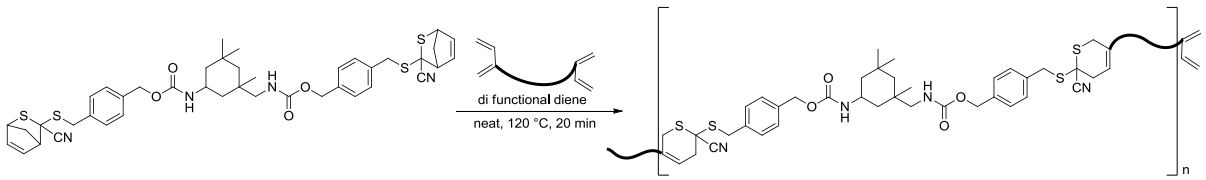

3 **6 , HDA polymer**

Di-linker **3** and a molar equivalent amount of the suitable diene di-linker Cp_2-P(iBoA-BA) or IPDI-SA were dissolved in DCM and stirred for 5 min. After the solids were dissolved, the solution was transferred to a 5 mL flask. The flask was coated with a thin layer of starting material mixture by removing the solvent under reduced pressure. The flask was subsequently placed in an oil bath and heated to 120 °C. After 20-60 min reaction time the oil bath was removed and the obtained polymer was analyzed via SEC.

11.2 Alternative cyanodithioester synthesis approaches

Styrene oxide ring opening with cyanodithioate salt

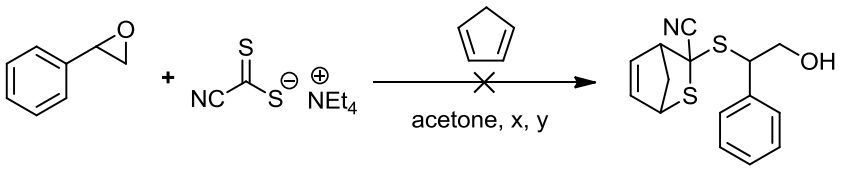

Styrene oxide (36.0 mg, 0.030 mmol, 1 eq) was dissolved in 1 mL aceton (in some cases with 1 eq of either TosOH, $ZnCl_2$, $AlCl_3$ or Al(*i*Bu)$_3$) and stirred at ambient temperature for 10 min in a 100 mL round bottom flask. Next, a solution of cyanodithioate salt (69.0 mg, 0.030 mmol, 1 eq) and cyclopentadiene (5.40 mg, 0.090 mmol, 3 eq) in 1 mL acetone was added to the flask and stirred overnight (a sample was taken after 4 h to check the conversion). To stop the reaction, water was added in order to quench the Lewis acid. The mixture was extracted with DCM which was subsequently evaporated. Zooms into the resulting ^{1}H NMR spectrum are presented in chapter 5. The experiment was repeated at 50 °C with a reflux condenser following the same procedure.

Michael addition on hydroxylethylacrylate

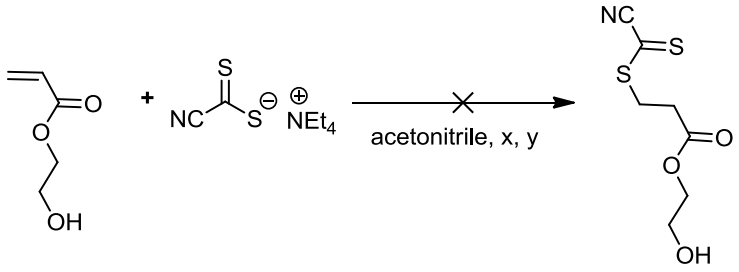

Hydroxylethylacrylate (34.8 mg, 0.300 mmol, 1 eq) and cyanodithioate salt (0.069 g, 0.300 mmol, 1 eq) were dissolved in 1 mL acetonitrile and stirred at ambient temperature overnight (a sample was taken after 4 h to check the conversion). To stop the reaction, the acetonitrile was removed and water as well as DCM were added. The organic layer was separated dried and concentrated. A zoom into the resulting ^{1}H NMR spectrum are presented in chapter 5. The experiment was repeated at 50 °C with a reflux condenser following the same procedure.

Synthesis of tosylethanol

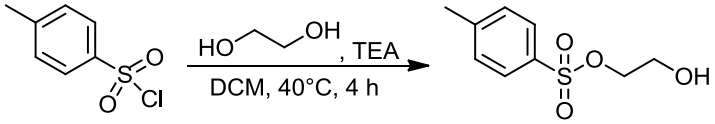

Ethylen glycol (1.00 g, 7.89 mmol, 1.5 eq), triethylamine (0.525 g, 5.26 mmol, 1 eq) and Tosylchloride (1.00 g, 5.26 mmol, 1 eq) were dissolved in 30 mL DCM and stirred over night at ambient temperature. For the work up the DCM phase was washed with water, saturated bicarbonate solution, 5%-HCl solution and brine, each time with 40 mL. The aqueous phases were every time reextracted with 10 mL DCM. The combined organic layers were dried over $MgSO_4$ and concentrated. The obtained residue was recrystalized in ethylacetate/hexane (1:2) to yield 1.00 g of crude tosylethanol from the filtrate. Yield = 88%.

^{1}H NMR ($CDCl_3$-d, 400 MHz) δ (ppm): 7.82-7.80 (d, *J* = 8.3 Hz, 2H, Ar*H*), 7.37-7.35 (d, *J* = 8.0 Hz, 2H, Ar*H*), 4.16-4.14 (t, *J* = 4.8 Hz, 2H, C–CH_2OSO_2), 3.83-3.81 (t, *J* = 4.8 Hz, 2H, C–CH_2OH), 2.45 (s, 3H, CH_3).

SN2 reaction with tosylethanol

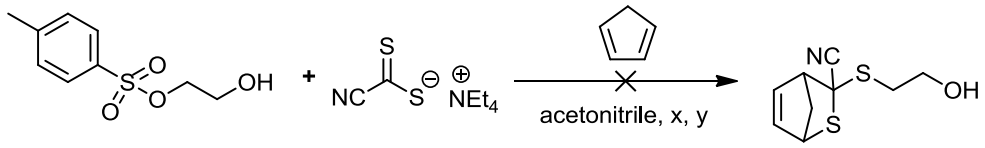

Tosylethanol (0.020 g, 0.092 mmol, 1 eq), cyanodithioate salt (0.017 g, 0.007 mmol, 0.8 eq) and cyclopentadiene (0.018 g, 0.270 mmol, 3 eq) were dissolved in 0.8 mL acetonitrile and stirred over night at ambient temperature (a sample was taken after 4 h to check the conversion). To stop the reaction, the acetonitrile was removed and water as well as DCM were added. The organic layer was separated dried and concentrated. A zoom into the resulting ^{1}H NMR spectrum is presented in chapter 5. The experiment was repeated at 50 °C with a reflux condenser following the same procedure.

SN2 reaction with methyl-2-bromoacetate (7)

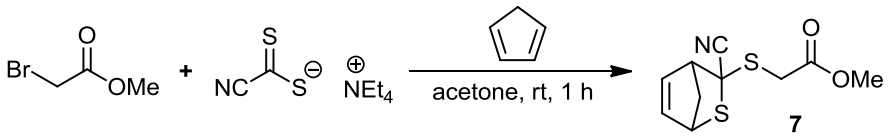

Cyanodithioate salt (50.0 mg, 0.021 mmol, 1 eq) and cyclopentadiene (0.060 mL, 4.22 mg, 0.064 mmol, 3 eq) were dissolved in 1 mL acetone and stirred at ambient temperature. To the mixture, a solution of methyl-2-bromoacetate in 1 mL acetone was added dropwiese. After 1 h the solvent was removed and the residue taken in 10 mL DCM. The DCM phase was washed with 10 mL water, dried over $MgSO_4$ and concentrated to yield 50 mg of a yellowish oil. Yield = 96%

^{1}H NMR ($CDCl_3$, 400 MHz) δ (ppm): 6.69-6.67 (dd, *J* = 5.4, 2.9 Hz, 0.4H, C=CH_{exo}), 6.52-6.50 (dd, *J* = 5.4, 2.9 Hz, 0.6H, C=CH_{endo}), 6.17-6.15 (dd, *J* = 5.4, 3.2 Hz, 0.4H, C=CH_{exo}), 6.09-6.07 (dd, *J* = 5.4, 3.2 Hz, 0.6H, C=CH_{endo}), 4.29 (s, 0.6H, C*H*SC), 4.22 (s, 8H, C*H*SC, 0.4H, C*H*SC), 3.83-3-45 (m, 2H, CH_2C=O, 1H, C*H*C-CN), 3.73 (s, 3H, COCH_3),2.18-1.93 (d+ddt+d,*J* = 10.2, 18.1, 10.2, 2.1, 10.4 Hz, 2H, bridge CH_2).

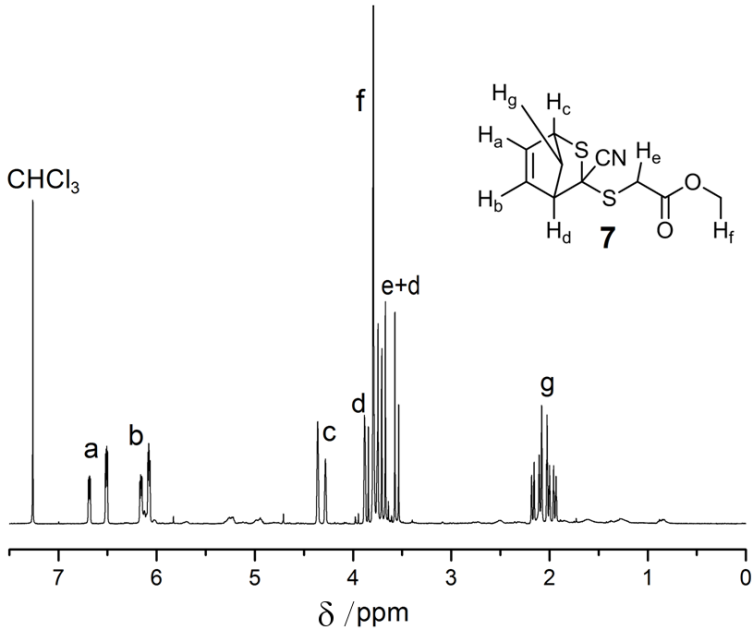
CHCl3
a
b
c
d
e+d
f
g
Hg
Hc
Ha
S
CN
He
Hb
S
O
Hd
7
O
Hf
7
6
5
4
3
2
1
0
δ /ppm

11.3 Reversible networks based on cyanodithioester chemistry

Bromo-quatro-linker precursor (8)

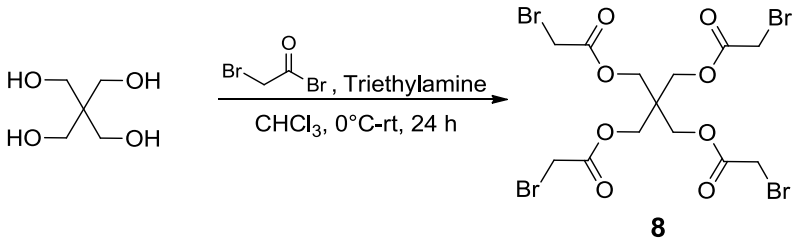

8

1.00 g (7.40 mmol, 1.0 eq) pentaerythritol was suspended, under a nitrogen atmosphere, in 110 mL $CHCl_3$, which was stored over $CaCl_2$. After adding 4.96 mL (3.71 g, 36.7 mmol, 5.0 eq) triethylamine the solution was cooled with an ice bath to 0 °C. Under strong stirring, 3.18 mL (7.39 g, 36.7 mmol, 5.0 eq) bromoacetyl bromide, diluted in 30.0 mL $CHCl_3$, were added dropwise over a period of approximately 30 min. Subsequent complete addition, the ice bath was removed and the reaction stirred further. After 24 h the solid was filtered, and the organic layer washed with water, three times with saturated sodium carbonate solution, twice with 10% HCl solution and finally water and brine (each time with 50.0 mL). A brownish liquid was obtained when the organic phase was dried over $MgSO_4$ and concentrated. The liquid was purified by flash column chromatography (n-hexane/ethylacetate, 4:1).The combined pure fractions were dried over $MgSO_4$ and concentrated to give the desired product as pale yellow oil. Yield: 31% (1.4 g, 2.27 mmol). ^{1}H NMR ($CDCl_3$-d, 400 MHz) δ (ppm): 4.28 (s, 8H, C*H*2OC=O), 3.86 (s, 8H, C*H2*Br)

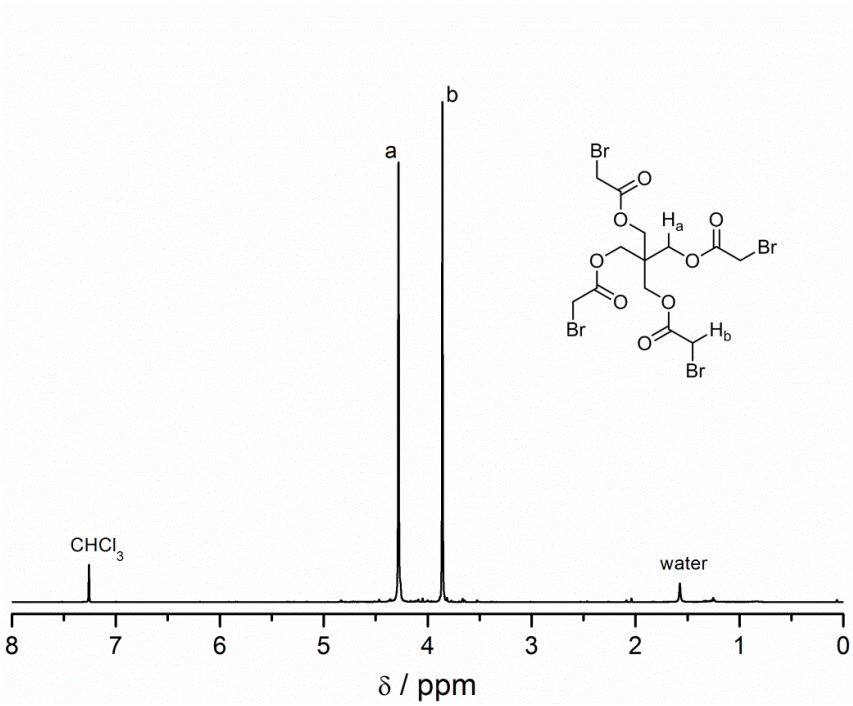

Cp protected cyanodithioester quattro–linker (9)

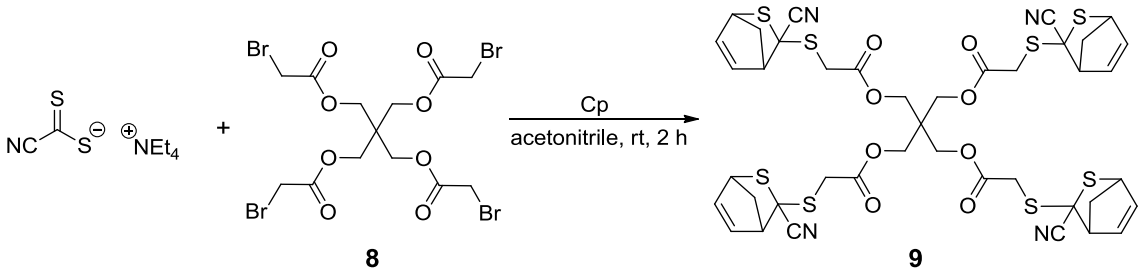

A mixture of 0.665 g (1.08 mmol, 1.0 eq) quattro-linker precursor and 0.860 mL (0.560 g, 8.60 mmol, 8.0 eq) cyclopentadiene, in 25.0 mL acetonitrile, was stirred at ambient temperature. Over a period of 30 min, a solution of 25 mL acetonitrile, containing 1.00 g (4.30 mmol, 4 eq) cyano salt, was added dropwise to the solution. The reaction was stirred for an additional 1.5 h and subsequently stopped by evaporating the acetonitrile. The residue was taken up in 50.0 mL DCM and washed with 10% HCl, saturated sodium carbonate solution and water (each time 40.0 mL). After drying over $MgSO_4$ and concentrating on an evaporator, 1.05 g of a dark green solid (foam) were obtained. Yield: 99% (1.05 g, 1.07 mmol). MS (ESI) calculated for sum formula $[M+Na]^+$: (found) 995.1 *m / z*, (expected) 995.05 *m / z*.

^{1}H NMR ($CDCl_3$-d, 400 MHz) δ (ppm): 6.69-6.67 (dd, *J* = 5.4, 2.9 Hz, 2H, C=C*H*$_{exo}$), 6.52-6.50 (dd, *J* = 5.4, 2.9 Hz, 2H, C=C*H*$_{endo}$), 6.17-6.15 (dd, *J* = 5.4, 3.2 Hz, 2H, C=C*H*$_{exo}$), 6.09-6.07 (dd, *J* = 5.4, 3.2 Hz, 2H, C=C*H*$_{endo}$), 4.39 (s, 2H, C*H*SC), 4.30 (s, 8H, C*H*SC, 2H, C*H*SC), 3.89 (s, 2H, C*H*C-CN), 3.75-3-63 (m, 8H, C*H*$_2$C=O, 2H, C*H*C-CN), 2.18-1.93 (d+ddt+d,*J* = 10.2, 18.1, 10.2, 2.1, 10.4 Hz, 8H, bridge C*H*$_2$).

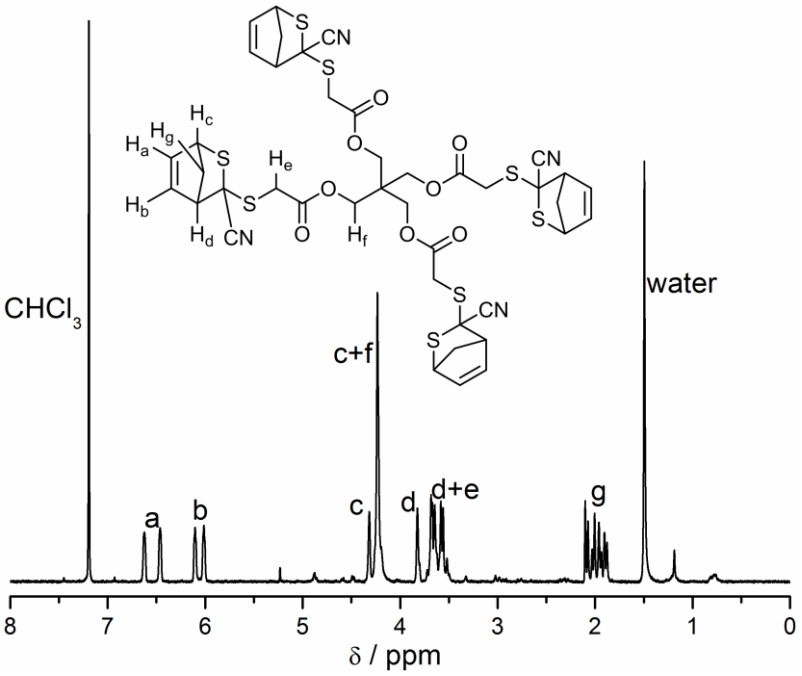

Formation of CDTE/Cp network (**10**)

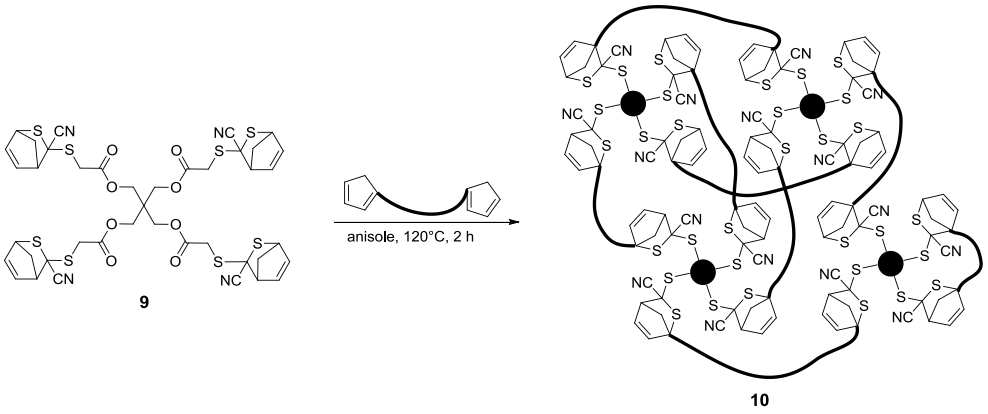

Quatro-linker **9** and a double molar amount of di-linker Cp_2-P(iBoA-BA) were dissolved in anisol at a mass concentration of 300 mg·mL^{-1} of Cp_2-P(iBoA-BA). The viscous solution was added to the network template, already heated on a heater to 125° C and kept at this temperature for 2 h. After 2 h, the heater was turned off and the template allowed to cool (the cooling took approximately 30 min). At 50 °C the formed network was removed from the template and subsequently pressed in a hot

press at 120° C with 1 kN under vacuum. The obtained pellet (whose shape can be selected by choosing the press template) was used for the analytical measurements.

Tensile test healing

The broken specimen parts were added to the heatable press in a rod template and heated under vacuum to 120 °C at 1 kN. The heating of the press to 120 °C took 10 min. When 120 °C were reached, the thermo element was turned off to allow the press to cool to 50 °C over 30 min. At 50 °C, the rod template was removed from the press and the rod shaped sample separated from the template.

11.4 The thioaldehyde-cyclopentadiene pair

Phenacylsulfide precursor

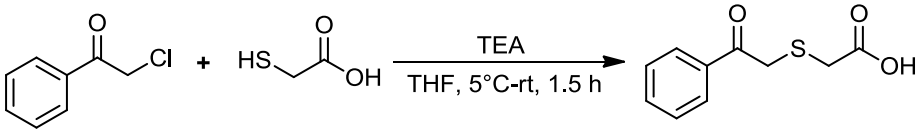

Thioglycolic acid (920 mg, 10.0 mmol) was taken up in 25 mL of THF and cooled to 5 °C with stirring under nitrogen (flow). Triethylamine (2.10 g, 2.90 mL, 20.8 mmol, 2.08 eq) was added (neat), followed by phenacyl chloride (1.56 g, 10.1 mmol, 1.01 eq) in 5 mL of THF, whereupon a thick precipitate developed. The mixture was stirred at 5 °C for 30.0 min and at room temperature for 1 h and then was poured into a stirred mixture of ice-cold 0.5 M HCl (100 mL) and 50.0 mL of ether. The aqueous layer was extracted with 2 times with diethylether. The combined organic layers were dried over $MgSO_4$, filtered and concentrated. The obtained white solid was recrystalized from $CHCl_3$, to yield 1.87 g phenacylsulfide acid. Yield: 89%

^{1}H NMR ($CDCl_3$-d, 400 MHz) δ (ppm): 7.98–7.96 (d, J = 7.3 Hz, 2H), 7.61–7.57 (t, J = 7.4 Hz, 1H), 7.50–7.46 (t, J = 7.7 Hz, 2H), 4.06 (s, 2H), 3.36 (s, 2H).

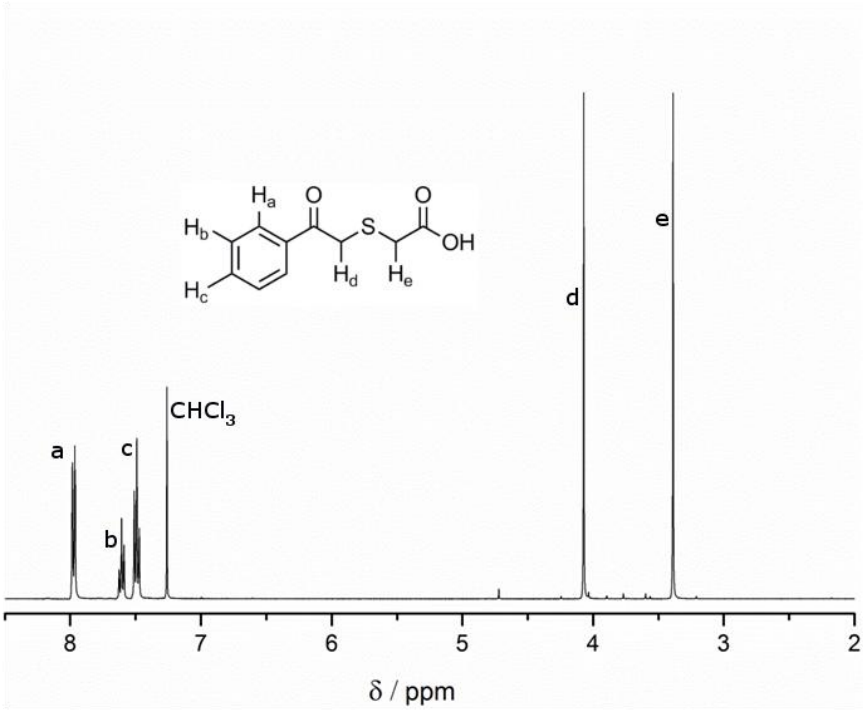

Poly(ethylene glycol) esterification

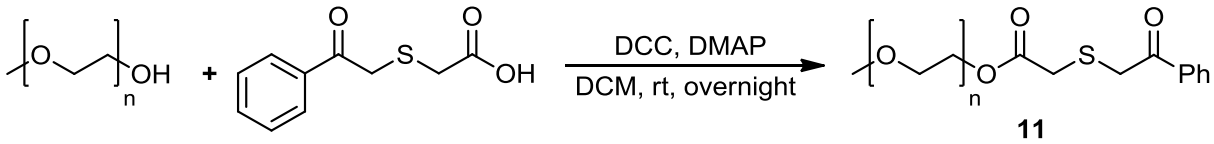

Poly(ethylene glycol) monomethyl ether (2.00 g, 1.00 mmol), 4-dimethylaminopyridine (7.00 mg, 0.600 mmol) and (phenacylthio)acetic acid (631 mg, 3.00 mmol) were dissolved in 10.0 mL dry DCM. A solution of DCC (619 mg, 3.00 mmol) in 2 mL dry DCM was added and the reaction mixture stirred overnight at ambient temperature. The solution was filtered and the polymer precipitated in cold diethyl ether to give a white solid.

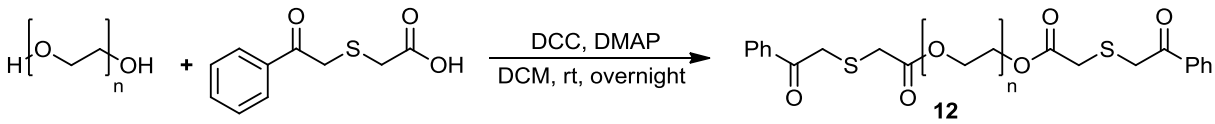

The bis-phenacylsulfid PEG was synthesized with the same functional group ratios and concentration as the mono functionalized one. A 8 kDA bis hydroxyl poly(ethylenglycol) was used for the di-linker synthesis.

^{1}H NMR ($CDCl_3$-d, 400 MHz) δ (ppm): 7.98–7.96 (d, *J* = 7.3 Hz, 2H), 7.61–7.57 (t, *J* = 7.4 Hz, 1H), 7.50–7.46 (t, *J* = 7.7 Hz, 2H), 4.30-4.27 (t, *J* = 4.8 Hz, 2H), 4.06 (s, 2H), 3.81-3.80 (t, *J* = 4.6 Hz, 2H), 3.64 (s, PEG back bone), 3.36 (s, 2H).

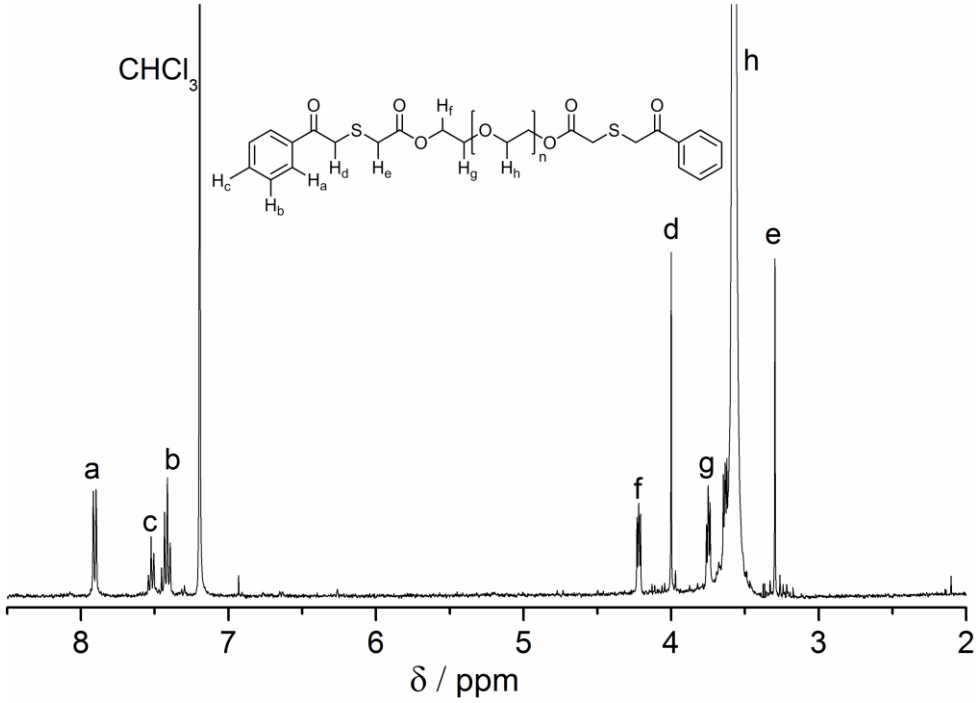

Photo-reactions with small molecule dienes

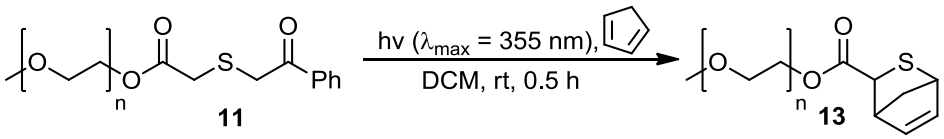

Phenacyl sulfide mono functionalized PEG **11** (10.0 mg, 5 μmol) and cyclopentadiene (0.500 mg, 0.610 μL, 7.50 μmol) were dissolved in 1.00 mL dry CH_2Cl_2 in a headspace vial (Pyrex, dia. 20 mm), which was crimped airtight using styrene/butadiene rubber seals with PTFE inner liner. The solution was deoxygenated by purging with nitrogen for 5 min. The vessel was irradiated by revolving around a 36 W compact low-pressure fluorescent lamp (Philips CLEO Compact PL-L, λ_{max} = 355 nm) at a distance of 40-50 mm in a custom built photo reactor (see Ref 10 of the main manuscript for a drawing). After 30 min the irradiation was stopped and the solvent removed under a stream of nitrogen. The residue was redissolved in THF and analyzed by SEC/ESI-MS (refer to chapter 7).

Diene exchange study

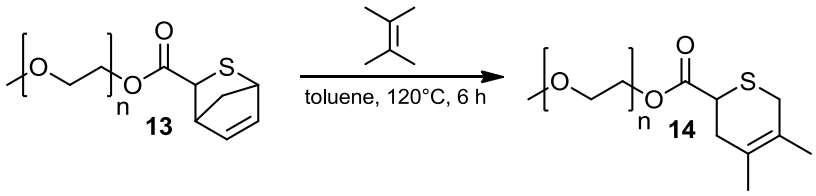

Cp trapped mono functionalized PEG **13** (10.0 mg, 5.00 μmol, 1 eq) and 2,3-dimethylbutadiene (0.410 mg, 10.0 μmol, 2 eq) were dissolved in 1 mL toluene in a headspace vial (Pyrex, dia. 20 mm) which was crimped airtight using styrene/butadiene rubber seals with PTFE inner liner. The solution was deoxygenated by purging with nitrogen for 5 min. After 6 h refluxing the reaction was stopped and cooled down to room temperature. At room temperature the toluene was removed and the residue was redissolved in THF and analyzed by SEC/ESI-MS.

MS spectra evaluation:

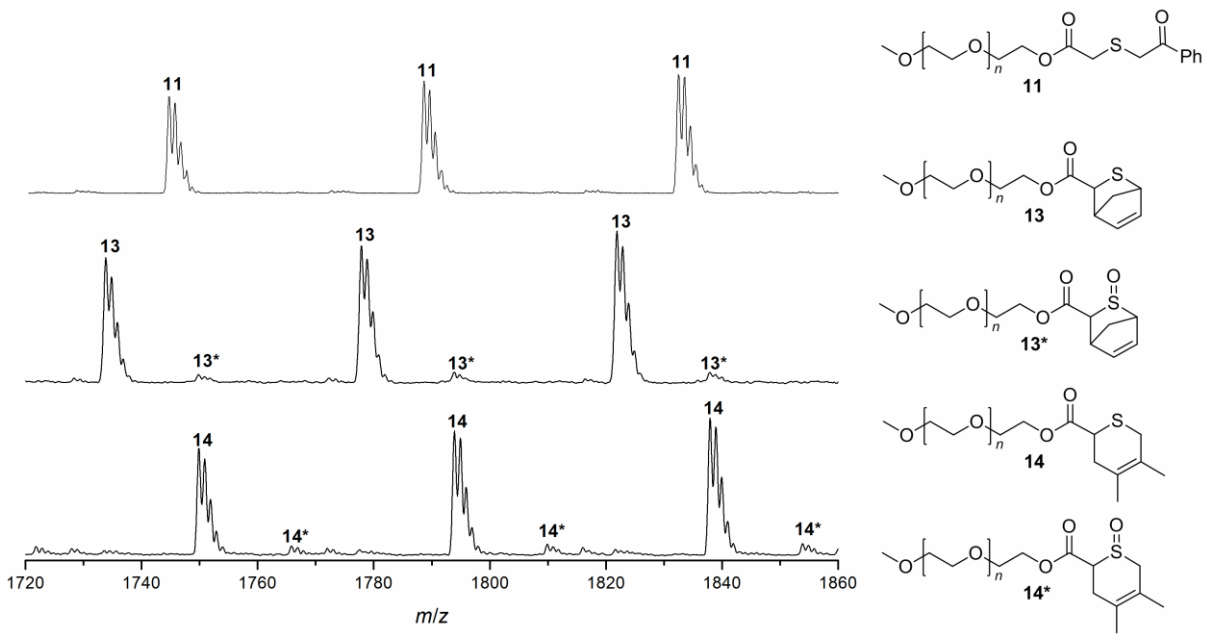

Compound	n (EG)	Summa Formula	m / z^{theo}	m / z^{meas}	$\Delta m / z$
11	34	$C_{79}H_{148}NaO_{37}S^+$	1743.93	1743.91	0.02
13	35	$C_{78}H_{150}NaO_{37}S^+$	1733.94	1733.83	0.11
13*	35	$C_{79}H_{150}NaO_{38}S^+$	1794.83	1794.94	0.11
14	35	$C_{79}H_{154}NaO_{37}S^+$	1749.91	1749.97	0.06
14*	35	$C_{79}H_{154}NaO_{38}S^+$	1765.97	1765.83	0.14

Light-induced HDA polymerization

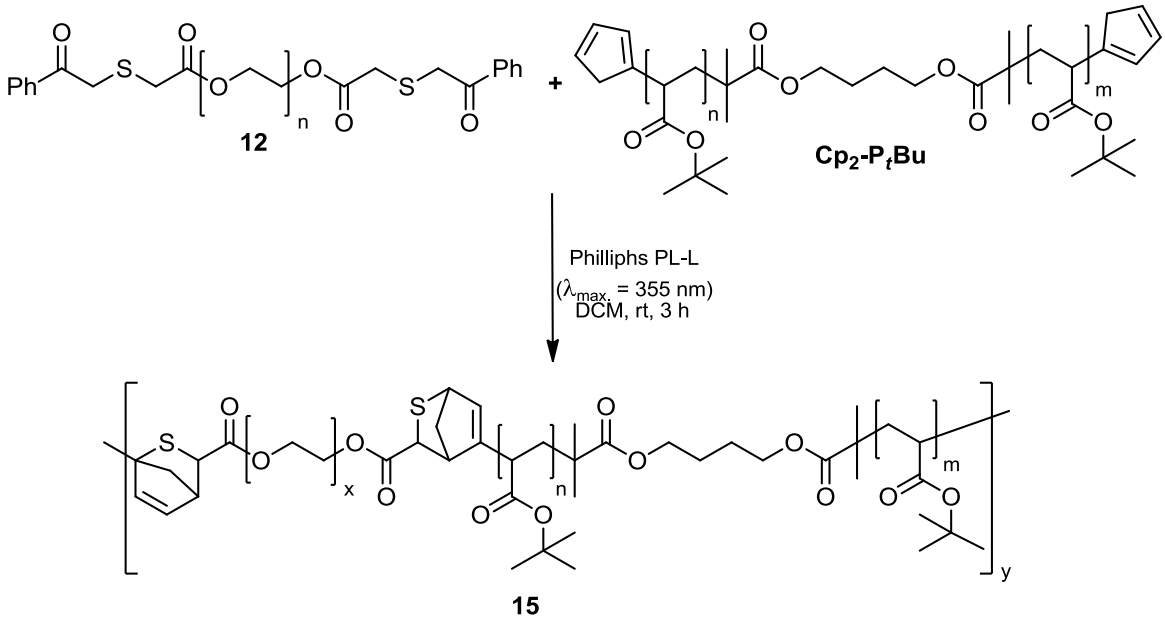

An equimolar ratio of polymer **12** and **Cp_2-P_tBu** was weighted in a headspace vial (Pyrex, diameter 20 mm), and crimped air-tight using SBR seals with PTFE inner liner. The vial was flushed with nitrogen before dry DCM was added to the vial (polymer concentration 10.0 $mg \cdot mL^{-1}$). The solution was deoxygenated by further purging with nitrogen for 5 min. The vial was subsequently irradiated for 3 h in the photo reactor. After irradiation, the solvent was removed and the residue analyzed by SEC.

Depolymerization reaction

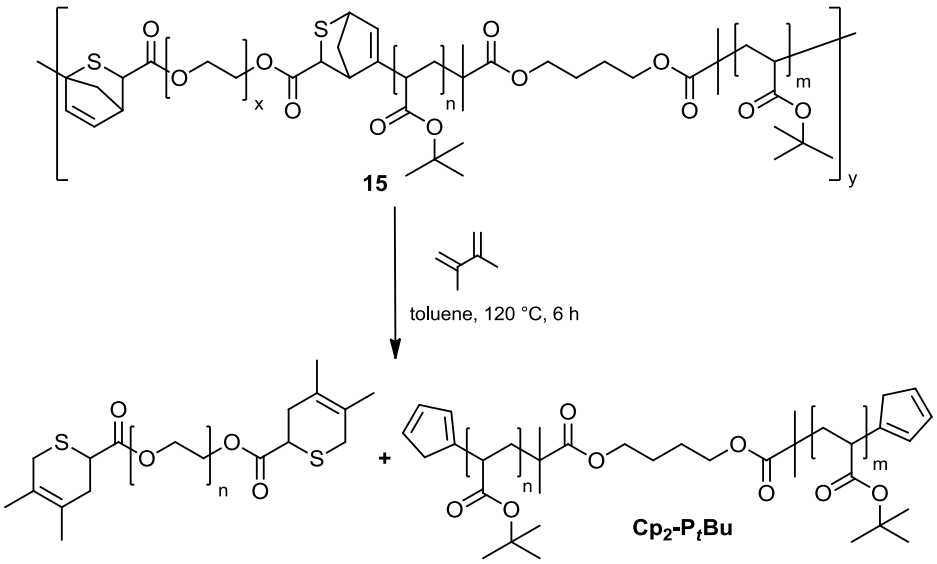

A sample of 20.0 mg step-growth polymer **15** was dissolved in 0.500 mL toluene and heated with 10 eq of 2,3-dimethylbutadiene (eq were calculated by the mass and M_n of **15**) to 120 °C for 6 h. After cooling to ambient temperature the toluene was evaporated and the remaining material analyzed by SEC (see main texts for the data).

11.5 Light-induced RAFT hetero Diels–Alder chemistry

RAFT polymerization of methyl methacrylate with CPDB (**16**)

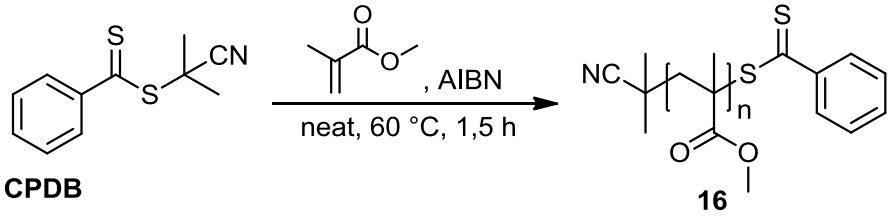

MMA (50.0 mL, 47.0 g, 470 mmol, 200 eq), 2-cyanopropyl dithiobenzoate (0.538 g, 2.43 mmol, 1.00 eq) and 2,2'-azobis(isobutyronitrile) (0.042 g, 0.256 mmol, 0.10 eq) were weighted into a round bottom flask. The flask was sealed with a rubber septum and the solution was deoxygenated by purging with nitrogen for 20 min. The mixture was subsequently heated to 60 °C for 90 min. After 90 min the solution was exposed to air and cooled with an ice bath. Three consecutive precipitations from cold *n*-

hexane yielded 7 g of a pink powder, which was analyzed via SEC (M_n = 3300 g·mol^{-1}, $Đ_M$ = 1.27) and SEC/ESI-MS.

Synthesis of photoenol precursor 2-methoxy-6-methylbenzaldehyde (17)

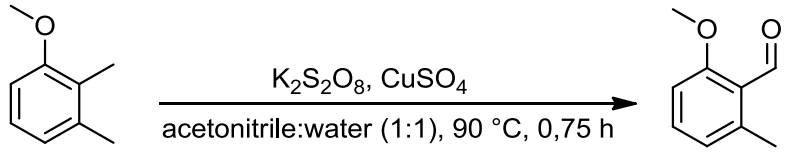

17

2,3-Dimethyl anisole (7.03 g, 51.6 mmol, 1.00 eq), copper sulfate pentahydrate (13.1 g, 52.5 mmol, 1.02 eq) and potassium peroxodisulfate (41.9 g, 154 mmol, 3.00 eq) were added to a mixture of MeCN/water (1:1, 500 mL) in a round bottom flask. The suspension was vigorously stirred and heated at 90 °C in a temperature regulated oil bath until thin layer chromatography (TLC) revealed that all the starting material had been consumed. At this point, 45 min after the start of the reaction, the mixture was allowed to cool down to ambient temperature and the non-dissolved copper salt was removed by filtration. DCM (150 mL) was added and the phases were separated. The aqueous phase was extracted two times with DCM (100 mL) and the combined organic layers were dried over magnesium sulfate. After removal of the solvent under reduced pressure, the crude product was purified by flash chromatography (silica gel, hexane/ethyl acetate 5:1 v/v), yielding 5.2 g of a yellow solid. Yield: 68%

^{1}H NMR ($CDCl_3$-d, 250 MHz) δ (ppm): 10.64 (s, 1H, C*H*O), 7.38 (t, ^3J = 7.97 Hz, 1H, Ar*H*), 6.81 (t, ^3J = 7.97 Hz, 2H, Ar*H*), 3.89 (s, 3H, OCH_3), 2.57 (s, 3H, CH_3).

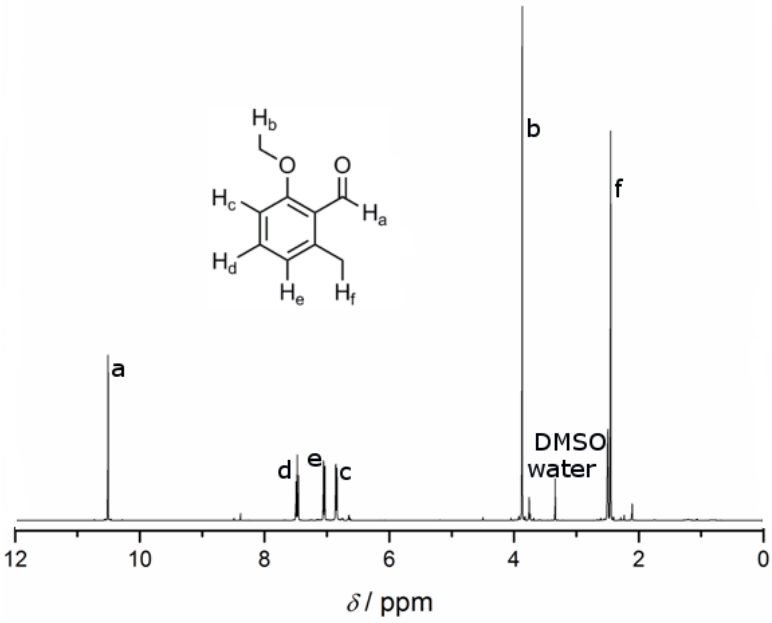

Synthesis of functionalized photoenol 2-hydroxy-6-methylbenzaldehyde

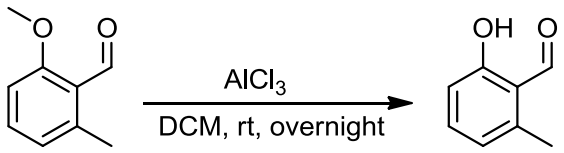

17

2-Methoxy-6-methylbenzaldehyde (5.20 g, 34.6 mmol, 1.00 eq) was dissolved in anhydrous DCM (75.0 mL) and cooled to 0 °C. $AlCl_3$ (13.9 g, 103 mmol, 3.00 eq) was added and the mixture was stirred at ambient temperature overnight. The reaction was quenched with H_2O and the phases were separated. The aqueous layer was extracted three times with DCM (100 mL). The combined organic layers were dried over magnesium sulfate and the solvent was evaporated. The final purification was carried out by flash chromatography (silica gel, cyclohexane/ethyl acetate 2:1 v/v) yielding 3.90 g of a yellow solid. Yield: 82%

^{1}H NMR ($CDCl_3$-d, 250 MHz) δ (ppm): 11.91 (s, 1H, O*H*), 10.32 (s, 1H, C*H*O), 7.38 (t, ^3J = 7.9 Hz, 1H, Ar*H*), 6.76 (dd, ^3J = 25.3, 7.9 Hz, 2H, Ar*H*), 2.61 (s, 3H, CH_3).

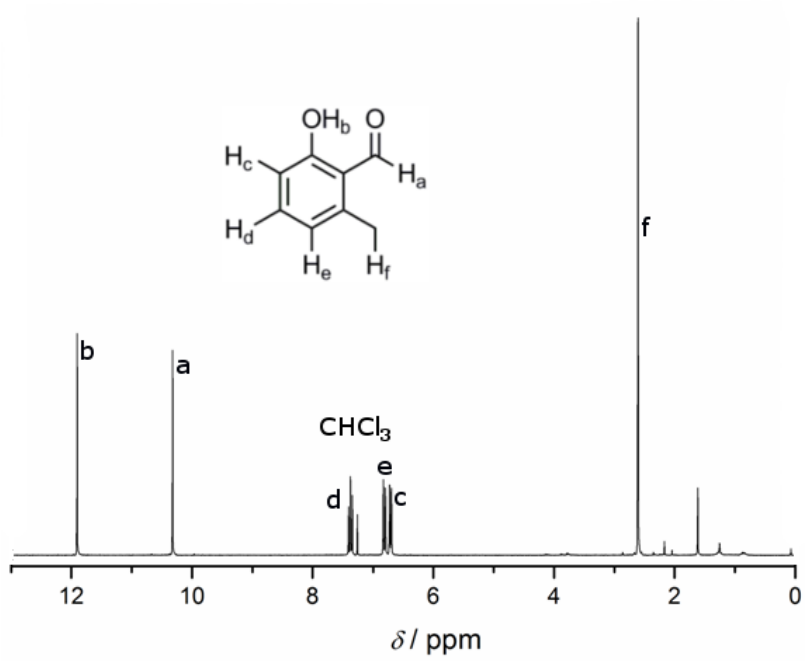
OHb
O
Hc
Ha
Hd
He
Hf
b
a
CHCl3
e
d
c
f
12
10
8
6
4
2
0
δ / ppm

Photoenol-ROP initiator 2-((11-hydroxyundecyl)oxy)-6-methylbenzaldehyde

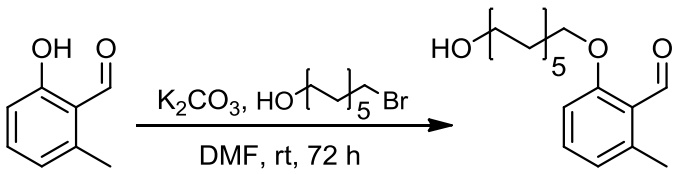

To a suspension of K_2CO_3 (394 mg, 2.85 mmol, 1.67 eq) in anhydrous DMF (5.20 mL) 2-hydroxy-6-methylbenzaldehyde (909 mg, 6.68 mmol, 1.23 eq) was added and the mixture was stirred for 30 min. A solution of 11-bromo-undecanol (1.36 g, 5.47 mmol, 1.00 eq) in anhydrous DMF (2.00 mL) was added dropwise over a period of 30 min. After stirring for 72 h the reaction was quenched with H_2O (50 mL). The mixture was extracted with diethyl ether three times and the combined organic layers were washed with 5% NaOH (2 x 50.0 mL) and H_2O (2 x 100 mL). After drying over magnesium sulfate and evaporating the solvent, the crude product was purified by flash chromatography (silica gel, cyclohexane/ethyl acetate 2:1 v/v) yielding 0.770 g of a yellow solid. Yield: 45%

^{1}H NMR ($CDCl_3$-d, 250 MHz) δ (ppm): 10.67 (s, 1H, C*H*O), 7.34 (t, ^3J = 7.9 Hz, 1H, Ar*H*), 6.80 (t, ^3J = 8.2 Hz, 2 H, Ar*H*), 4.03 (t, ^3J = 6.3 Hz, 2H, HOCH_2), 3.64 (t, ^3J = 6.6 Hz, 2H, ArOCH_2), 2.57 (s, 3H, CH_3), 1.89-1.74 (m, 2H, HOCH2-CH_2), 1.62-1.25 (m, 16H, CH_2).

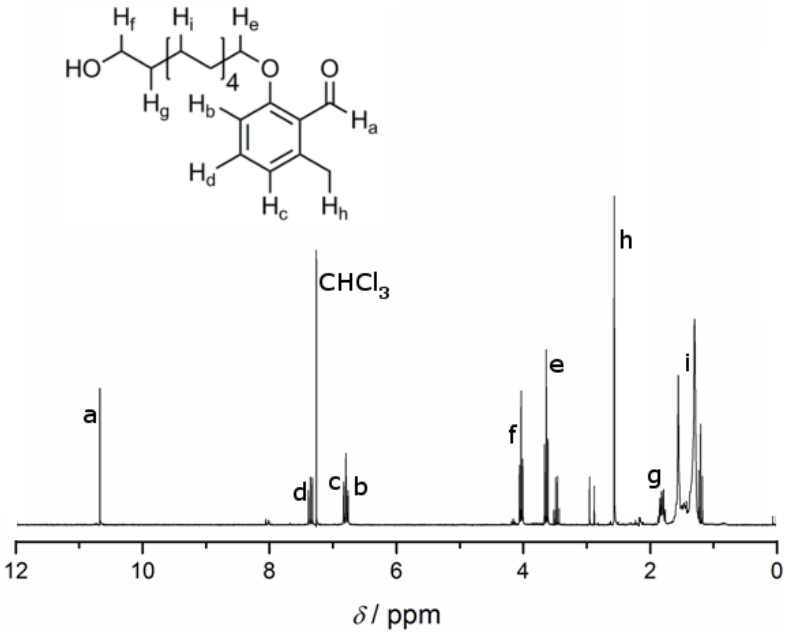

Photoenol end capped poly(ε-caprolactone) (19)

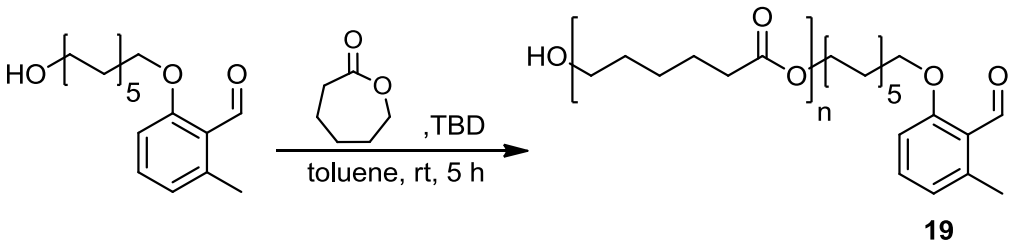

19

2-((11-hydroxyundecyl)oxy)-6-methylbenzaldehyde (121 mg, 0.396 mmol, 0.08 eq) and TBD (6.00 mg, 0.043 mmol, 0.008 eq) were dissolved in toluene (2.5 mL) in an inert atmosphere (Ar). ε-CL (565 mg, 4.95 mmol, 1.00 eq) was added and the solution was stirred at ambient temperature for 5 h. The reaction was quenched with benzoic acid (50.0 mg, 0.400 mmol, 0.08 eq) and the polymer was precipitated in cold hexane/Et_2O (1:1 v/v, 200 mL).

^{1}H NMR ($CDCl_3$, 250 MHz) δ (ppm): 10.67 (s, 1H, C*H*O), 7.37 (t, *J* = 7.9 Hz, 1H, Ar*H*), 6.80 (t, *J* = 8.3 Hz, 2H, Ar*H*), 4.05 (t, *J* = 6.6 Hz, OCH_2 initiator, OCH_2 along polymer backbone), 3.64 (t, *J* = 6.4 Hz, 2H, COOCH_2), 2.56 (s, 3H, CH_3), 2.30 (t, *J* = 7.5 Hz, 2H, OOC-CH_2), 1.86-1.24 (m, CH_2 along polymer backbone). (M_n = 2000 g·mol^{-1}, $Đ_M$ = 1.25).

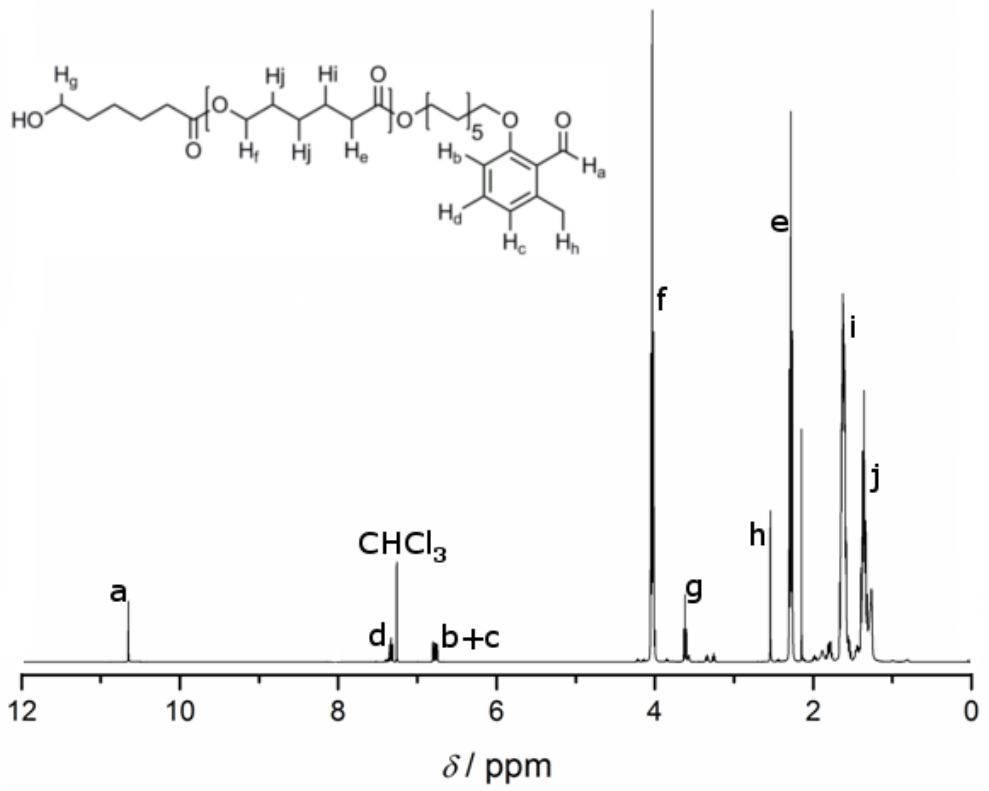

Light-triggered reaction of 2-methoxy-6-methylbenzaldehyde (17) with RAFT - poly(methyl methacrylate) (16)

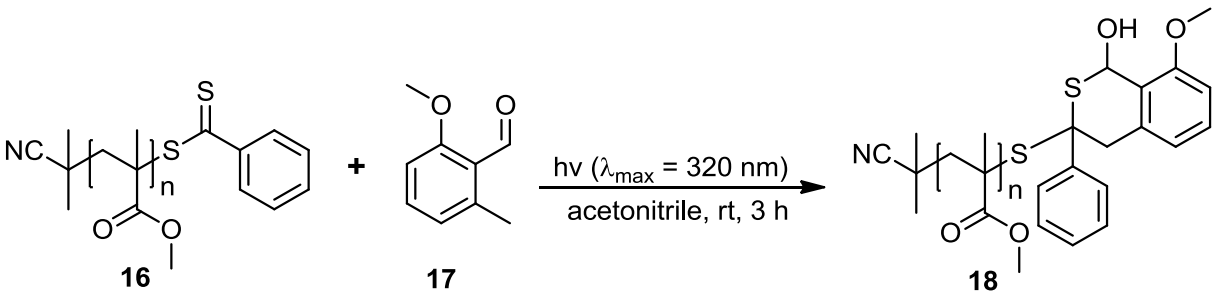

Both reagents were weighted up into a headspace vial (Pyrex, dia. 20 mm) in a ratio of 1 (PMMA **16**) to 1.1 (**17**) and dissolved in MeCN to give a polymer concentration of 10.0 $g \cdot L^{-1}$. The vial was crimped airtight using a styrene/butadiene rubber seal with a PTFE inner liner. The reaction mixture within the vial was subsequently deoxygenated by bubbling nitrogen through the solution for 20 min. The vial was irradiated by revolving it around a compact low-pressure fluorescent lamp (Arimed B6, Cosmedico GmbH, Stuttgart, Germany), emitting at 320 nm (± 30 nm), at a distance of 40–50 mm in a custom-built photoreactor. After ending the reaction, the solution was concentrated under reduced pressure and the polymer was precipitated from cold *n*-hexane. The polymer was filtered and dissolved in THF for SEC/ESI-MS analysis.

Light-triggered reaction of photoenol end capped poly-(ε-caprolactone) (19) with the RAFT-poly(methyl methacrylate) (16)

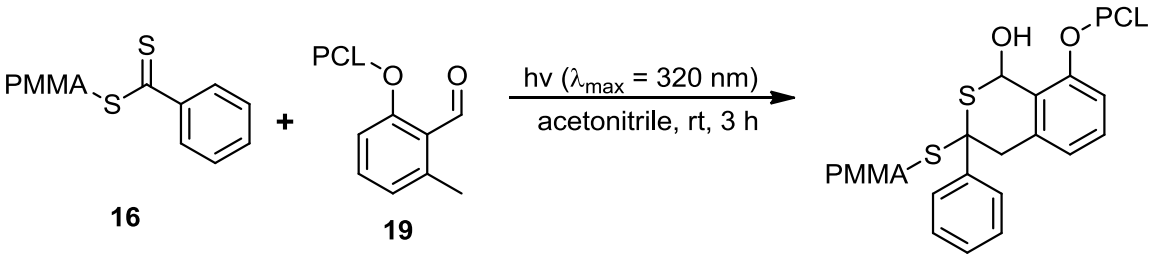

Equimolar amounts of both polymers were weighted up into a headspace vial (Pyrex, dia. 20 mm) and dissolved in MeCN to give a polymer concentration of 5.00 $g \cdot L^{-1}$. The solution was deoxygenated by purging with nitrogen for 20 min. The vial was irradiated (3 h) by revolving it around a compact low-pressure fluorescent lamp (Arimed B6, Cosmedico GmbH, Stuttgart, Germany) emitting at 320 nm (± 30 nm) at

a distance of 40–50 mm in a custom-built photo reactor. After ending the reaction, the solvent was evaporated under reduced pressure and the polymer was dissolved in THF for SEC/ESI-MS analysis (M_n = 5900 g·mol^{-1}, $Đ_M$ = 1.26).

12 Schemes

13 Figures

14 Abbreviations

AIBN = 2,2′-Azobis(2-methylpropionitril)

ATRP = atom transfer radical polymerization

Cp = cyclopentadiene

CDTE = cyanodithioester

CuAAC = copper catalyzed azide alkyne 1,3 dipole cycloaddition

CPDB = 2-cyanopropyl-dithiobenzoate

CRP = controlled radical polymerization

DA = Diels–Alder

DCM = dichlormethane

DHTP = 3,6-dihydro-2H-thiopyrane

DLS = dynamic light scattering

DMF = N,N-dimethylformamide

ESI-MS = electro-spray ionization mass spectrometry

FRP = free radical polymerization

HDA = hetero Diels–Alder

HOMO = highest occupied molecular orbital

IC = internal conversion

IPDI = isophorone diisocyanate

IPDI-SA = isophorone di-sorbic alcohole

ISC = inter-system crossing

k_a = rate coefficient of activation

k_{add} = rate coefficient of addition

K_{ATRP} = equilibrium constant of atom transfer radical polymerization process

k_d = rate coefficient of dissociation

k_{DA} = rate coefficient of Diels–Alder reaction

k_{do} = rate coefficient of deactivation

K_{eq} = equilibrium constant of Diels–Alder process

k_i = rate coefficient of initiation

k_{rDA} = rate coefficient of retro Diels–Alder reaction

k_t = rate coefficient of termination

$k_{t\ comb}$ = rate coefficient of termination by combination

$k_{t\ dispro}$ = rate coefficient of termination by disproportionation

LUMO = lowest unoccupied molecular orbital

M_n = number average molar mass

MO = molecular orbital

M_p = molar mass

M_w = weight average molar mass

m / z = mass to charge ratio

NMP = nitroxide mediated radical polymerization

NMR = nuclear-magnetic-resonance-spectroscopy

P^{n}BA = poly(*n*-butylacrylate)

PCL = poly(ε-caprolactone)

Đ (PDI) = polydispersity

PE = photoenol precursor end group

PEG = poly(ethylenglycol)

P^{i}BoA = poly(isobornylacrylate)

PMMA = poly(methyl methacrylate)

P^{t}BA = poly(*tert*-butylacrylate)

PS = poly(styrene)

RAFT = reversible addition fragmentation chain transfer

RI = refractive index

ROMP = ring opening metathesis polymerization

ROP = ring opening polymerisation

SEC = size exclusion chromatography

SN2 = nucleophilic substitution of second order

SOMO = single occupied molecular orbital

TFA = trifluoraceticacid

THF = tetrahydrofuran

UV-Vis = ultraviolet / visible light

15 References

[1] C. J. Kloxin, C. N. Bowman, *Chem. Soc. Rev.* **2013**, *42*, 7161-7173.

[2] S. J. Rowan, S. J. Cantrill, G. R. L. Cousins, J. K. M. Sanders, J. F. Stoddart, *Angew. Chem. Int. Ed.* **2002**, *41*, 898-952.

[3] Y.-L. Liu, T.-W. Chuo, *Polymer Chemistry* **2013**, *4*, 2194-2205.

[4] J. Zhou, N. K. Guimard, A. J. Inglis, M. Namazian, C. Y. Lin, M. L. Coote, E. Spyrou, S. Hilf, F. G. Schmidt, C. Barner-Kowollik, *Polymer Chemistry* **2012**, *3*, 628-639.

[5] J. K. Stille, L. Plummer, *The Journal of Organic Chemistry* **1961**, *26*, 4026-4029.

[6] a) S. Sinnwell, A. J. Inglis, T. P. Davis, M. H. Stenzel, C. Barner-Kowollik, *Chem. Commun.* **2008**, 2052-2054; b) A. J. Inglis, S. Sinnwell, M. H. Stenzel, C. Barner-Kowollik, *Angew. Chem. Int. Ed.* **2009**, *48*, 2411-2414; c) A. J. Inglis, M. H. Stenzel, C. Barner-Kowollik, *Macromol. Rapid Commun.* **2009**, *30*, 1792-1798; d) L. Nebhani, S. Sinnwell, A. J. Inglis, M. H. Stenzel, C. Barner-Kowollik, L. Barner, *Macromol. Rapid Commun.* **2008**, *29*, 1431-1437.

[7] H. C. Kolb, M. G. Finn, K. B. Sharpless, *Angew. Chem. Int. Ed.* **2001**, *40*, 2004-2021.

[8] J. E. Moses, A. D. Moorhouse, *Chem. Soc. Rev.* **2007**, *36*, 1249-1262.

[9] a) C. Barner-Kowollik, A. J. Inglis, *Macromol. Chem. Phys.* **2009**, *210*, 987-992; b) A. S. Goldmann, M. Glassner, A. J. Inglis, C. Barner-Kowollik, *Macromol. Rapid Commun.* **2013**, *34*, 810-849.

[10] a) J.-F. Lutz, H. G. Börner, K. Weichenhan, *Macromolecules* **2006**, *39*, 6376-6383; b) U. Mansfeld, C. Pietsch, R. Hoogenboom, C. R. Becer, U. S. Schubert, *Polymer Chemistry* **2010**, *1*, 1560-1598.

[11] M. Glassner, K. K. Oehlenschlaeger, T. Gruendling, C. Barner-Kowollik, *Macromolecules* **2011**, *44*, 4681-4689.

[12] S. Sinnwell, A. J. Inglis, M. H. Stenzel, C. Barner-Kowollik, *Macromol. Rapid Commun.* **2008**, *29*, 1090-1096.

[13] M. Glassner, J. P. Blinco, C. Barner-Kowollik, *Macromol. Rapid Commun.* **2011**, *32*, 724-728.

[14] a) N. V. Tsarevsky, K. V. Bernaerts, B. Dufour, F. E. Du Prez, K. Matyjaszewski, *Macromolecules* **2004**, *37*, 9308-9313; b) R. M. Hensarling, V. A. Doughty, J. W. Chan, D. L. Patton, *J Am Chem Soc* **2009**, *131*, 14673-14675.

[15] a) P. Wu, A. K. Feldman, A. K. Nugent, C. J. Hawker, A. Scheel, B. Voit, J. Pyun, J. M. J. Fréchet, K. B. Sharpless, V. V. Fokin, *Angew. Chem. Int. Ed.* **2004**, *43*, 3928-3932; b) K. L. Killops, L. M. Campos, C. J. Hawker, *J Am Chem Soc* **2008**, *130*, 5062-5064; c) M. L. Szalai, D. V. McGrath, D. R. Wheeler, T. Zifer, J. R. McElhanon, *Macromolecules* **2007**, *40*, 818-823.

[16] C. Barner-Kowollik, F. E. Du Prez, P. Espeel, C. J. Hawker, T. Junkers, H. Schlaad, W. Van Camp, *Angew. Chem. Int. Ed.* **2011**, *50*, 60-62.

[17] a) C. J. Hawker, K. L. Wooley, *Science* **2005**, *309*, 1200-1205; b) A. J. Inglis, C. Barner-Kowollik, *Macromol. Rapid Commun.* **2010**, *31*, 1247-1266; c) R. K. Iha, K. L. Wooley, A. M. Nyström, D. J. Burke, M. J. Kade, C. J. Hawker, *Chem. Rev.* **2009**, *109*, 5620-5686.

[18] a) J.-A. Funel, S. Abele, *Angew. Chem. Int. Ed.* **2013**, *52*, 3822-3863; b) A. Gandini, *Prog. Polym. Sci.* **2013**, *38*, 1-29; c) M. A. Tasdelen, *Polymer Chemistry* **2011**, *2*, 2133-2145; d) G. Hizal, U. Tunca, A. Sanyal, *J. Polym. Sci., Part A: Polym. Chem.* **2011**, *49*, 4103-4120.

[19] a) W. H. Binder, R. Sachsenhofer, *Macromol. Rapid Commun.* **2008**, *29*, 952-981; b) W. Li, T. Tian, W. Zhu, J. Cui, Y. Ju, G. Li, *Polymer Chemistry* **2013**, *4*, 3057-3068.

[20] a) A. B. Lowe, *Polymer Chemistry* **2010**, *1*, 17-36; b) V. X. Truong, A. P. Dove, *Angew. Chem. Int. Ed.* **2013**, *52*, 4132-4136.

[21] K. N. Matyjaszewski, **2010**, pp. 103.

[22] a) A. P. Haehnel, M. Schneider-Baumann, K. U. Hiltebrandt, A. M. Misske, C. Barner-Kowollik, *Macromolecules* **2012**, *46*, 15-28; b) M. Buback, R. G. Gilbert, R. A. Hutchinson, B. Klumperman, F.-D. Kuchta, B. G. Manders, K. F. O'Driscoll, G. T. Russell, J. Schweer, *Macromol. Chem. Phys.* **1995**, *196*, 3267-3280; c) S. Beuermann, M. Buback, T. P. Davis, R. G. Gilbert, R. A. Hutchinson, O. F. Olaj, G. T. Russell, J. Schweer, A. M. van Herk, *Macromol. Chem. Phys.* **1997**, *198*, 1545-1560.

[23] T. Junkers, C. Barner-Kowollik, *J. Polym. Sci., Part A: Polym. Chem.* **2008**, *46*, 7585-7605.

[24] J. Barth, M. Buback, G. T. Russell, S. Smolne, *Macromol. Chem. Phys.* **2011**, *212*, 1366-1378.

[25] S. Beuermann, M. Buback, *Prog. Polym. Sci.* **2002**, *27*, 191-254.

[26] M. Szwarc, *Nature* **1956**, *178*, 1168.

[27] W. A. Braunecker, K. Matyjaszewski, *Prog. Polym. Sci.* **2007**, *32*, 93-146.
[28] J. Nicolas, Y. Guillaneuf, C. Lefay, D. Bertin, D. Gigmes, B. Charleux, *Prog. Polym. Sci.* **2013**, *38*, 63-235.
[29] K. Matyjaszewski, *Macromolecules* **2012**, *45*, 4015-4039.
[30] L. Barner, T. P. Davis, M. H. Stenzel, C. Barner-Kowollik, *Macromol. Rapid Commun.* **2007**, *28*, 539-559.
[31] T. Fukuda, T. Terauchi, A. Goto, K. Ohno, Y. Tsujii, T. Miyamoto, S. Kobatake, B. Yamada, *Macromolecules* **1996**, *29*, 6393-6398.
[32] H. Fischer, *Chem. Rev.* **2001**, *101*, 3581-3610.
[33] V. Sciannamea, R. Jérôme, C. Detrembleur, *Chem. Rev.* **2008**, *108*, 1104-1126.
[34] a) M. Gomberg, *J Am Chem Soc* **1898**, *20*, 773-780; b) M. Gomberg, *J Am Chem Soc* **1900**, *22*, 757-771.
[35] T. Junkers, L. Zang, E. H. H. Wong, N. Dingenouts, C. Barner-Kowollik, *J. Polym. Sci., Part A: Polym. Chem.* **2011**, *49*, 4841-4850.
[36] S. Fleischmann, H. Komber, D. Appelhans, B. I. Voit, *Macromol. Chem. Phys.* **2007**, *208*, 1050-1060.
[37] D. Benoit, S. Grimaldi, S. Robin, J.-P. Finet, P. Tordo, Y. Gnanou, *J Am Chem Soc* **2000**, *122*, 5929-5939.
[38] W. Tang, Y. Kwak, W. Braunecker, N. V. Tsarevsky, M. L. Coote, K. Matyjaszewski, *J Am Chem Soc* **2008**, *130*, 10702-10713.
[39] J.-S. Wang, K. Matyjaszewski, *J Am Chem Soc* **1995**, *117*, 5614-5615.
[40] M. Kato, M. Kamigaito, M. Sawamoto, T. Higashimura, *Macromolecules* **1995**, *28*, 1721-1723.
[41] a) T. K. Hayes, R. Villani, S. M. Weinreb, *J Am Chem Soc* **1988**, *110*, 5533-5543; b) D. P. Curran, *Synthesis* **1988**, *1988*, 489-513.
[42] J.-F. Lutz, K. Matyjaszewski, *J. Polym. Sci., Part A: Polym. Chem.* **2005**, *43*, 897-910.
[43] V. Coessens, T. Pintauer, K. Matyjaszewski, *Prog. Polym. Sci.* **2001**, *26*, 337-377.
[44] W. Jakubowski, K. Matyjaszewski, *Angew. Chem. Int. Ed.* **2006**, *45*, 4482-4486.
[45] J. Chiefari, Y. K. Chong, F. Ercole, J. Krstina, J. Jeffery, T. P. T. Le, R. T. A. Mayadunne, G. F. Meijs, C. L. Moad, G. Moad, E. Rizzardo, S. H. Thang, *Macromolecules* **1998**, *31*, 5559-5562.
[46] G. Moad, E. Rizzardo, S. H. Thang, *Aust J Chem* **2005**, *58*, 379-410.
[47] G. Johnston-Hall, A. Theis, M. J. Monteiro, T. P. Davis, M. H. Stenzel, C. Barner-Kowollik, *Macromol. Chem. Phys.* **2005**, *206*, 2047-2053.
[48] C. Barner-Kowollik, *Handbook of RAFT Polymerization*, Wiley-VCH , Weinheim, Germany **2008**.
[49] G. Moad, E. Rizzardo, S. H. Thang, *Aust J Chem* **2009**, *62*, 1402-1472.
[50] G. Moad, E. Rizzardo, S. H. Thang, *Aust J Chem* **2006**, *59*, 669-692.
[51] D. J. Keddie, G. Moad, E. Rizzardo, S. H. Thang, *Macromolecules* **2012**.
[52] L. Albertin, M. H. Stenzel, C. Barner-Kowollik, L. J. R. Foster, T. P. Davis, *Macromolecules* **2005**, *38*, 9075-9084.
[53] O. Altintas, A. P. Vogt, C. Barner-Kowollik, U. Tunca, *Polymer Chemistry* **2012**, *3*, 34-45.
[54] C. Barner-Kowollik, T. P. Davis, J. P. A. Heuts, M. H. Stenzel, P. Vana, M. Whittaker, *J. Polym. Sci., Part A: Polym. Chem.* **2003**, *41*, 365-375.
[55] F. Sanda, T. Endo, *J. Polym. Sci., Part A: Polym. Chem.* **2001**, *39*, 265-276.
[56] O. Nuyken, S. Pask, *Polymers* **2013**, *5*, 361-403.
[57] H. Mori, S. Masuda, T. Endo, *Macromolecules* **2006**, *39*, 5976-5978.
[58] N. Calderon, H. Y. Chen, K. W. Scott, *Tetrahedron Lett* **1967**, *8*, 3327-3329.
[59] L. R. Gilliom, R. H. Grubbs, *J Am Chem Soc* **1986**, *108*, 733-742.
[60] R. Grubbs, W. Tumas, *Science* **1989**, *243*, 907-915.
[61] a) A. Dag, H. Sahin, H. Durmaz, G. Hizal, U. Tunca, *J. Polym. Sci., Part A: Polym. Chem.* **2011**, *49*, 886-892; b) J. A. Johnson, Y. Y. Lu, A. O. Burts, Y.-H. Lim, M. G. Finn, J. T. Koberstein, N. J. Turro, D. A. Tirrell, R. H. Grubbs, *J Am Chem Soc* **2010**, *133*, 559-566; c) S. R. White, N. R. Sottos, P. H. Geubelle, J. S. Moore, M. R. Kessler, S. R. Sriram, E. N. Brown, S. Viswanathan, *Nature* **2001**, *409*, 794-797.
[62] O. Diels, K. Alder, *Justus Liebigs Ann. Chem.* **1928**, *460*, 98-122.
[63] W. Albrecht, *Justus Liebigs Ann. Chem.* **1906**, *348*, 31-49.
[64] O. Diels, J. Blom, W. Koll, *Justus Liebigs Ann. Chem.* **1925**, *443*, 242.
[65] H. v. Euler, K. O. Josephson, *Berichte der deutschen chemischen Gesellschaft (A and B Series)* **1920**, *53*, 822-826.
[66] a) O. Diels, K. Alder, *Justus Liebigs Ann. Chem.* **1931**, *490*, 236-242; b) O. Diels, K. Alder, *Berichte der deutschen chemischen Gesellschaft (A and B Series)* **1929**, *62*, 554-562; c) O.

Diels, K. Alder, *Berichte der deutschen chemischen Gesellschaft (A and B Series)* **1929**, *62*, 2081-2087; d) O. Diels, K. Alder, *Justus Liebigs Ann. Chem.* **1929**, *470*, 62-103; e) O. Diels, K. Alder, *Justus Liebigs Ann. Chem.* **1931**, *490*, 277-294; f) O. Diels, K. Alder, *Justus Liebigs Ann. Chem.* **1931**, *486*, 191-202; g) O. Diels, K. Alder, *Justus Liebigs Ann. Chem.* **1931**, *486*, 211-225; h) O. Diels, K. Alder, *Justus Liebigs Ann. Chem.* **1931**, *490*, 243-257; i) O. Diels, K. Alder, *Justus Liebigs Ann. Chem.* **1931**, *490*, 257-266; j) O. Diels, K. Alder, *Justus Liebigs Ann. Chem.* **1931**, *490*, 267-276; k) O. Diels, K. Alder, E. Petersen, *Justus Liebigs Ann. Chem.* **1931**, *486*, 202-210; l) O. Diels, K. Alder, *Berichte der deutschen chemischen Gesellschaft (A and B Series)* **1929**, *62*, 2337-2372; m) O. Diels, K. Alder, *Justus Liebigs Ann. Chem.* **1930**, *478*, 137-154.

[67] M. Petrzilak, I. J. Grayson, *synthesis* **1981**, *10*, 753.

[68] K. Alder, *Neuere Methoden der preparativen organsichen Chemie*, Verlag Chemie, Weinheim, **1943**.

[69] a) S. M. Weinreb, R. R. Staib, *Tetrahedron* **1982**, *38*, 3087-3128; b) J. Hamer, *1,4-Cycloaddition Reactions*, Academic Press, New York, **1967**; c) S. B. Needleman, M. C. Chang Kuo, *Chem. Rev.* **1962**, *62*, 405-431.

[70] G. Desimoni, G. Tacconi, *Chem. Rev.* **1975**, *75*, 651-692.

[71] a) W. J. Middleton, *The Journal of Organic Chemistry* **1965**, *30*, 1390-1394; b) W. J. Middleton, *The Journal of Organic Chemistry* **1965**, *30*, 1395-1398; c) M. S. Raasch, *The Journal of Organic Chemistry* **1979**, *44*, 632-633.

[72] E. Vedejs, T. H. Eberlein, D. J. Mazur, C. K. McClure, D. A. Perry, R. Ruggeri, E. Schwartz, J. S. Stults, D. L. Varie, *The Journal of Organic Chemistry* **1986**, *51*, 1556-1562.

[73] B. König, J. Martens, K. Praefcke, A. Schönberg, H. Schwarz, R. Zeisberg, *Chem. Ber.* **1974**, *107*, 2931-2937.

[74] K. Hartke, T. Kissel, J. Quante, G. Henssen, *Angewandte Chemie International Edition in English* **1978**, *17*, 953-954.

[75] a) J. Sauer, R. Sustmann, *Angewandte Chemie International Edition in English* **1980**, *19*, 779-807; b) E. Goldstein, B. Beno, K. N. Houk, *J Am Chem Soc* **1996**, *118*, 6036-6043.

[76] a) S. Sakai, *The Journal of Physical Chemistry A* **2000**, *104*, 922-927; b) L. A. Telan, R. A. Firestone, *Tetrahedron* **1999**, *55*, 14269-14280; c) J. S. Chen, K. N. Houk, C. S. Foote, *J Am Chem Soc* **1998**, *120*, 12303-12309.

[77] R. B. Woodward, R. Hoffmann, *J Am Chem Soc* **1965**, *87*, 395-397.

[78] R. B. Woodward, R. Hoffmann, *Angewandte Chemie International Edition in English* **1969**, *8*, 781-853.

[79] R. Hoffmann, R. B. Woodward, *J Am Chem Soc* **1965**, *87*, 2046-2048.

[80] G. N. Lewis, *Proceedings of the National Academy of Sciences* **1925**, *11*, 179-183.

[81] A. J. Inglis, L. Nebhani, O. Altintas, F. G. Schmidt, C. Barner-Kowollik, *Macromolecules* **2010**, *43*, 5515-5520.

[82] G. Mantovani, F. Lecolley, L. Tao, D. M. Haddleton, J. Clerx, J. J. L. M. Cornelissen, K. Velonia, *J Am Chem Soc* **2005**, *127*, 2966-2973.

[83] L. Rulíšek, P. Šebek, Z. Havlas, R. Hrabal, P. Čapek, A. Svatoš, *The Journal of Organic Chemistry* **2005**, *70*, 6295-6302.

[84] N. K. Guimard, J. Ho, J. Brandt, C. Y. Lin, M. Namazian, J. O. Mueller, K. K. Oehlenschlaeger, S. Hilf, A. Lederer, F. G. Schmidt, M. L. Coote, C. Barner-Kowollik, *Chemical Science* **2013**, *4*, 2752-2759.

[85] a) A. Gandini, A. Silvestre, D. Coelho, *Polymer Chemistry* **2013**, *4*, 1364-1371; b) A. Gandini, M. N. Belgacem, *Prog. Polym. Sci.* **1997**, *22*, 1203-1379; c) A. Gandini, A. J. D. Silvestre, D. Coelho, *Polymer Chemistry* **2011**, *2*, 1713-1719.

[86] E. Goiti, M. B. Huglin, J. M. Rego, *Macromol. Rapid Commun.* **2003**, *24*, 692-696.

[87] X. Chen, M. A. Dam, K. Ono, A. Mal, H. Shen, S. R. Nutt, K. Sheran, F. Wudl, *Science* **2002**, *295*, 1698-1702.

[88] a) D. Boger, S. M. Weinreb, *Hetero Diels-Alder ethodology in organic synthesis*, Elsevier, New York, **1987**; b) W. M. McGregor, D. C. Sherrington, *Chem. Soc. Rev.* **1993**, *22*, 199-204.

[89] K. K. Oehlenschlaeger, N. K. Guimard, J. Brandt, J. O. Mueller, C. Y. Lin, S. Hilf, A. Lederer, M. L. Coote, F. G. Schmidt, C. Barner-Kowollik, *Polymer Chemistry* **2013**, *4*, 4348-4355.

[90] a) G. W. Kirby, W. M. McGregor, *J. Chem. Soc., Perkin Trans. 1* **1990**, 3175-3181; b) T. L. Gilchrist, J. E. Wood, *J. Chem. Soc., Chem. Commun.* **1992**, 1460-1461.

[91] a) E. Vedejs, J. S. Stults, R. G. Wilde, *J Am Chem Soc* **1988**, *110*, 5452-5460; b) J. Rapp, R. Huisgen, *Tetrahedron* **1997**, *53*, 961-970.

[92] a) H. Jiang, D. C. Cruz, Y. Li, V. H. Lauridsen, K. A. Jørgensen, *J Am Chem Soc* **2013**, *135*, 5200-5207; b) H. Dentel, I. Chataigner, F. Le Cavelier, M. Gulea, *Tetrahedron Lett* **2010**, *51*, 6014-6017.

[93] a) D. M. Vyas, G. W. Hay, *Journal of the Chemical Society D: Chemical Communications* **1971**, 1411-1412; b) D. M. Vyas, G. W. Hay, *Can. J. Chem.* **1971**, *49*, 3755-3758; c) D. M. Vyas, G. W. Hay, *J. Chem. Soc., Perkin Trans. 1* **1975, 180-186.**

[94] M. Glassner, G. Delaittre, M. Kaupp, J. P. Blinco, C. Barner-Kowollik, *J Am Chem Soc* **2012**, *134*, 7274-7277.

[95] S. Sinnwell, M. Lammens, M. H. Stenzel, F. E. Du Prez, C. Barner-Kowollik, *J. Polym. Sci., Part A: Polym. Chem.* **2009**, *47*, 2207-2213.

[96] D. Hönicke, R. Födisch, P. Claus, M. Olson, in *Ullmann's Encyclopedia of Industrial Chemistry*, Wiley-VCH Verlag GmbH & Co. KGaA, **2000**.

[97] E. B. Murphy, E. Bolanos, C. Schaffner-Hamann, F. Wudl, S. R. Nutt, M. L. Auad, *Macromolecules* **2008**, *41*, 5203-5209.

[98] F. Günzler, T. Junkers, C. Barner-Kowollik, *J. Polym. Sci., Part A: Polym. Chem.* **2009**, *47*, 1864-1876.

[99] L. Tschugaeff, *Berichte der deutschen chemischen Gesellschaft* **1899**, *32*, 3332-3335.

[100] a) B. A. Jones, J. S. Bradshaw, *Chem. Rev.* **1984**, *84*, 17-30; b) S. Scheibye, J. Kristensen, S. O. Lawesson, *Tetrahedron* **1979**, *35*, 1339-1343.

[101] M. Jesberger, T. P. Davis, L. Barner, *Synthesis* **2003**, *2003*, 1929-1958.

[102] H. Pellissier, *Tetrahedron* **2009**, *65*, 2839-2877.

[103] M. F. Ansell, A. A. Charalambides, *J. Chem. Soc., Chem. Commun.* **1972**, 739-740.

[104] W. J. Dale, A. J. Sisti, *J Am Chem Soc* **1954**, *76*, 81-82.

[105] E. Vedejs, D. A. Perry, K. N. Houk, N. G. Rondan, *J Am Chem Soc* **1983**, *105*, 6999-7001.

[106] a) R. P. Wool, *Polym. Eng. Sci.* **1978**, *18*, 1056-1061; b) R. P. Wool, *Adhesion and Adsorption of Polymers* **1980**, *A*, 341; c) S. L. Cannon, G. B. McKenna, W. O. Statton, *J Polym Sci Macromol Rev* **1976**, *11*, 209-275.

[107] a) Y. Chen, A. M. Kushner, G. A. Williams, Z. Guan, *Nat Chem* **2012**, *4*, 467-472; b) K. Imato, M. Nishihara, T. Kanehara, Y. Amamoto, A. Takahara, H. Otsuka, *Angew. Chem. Int. Ed.* **2012**, *51*, 1138-1142.

[108] a) S. R. Trenor, A. R. Shultz, B. J. Love, T. E. Long, *Chem. Rev.* **2004**, *104*, 3059-3077; b) Y. Chujo, K. Sada, R. Nomura, A. Naka, T. Saegusa, *Macromolecules* **1993**, *26*, 5611-5614; c) C. M. Chung, Y. S. Roh, S. Y. Cho, J. G. Kim, *Chem. Mater.* **2004**, *16*, 398; d) P. Froimowicz, H. Frey, K. Landfester, *Macromol. Rapid Commun.* **2011**, *32*, 468-473; e) H. Otsuka, S. Nagano, Y. Kobashi, T. Maeda, A. Takahara, *Chem. Commun.* **2010**, *46*, 1150-1152; f) T. F. Scott, A. D. Schneider, W. D. Cook, C. N. Bowman, *Science* **2005**, *308*, 1615-1617; g) Y. Amamoto, J. Kamada, H. Otsuka, A. Takahara, K. Matyjaszewski, *Angew. Chem. Int. Ed.* **2011**, *123*, 1698; h) B. Ghosh, M. W. Urban, *Science* **2009**, *323*, 1458-1460.

[109] a) Y. Zhang, A. A. Broekhuis, F. Picchioni, *Macromolecules* **2009**, *42*, 1906-1912; b) H. Otsuka, K. Aotani, Y. Higaki, Y. Amamoto, A. Takahara, *Macromolecules* **2007**, *40*, 1429-1434; c) A. J. Inglis, L. Nebhani, O. Altintas, F. G. Schmidt, C. Barner-Kowollik, *Macromolecules* **2010**, *43*, 5515-5520.

[110] a) D. Kowalski, M. Ueda, T. Ohtsuka, *J. Mater. Chem.* **2010**, *20*, 7630-7633; b) K. A. Williams, A. J. Boydston, C. W. Bielawski, *J R Soc Interface* **2007**, *4*, 359-362.

[111] a) S. J. Kalista Jr, T. C. Ward, *J R Soc Interface* **2007**, *4*, 405-411; b) S. J. Kalista Jr, T. C. Ward, Z. Oyetunji, *Mechanics of Advanced Materials and Structures* **2007**, *14*, 391-397.

[112] a) T. Ono, T. Nobori, J. M. Lehn, *Chem. Commun.* **2005**, 1522-1524; b) R. K. Schultz, R. R. Myers, *Macromolecules* **1969**, *2*, 281-285.

[113] a) C. Dry, *J. Mod. Phys. B* **1992**, *6*, 2763; b) C. M. Dry, *Materials Research Society Proceedings* **1992**, *276*, 331.

[114] a) S. Burattini, B. W. Greenland, D. Chappell, H. M. Colquhoun, W. Hayes, *Chem. Soc. Rev.* **2010**, *39*, 1973-1985; b) E. B. Murphy, F. Wudl, *Progress in Polymer Science (Oxford)* **2010**, *35*, 223-251; c) R. J. Wojtecki, M. A. Meador, S. J. Rowan, *Nature Materials* **2011**, *10*, 14-27; d) R. P. Wool, *Soft Matter* **2008**, *4*, 400-418; e) D. Y. Wu, S. Meure, D. Solomon, *Progress in Polymer Science (Oxford)* **2008**, *33*, 479-522.

[115] S. M. Bleay, C. B. Loader, V. J. Hawyes, L. Humberstone, P. T. Curtis, *Composites - Part A: Applied Science and Manufacturing* **2001**, *32*, 1767-1776.

[116] a) M. Hucker, I. Bond, S. Bleay, S. Haq, *Composites Part A: Applied Science and Manufacturing* **2003**, *34*, 927-932; b) M. Hucker, I. Bond, A. Foreman, J. Hudd, *Advanced Composites Letters* **1999**, *8*, 181-189; c) E. N. Brown, M. R. Kessler, N. R. Sottos, S. R. White, *J. Microencaps.* **2003**, *20*, 719-730.

[117] a) E. N. Brown, S. R. White, N. R. Sottos, *Journal of Materials Science* **2004**, *39*, 1703-1710; b) J. D. Rule, N. R. Sottos, S. R. White, *Polymer* **2007**, *48*, 3520-3529.

[118] a) X. Liu, J. K. Lee, S. H. Yoon, M. R. Kessler, *J. Appl. Polym. Sci.* **2006**, *101*, 1266-1272; b) G. O. Wilson, J. S. Moore, S. R. White, N. R. Sottos, H. M. Andersson, *Adv. Funct. Mater.* **2008**, *18*, 44-52.

[119] J. D. Rule, E. N. Brown, N. R. Sottos, S. R. White, J. S. Moore, *Adv. Mater.* **2005**, *17*, 205-208.

[120] E. N. Brown, S. R. White, N. R. Sottos, *Journal of Materials Science* **2006**, *41*, 6266-6273.

[121] A. R. Hamilton, N. R. Sottos, S. R. White, *Adv. Mater.* **2010**, *22*, 5159-5163.

[122] C. J. Hansen, W. Wu, K. S. Toohey, N. R. Sottos, S. R. White, J. A. Lewis, *Adv. Mater.* **2009**, *21*, 4143-4147.

[123] K. S. Toohey, C. J. Hansen, J. A. Lewis, S. R. White, N. R. Sottos, *Adv. Funct. Mater.* **2009**, *19*, 1399-1405.

[124] W. L. Dilling, *Chem. Rev.* **1983**, *83*, 1-47.

[125] Y. Amamoto, J. Kamada, H. Otsuka, A. Takahara, K. Matyjaszewski, *Angew. Chem. Int. Ed.* **2011**, *50*, 1660-1663.

[126] M. Burnworth, L. Tang, J. R. Kumpfer, A. J. Duncan, F. L. Beyer, G. L. Fiore, S. J. Rowan, C. Weder, *Nature* **2011**, *472*, 334-337.

[127] a) A. P. Esser-Kahn, J. S. Moore, *Materials with Purpose: Designer Materials for Applications from Every Approach* **2010**; b) G. Deng, C. Tang, F. Li, H. Jiang, Y. Chen, *Macromolecules* **2010**, *43*, 1191-1194; c) D. C. Tuncaboylu, M. Sari, W. Oppermann, O. Okay, *Macromolecules* **2011**, *44*, 4997-5005.

[128] A. P. Vogt, B. S. Sumerlin, *Soft Matter* **2009**, *5*, 2347-2351.

[129] J. I. Jay, K. Langheinrich, M. C. Hanson, A. Mahalingam, P. F. Kiser, *Soft Matter* **2011**, *7*, 5826-5835.

[130] Z. Ge, J. Hu, F. Huang, S. Liu, *Angew. Chem. Int. Ed.* **2009**, *48*, 1798-1802.

[131] J. Canadell, H. Goossens, B. Klumperman, *Macromolecules* **2011**, *44*, 2536-2541.

[132] T. Ono, T. Nobori, J.-M. Lehn, *Chem. Commun.* **2005**, 1522-1524.

[133] a) P. Reutenauer, E. Buhler, P. J. Boul, S. J. Candau, J. M. Lehn, *Chemistry - A European Journal* **2009**, *15*, 1893-1900; b) P. Reutenauer, P. J. Boul, J.-M. Lehn, *Eur J Org Chem* **2009**, *2009*, 1691-1697; c) J. R. Jones, C. L. Liotta, D. M. Collard, D. A. Schiraldi, *Macromolecules* **1999**, *32*, 5786-5792.

[134] a) Y. Higaki, H. Otsuka, A. Takahara, *Macromolecules* **2006**, *39*, 2121-2125; b) Y. Amamoto, M. Kikuchi, H. Masunaga, S. Sasaki, H. Otsuka, A. Takahara, *Macromolecules* **2010**, *43*, 1785-1791; c) C. J. Kloxin, T. F. Scott, B. J. Adzima, C. N. Bowman, *Macromolecules* **2010**, *43*, 2643-2653.

[135] a) S. Burattini, H. M. Colquhoun, J. D. Fox, D. Friedmann, B. W. Greenland, P. J. F. Harris, W. Hayes, M. E. Mackay, S. J. Rowan, *Chem. Commun.* **2009**, 6717-6719; b) J. Cui, A. d. Campo, *Chem. Commun.* **2012**, *48*, 9302-9304; c) X. Hao, H. Liu, Y. Xie, C. Fang, H. Yang, *Colloid. Polym. Sci.* **2013**, 1-10.

[136] P. Reutenauer, E. Buhler, P. J. Boul, S. J. Candau, J. M. Lehn, *Chemistry – A European Journal* **2009**, *15*, 1893-1900.

[137] a) C. Barner-Kowollik, A. J. Inglis, L. Nebhani, O. Altintas, F. G. Schmidt, S. Fengler, S. Hilf, S. Krause, A. Henning, *International Patent PCT, WO/2011/101176*; b) C. Barner-Kowollik, A. J. Inglis, L. Nebhani, F. G. Schmidt, S. Fengler, S. Hilf, S. Krause, A. Henning, *International Patent PCT, WO/2011/101175*; c) C. Barner-Kowollik, F. G. Schmidt, S. Hilf, J. Zhou, *International Patent PCT, WO/2012/065786.*

[138] S. D. Bergman, F. Wudl, *J. Mater. Chem.* **2008**, *18*, 41-62.

[139] J. M. Craven, in *3435003, Vol. 3435003*, 3435003 ed. (Ed.: 3435003), 3435003, USA, **1969**, p. 3435003.

[140] C. Goussé, A. Gandini, *Polym. Int.* **1999**, *48*, 723-731.

[141] a) A. A. Kavitha, N. K. Singha, *Macromol. Chem. Phys.* **2007**, *208*, 2569-2577; b) H. S. Patel, B. P. Patel, D. B. Patel, *International Journal of Polymeric Materials and Polymeric Biomaterials* **2009**, *58*, 625-635; c) H. S. Patel, B. P. Patel, D. B. Patel, *Polymer-Plastics Technology and Engineering* **2010**, *49*, 394-399; d) J. R. McElhanon, D. R. Wheeler, *Org Lett* **2001**, *3*, 2681-2683.

[142] F. Ghezzo, D. R. Smith, T. N. Starr, T. Perram, A. F. Starr, T. K. Darlington, R. K. Baldwin, S. J. Oldenburg, *J. Compos. Mater.* **2010**, *44*, 1587-1603.

[143] A. M. Peterson, R. E. Jensen, G. R. Palmese, *ACS Applied Materials & Interfaces* **2010**, *2*, 1141-1149.

[144] A. A. Kavitha, N. K. Singha, *Macromolecules* **2010**, *43*, 3193-3205.

[145] J. A. Syrett, G. Mantovani, W. R. S. Barton, D. Price, D. M. Haddleton, *Polymer Chemistry* **2010**, *1*, 102-106.
[146] C. e. Yuan, M. Z. Rong, M. Q. Zhang, Z. P. Zhang, Y. C. Yuan, *Chem. Mater.* **2011**, *23*, 5076-5081.
[147] Z. P. Zhang, M. Z. Rong, M. Q. Zhang, C. e. Yuan, *Polymer Chemistry* **2013**, *4*, 4648-4654.
[148] S. Burattini, B. W. Greenland, D. H. Merino, W. Weng, J. Seppala, H. M. Colquhoun, W. Hayes, M. E. MacKay, I. W. Hamley, S. J. Rowan, *J Am Chem Soc* **2010**, *132*, 12051-12058.
[149] Trommsdorf, *Ann. Chem. Pharm.* **1834**, *11*.
[150] A. Einstein, *Annalen der Physik* **1905**, *322*, 132-148.
[151] M. Planck, *Verhandlungen der Deutschen Physikalischen Gesellschaft* **1900**, *2*, 237.
[152] A. Einstein, *Verhandlungen der Deutschen Physikalischen Gesellschaft* **1916**, *18*, 318-323.
[153] A. Einstein, *Naturwissenschaften* **1922**, *10*, 823-826.
[154] A. Jablonski, *Zeitschrift für Physik* **1935**, *94*, 38-46.
[155] J. C. Collie, *J. Chem. Soc.* **1904**, *85*, 971.
[156] a) J. N. Pitts, R. L. Letsinger, R. P. Taylor, J. M. Patterson, G. Recktenwald, R. B. Martin, *J Am Chem Soc* **1959**, *81*, 1068-1077; b) G. S. Hammond, W. M. Moore, *J Am Chem Soc* **1959**, *81*, 6334-6334.
[157] N. C. Yang, C. Rivas, *J Am Chem Soc* **1961**, *83*, 2213-2213.
[158] a) J. N. Moorthy, S. Samanta, *ARKIVOC* **2007**, 324-340; b) E. F. Ullman, K. R. Huffman, *Tetrahedron Lett* **1965**, *6*, 1863-1867.
[159] E. F. Zwicker, L. I. Grossweiner, N. C. Yang, *J Am Chem Soc* **1963**, *85*, 2671-2672.
[160] a) G. Porter, M. F. Tchir, *Journal of the Chemical Society D: Chemical Communications* **1970**, 1372-1373; b) G. Porter, M. F. Tchir, *Journal of the Chemical Society A: Inorganic, Physical, Theoretical* **1971**, 3772-3777.
[161] L. Salem, C. Rowland, *Angewandte Chemie International Edition in English* **1972**, *11*, 92-111.
[162] S. M. Mellows, P. G. Sammes, *Journal of the Chemical Society D: Chemical Communications* **1971**, 21-22.
[163] B. J. Arnold, P. G. Sammes, T. W. Wallace, *J. Chem. Soc., Perkin Trans. 1* **1974**, 415-420.
[164] P. G. Sammes, *Tetrahedron* **1976**, *32*, 405-422.
[165] K. R. Huffman, M. Loy, E. F. Ullman, *J Am Chem Soc* **1965**, *87*, 5417-5423.
[166] K. C. Nicolaou, D. L. F. Gray, J. Tae, *J Am Chem Soc* **2003**, *126*, 613-627.
[167] a) T. Gruendling, K. K. Oehlenschlaeger, E. Frick, M. Glassner, C. Schmid, C. Barner-Kowollik, *Macromol. Rapid Commun.* **2011**, *32*, 807-812; b) M. Kaupp, T. Tischer, A. F. Hirschbiel, A. P. Vogt, U. Geckle, V. Trouillet, T. Hofe, M. H. Stenzel, C. Barner-Kowollik, *Macromolecules* **2013**, *46*, 6858-6872.
[168] T. Pauloehrl, G. Delaittre, V. Winkler, A. Welle, M. Bruns, H. G. Börner, A. M. Greiner, M. Bastmeyer, C. Barner-Kowollik, *Angew. Chem. Int. Ed.* **2012**, *51*, 1071-1074.
[169] a) S. Arumugam, V. V. Popik, *J Am Chem Soc* **2009**, *131*, 11892-11899; b) S. Arumugam, V. V. Popik, *J Am Chem Soc* **2011**, *133*, 15730-15736; c) S. Arumugam, V. V. Popik, *J Am Chem Soc* **2011**, *133*, 5573-5579.
[170] S. Arumugam, V. V. Popik, *J Am Chem Soc* **2012**, *134*, 8408-8411.
[171] E. Vedejs, T. H. Eberlein, R. G. Wilde, *The Journal of Organic Chemistry* **1988**, *53*, 2220-2226.
[172] M. Glassner, K. K. Oehlenschlaeger, A. Welle, M. Bruns, C. Barner-Kowollik, *Chem. Commun.* **2013**, *49*, 633-635.
[173] T. Pauloehrl, A. Welle, K. K. Oehlenschlaeger, C. Barner-Kowollik, *Chemical Science* **2013**, *4*, 3503-3507.
[174] a) D. Y. Wu, S. Meure, D. Solomon, *Prog. Polym. Sci.* **2008**, *33*, 479-522; b) M. Wouters, E. Craenmehr, K. Tempelaars, H. Fischer, N. Stroeks, J. van Zanten, *Prog. Org. Coat.* **2009**, *64*, 156-162.
[175] a) S. van der Zwaag, *Self healing materials an alternative approach to 20 centuries of materials science*, Springer Verlag, Dordrecht, The Netherlands, **2007**; b) J. M. Carven*, Vol. 3435003*, US, **1969**.
[176] a) P. A. Pratama, A. M. Peterson, G. R. Palmese, *Polymer Chemistry* **2013**, *4*, 5000-5006; b) S. Yu, R. Zhang, Q. Wu, T. Chen, P. Sun, *Adv. Mater.* **2013**, *25*, 4912-4917.
[177] L. Nebhani, S. Sinnwell, C. Y. Lin, M. L. Coote, M. H. Stenzel, C. Barner-Kowollik, *J. Polym. Sci., Part A: Polym. Chem.* **2009**, *47*, 6053-6071.
[178] L. Nebhani, D. Schmiedl, L. Barner, C. Barner-Kowollik, *Adv. Funct. Mater.* **2010**, *20*, 2010-2020.
[179] W. J. Middleton, E. G. Howard, W. H. Sharkey, *J Am Chem Soc* **1961**, *83*, 2589-2590.
[180] G. Bähr, G. Schleitzer, *Chem. Ber.* **1955**, *88*, 1771-1777.

[181] H. E. Simmons, D. C. Blomstrom, R. D. Vest, *J Am Chem Soc* **1963**, *84*, 4756-4771.
[182] R. Mayer, W. Thiel, H. Viola, *Zeitschrift für Chemie* **1979**, *19*, 56-56.
[183] A. Maciejewski, R. P. Steer, *Chem. Rev.* **1993**, *93*, 67-98.
[184] T. Paulöhrl, A. J. Inglis, C. Barner-Kowollik, *Adv. Mater.* **2010**, *22*, 2788-2791.
[185] a) W. Thiel, R. Mayer, *Journal für Praktische Chemie* **1989**, *331*, 243-262; b) W. Thiel, R. Mayer, *Sulfur reports* **1988**, *8*, 1-52; c) F. Durton-Woitrine, R. Merenyi, H. G. Viehe, *Synthesis* **1985**, 79-80.
[186] I. Gadwal, A. Khan, *Polymer Chemistry* **2013**.
[187] a) F. Fringuelli, F. Pizzo, S. Tortoioli, L. Vaccaro, *The Journal of Organic Chemistry* **2003**, *68*, 8248-8251; b) H. Kotsuki, T. Shimanouchi, R. Ohshima, S. Fujiwara, *Tetrahedron* **1998**, *54*, 2709-2722; c) C. Mangold, F. Wurm, H. Frey, *Polymer Chemistry* **2012**, *3*, 1714-1721.
[188] a) C. N. Bowman, W. Xi, C. Kloxin, M. Krieger, *Chem. Commun.* **2013**; b) J. W. Chan, C. E. Hoyle, A. B. Lowe, M. Bowman, *Macromolecules* **2010**, *43*, 6381-6388.
[189] L. H. Sperlig, *Troduction to Physical polymer science, Wiley-VCH, Weinheim, Germany* **2006**, *forth eddition*, Ch. 8.
[190] a) M. R. Kessler, N. R. Sottos, S. R. White, *Composites Part A: Applied Science and Manufacturing* **2003**, *34*, 743-753; b) G. W. Greenwood, *Materials Science and Engineering* **1976**, *25*, 241-245; c) G. J. Weng, *Materials Science and Engineering* **1983**, *57*, 127-133; d) R. W. Penn, G. E. Fulmer, *Rev. Sci. Instrum.* **1965**, *36*, 1230-1232.
[191] M. C. Caserio, W. Lauer, T. Novinson, *J Am Chem Soc* **1970**, *92*, 6082-6084.
[192] T. L. Gilchrist, J. E. Wood, *J. Chem. Soc. Chem. Comm.* **1992**, *0*, 1460-1461.
[193] a) T. Josse, O. Altintas, K. K. Oehlenschlaeger, P. Dubois, P. Gerbaux, O. Coulembier, C. Barner-Kowollik, *Chem. Commun.* **2014**, *50*, 2024-2026; b) M. Winkler, J. O. Mueller, K. K. Oehlenschlaeger, L. Montero de Espinosa, M. A. R. Meier, C. Barner-Kowollik, *Macromolecules* **2012**, *45*, 5012-5019.
[194] S. Perrier, C. Barner-Kowollik, J. F. Quinn, P. Vana, T. P. Davis, *Macromolecules* **2002**, *35*, 8300-8306.
[195] a) L. Charles, M. Lejars, A. Margaillan, C. Bressy, *Int. J. Mass spectrom.* **2012**, *311*, 31-39; b) A. T. Jackson, S. E. Slade, J. H. Scrivens, *Int. J. Mass spectrom.* **2004**, *238*, 265-277.

16 Complete List of Publications

15. *Ambient Temperature Ligation of Diene Functional Polymer and Peptide Strands onto Cellulose via Photochemical and Thermal Protocol*

Tischer, T.; Claus, T. K.; **Oehlenschlaeger, K. K.**; Trouillet, V.; Bruns, M.; Welle, A.; Linkert, K.; Goldmann, A. S.; Börner, H. G.; Barner-Kowollik, C. ***Macromol. Rapid Comm.*** **2014**, in press.

14. *State-of-the-Art Analytical Methods for Assessing Dynamic Bonding Soft Matter Materials*

Brandt, J.; **Oehlenschlaeger, K. K.**; Schmidt, F. G.; Barner-Kowollik, C.; Lederer, A. ***Adv. Mat.*** **2014**, in press.

13. *Adaptable Hetero Diels –Alder Networks for Fast Self-Healing under Mild Conditions*

Oehlenschlaeger, K. K.; Mueller, J. O.; Brandt, J.; Hilf, S.; Lederer, A.; Wilhelm, M.; Graf, R.; Coote, M. L.; Schmidt, F. G.; Barner-Kowollik, C. ***Adv. Mat.*** **2014**, in press.

12. *Ambient Temperature Catalyst-Free Light-induced Preparation of Macrocyclic Aliphatic Polyesters*

Josse, T.; Altintas, O.; **Oehlenschlaeger, K. K.**; Dubois, P.; Gerbaux, P.; Coulembier, O.; Barner-Kowollik, C. ***Chem. Commun.*** **2014**, *50*, 2024–2026.

11. *Sunligh- induced Crosslinking of 1,2-Polybutadienes: Access to Flourescent Polymer Networks*

Mueller, J. O; Guimard, N. K.; **Oehlenschlaeger, K. K.**; Schmidt, F. G.; Barner-Kowollik, C. ***Polym. Chem.*** **2014**, *5*, 1447–1456.

10. *A Mild and Efficient Approach to Functional Single-Chain Polymeric Nanoparticles via Photoinduced Diels-Alder Ligation*

Altintas, O.; Willenbacher, J.; Wuest, K.; **Oehlenschlaeger, K. K.**; Krolla-Sidenstein, P.; Gliemann, H.; Barner-Kowollik, C. ***Macromolecules*** **2013**, 46, 8092–8101.

9. *Spatially Controlled Surface Immobilization of Nucleophiles via Trapping of Photo-Generated Thioaldehydes*

Pauloehrl, T.; Welle, A.; **Oehlenschlaeger, K. K.**; Barner-Kowollik, C. ***Chem. Sci.*** **2013**, 4, 3503–3507.

8. *Fast and Catalyst Free Hetero-Diels-Alder Chemistry for Cyclable Bonding/Debonding on Demand Material Design*

Oehlenschlaeger, K. K.; Guimard, N. K.; Brandt, J.; Mueller, J. O.; Lin, C. Y.; Hilf, S.; Lederer, A.; Coote, M. L.; Schmidt, F. G.; Barner-Kowollik, C. ***Polym. Chem.*** **2013**, 4, 4348-4355

7. *Harnessing Entropy to Direct the Bonding/Debonding of Polymer Systems Based on Reversible Chemistry*

Guimard, N. K.; Ho, J.; Brandt, J.; Lin, C. Y.; Namazian, M.; Mueller, J. O.; **Oehlenschlager, K. K.**; Hilf, S.; Lederer, A.; Schmidt, F. G.; Coote, M.; Barner-Kowollik, C. ***Chem. Sci.*** **2013**, 4, 2752-2759

6. *Polymer Surface Patterning via Diels-Alder Trapping of Photo-Generated Thioaldehydes*

Glassner, M.; **Oehlenschlaeger, K. K.**; Welle, A.; Bruns, M.; Barner-Kowollik, C. ***Chem. Commun.*** **2013**, 49, 633-635.

5. *Light-Induced Modular Ligation of Conventional RAFT Polymers*

Oehlenschlaeger, K. K.; Mueller, J. O.; Heine, N. B.; Glassner, M.; Guimard, N. K.; Delaittre, G.; Schmidt, F. G.; Barner-Kowollik, C. ***Angew. Chem. Int. Ed.*** **2013**, 52, 762–766.

4. *Highly Orthogonal Fucntionalization of ADMET Polymers via Photoinduced Diels-Alder Reactions*

Winkler, M.; Müller, J. O; **Oehlenschlaeger, K. K.**; Montero de Espinosa, L.; Meier, M. A. R.; Barner-Kowollik, C. ***Macromolecules*** **2012**, 45, 5012−5019.

3. *Current Trends in the Field of Self-Healing Materials*

Guimard, N. K.; **Oehlenschlaeger, K. K.**; Zhou, J.; Hilf, S.; Schmidt, F. G.; Barner-Kowollik, C. ***Macromol. Chem. Phys.*** **2012**, 213, 131−143.

2. *Ambient Temperature Synthesis of Triblock Coplymers via Orthogonal Photochemically and Thermally Induced Modular Conjugation*

Glassner, M.; **Oehlenschlaeger, K. K.**; Gruendling, T.; Barner-Kowollik, C. ***Macromolecules*** **2011**, 44, 4681–4689.

1. *UV Light-Triggered Macromolecular Click Conjugations via the Use of o-Quinodimethanes*

Gruendling, T.; **Oehlenschlaeger, K. K.**; Frick, E.; Glassner, M.; Schmid, C.; Barner-Kowollik, C. ***Macromol. Rapid Comm.*** **2011**, 32, 807–812.

17 Acknowledgments

The current thesis is not only a product of mine. Without the help and support of several people I would have not been able to master all the projects and research. In the following their names should be honored.

I want to thank the most understanding, friendly, obliging and supporting professor I ever met, Christopher. You are a phenomenon. I never met somebody who is so motivating, pushing and ambitious like you, by still taking so much care of every single coworker. Without your motivation I wouldn't be the chemists I am, which I will never forget. I'm very proud of being a CBK student.

The quote "behind every hard working man stands a great woman" describes extremely well the entire periode of my study and my PhD-student time. Therefore, the one of the first persons I have to acknowledge is my beloved Tanja. You were the person who supported me most and gave me a home as well as comfort in hard times. Thank you so much for being there. I don't know where I would be without you.

Similarly my whole family is acknowledged for their understanding and support over the last three years, especially my parents who enabled my study and always kept faith in me during my entire life. Thank you.

Plenty of thanks to my collaboration partners from Evonik (Dr. Stefan Hilf, Dr. Markus Pridöhl and Dr. Uwe Paulmann), who always created a very comfortable atmosphere during the business meetings and encouraged me in my work. Special thanks to Dr. Stefan Hilf for providing the Cp_2-polymer I used throughout my thesis.

Dr. Friedrich Georg Schmidt shall be acknowledged in particular for the trust in me and the amazing support. Thank you very much. My PhD time with you was really great. I hope we can stay in touch.

Special thanks to my PhD "mum" Dr. Nathalie Guimard, who guided me at the beginning of my PhD time and thought me a lot about correct scientific working and writing (sometimes the hard way !-). Merci beaucoup maman.

In this context I also wish to thank Dr. Adrew Vogt, who improved (together with Nathalie) my english with every single talk. Thanks mate, I will never forget my first rodeo cowboy.

Thank you Dr. Till Gründling for taking care of me when I was a young, naive diploma greenhorn.

Thank you Evelyn Stühring, Dr. Anja Goldmann, Vincent Schüler and Peter Gerstel for running the ship and keeping everything in order.

большое спасибо Dr. Maria Schneider для красивой времени. Я не забуду

Many thanks to Dr. Adrew Vogt, Dr. Mathias Glassner, Dr. Dominik Voll, Tiny Tanja and Kai Hiltebrandt for proof reading parts of the thesis. (And of course thank you to the team who corrected the final errors and helped me to eliminate the last typos)

I wish to acknowledge my collaboration partners from Canberra, Dresden, Karsruhe and Mainz for the fruitful work (Prof. Michelle Coote, Dr. Ching Yen Lin, Dr. Albena Lederer, Josef Brandt, Prof. Manfred Wilhelm and Dr. Robert Graf).

I want to thank my old diploma student and later co-Evonik PhD student Jan Müller. You are an awesome dude, and you impressed me a lot with your calm attitude. I'm looking forward and will be happy to call you Dr. Müller (And maybe share a desk with you in Marl).

Kai Pahnke, the latest Evonik-CBK product, shall be acknowledged for taking over the CDTE topic and driving the project further. Additionally, the multiple trips to the business meetings were fun with you. All the best.

Thank you Dr. Mathias Glassner for the countless scientific discussions. We are a really good tandem.

Many thanks to Larissa Bergmann, Linus Reichenbach and Marius Kuhn who are great friends. You guys managed to let me smile every day during my student time.

Thank you (Dr.) Alex Hähnel for the long time we spent together and the great PhD party which will leave our legacy.

Muchas gracias mi hermano Dr. Cesar Rodriguez-Emmenegger. You are a true friend.

Thank you to all the visiting students (Susanne Handson, Pietre Derboven, Stijn Billiet, Thomas Josse, Dagmar D'hooge, Clara G.A.) for the great time I had with you and for your friendship.

I have to thank the post-docs of course as well, so thank you Dr. Andrew Vogt, Dr. James Blinco, Dr. Elise "ma bell" Deniau, Dr. Lebohang "Lebo" Hlalele, Dr. Jiawen Zhou, Dr. Guillaume Delaittre (I count you here) and of course Dr. Basit Yameen for a great time and lots of lessons. Special thanks to Basit for staying up with me in the lab during so many nights and being such an impressive, intelligent and humbling person.

Thank you to the KHYS and Prof. Martina Stenzel for giving me the opportunity to work at the UNSW (Sydney). It was a formative experience I will never forget.

Many members in the Stenzel group made it easy for me to feel home at the UNSW. Therefore I have to say thank you to, Johnny, Alice, Yanyan, Ted, Aydan, Manuela, Krystof, Wei and Sam. You are all very special people. Thank you for your friendship

Thanks to Astrid Hirschbiel for her funny personality, which simplified working in the lab. The same acknowledgement applies to Dr. Nicolas Zydziak.

Thank you Dr. Eva Blasco-Pomar. Your friendship has a high value for me. You gave me a view inside the spanish culture and taught me what is important in life. I certainly will never forget that.

I'm glad and proud to be part of the original big five, a brotherhood who brought light to the darkness of the group. Thank you Johannes "mad dog" Willenbacher, Jan "lucky hand" Müller, Michi "charly" Kaupp and Alex "fox" Quick for being great brothers. I will never forget you guys and the countless hours we spend together. You are great.

Thank you squash-team, especially Christiane, for the funny evenings.

Thanks a lot to all people in the old building in the lab and the office, for a great working atmosphere.

I also have to acknowledge Tanja's family, who always showed keen interest in my work.

Finally I want to acknowledge the entire macroarc family (alumni members such as Berni, Christoph and Christina; but also new colleagues like Alex S., Kai H. and Thomas G.) for being a great team. I couldn't imagine a better group and I will miss every single one of you very much.

In the end I have to thank to my beloved Tanja again, as I can never say it often enough.

…dary! High Five!

(Barney Stinson)